Synthesis, Characterization, and Properties of Tailored Functional Block Copolymers

Dissertation

zur Erlangung des akademischen Grades

Doktor der Naturwissenschaften (Dr. rer. nat.)

im Fach Chemie der Fakultät für Biologie, Chemie und Geowissenschaften

der Universität Bayreuth

vorgelegt von

Robin Pettau

geboren in Wesel

Bayreuth, 2011

Die vorliegende Arbeit wurde in der Zeit von November 2006 bis Mai 2011 am Lehrstuhl für Makromolekulare Chemie I der Universität Bayreuth unter der Betreuung von Prof. Dr. Hans-Werner Schmidt angefertigt.

Datum der Einreichung: 13. Mai 2011

Datum der Zulassung durch die Prüfungskommission: 18. Mai 2011

Datum des wissenschaftlichen Kolloquiums: 02. November 2011

Prüfungsausschuss:

Prof. Dr. Hans-Werner Schmidt (Erstgutachter)

Prof. Dr. Axel H. E. Müller (Zweitgutachter)

Prof. Dr. Stephan Förster (Vorsitz)

Prof. Dr. Lothar Kador

Table of contents

1   Introduction

Research and development of block copolymers and their entropically and enthalpically driven phase separation[1,2] has stimulated a broad range of research areas and opened numerous applications in the last decades.[3,4] Liquid crystals as an important material class that exhibit exceptional anisotropic properties due to their molecular shape are much longer known[5–7] and are used successfully in display applications.[8,9] Still, ongoing and future research opens and will open opportunities to new applications, especially when liquid crystalline properties are combined with block copolymer materials and two ways of self-assembly are present. By this, complex order on hierarchical levels is achieved.[10] In the introduction of this thesis, a brief overview will be given concerning selected topics on functional block copolymers that are important within the scope of this thesis. These topics include i) the synthesis and properties of block copolymers, ii) functional block copolymers and iii) liquid crystalline side-group block copolymers, as well as specific applications of functional block copolymers, as photo addressable materials and gelators for liquid crystals.

1.1   Block copolymers

Block copolymers are macromolecules composed of at least two chemically different blocks (segments) that are covalently connected. The chemically distinct blocks generally undergo microphase separation and block copolymers are well-known for their self-assembly into well defined, ordered morphologies on the nanometer scale. The formation of microphase-separated morphologies is driven by two counteracting forces. Enthalphic effects cause the tendency to minimize the unfavorable interaction energy between dissimilar blocks (A and B) via the formation of A- and B-rich regions in order to achieve the smallest possible interface to volume ratio (e.g. via creating curvature and chain stretching normal to the interface). Entropic effects counteract this minimization of the interface. This phase separation is accomplished with some loss of translational and configurational entropy by local compositional ordering to maintain a constant homogenous segment density. The localization of the junction points of the different segments at the domain interface causes an additional loss of entropy.[11,12]

The phase behavior of AB diblock copolymers can be described by the Flory–Huggins segment–segment interaction parameter (χ), the overall degree of polymerization (N), and the volume fraction (ϕ) of the individual blocks that is determined by the ratio of the two monomers and their molar volume. The product N times χ ($N\chi$) is used to express the enthalpic-entropic balance and determines the degree of segregation and therefore if an ordered or disordered phase results. The volume fraction (ϕ) determines to a large extend

which morphology is obtained as long as the block copolymer remains in the range of an ordered phase.

If $N\chi \leq 10$, the entropic effects dominate, resulting in the formation of a mixed, disordered phase and the chain segments of both components penetrate each other. If $10 \leq N\chi < 100$ the weak segregation limit (WSL) is reached and the system is governed by enthalpic effects, causing an order-disorder transition (ODT) where the dissimilar segments segregate into a variety of ordered periodic microstructures. This microphase separation within the WSL was firstly theoretically described by Leibler.[1]

For $N\chi \geq 100$ the strong segregation limit (SSL) is reached and the interphases between the domains are narrow and well separated. Meier[13] established a theory for diblock copolymers in the SSL describing the classical morphologies. Neither the SSL nor the WSL describes the morphological behavior of diblock copolymers completely. In 1996 Matsen and Bates used a self-consistent field theory (SCFT) and could mostly bridge the gap between weak and strong segregation limit.[14]

In the case of AB diblock copolymers typically four stable morphologies (i.e. spheres, cylinders, gyroids and lamellae) can be found under equilibrium conditions for distinct compositions.[11,12,15]

In Figure 1.1 a phase diagram ($N\chi$ vs. ϕ) calculated after Matsen[14] (Figure 1.1, a) is compared to an experimentally determined phase diagram for polyisoprene-*block*-polystyrene presented by Khandpur *et al.*[15] (Figure 1.1, b). The respective morphologies are shown below with increasing ϕ_A in the order: body centered cubic spheres (bcc, $Im\overline{3}m$) of A in a matrix of B, hexagonal cylinders (H, HEX,) of A in a matrix of B, bicontinuous cubic (gyroid, $Ia\overline{3}d$), perforated layers (HPL) and lamellae (L, LAM). With further increase of ϕ_A the order is reversed with A being the matrix.

In more complex block copolymer systems, i.e. ABC triblock copolymers, the number of morphologies and their complexity are considerably extended.[12,16]
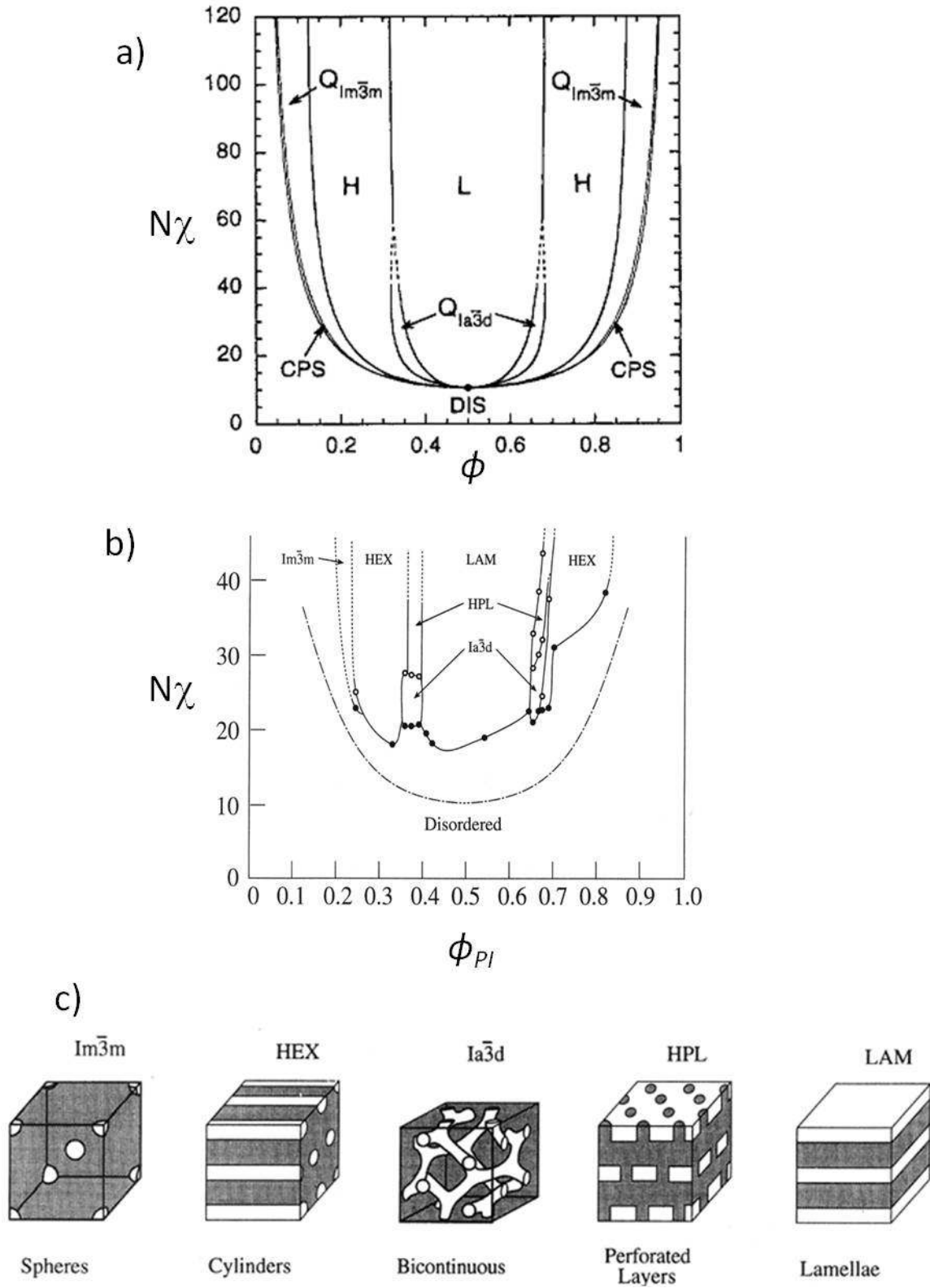
Figure 1.1:   a) Phase diagram for AB diblock copolymers in the strong segregation limit (SSL) calculated by Matsen *et al*.;[14] b) experimental results for the phase diagram for polyisoprene-*block*-polystyrene diblock copolymer near the order-disorder transition by Khandpur *et al*.;[15] c) illustration of the respective morphologies[15] close-packed spheres (CPS), body centered cubic spheres ((bcc, lm$\overline{3}$m), hexagonal cylinders (H, HEX), bicontinuous la$\overline{3}$d cubic (gyroid, la$\overline{3}$d), perforated layers (HPL), lamellae (L, LAM).

Functional block copolymers

According to IUPAC, "The term *functional polymer* has two meanings: (a) a polymer bearing functional groups (such as hydroxy, carboxy, or amino groups) that make the polymer reactive and (b) a polymer performing a specific function for which it is produced and used."[17]

In general, this definition covers two sets of polymers. Accordingly, in the frame of this thesis mainly targeting block copolymers, the term *functional* will be used if at least one block bears functional groups that allow chemical reactions or the block copolymers fulfill a specific function due to their physical properties or induced changes in these properties. To facilitate a more easy distinction between these two different cases of block copolymers carrying reactive chemical functions in one block copolymer segment will be denoted as *functionalizable*.

Functionalizable block copolymers with reactive side-groups

In Figure 1.2 three examples for functionalizable block copolymers are shown as an illustration. The first example is a block copolymer bearing a poly(1,2-butadiene) segment. The olefinic double bond can be used for a variety of different polymer analogous reactions. Hydroboration and subsequent oxidation yields a hydroxy functionalized side-group, that again can be used for further reactions.[18,19] A direct attachment of a side-group can be carried out by a hydrosilylation reaction.[20] By converting the double bond into a epoxy group[21] it is possible to attach functional amines. The double bond can be also used for inter-chain crosslinking reactions.[22] Secondly block copolymers with silyl protected poly(2-hydroxyethyl methacrylate) segments can be mentioned. Cleavage of the protection group under mild acidic conditions in a polymer analogous reaction uncovers hydroxyl functions that subsequently can be used for further attachment reactions of e.g. photo-addressable moieties.[23]
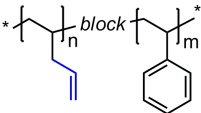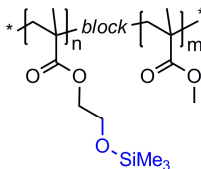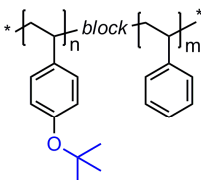
Block copolymer:

Chemical function:

olefinic double bond

trimethylsilyl protected
hydroxy function

tert-butoxy protected
hydroxy function

Possible polymer analogous reactions:

- hydrosilylation

- crosslinking

- conversion to hydroxy group

- attachment of side-group via ester linkage

- deprotection with mild acid yields hydroxy group

- attachment of side-group via ester linkage

- deprotection with strong acid yields hydroxy group

- attachment of side-group via ester or ether linkage

Figure 1.2: Examples of AB diblock copolymers bearing reactive groups: double bond (left), silyl protected hydroxy function (middle) and *tert*-butoxy protected hydroxy function (right).

A third example features a block copolymer with a poly(*tert*-butoxystyrene) segment. In this case the phenolic function is protected by a *tert*-butoxy ether group. Compared to the previous example a much stronger acid is required for the polymer analogous deprotection.[24,25] In contrast to aliphatic hydroxyl groups, the phenolic character allows more easily the formation of ether linkages additionally to the ester linkages. This thesis focuses mainly on block copolymers of the last type and thus, it will be discussed in more detail in the following chapters.

Functional block copolymers with special physical properties

Functionalizable block copolymers with chemical reactive side-groups can be used in the synthesis of functional block copolymers that are able to fulfill a function due to their physical properties. Examples are azobenzene-containing block copolymers. They are promising candidates for the applications such as holographic data storage,[26–29] or photocontrolled deformation[30] (e.g. artificial muscles[31]). Numerous azobenzene-containing block copolymers are side-group functionalized block copolymers with isotropic or liquid crystalline moieties.

The functions of functional block copolymers can also arise from their microphase separated morphology:

An example of commercial successful functional block copolymers are poloxamers, sold for example by BASF under the trade name Pluronics.[32] Poloxamers are symmetrical ABA triblock copolymers consisting of hydrophilic poly(ethylene oxide) (PEO) A-blocks and a hydrophobic poly(propylene oxide) (PPO) B-block (PEO-*block*-PPO-*block*-PEO)n

as shown in Figure 1.3, that can be used as non-ionic surfactants as well as drug delivery systems in medical applications.[33] Other examples are polystyrene and polybutadiene based block copolymers, i.e. polystyrene-*block*-polybutadiene-*block*-polystyrene ABA triblock copolymers called "SBS rubber", sold for example under the names Kraton®[34] or Styroflex®,[35] that is a thermoplastic elastomer and used for a wide range of applications. In this thermoplastic elastomer the polystyrene domains form physical crosslinks that are connected by polybutadiene segments. Transparent modified polystyrene, a polystyrene-*block*-polybutadiene block copolymer, sold as Styrolux[36] is another member of this class. The transparency arises from the microphase separated morphology on the 10-20 nm level that does not scatter visible light.
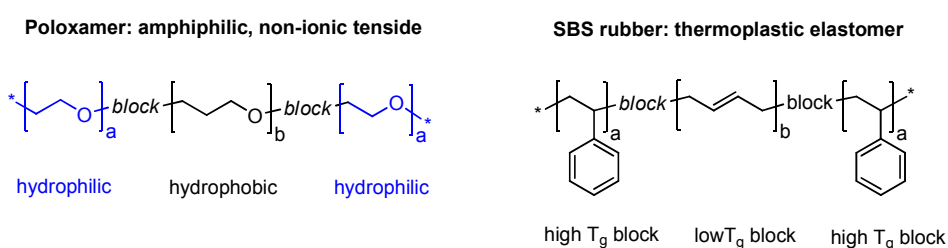
Figure 1.3:   Examples of commercial available functional block copolymers. *left:* Poloxamer (Pluronics®); *right:* SBS rubber (Kraton®, Styroflex®).

A wide range of possible application for functional block copolymers can be found in recent literature reviews.[3,37–40] Examples are: Highly ordered, nano-structured block copolymers templates are suitable for advanced potential applications like nano lithography (e.g. for high density magnetic disks)[4,39,41–43] or templates for mesostructured hybrids and inorganic materials.[40,44] Block copolymers with cylindrical or bicontinuous microdomains can be directly used as nanoporous membrane in filter applications,[38,39] also biomedical applications of hyperbranched block copolymers were explored due to their assembly into micelles, fibers, membranes.[45] Recently, donor–acceptor block copolymers have been introduced for photovoltaic applications.[46]

For the above mentioned applications block copolymers with a highly uniform domain size is required. Therefore the molecular weight distribution should be as narrow as possible to achieve the best control of the nanostructures. Hence, a controlled polymerization is a prerequisite and usually utilized for the synthesis of well defined block copolymers.[47]

Block copolymer synthesis

Anionic polymerization, as the oldest living polymerization method, was first demonstrated by Szwarc in 1956.[48,49] Since then it has been been proven as a reliable and versatile method for preparation of well-defined polymers and block copolymers with narrow molecular weight distribution.[50–52] Anionic polymerization has been in addition successfully applied for the synthesis of more complex polymer architectures such as comb-shaped and star-block copolymers.[53,54]

Anionic polymerization is a chain growth polymerization with carbanions as active species. As a consequence, no recombination or disproportionation of the negative charged propagation species can occur resulting among others in a so called *living polymerization*. In general, the term *living polymerization* is used for a polymerization without termination and transfer reactions.[49–52] If additionally the rate of initiation is much higher than the rate of propagation these factors allow control over the degree of polymerization (DP) respectively the molecular weight (MW) and a narrow molecular weight distribution of the resulting polymer (*Poisson* distribution). As a main feature of anionic polymerization -due to the living nature of the chain ends- the preparation of block copolymers is possible (see Figure 1.4). For the preparation of block copolymers the second monomer has to be more reactive than the first. Since the rate of initiation of the second block by the anionic end of the first block has to be much higher than the propagation rate of the second monomer. If the reactivity of the chain end of the first block is too high, side reactions with the second monomer can occur. In these cases special derivatives have to be added to reduce the reactivity of the chain-end of the first block.[53] The living nature of the chain ends also facilitate functionalization of the chain-end with suitable endcapping agents.[55,56] Using multifunctional linking agents instead of endcapping agents is one approach for the synthesis of star-block copolymers.[53,55,57]
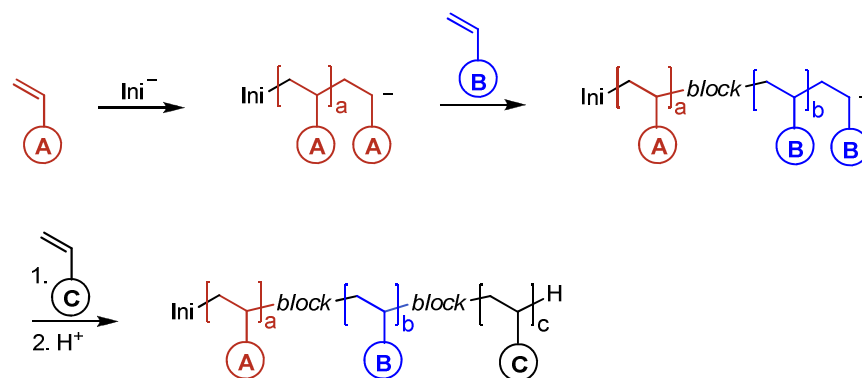
Figure 1.4: Schematic representation of an anionic polymerization of a ABC triblock copolymer.

However, anionic polymerization is restricted to a limited number of monomers due to high reactivity of initiator and chain-ends. Especially the use of functional monomers (bearing an amine, alcohol, thiol, etc. function) is restricted due to termination reactions with the anionic chain-end. The monomer range can be extended by using previously protected functional monomers.[58,59]

Several other polymerization techniques have been demonstrated for the synthesis of block copolymers. Cationic polymerization,[60] as counterpart to anionic polymerization, can be used for a range of different monomers. Also possible but more limited are the group transfer polymerization (GTP)[61] that is mainly applied for the polymerization of methaycrylate and acrylate based monomers[53,62] and the ring opening metathesis (ROMP)[63] of strained olefinic cycles using Schrock- or Grubbs-type catalysts.[64]

Recently introduced were the controlled radical polymerization (CRP) methods like the atom transfer radical polymerization (ATRP),[65] nitroxide-mediated polymerization (NMP)[66] and reversible addition/fragmentation chain transfer polymerization (RAFT).[67] ATRP and NMP allow for a wide range of different complex monomers that can be polymerized under mild conditions with good control over molecular weight and molecular weight distribution.

1.2   Liquid crystalline polymers

Liquid crystals (LCs) form thermodynamically stable mesomorphic phases (mesophases) between the (crystalline) solid state and the isotropic liquids. Liquid crystalline systems can be divided into two categories: lyotropic liquid crystals and thermotropic liquid crystals. Lyotropic liquid crystalline phases are formed in solution and depend on the concentration. Thermotropic liquid crystalline phases are formed depending on the temperature. This is often the result of the shape anisotropic molecules or at least molecular parts. Exemplarily, on heating thermotropic liquid crystals undergo a phase transition from the crystalline into the liquid crystalline phase at the melting point. When the temperature reaches the clearing point (T_{cl}) the molecules lose their liquid crystalline order and become isotopic. The temperature range in between these two points is the mesophase range. Different liquid crystalline phases (more than one) might be existent in one compound. In the following only thermotropic liquid crystal will be discussed.

From a historical viewpoint, thermotropic liquid crystals were discovered by Reinitzer during the investigations of cholesterylbenzoates in 1888.[5] The term *liquid crystal* was coined by Lehmann.[6,68] Later on, Vorländer[69] started the first systematical investigation of these compounds.[7] Mesogens, the molecules that form a thermotropic liquid crystalline phase, commonly exhibit formanisotropic shape mostly rod-like (calamitic) or disk-like (discotic). Molecules with these anisotropic shapes have different degrees of order in the liquid crystalline phase. Figure 1.5 shows examples of calamitic LC phases. The simplest LC phase, the nematic (N) phase, exhibits long range orientational order. This is possible when the symmetry axes of the ordering molecules are on average parallel to a well defined spatial direction know as *director*.

nematic phase   smectic A phase   isotropic liquid
N   SmA   I
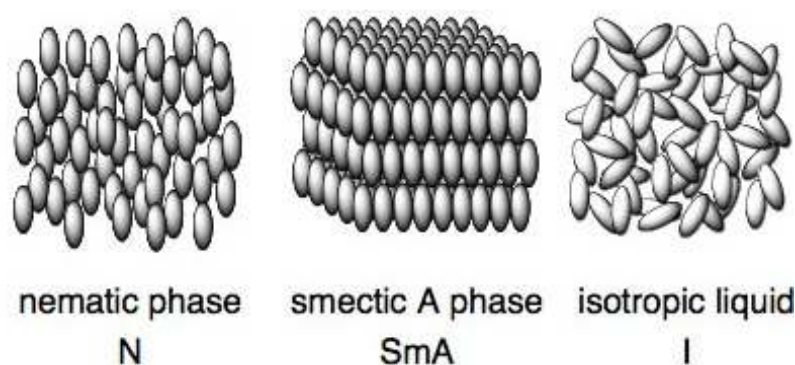
Figure 1.5:   Examples of liquid crystalline phases for calamitic mesogens. (*left*) nematic phase, (*middle*) smecticA phase and (*right*) the isotropic phase (ref.[71], altered).

If positional or translational order in one direction is present the molecules order in smectic (Sm) phases that are characterized by the director and the layer normal. The angle

of the director with the layer normal determines the smectic phase. In the simplest case, if both are collinear, the mesophase is called a smectic-A phase (SmA). This phase exhibits a short range positional order in the layer and a quasi long range positional order perpendicular to the planes and might be viewed as a two-dimensional stack of fluid layers.[70] No long range order is present in the isotropic (I) phase.

Due to their anisotropic shape LCs possess interesting properties such as birefringence (Δn), dielectric anisotropy ($\Delta \varepsilon$), diamagnetic anisotropy and orientational elasticity.[72] Because of these anisotropic properties liquid crystals can be influenced by external fields (electric, magnetic). For this reason predominantly nematic LCs have been intensively used in electrooptical applications, e.g., liquid crystal displays. In those, the twisted nematic (TN) mode was introduced in the early 1970s and has extensively been used since then.[9,73]

Three examples for nematic liquid crystals are shown in Figure 1.6. All of them consist of a rigid core (two or more rings), that mainly determines the anisotropy of the molecule, a flexible terminal group on one end, that decreases the melting temperatures, and substituents laterally attached or on the opposite end to the flexible group to adjust the electrical dipole of the molecule.[72] The first example N-(4-methoxybenzylidene)-4-butylaniline (MBBA) is a Schiff base and one of the first nematic liquid crystals that was synthesized in 1969 by Kelker.[74] MBBA could not be used in display applications due to its yellowish color and the sensitivity of the Schiff base to hydrolysis. The next example 4-cyano-4'-(pentyl)biphenyl (CB) is one of the most commonly used nematic LCs. It is a prominent member of the cyanobiphenyl class that was synthesized by Gray *et al.* in 1972 and used in TN displays until today.[75] The strongly polar cyano substituent leads to a higher dipole moment in this liquid crystal compared to MBBA. The third mesogen (1S,1'S,4R,4'S)-4-butyl-4'-(3,4,5-trifluorophenyl)-1,1'-bi(cyclohexane) is an example for a three-ring calamitic liquid crystal. In this case the fluoro substituents result in a high dielectric anisotropy. Cyclohexane derivatives with two or more rings are among the most important substances for the application in displays.[9,72]
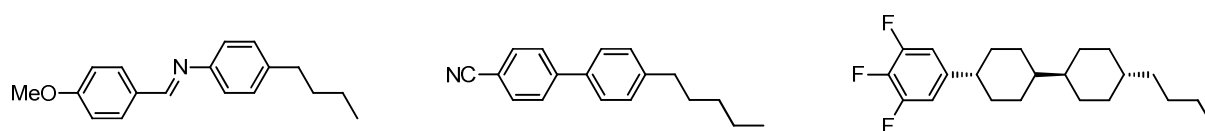
Figure 1.6: Examples for calamitic liquid crystals: N-(4-methoxybenzylidene)-4-butylaniline (MBBA) (*left*), 4-cyano-4'-(pentyl)biphenyl (5CB) (*middle*) and (1s,1's,4R,4'S)-4-butyl-4'-(3,4,5-trifluorophenyl)-1,1'-bi(cyclohexane) (*right*).

Today mostly mixtures of different liquid crystals are used in display applications to achieve a broad mesophase range and to tailor the birefringence, dielectric anisotropy and rotational viscosity of the materials for the desired purpose.

Liquid crystalline polymers

Mesogens can be incorporated into polymers in several ways yielding liquid crystalline polymers. The most basic types are shown in Figure 1.7. The mesogens can be directly connected to on another forming rigid rod-like liquid crystalline main chain polymers (Figure 1.7, a). Another possibility of main chain LC polymer contain mesogens connected via flexible spacers (Figure 1.7, b). The spacers in these semi-flexible main chain LC polymers allow for a better mobility of the mesogens and result in overall more flexible polymers. If the mesogens as side-groups are attached to the polymer backbone via flexible spacers the resulting polymers are called side-group liquid crystalline polymers (Figure 1.7, c). This type of LC polymers will be discussed in the following chapter because this motif is used in one segment of the block copolymers discussed in this thesis.
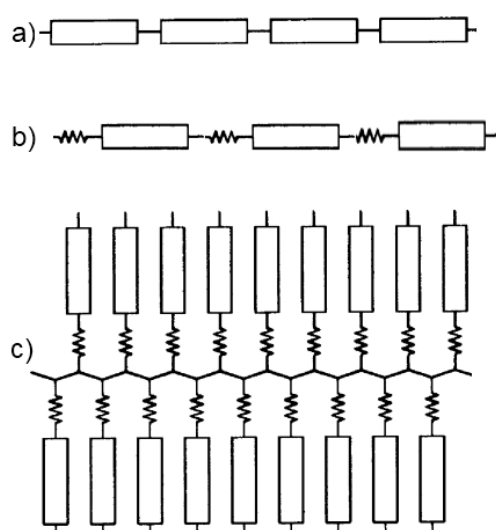
Figure 1.7:   Schematic representation of principle variations of incorporating mesogens in LC polymers. a) main chain LC polymers with mesogens directly connected; b), semiflexible main chain LC polymers with mesogens connected via flexible spacers and c) side-group LC polymers.

1.2.1   Side-group liquid crystalline polymers

Polymers that carry mesogens laterally attached to the polymer backbone (*comb-shaped*) exhibit thermotropic liquid crystalline mesophases and are called side-group LC polymers. They contain three major constituents: (i) the polymer backbone, (ii) the

mesogenic groups and (iii) the flexible spacers connecting both other elements. This concept, depicted in Figure 1.8, was presented by Finkelmann, Ringsdorf, and Wendorff in 1978.[76] The spacer is required to decouple the motions of the mesogens from the polymer backbone. As a result, the former is able to form a mesophase, whereas the latter tends to adopt a random coil conformation. Neutron scattering experiments have revealed that the polymer backbone is deformed in both nematic and smectic mesophases. It can be concluded that it is impossible to completely decouple the backbone motions from those of the mesogens.[77,78]
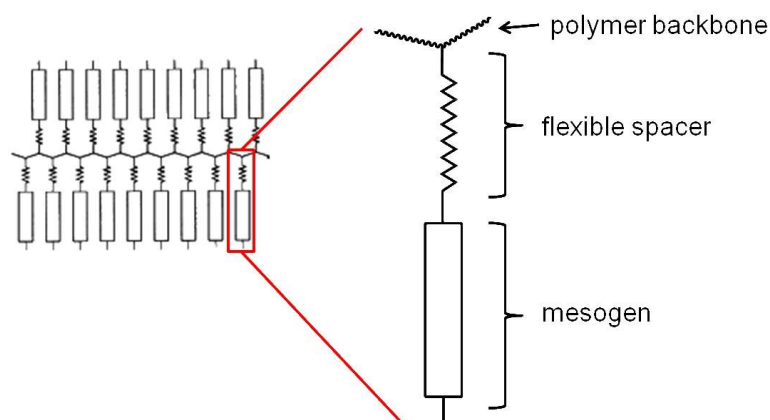
Figure 1.8:   Schematic representation of side-group liquid crystalline polymers.

Regarding the aforementioned three constituents of side-group liquid crystalline polymers several influences on the thermal and mesophase properties can be distinguished.[79,80]

The thermal transitions of liquid crystalline polymers are depended on the molecular weight and the number of repeating units respectively.[81] With increasing molecular weight the temperature range of the mesophase increases. If more than one mesophase exist, at least the range of the highest temperature mesophase is extended.[82,83] The influence on the glass transition is less pronounced. This can be explained with the greater decrease in entropy and increase in free energy of the isotropic liquid with increasing molecular weight compared to that of the more ordered phases.[84] Depending on the polymer system this dependency reaches the plateau values at less than 50 repeat units.

The decoupling of the mesogen from the polymer backbone increases with the increasing flexibility of the polymer backbone. A more flexible backbone results in more arrangement possibilities of the mesogen and therefore increases the tendency to form higher ordered mesophases. With increasing backbone flexibility the glass transition temperatures tend to decrease while the clearing point increases for a given spacer length

and mesogenic group. Also the side-chain crystallization becomes possible at shorter spacer length for more flexible polymers.[85]

The influence of the length of the spacer can be compared to the length of the flexible substituent for small molecule LCs. Increasing spacer length decreases the glass transition temperature due to the decreased packing density, an effect that is often referred to as "internal plasticization".[86] Consequently the introduction of (longer) spacers can result in the appearance of mesophase(s) not present in the comparable polymer with shorter/no spacers in which the higher glass transition temperature prohibited the formation of the mesophase. This trend often exhibits an odd-even effect that gets weaker with increasing spacer length.[85,87] Analogous to the trend observed for alky substituents in low molecular liquid crystals, short spacers also favor nematic mesophases whereas long spacers favor smectic mesophases. In the nematic mesophase of side-group liquid crystalline polymers the transition temperatures tend to decrease with increasing spacer length. In contrast the transition temperatures in the smectic phase, at least in the SmA, increase with the length of the methylene spacer showing an odd-even effect. It has to be noted that these trends depend on the specific polymer system. For example for polymethacrylate based LC side-group polymers with cyanobiphenyl mesogens an increasing of the clearing temperature is observed. In contrast, if methoxybiphenyl mesogens are used, the clearing temperature decrease with increasing spacer length.[86] The odd-even effect is dependent on the respective polymer backbone and the linkage connecting it to the spacer. An example are poly(meth)acrylate based LC side-group polymers, when a methylene spacer with ether linkages is used. For odd-membered spacers, the mesogenic unit is orthogonal with respect to the backbone not only for the all-*trans* conformation of the spacer but also for selected conformations that include a single *gauche* defect. Therefore, there are more possibilities of maximum interactions between the mesogenic groups and these results in higher transition temperatures. With even-membered spacer there are much more conformations where the mesogens are positioned with some angle with respect to the backbone. These conformations prevent the efficient packing and, therefore, reduce the transition temperature.[80,86]

The mesogen density at the polymer backbone is often below 100% for polymer analogous attachment reactions, i.e. not every repeating unit carries a mesogenic side-group. The glass transition temperature and clearing temperature are functions of this degree of attachment and exhibit an increase with increasing degree of conversion.[20,88] The mesogen density at the polymer backbone can be increased by introducing two or even three mesogens per repeating unit. In this case the mesophase range is enhanced and the polymers with two and three mesogens per unit may exhibit additional lower ordered mesophases at higher temperatures compared to the polymers with less mesogenic groups per monomer unit. [80,89]

13

1.2.2 Block copolymer with liquid crystalline segments

If mesogenic units are chemically incorporated into a block copolymer, several combinations are possible. Examples are shown in Figure 1.9. The two simplest combinations combine both an amorphous block and a liquid crystalline block. LC main-chain block copolymers are obtained if the mesogens form one segment that is connected to an amorphous block. (Figure 1.9, a). An example for graft copolymers are the LC main-chain graft copolymer (Figure 1.9, b). Side-group LC block copolymers are comprised of an amorphous segment and a segment, in which the mesogens are laterally attached to the polymer backbone (Figure 1.9, c).

In the following the focus will be on the last type, the combination of an isotropic block and a liquid crystalline block in the form of a side-group LC block copolymer.
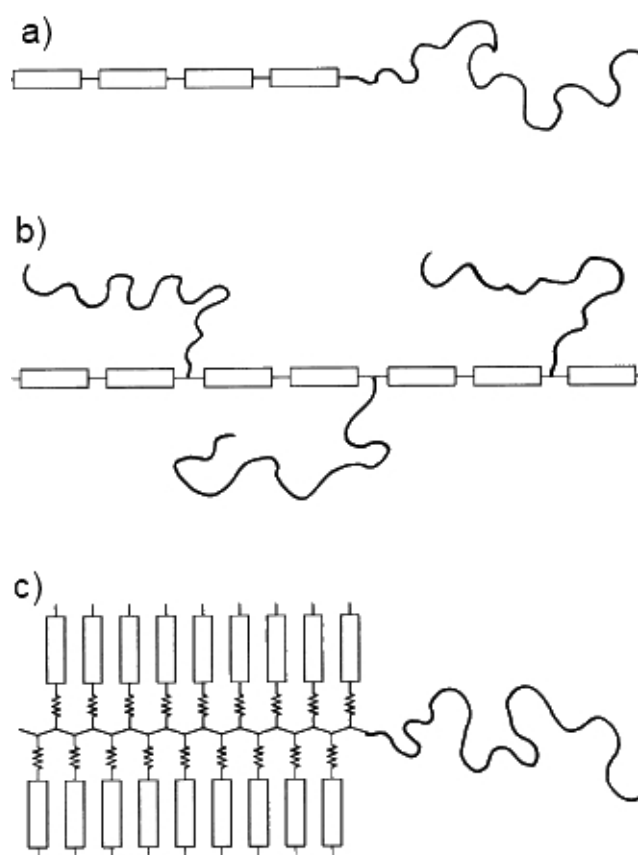
Figure 1.9:   Schematic representation of liquid crystalline block and graft copolymers with calamitic mesogens. a) liquid crystalline main chain block copolymers; b) liquid crystalline main chain graft copolymers; c) liquid crystalline side-group block copolymers.

Synthesis of side-group liquid crystalline block copolymers

For the investigation of side-group LC block copolymers, the synthesis of samples with well defined molecular structure for each block over a wide range of molecular weights is required. All kinds of living polymerization methods have been employed for the controlled synthesis of side-group liquid crystalline block copolymers.

Direct anionic synthesis of a side-group liquid crystalline block copolymer has been achieved with mesogenic methacrylates containing for example azobenzene moieties,[90,91] biphenyl moieties,[82,92,93] as well a chiral mesogens.[93] In this case, the challenging issues are the required high purity of the monomers and solvents as well as the often low temperatures (e.g. -78°C) that are typical prerequisites for anionic polymerization. The purification of the mesogenic monomers is not easy to achieve due to the relatively higher molecular weights which do not allow purification via distillation under high vacuum. As a consequence, the degree of polymerization was not very high for the functional block in the direct anionic polymerization approaches. Direct cationic polymerization was achieved for example for a cyanobiphenyl mesogenic block[94] as well as for an chiral LC block combined with a poly(isobutyl vinyl ether) block forming a AB diblock copolymer.[95] Group transfer polymerization (GTP) was first used by Ringsdorf *et al.*[96] for the synthesis of side-group liquid crystalline polymers but the first liquid crystalline AB diblock copolymers were reported in 1990 by Springer *et al.*[97] based on PMMA and methoxybiphenyl containing liquid crystalline blocks. All of the living polymerizations allow a good control over molecular weight and molecular weight distribution but normally do not result in a high degree of polymerization and are very limited regarding the functional groups or require special monomers.[98] Termination reactions as a result of impurities are still a problem.

Radical polymerization presents a much more versatile approach because a wide range of functions are tolerated, the requirements on the monomer and solvent purity are less strict and the polymerization can often be carried out at a more convenient temperature range. For the synthesis of block copolymers a controlled radical polymerization (CRP) methods has to be used.[47] Prominent CRP methods are the atom transfer radical polymerization (ATRP),[65] nitroxide-mediated polymerization (NMP)[66] and reversible addition/fragmentation chain transfer polymerization (RAFT).[67] ATRP, that was introduced by Matyjaszewski,[99] allows for the use of different functional monomers, results in narrow polymer weight distributions, enables the control of molecular weight, block copolymer composition and chain topology. Therefore this method has been used extensively for the syntheses of side-group liquid crystalline block copolymers containing for example quinquephenyl units,[100] cyanobiphenyl-functionalized blocks,[101] or azobenzene functionalized blocks.[102–106] Other CRP techniques such as nitroxide-

mediated polymerization (NMP)[66,107] and reversible addition/fragmentation chain transfer polymerization (RAFT),[67,108,109] were also used to synthesize side-group LC block copolymers with well-defined compositions.

Another approach is the use of ring-opening-metathesis-polymerization (ROMP) of functional, olefinic, cyclic monomers (e.g. norbornene or cyclopentene) by metal catalysts of the Schrock or Grubbs type.[110] Series of liquid crystalline block copolymers have been prepared by ROMP to study the influence of spacer, backbone and mesogen on the thermal properties.[80] Examples of AB diblock copolymers include methoxybiphenyl mesogens,[111] semifluorinated mesogens[112] or cyanostilben mesogens.[113] Side-group liquid crystalline ABA block copolymers with a chiral mesogenic B block were reported by Schrock *et al.*.[114]

A convenient approach for the synthesis of well defined side-group liquid crystalline block copolymers is the polymer analogous reaction.[18,115,116] This approach was used for in this thesis. The block copolymer backbone is synthesized first and the desired mesogen is attached to one block in a second step. The schematic reaction scheme is shown in Figure 1.10. Anionic polymerization has been proven the most valuable way and is employed for the backbone synthesis. For the polymer analogous synthesis of side-group LC block copolymers the block copolymer backbone has to contain one block composed of monomers that enable polymer analogous reactions. Commonly alcohol functions are employed that allow a polymer analogous esterification or etherification reactions. These reactions can be driven to high yields. For an anionic polymerization these functions have to be protected to prevent side reactions and termination reactions. After polymerization of the block copolymer backbone the alcohol functions are deprotected or another chemical group is converted into an alcohol function. The polymer analogous functionalization is then carried out with activated low molecular weight functional side groups.

Sequential anionic polymerization to the block copolymers
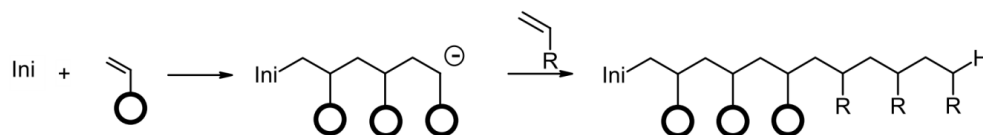
Conversion to functional groups
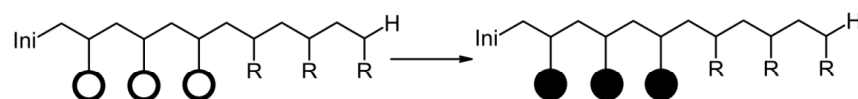
Polymeranalogous reaction with activated side-groups
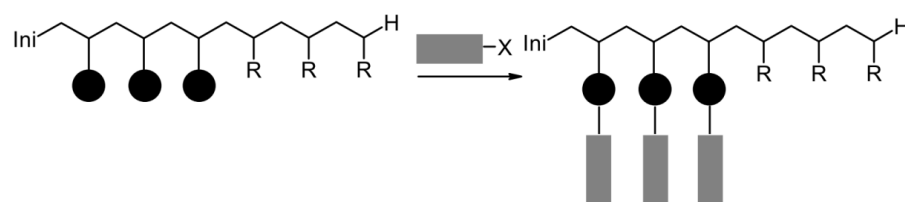
Figure 1.10: General strategy for the synthesis of side-group functionalized block copolymers via sequential anionic polymerization of the block copolymer, conversion to functional groups in one block and the polymer analogous reaction to attach the functional side-group; (○) protected functional groups, (●) functional groups, (━) mesogenic side-group units.[29]

This synthesis approach, also used in this thesis, has several distinct advantages:

- anionic polymerization allows for high molecular weight block copolymers with excellent control of molecular weight distribution as well as the polymerization of larger quantities of block copolymer

- commercial monomers can be used that are easy to purify and polymerize; monomers that already carry the side-groups are synthetically more challenging and harder to purify

- the polymer analogous reaction allows for an easy variation of the side-groups utilizing the same precursor block copolymer

- using the activation of the low molecular weight functional side-group improves the degree of functionalization and in principle eliminates the crosslinking reactions that are often present if the block copolymer is activated itself.

In 1989 Adams and Gronski[18] were the first demonstrating this approach for the synthesis of a side-group liquid crystalline block copolymers. As a functionalizeable backbone a poly(2-hydroxyethylethylene) segment was chosen, that was obtained by hydroboration of the initial poly(1,2-butadiene) (1,2-PB) segment. Ober *et. al.*[115,116] used an poly(1,2-&3,4-isoprene) based segment for the same kind of functionalization. Exemplarily, in Figure 1.11 the complete synthesis sequence based on a 1,2-PB is

presented. The precursor diblock copolymer is prepared via sequential anionic polymerization of styrene and butadiene. The double bonds are converted into hydroxy groups via hydroboration and subsequent oxidation. The mesogens are attached by an esterification reaction utilizing the corresponding acid chloride as reactive intermediate. This highly reliable approach has been chosen by different groups for the syntheses of functionalized block copolymers.[19,29,117]
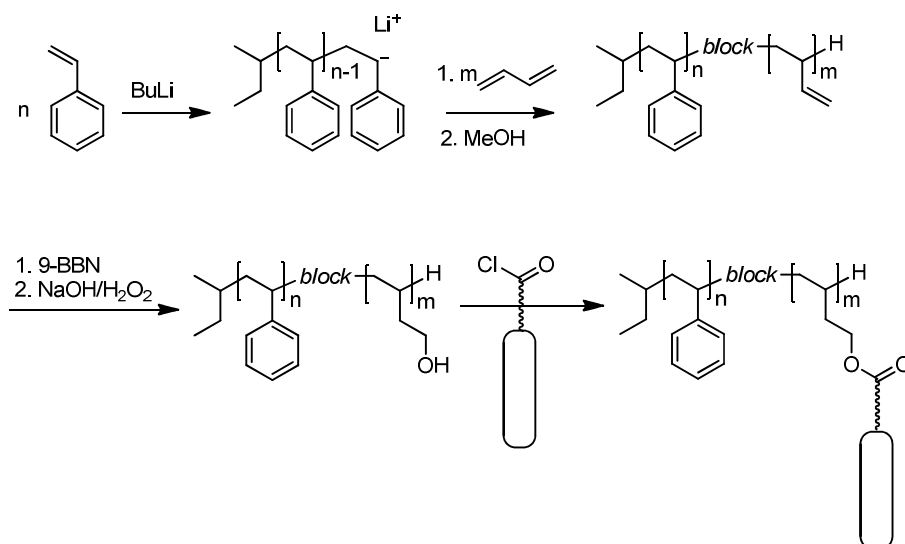
Figure 1.11: Reaction sequence for the synthesis of side-group liquid crystalline block copolymers based on anionic polymerization of polystyrene-*block*-poly(1,2-butadiene) and subsequent polymer analogous reactions reported by Adams and Gronski[18] (BuLi: buthyl lithium; 9-BBN: 9-borabicyclo[3.3.1]nonane).

As aforementioned the double bonds in 1,2-PB can also be used for other functionalization methods. SiH-containing mesogens can be attached to the backbone via a hydrosilylation reaction using a Pt catalyst thus forming a silicon-carbon bond.[118,119] The same type of reaction can be conducted using other polymer backbones with olefinic double bonds like a poly(vinylmethylsiloxane) based polymer.[20] Recently, a novel polymer analogous functionalization based on an polybutdadiene segment was presented by Fernández *et al*. by converting the double bonds into a epoxy group that was subsequently used for the attachments of functional amines.[21]

A different functional backbone for a polymer analogous synthesis of side-group liquid crystalline block copolymers was introduced by Zaschke *et al*..[120] The synthesis of AB block copolymers with a completely hydroxy-functionalized segment was achieved by the anionic polymerization of (2-trimethylsilyl)oxyethyl methacrylate with conventional monomers such as styrene, butadiene, n-butyl methacrylate for the second block. The

attachment of the mesogens was realized via a polymer analogous reaction with a activated acide chloride mesogen.

Besides this esterification reaction also polymer analogous etherifications based on a poly(4-hydroxystyrene) backbone resulting in side-group liquid crystalline homopolymers were described.[121,122]

A relatively new approach is the use of a "click" reaction. This type of reaction normally proceeds with a high degree of conversion and does not need the anhydrous conditions required for the high conversions by the acid chloride reactions mentioned above. Recently, this copper(I)-catalyzed Huisgen 1,3-dipolar cycloaddition reaction between functional azides and an alkyne functionalized homopolymer has been used for the synthesis of side-group liquid crystalline polymers based on a polymethacrylate backbone.[123] Up to now, no functionalized block copolymers were prepared using this method.

An inherent issue in the polymer analogous approach in the degree of conversions that is commonly not quantitative. Verploegen *et al.* conducted an investigation concerning the influence of the degree of conversion on the mesophase as well as the resulting block copolymer bulk morphology.[20] Using a poly(vinylmethylsiloxane)-*block*-polystyrene based side-group liquid crystalline block copolymers with a chiral mesogen they revealed that the glass transition temperature and clearing temperature as well as the morphology are functions of the degree of conversion. The clearing temperature and the order-disorder-transition exhibited an increase with increasing degree of conversion. A smectic mesophase was found for degrees of conversion as low as 30%.[20]

Phase and morphology behavior of side-group liquid crystalline block copolymers

Side-group LC block copolymers are of special interest due to the combination of two different order principles on different length scales in one material at the same time.

As mentioned in chapter 1.1, in block copolymers the driving force for microphase separation is the balance of minimizing the interfacial energy and maximizing the conformational entropy of the macromolecules, yielding self-assembled well-defined structures on the nanometer scale. On the other hand, orientational and long–range order on the molecular scale is the basic principle in liquid crystalline polymers where the mesogens are laterally attached to the polymer chain as side-groups. In side-group liquid crystalline block copolymers those two properties are combined by covalently connecting a liquid crystalline block to a flexible amorphous block, thus forming a LC/coil-block copolymer. These systems are expected to show microphase separation between coexisting isotropic and anisotropic phases. Generally, it is assumed that the χ parameters

in side-group liquid crystalline block copolymers systems are much larger compared to coil - coil block copolymers (described in chapter 1.1) due to the mesophase formation.[115] In a liquid crystalline phase, the dissolution of the isotropic segment is unfavorable because it drastically decreases the entropy of the isotropic polymer that has to adopt to ordered phase. On the one hand, the confined geometry of the microstructure will influence the liquid crystalline phase behavior due to packing restrictions. On the other hand, the interfaces between the blocks will be influenced by the isotropic – liquid crystalline interactions. In LC phases additional elastic forces influence the curvature of the interface; therefore, the resulting morphology of the microphase separation might be affected and altered.

The liquid crystalline segment has a higher surface area per chain segment compared to the isotropic segment because of the attached side groups. Therefore due to the localization of the block joints in a narrow interface a highly convexly curved interface would result from packing arguments stabilizing isotropic spheres or cylinders in a liquid crystalline matrix. This high curvature interfaces will cause a director deformation and the free elastic energy of the liquid crystalline system rendering theses microstructures unfavorable. The observed morphologies are therefore determined by the balancing of the geometrical factors and the elastic energy of the liquid crystalline phase.[124]

For the process of microphase separation in side-group liquid crystalline block copolymers two pathways exist. In Figure 1.12 this process is schematically illustrated. On cooling, starting from the isotropic melt microphase separation occurs and ordered structures are formed. The LC formation may deform the rubbery isotropic block, if the isotropic-LC transition temperature of the liquid crystalline block is higher than the T_g of the isotropic segment. Thus morphologies with lower curvature may be obtained. In the opposite case, the LC formation will take place in a confined microdomain within the glassy matrix.
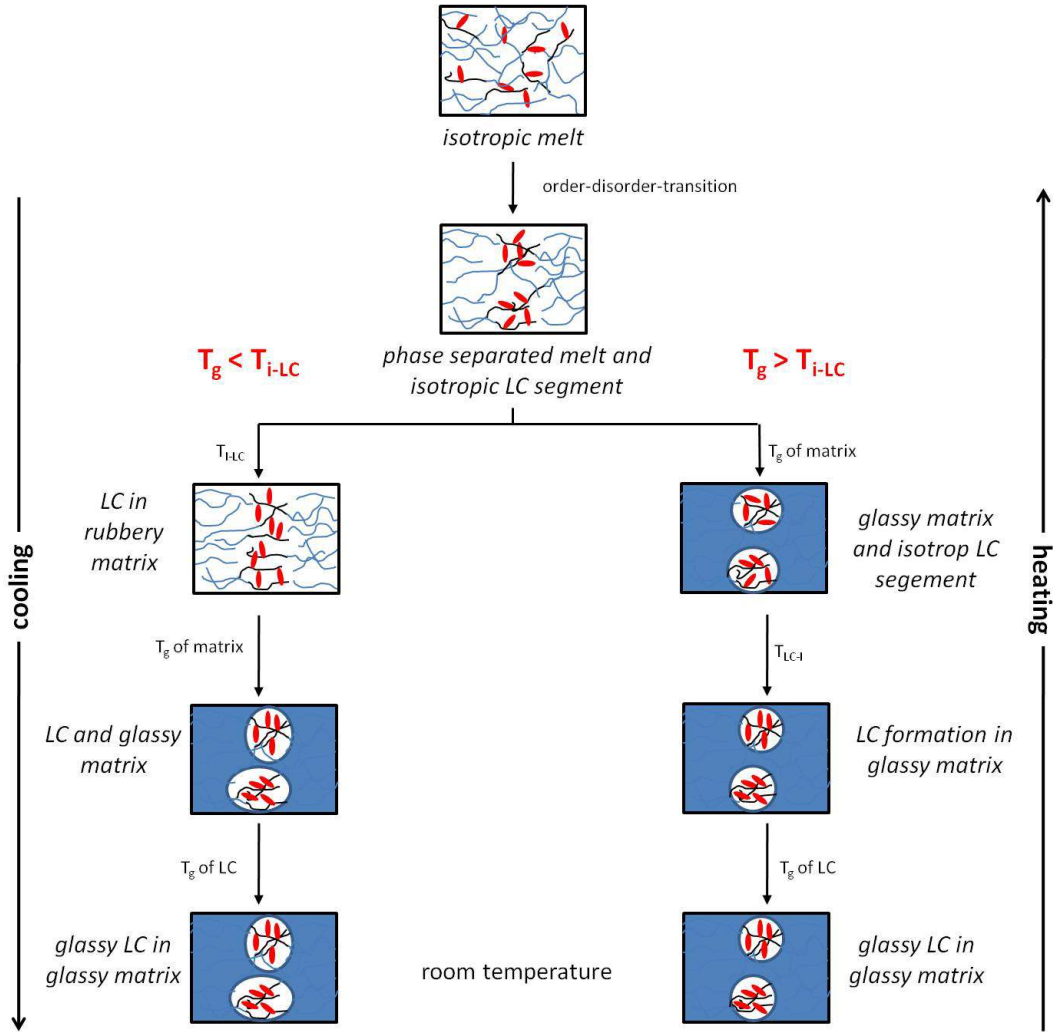
Figure 1.12: Microphase separation process for side-group liquid crystalline block copolymers. If $T_g < T_{i\text{-}LC}$ the LC phase is formed in a rubbery matrix whereas if $T_g > T_{i\text{-}LC}$ the LC formation takes place in a glassy matrix (based on ref.[98]).

Generally, side-group liquid crystalline block copolymers exhibit similar mesophases as the respective side-group liquid crystalline homopolmyer. Fischer *et al.* were the first to report a morphology diagram for a SmA side-group liquid crystalline diblock copolymer with polystyrene[125] as well as poly(*n*-butyl methacrylate)[126] as amorphous block and a cholesteryl based methacrylate as liquid crystalline block. In both cases no LC cylinders were observed and the LC spheres exhibited only a nematic mesophase. It was assumed that a smectic phase can only be realized in continuous subphases like the lamellar or matrix phases, not in rods or spheres of the LC subphase with a very small diameter compared to the layer spacing.[126] Ober *et al.* reported a morphology diagram of a diblock copolymer with a azobenzene mesogen and polystyrene as amorphous block. In contrast to the reports by Fischer *et al.,* they found LC cylinders exhibiting a SmA mesophase and also a 22 °C higher clearing temperature (T_{cl}) compared to the respective

lamellar morphology.[115] This effect was explained by the confinement of the cylinders that stabilizes the smectic mesophase. In the same paper this group also reported the formation a bicontinuous morphology.

Watanabe *et al.* prepared LC block copolymers of different molecular weights with about 50 wt% of an amorphous PS block with different molecular weights. Interestingly, they found not only the expected lamellar morphology but also one side-group liquid crystalline block copolymer showed a cylindrical structure.[82] Hammond *et al.* investigated the phase diagram of LC block copolymers with a polystyrene segment and a chiral mesogenic methacrylate and found lamellar morphologies even at LC fractions as low as 30 wt%.[127] It has been shown that in LC cylinders the mesogens orient parallel to the axis of the cylinders[115] and also the liquid crystalline groups can be efficient to stabilize perpendicular orientating of the amorphous domains (cylinders and lamellae) in thin films.[128]

Theoretical models have been developed focusing on the order-disorder transitions of both liquid crystalline orientation and microphase segregation.[129] Novel stable lamellar microstructures were predicted by theoretical calculations and modeling that could be confirmed experimentally.[127,130]

An fascinating branch of this topic is the photoinduced morphology change or ordering and patterning in side-group liquid crystalline block copolymers using azobenzene-containing block copolymers that was reviewed by Zhao *et al.*.[131]

1.3   Functional block copolymers for holographic data storage

Data storage

Modern-day society is heavily based on information. For this reason our era might be called the "Information Age". The volume of information produced and stored annually is growing exceptionally and has already reached amounts which could not be imagined in the last century. This digital information is stored in a binary form i.e. in terms of "zeros" and "ones" known as bits (1b). A letter of the alphabet utilizes eight bits and is termed a byte (1B). According to some estimates, the total amount of hard disk storage worldwide at the end of 2008 was roughly 200 exabytes (exabyte = 10^{18} bytes).[132]

To store and process these data several storage media are used today. Magnetic disks, commonly known as hard drives, are still the best medium for storage of large amounts of information which have to be accessed and altered often and fast. Magnetic disk and conventional magneto-optical data storage technology uses the surface of the medium to store bits of data. The super-paramagnetic effect, that is the basis for today's magnetic

disks, limits the compression of magnetic domains to roughly 10 nm. Below that point thermal self-erasure occurs and the magnetized bit flips randomly.[133]

Blu-Ray Disk is the state of the art consumer medium for optical data storage and is based on a blue laser light source (405 nm) combined with optics of numerical aperture 0.85, which allows for a smaller, focused spot-size, thus increasing the area available for storage. Thereby the Blu-Ray Disk has a storage capacity of 25 GB and is superior to the related optical media, the CD (750 MB) or DVD (4.7 GB).

The capacity of the current Blu-Ray disk standard can theoretically be increased by stacking different layers. In 2008 Pioneer Corporation announced a prototype400 GB Blu-Ray disc containing 16 data layers of 25 GB each which is still not commercially available.[134]

However, up to now, individual bits are still stored as distinct magnetic or optical changes in the surface of a recording medium. As the feature sizes of surface recording media are further scaled down, they will eventually be closing in on physical limits as stated above. All storage media presented above use only the surface (2-D) of the media to store the data. An approach to further increase the storage density is a volumetric (3-D) approach. Inscription of holographic gratings, especially volume gratings, is such a volumetric approach, where an entire page of information can be stored in a photosensitive material.

Holographic data storage

Holography is an optical imaging technique that was discovered by the Hungarian physicist D. Gabor in 1948.[135] In 1971 he was awarded the Nobel prize in physics for his "invention and development of the holographic method".[136]

In holographic data storage, the information is stored as an optical interference pattern that is created by intersecting two coherent laser beams within the storage material. In Figure 1.13 the principle of holographic data storage is presented. A coherent beam is split into two beams. The first beam, called the signal or object beam, contains the information. In this case, a spatial light modulator is used to store a huge amount of bits at the same time. The second beam, called the reference beam, generates a coherent background. Both beams are superimposed in the storage medium. The resulting optical interference pattern with areas of different intensity and/or polarization (depending on laser polarization) is then stored in the photosensitive material as a local change of the refractive index. In the reading process a subsequent illumination of the recorded pattern in the storage medium with the reference beam alone reconstructs the inscribed information.
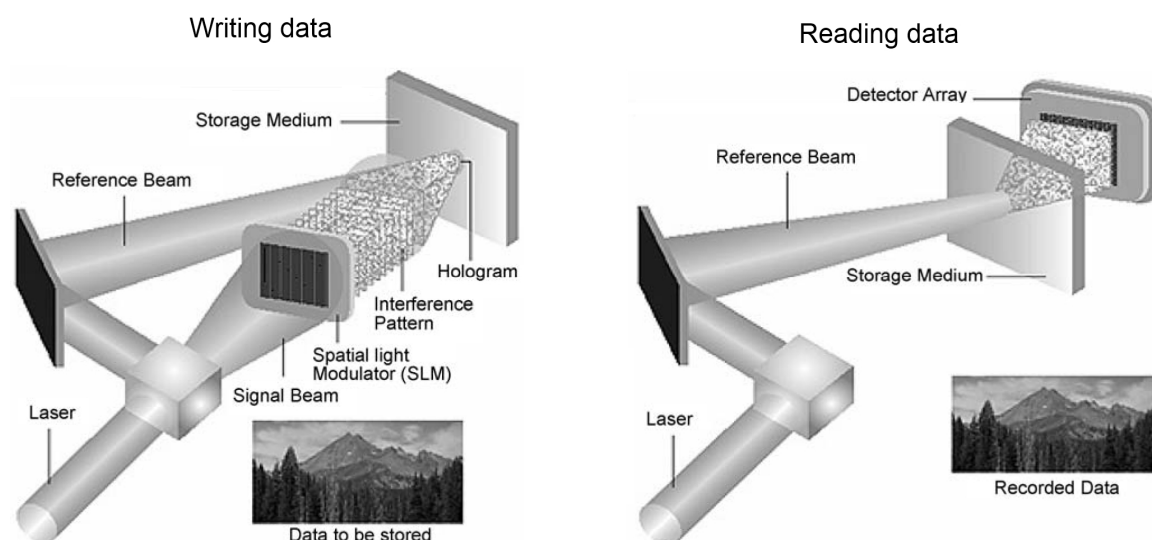
Figure 1.13:   Principle of holographic recording (*left*) and reading (*right*).[137]

One major advantage of holographic media is that a large number of these interference patterns can be superimposed in the same volume element of a holographic material by inscribing the holograms under different angles thus multiplying the storage density ("angle multiplexing").[137,138]

As for all optical data storage, holographic media are divided into "write once" and "rewritable" media. Write-once media for holographic data storage are mainly based on photopolymers.[137,139,140] In these systems photo polymerization of a monomeric species is induced in defined regions. The refractive index modulation, which is basically the contrast and an essential paramete for data storage is created by a concentration gradient between irradiated and non irradiated areas. This gradient arises from a diffusion driven process of a monomeric species caused by light-induced initiation of the polymerization in the irradiated regions. The first commercially available product is the InPhase Technologies Tapestry^{TM} media that already announces a capacity of 300GB to 1,6TB at a 20MB/s to 120MB/s transfer rate and milliseconds data access time on a 130 mm disk.[137,141]

Azobenzene chromophores

In general, rewriteable holographic media are based on photochromic materials. The most important and widely studied class consists of azobenzene compounds and especially azobenzene-containing polymers. Photoaddressable homopolymers containing laterally attached azobenzene side-groups were first reported by Ringsdorf *et al.*.[142,143] Eich *et al.* were the first to study the photoisomerization of the azobenzene chromophores and their application as holographic data storage materials.[144] These chromophores exhibit two

configuration isomers, the *trans-* and the *cis*-state. Hereby the *trans*-state is thermodynamically more stable. Upon irradiation with UV light a conversion to the *cis*-state is exited. The back conversion to the more stable *trans*-state can be induced by visible light or thermally (see Figure 1.14). When irradiated with light, the azobenzene moieties undergo photochemical electronic excitation that results in multiple *trans-cis-trans* photo-isomerization cycles inducing a motion of the chromophores.[145]
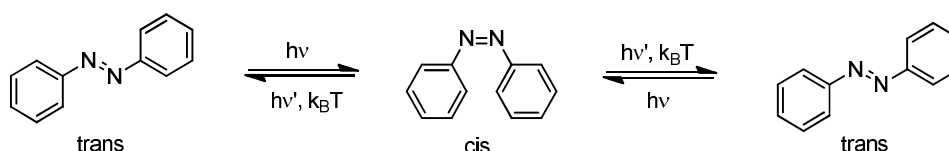
Figure 1.14:   Schematic representation of the reversible *trans-cis-trans* photo-isomerization of azobenzene. Upon absorption of UV light, a *trans-to-cis* conversion is induced; with visible (blue) light, a *cis-to-trans* conversion occurs until an equilibrium between both isomers is reached. The thermodynamically less stable *cis* isomer can thermally return to the *trans* isomer.

If linear polarized light is used in this process, the above mentioned chromophore reorientation continues until the molecular transition moment is oriented perpendicular to the polarization direction of the incident light. Once *trans*-azobenzene chromophores are oriented perpendicular to the direction of polarization of the light, they become inactive with respect to incident light (*Weigert* effect)[146] and electronic excitation is no longer possible. Using this mechanism reorientation of the chromophores in the solid state can be induced.

Holographic writing process

In the simplest case of transmission holographic writing, an interference pattern is created by intersecting two coherent plane waves (no object) in the storage material. The resulting intensity grating is a sinusoidal light intensity gradient as shown in Figure 1.15. Only in the areas of the intensity maxima the photo-induced reorientation of the chromophores occurs. Since the shape anisotropic azobenzene moiety has different polarizabilities parallel and perpendicular to its axis, the irradiated areas have a different refractive index (n*) compared to the non-irradiated areas (n_0). As consequence, the exposed areas become macroscopically birefringent.
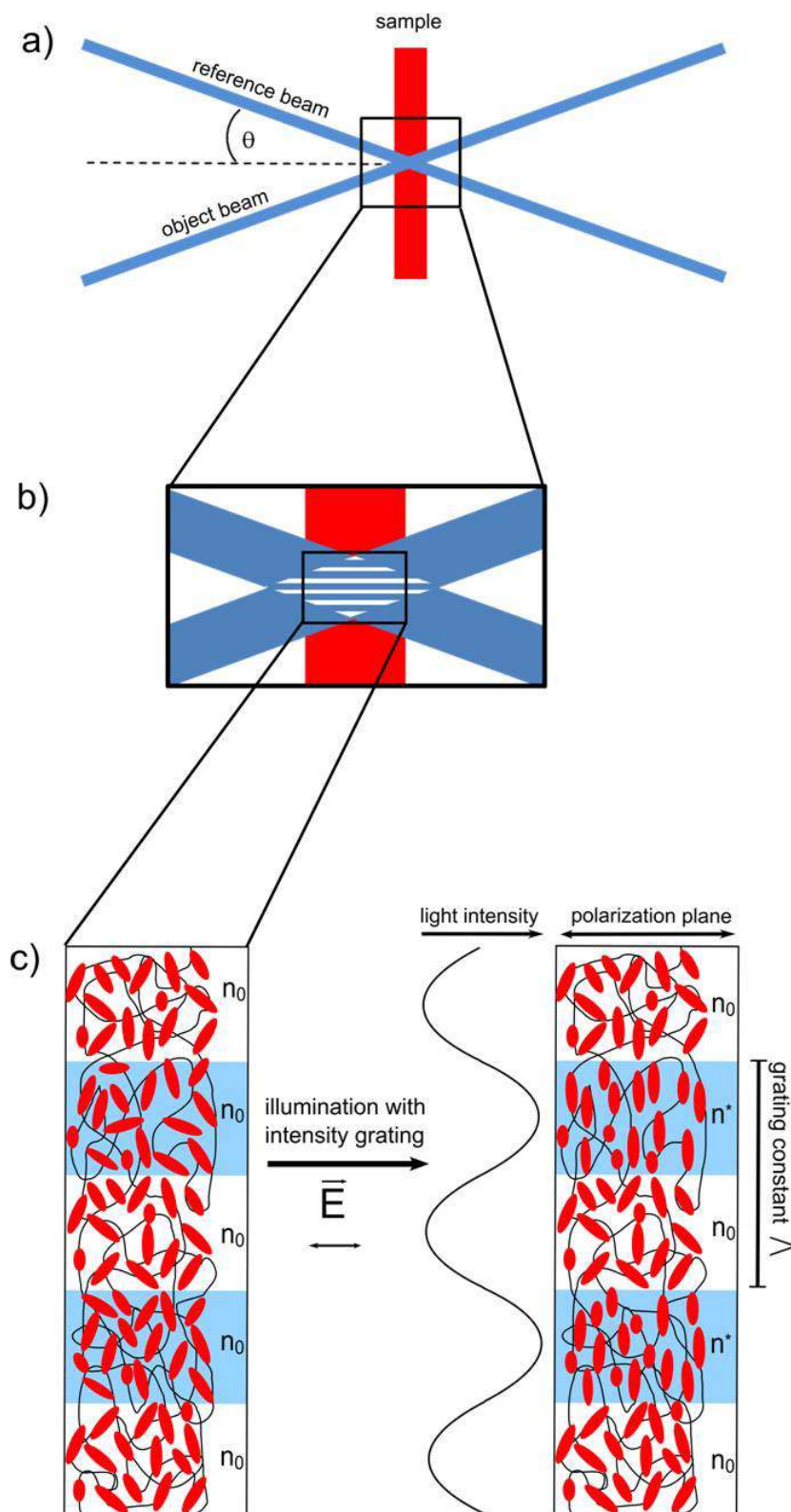
Figure 1.15: Principles of writing holographic gratings in azobenzene-containing materials. a) Writing of a hologram with reference and object beam b) enlarged region of interference with the resulting intensity grating c) schematic representation of the reorientation of azobenzene chromophores in the storage material by excitation with the intensity grating. Excitation occurs only in the blue highlighted areas of maximum intensity, resulting in a different refractive index in the irradiated areas (n^*) compared to the non-irradiated (n_0).

1.4 Liquid crystalline gels

Gels consist of at least two components: the minor component (i.e. the gelator) forms an elastic network within the liquid major component (i.e. the solvent). As a result, gels can be regarded as soft solid materials that can easily be deformed by mechanical forces. Liquid crystals are anisotropic fluids with an orientational long-range order and thus show a very sensitive response to external fields. Gels of liquid crystals form an interesting class of functional soft materials because they combine the properties of gels and liquid crystals.

On the on hand, these gels can undergo controlled and reversible shape changes using different stimuli. The applied stimulus or external field might be thermal, magnetic, electrical, UV/visible light, or pH change. The shape change can be a two-dimensional change, a bending motion, or three-dimensional actuation, a volume change. This reversible contraction and expansion of polymer gels as well as their mechanical properties are similar to that of biological muscles.[148]

On the other hand, in display applications LC gels can show faster responses in the twisted nematic (TN) mode than the respective neat liquid crystals, due to the elastic interaction between the liquid crystal and the network.[149] LC gels also have potential for use as an element in a light scattering display medium because they show high contrast switching in light scattering mode. The advantage of this display type is, that it does not require polarizers and therefore the brightness is enhanced compared to TN mode.[150]

Liquid crystalline gels are formed by three-dimensional, space-filling networks of gelators in the liquid crystal. Depending on the nature of their crosslinks, they are classified as chemical or physical gels.[148,149]

In a *chemical gel* the crosslinking is achieved via chemical reactions yielding covalent bonds. As a result the gelation is irreversible and a permanent network is obtained. Destroying the crosslinks causes chemical degradation of the system. Chemical LC gels are usually prepared by in situ polymerization of LC or non-LC monomers in a low molecular weight solvent.[151] This in-situ approach precludes a high degree of polymerization and a well defined crosslinking commonly resulting in slower reorientation of the director. Another approach is to produce a polymer network in the first step and subsequently swell it with the low molecular weight LC to yield a LC gel.[152,153] When telechelic polymers are used for this approach, a more controlled network structure is achievable.[152]

In contrast to the chemical gels, the gelation is a reversible process in *physical gels*. Most literature-known physical gels are obtained by the *self-assembly of fibrous solid networks of low molecular weight gelators* to a fibrous solid network.[149] This fibrous assembly of gelators exhibits a high aspect ratio and is driven by non-covalent interactions such as

hydrogen bonding and/or π–π interactions. LC gels of this type are dependent on the order of sol–gel transition temperature ($T_{sol–gel}$) and isotropic–LC transition temperature ($T_{iso–lc}$).[149,154] Two different types of LC gels can be differentiated (see Figure 1.16). For *Type I* the $T_{sol–gel}$ is higher than $T_{iso–lc}$, thus the gel is formed before the solvent becomes liquid crystalline. Type I gels are inherently not macroscopically oriented LC gels. For *type II* the opposite is the case. Here $T_{sol–gel}$ is lower than $T_{iso–lc}$. Therefore the solvent becomes liquid crystalline before the gelation occurs. For type II it is possible to obtain oriented LC gels if the system is oriented at $T > T_{sol–gel}$.
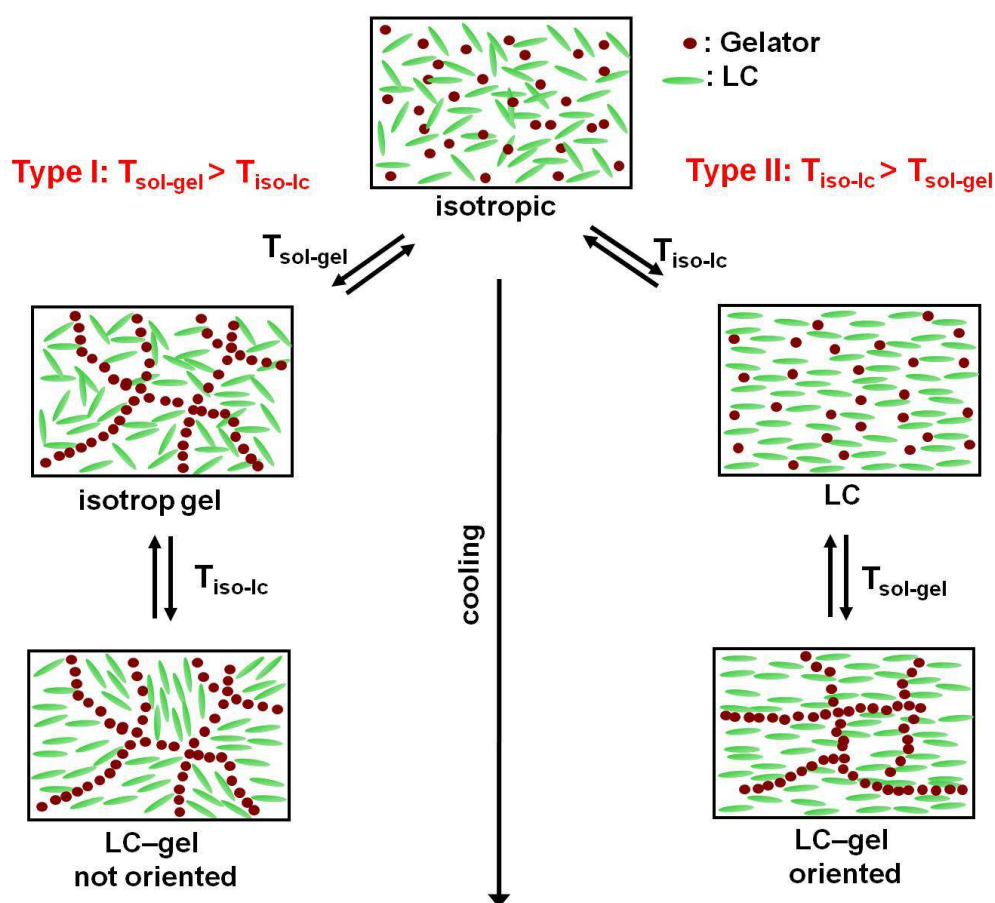
Figure 1.16:   Schematic illustration of two types of thermoreversible LC physical gels.
(*left*) Type I: $T_{sol–gel} > T_{iso–lc}$; (*right*) Type II: $T_{iso–lc} > T_{sol–gel}$ (based on lit.[149]).

In contrast to physical LC gels utilizing low molecular weight gelators, Kornfield *et al.* recently introduced a polymer based concept for physical gels.[118,119] Hereby, *ABA triblock copolymers* were used *as gelators* for low molecular weight liquid crystals consisting of a side-group functionalized polymer B-block and amorphous A-blocks. The main feature of these triblock copolymer is that the functionalized B-block is soluble in both, the LC state and the isotropic state of the low molecular weight LC, whereas the A-

blocks are only soluble in the isotropic liquid. As a consequence, a physical network is formed on cooling from an isotropic mixture of the polymer and the low molecular weight LC due to the self-assembly of the A-blocks (see Figure 1.17). In this concept the formation of the network by aggregation of the end blocks is due to microphase separation that is induced when the solvent is cooled down from the isotropic into the LC phase. In a nematically ordered solvent dissolution of the isotropic polymer is unfavorable because it drastically decreases the entropy of the dissolved polymer.[118] This can be regarded as a major difference of physical gels based of the self-assembly of low molecular weight gelators to polymer gelators. In the former the solvent quality changes gradually with temperature, thus permitting the distinction of the two LC gel types. In contrast in the latter, the change in solvent quality is abrupt and coincides with isotropic-LC transition and, thus, only one LC gel type can be observed.
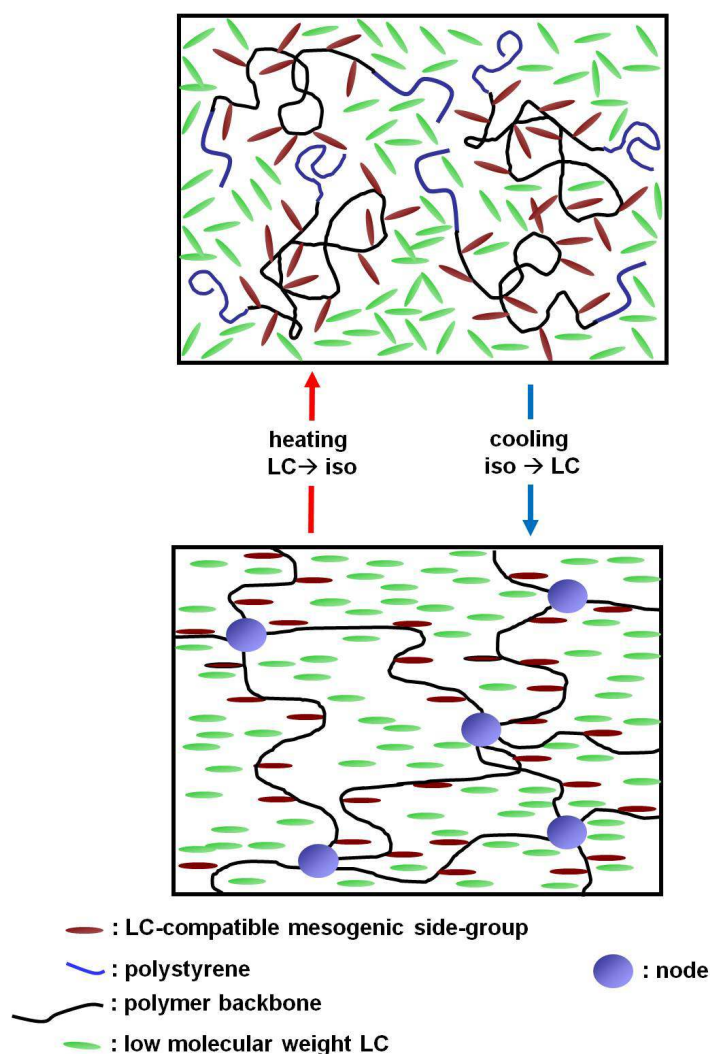
Figure 1.17:   Schematic illustration of a thermoreversible LC physical gel using ABA triblock copolymer gelators in a nematic solvent.

2   Aim and motivation of the thesis

The central goal of this thesis is the synthesis and application of functional block copolymers. The following synthesis sequence was carried out: i) block copolymers, that carry a protected functional groups, are prepared by anionic polymerization, ii) the block copolymers are subsequently converted into functionalizable block copolymers by deprotection of the side-group and iii) the side-groups with definite functions were attached by polymer analogous reaction resulting in functional block copolymers with specific properties. The functional block copolymers were tailored for applications as photoaddressable block copolymers or block copolymer gelators for liquid crystals. Three different subjects were pursued within the scope of this thesis:

Combinatorial synthesis of block copolymers by anionic polymerization

Combinatorial methods and techniques are an efficient synthetic approach for the preparation of well-defined block copolymers. The principle advantages of a combinatorial block copolymers series is based on the fact that an identical start block is used. The second block is varied in a combinatorial fashion in length or chemical structure. Series of block copolymers prepared in this way are on the one hand interesting for the fundamental investigations of morphologies and properties. On the other hand, combinatorial series can be beneficial for the investigation and efficient optimization of functionalized block copolymers.

This chapter covers the completion and implementation of a novel reactor setup that permits the anionic polymerization of block copolymers in a combinatorial fashion.

The main objectives of this chapter are:

a) completion of reactor setup for combinatorial anionic polymerization of block copolymers

b) implementation of reactor setup as well as establishing operating and polymerization procedures

c) demonstration of combinatorial block copolymer synthesis with model systems on the basis of:

- AB block copolymer series with different length of B-block

- AB block copolymer series with different monomers in B-block

- ABC block copolymer series with different length in C-block

d) synthesis of functional block copolymer precursors

- implementation of protected monomer suitable for anionic polymerization of block copolymers

Azobenzene-containing block copolymers

Azobenzene-containing block copolymers are promising class of materials for volume holographic data storage. Rewritable materials for the volume holographic data storage require a high maximal refractive index modulation that should be reached after a short writing time and should exhibit long term stability. These parameters are hard to combine in one material. For example liquid crystalline azobenzene-containing polymers normally exhibit stable gratings but the writing time is rather high due to the inherently high order of the liquid crystalline phase. Thick polymer samples that are required for holographic angular multiplexing must exhibit an optical density of 0.3 - 0.7. One approach to conveniently adjust the optical density is the blending of azobenzene-containing diblock copolymers with the pure homopolymer that form the optical inert matrix of the block copolymer.

The main objectives of this chapter are:

a)   implementation of polyhydroxystyrene as a functional monomer to achieve a high glass transition temperatures in resulting functionalized block copolymers

b)   synthesis of functionalizable block copolymers with poly(methyl methacrylate) as well as polystyrene as amorphous, optical inert matrix segments

c)   functionalization of these block copolymers to novel smectic azobenzene-containing block copolymers as schematically illustrated in Figure 2.1

d)   investigation of structure-property relations of the liquid crystalline mesophases

e)   processing of azobenzene-containing diblock copolymers into thin and thick photo-addressable samples suitable for holographic experiments

f)   holographic experiments on selected examples performed in cooperation with the Dr. Hubert Audorff and Prof. Lothar Kador (Bayreuther Institut für Makromolekül-forschung, BIMF) within the framework of SFB481
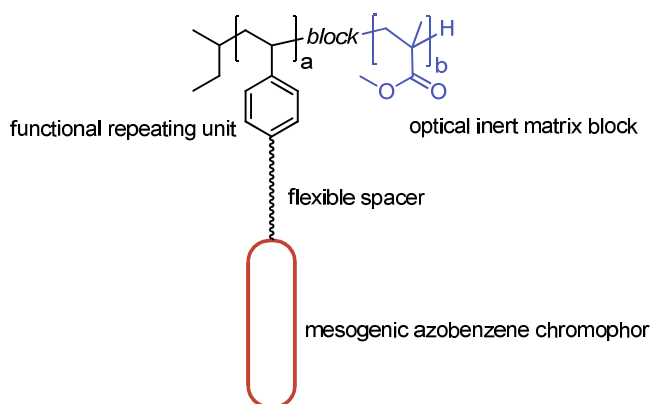
Figure 2.1:   Schematic representation of the targeted azobenzene-containing diblock copolymers for holographic data storage.

Cyanobiphenyl-functionalized ABA triblock copolymers as gelators for low molecular weight liquid crystals

Liquid crystalline gels are a special class of functional soft materials as they become soft solids upon gelation while preserving their stimuli-responsive properties. These materials are useful for fundamental studies concerning the liquid crystalline behavior in the gel state as well as potential applications in LC displays. Liquid crystalline gels can be prepared by using ABA triblock copolymer as gelators for the low molecular weight liquid crystals.

The main objectives of this chapter are:

a) synthesis and characterization of cyanobiphenyl-functionalized homopolymers and structure-property investigation with respect to the solubility in 4-cyano-4'-(pentyl)biphenyl (5CB)

b) synthesis of ABA triblock copolymers with functionalizable B-blocks of very high degree of polymerization

c) synthesis and characterization of novel cyanobiphenyl-functionalized ABA triblock copolymers as schematically shown in Figure 2.2

d) preparation of liquid crystalline gels based on 5CB using these block copolymer gelators

e) investigation of the influence of the polymer backbones of the gelators on the gelation of 5CB by rheological methods

f) investigation of gelation by electro-optical methods in cooperation with Dr. Maxim Khazimullin and Prof. Ingo Rehberg (Experimental Physics V) within the framework of FOR608
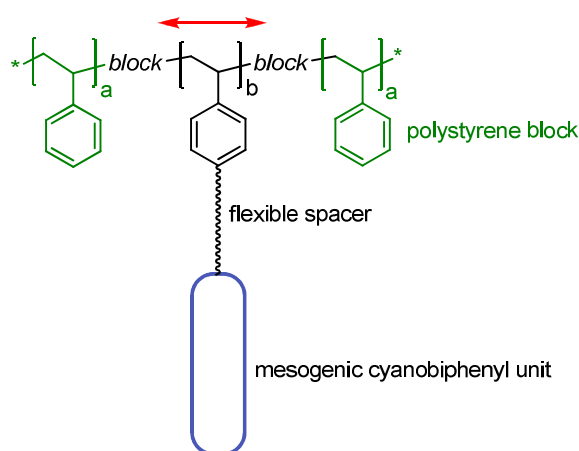
Figure 2.2:   Schematic representation of the targeted cyanobiphenyl-containing ABA triblock copolymers tailored to be used as gelators for low molecular weight crystals.

3   Combinatorial synthesis of block copolymers by anionic polymerization[1]

3.1   Introduction

Combinatorial experimentation as a technique to accelerate the development of new products and materials has drawn a lot of attention as a research strategy within the last decades. The principle of combinatorial experimentation is the use of parallel and high-throughput synthesis and screening that results in a reliable and comparable set of materials and material properties. Starting from drug research and pharmacology with the fundamental work by Furka,[156] Geysen,[157] and Houghten,[158] today it is a widely used technique in the fields of life science and catalysis. Compared to these fields, the usage of combinatorial methods is fairly new in material science.[159] Recently, these methods have advantageously been applied to many fields including polymer research[160] and device optimization for optoelectronic devices.[161]

Polymer synthesis by high throughput experimentation has been demonstrated for free radical polymerization including ATRP, RAFT, and cationic polymerization as well as for polycondensation.[160,162] Most polymers synthesized by these methods are homopolymers and random copolymers. These studies have mainly focused on optimizing the polymerization conditions or studying the kinetics. A limited number of combinatorial syntheses for block copolymers yielding ABA triblock copolymers and star-shaped block copolymers are known,[163] but in these cases no sequential anionic polymerization was used.

In the case of anionic synthesis for AB diblock copolymers the two basic possibilities for combinatorial variations are (i) variation of the B-block length and (ii) variation of the B-block`s chemical structure. In a classical, one pot, anionic setup the second option is not possible. It is possible to obtain block copolymers with increasing B-block lengths by taking multiple samples during the polymerization of the B-block.[164] However, the kinetics of the system must be known if a precise molecular weight is desired. Thus, highly reactive monomers (e.g. butylacrylates) cannot be used easily. In a sophisticated approach Abetz *et al.* also used two combined reactors for the preparation of two ABC triblock copolymers. The AB diblock was prepared in one reactor and the living anionic polymer was partly transferred into a second reactor, subsequently the C-block was polymerized with different length in both reactors.[165] Recently Schubert *et. al.* used an automated combinatorial system for anionic synthesis.[166] They were able to perform

---

[1] Parts of this chapter are already published: R. Pettau, C. Erdelen, H.-W. Schmidt, Design and Implementation of a Reactor Setup for Combinatorial Anionic Synthesis of Block Copolymer Series with Well-Defined Compositions; *Macromol. React. Eng.* **2010**, *4*, 65–72.

anionic polymerization in a parallel manner, demonstrating its use for kinetic studies and the synthesis of end functionalized polystyrene blocks.

Here a customized lab scale reactor setup for anionic combinatorial synthesis of block copolymers on a ten gram scale is presented that opens new possibilities in precision to synthesize block copolymer series. The reactor setup allows in the *first step* living anionic polymerization of the A-block (in ABC triblock copolymers the AB-block). In the *second step* the living blocks are distributed without termination to three additional reactors. In the *third step* the B-block (in ABC triblock copolymers the C-block) can be individually polymerized and tailored in four reactors (main reactor and three additional reactors).

3.2   Reactor setup

In order to implement the described combinatorial synthesis of block copolymers a customized reactor setup suitable for anionic polymerization procedures was designed. The whole reactor complex was initially designed and also built to a large extend by Dr. Christian Erdelen at the Chair of Macromolecular Chemistry I. There are three main issues that were addressed:

1. handling and transfer of the living polymer solution without termination,

2. defining/controlling the volume of the polymer solutions which are transferred from the main reactor into the secondary reactors,

3. individual temperature control for each reactor to allow the polymerization of differently reactive monomers.

Aside from these main issues, all common requirements of anionic polymerization have to be met. The purified solvents, initiators and additives must be introduced without contamination and the mixing speed in all reactors has to be sufficiently high to allow uniform initiation.

The complete setup consists of three parts and is schematically shown in Figure 3.1:

I   three distillation units for absolute solvents connected to the reactor setup via tubing system

II   two vacuum lines for high vacuum distillation of monomers; one line directly attached to the reactor setup

III   the polymerization reactor setup consisting of four reactors

Each part is described in detail in the following sections.

The whole system is kept under 300 mbar inert gas (N_2, quality 5.5) overpressure provided by an independent gas supply. The four glassware *distillation units* are

originally designed for three different solvents, tetrahydrofurane (THF), cyclohexane and toluene. Two units made of brown glass to reduce peroxide formation are used for THF. The solvent is pre-dried over CaH_2 in the first unit and the distilled solvent is then pumped into the second unit where potassium is used for drying. For cyclohexane and toluene in the other two distillation units only potassium is used. The whole hood of the distillation units is set up without electricity or water to minimize the danger potential. Thus, for the inline cooling system paraffin oil is used instead of water as cooling medium and all units are heated by hot silicon oil circulating through steel heating pipes in the distillation flasks. The distillation units are arranged in a way that the boiling point of the solvents decreases with the distance to the thermostats to reduce heat loss. Therefore, the toluene unit is placed next to the thermostats and THF is in the farthermost units (see Figure 3.1).
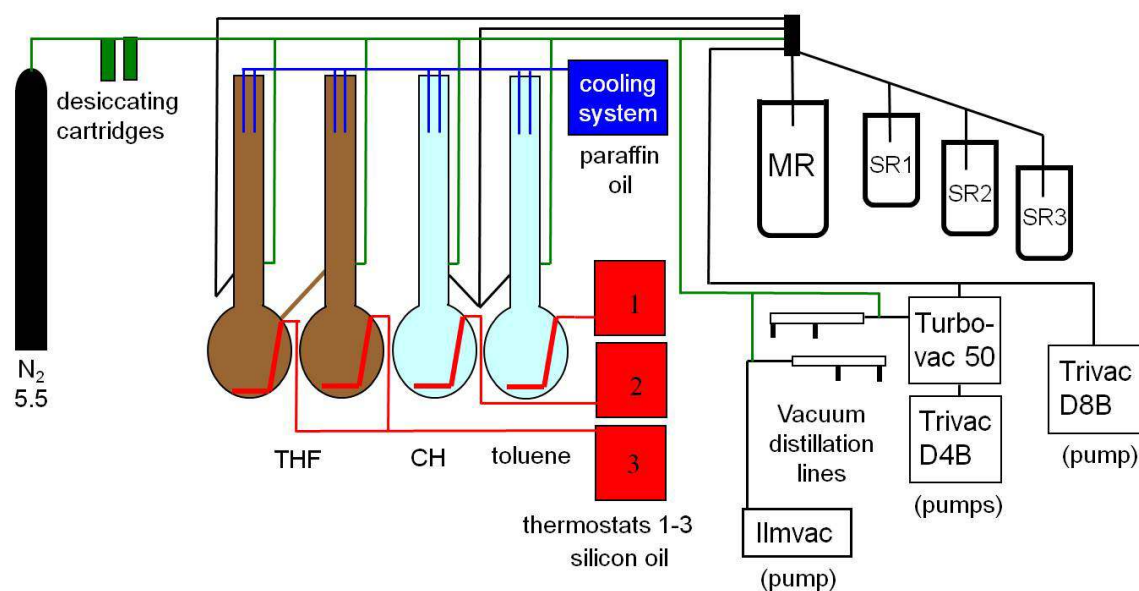
Figure 3.1: Schematics of the reactor setup and the adjacent distillation units and vacuum lines (THF: tetrahydrofurane; MR: main reactor; SR1-3: side reactor 1-3; red: heating; blue: cooling; green: N_2).

Vacuum lines are used to distill the monomers and additives for the anionic polymerizations under high vacuum. Two lines are implemented, a main line and a backup unit. The backup vacuum line uses an oil diffusion pump coupled with a rotary vane prepump (Ilmvac) reaching a minimal pressure of 10^{-5} mbar. The main vacuum line uses the same pump system that is connected to the reactor setup. Two different pumps can be used independently, a turbopump (Turbovac 50) coupled with a rotary vane prepump (Tricav D4B) reaching a minimal pressure of 10^{-6} mbar in the system or a rotary vane pump (Tricav D8B) with a minimal pressure of 10^{-4} mbar.

In Figure 3.2 a schematic illustration of the *rector setup* is shown. It consists of four reactors, i.e. one main reactor (MR) with a 1.6 l capacity and three secondary reactors (SRs) with 200 ml capacity. Dry solvents are directly fed into the reactors from the attached distillation units. Monomers, initiators, and additives can be injected into each reactor via a valve system through a septum.

Reactors: The reactor setup was mainly built from commercially available components. The main reactor is a 1.6 l glass vessel with cooling jacket (BüchiGlasUster EcoClave 075) and a high–torque drive with integrated magnetic couplings (cyclone 300; up to 3000 rpm). Swagelok-fittings in the lid of the MR allow a temperature sensor, one inflow tube (a) and two outflow tubes (b and c) to be passed through. One outflow tube is connected to *line 2* and the other to *line 3*. The orifices of the outflow tubes are placed below the T-mixer (e) at the bottom of the reactor. The inflow tube (a) is connected to *line 1* to feed monomers and solvents and to apply vacuum or inert gas. The three secondary reactors are 200 ml glass-pressure vessels (BüchiGlasUster Miniclave) each equipped with an external magnetic stirrer. Swagelok-fittings through the lid of each secondary reactor accommodate a temperature sensor, two inflow tubes (one from *line 3* (d) and the other (a) from *line 1*) and one outflow tube (b).

Pumping and pipeline systems: To facilitate the handling of the living polymer solutions without termination, the reactor setup constitutes an enclosed system interconnected by three separate lines under inert atmosphere (200 mbar gauge pressure of dry nitrogen). The reactors can be independently connected to each line by using the respective combination of valves. *Line 1* has three main functions. It is used first to evacuate the reactors with a turbo molecular pump (Turbovac 50 controlled by Leybold Turbotronik NT 10) prior to the polymerizations, second to apply inert gas and third to feed dry solvents into the reactors. *Line 2* is used to pump solutions out of the reactors with slight overpressure which is applied via *line 1*. *Line 3* is a double jacketed, temperature controlled pipeline (min. operation temperature: -70 °C), and is designed to transfer temperature sensitive liquids under controlled conditions. It is used to transfer and distribute the living polymer precursor solutions from the MR to the SRs. In addition, a custom-built, graduated 120 ml double jacketed glass vessel (Figure 3.2, T) is implemented in *line 3*. This transfer vessel allows controlling the transfer volume to each reactor. In step *II*, the polymer solution is pumped into this vessel using reduced pressure during the polymerization process. Subsequently a predetermined volume is pumped into each SR. Like *line 1*, *line 2* and *line 3* are connected to the supply of solvent, nitrogen and vacuum in that manner, that they can be rinsed with solvent, dried with vacuum and flushed with nitrogen any time during the experiment.
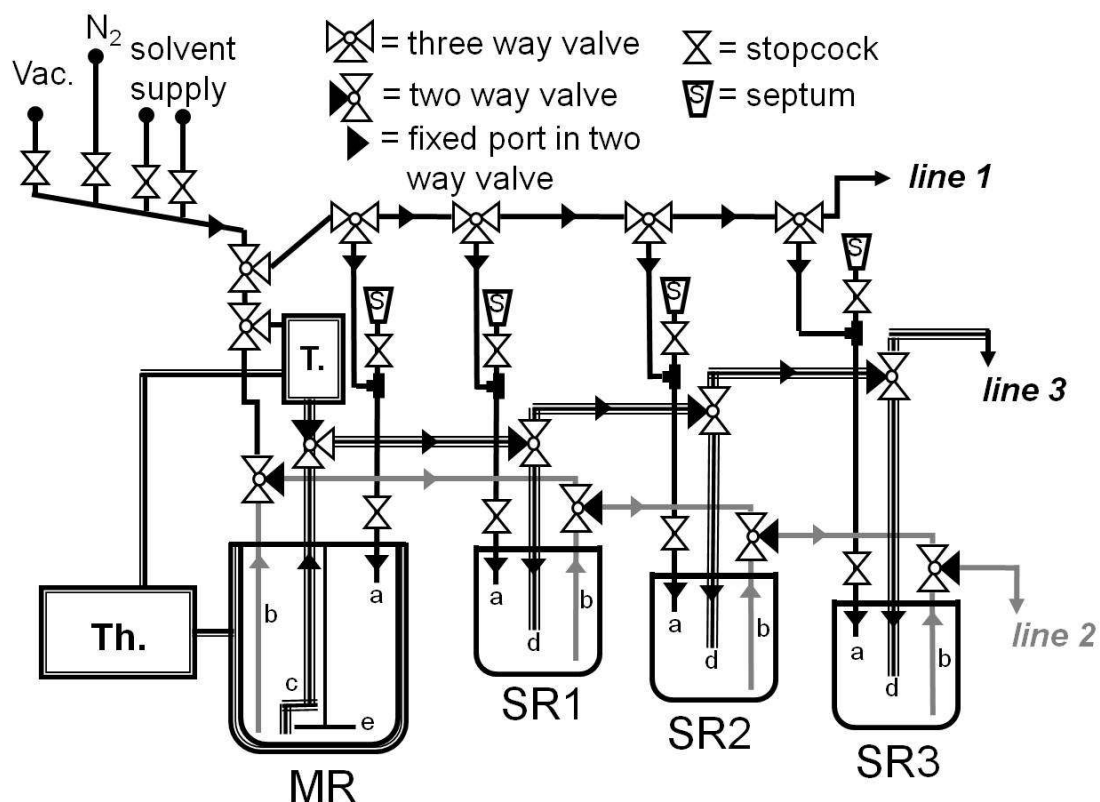
Figure 3.2:   *Top:* Schematic illustration of rector setup for combinatorial anionic synthesis (Vac. = connection to vacuum line, N$_2$ = connection to nitrogen line, solvent supply = connection to solvent distillation units, T. = graduated transfer vessel, Th. = thermostat, MR = main reactor, SR1-3 = secondary reactors 1-3); *Bottom:* photo of the reactor setup.

Temperature control: The temperature can be monitored (temperature Greisinger (electronic) GMH 175) and controlled in each reactor individually. The MR, the transfer *line 3* and the graduated transfer vessel are connected to a cryostat (huber cc80w). This allows reactor temperatures in the range of +55 °C to -70°C. The temperature of each SR is controlled externally. Thus the polymerization temperatures in every reactor can be adjusted individually with respect to the monomer used. For example dewars filled with an acetone/dry ice mixture can be used to cool down an anionic polymerization to -78°C.

3.3   Reactor setup features

A combinatorial reactor setup for a three step process was designed in order to realize a sequential anionic polymerization that is subsequently transformed into parallel syntheses based on an identical precursor. To demonstrate the capabilities of the novel setup series of model block copolymer system were prepared.

Figure 3.3 illustrates three example polymerization procedures realized with the described reactor setup. The top schematic in Figure 3.3 shows two variants for AB diblock copolymers. In the first step (*I*) monomer A is polymerized in the main reactor (MR) to the A-block. In the second step (*II*) defined volumes of the precursor solution are distributed to three secondary reactors (SRs). In the third step (*III*), two variants are possible. In variant one may inject the monomer B in different quantities in each reactor. After complete polymerization of the B-monomer a series of four AB diblock copolymers is obtained. These AB diblock copolymers have identical A-blocks but their B-block have a varied length. In this variant all B-blocks have the same chemical composition. In variant *ii* for the third step (*III*) different monomers are used in each reactor to form the B-blocks. In this case, after the polymerization of the B-block, the resulting AB diblock copolymer series features an identical A-block and a B-block with varying chemical composition. The length of the B-blocks can be varied or kept constant in this variant.

The bottom schematic in Figure 3.3 illustrates one variant for the synthesis of a ABC triblock copolymer series. Here the first step (*I*) contains the sequential polymerization of A-block and B-block in the MR. In the second step (*II*) the AB diblock precursor is distributed to the SRs. For the third step (*III*) the same monomer C is used in each reactor in different amounts, nevertheless the setup allows to use different monomers C as mentioned above. After the polymerization in the third step (*III*) a series of four ABC block copolymers based on an identical AB diblock and a C-block with increasing block length is obtained. The described examples are only a few demonstrating the feasibility of combinatorial block copolymer series with this setup.
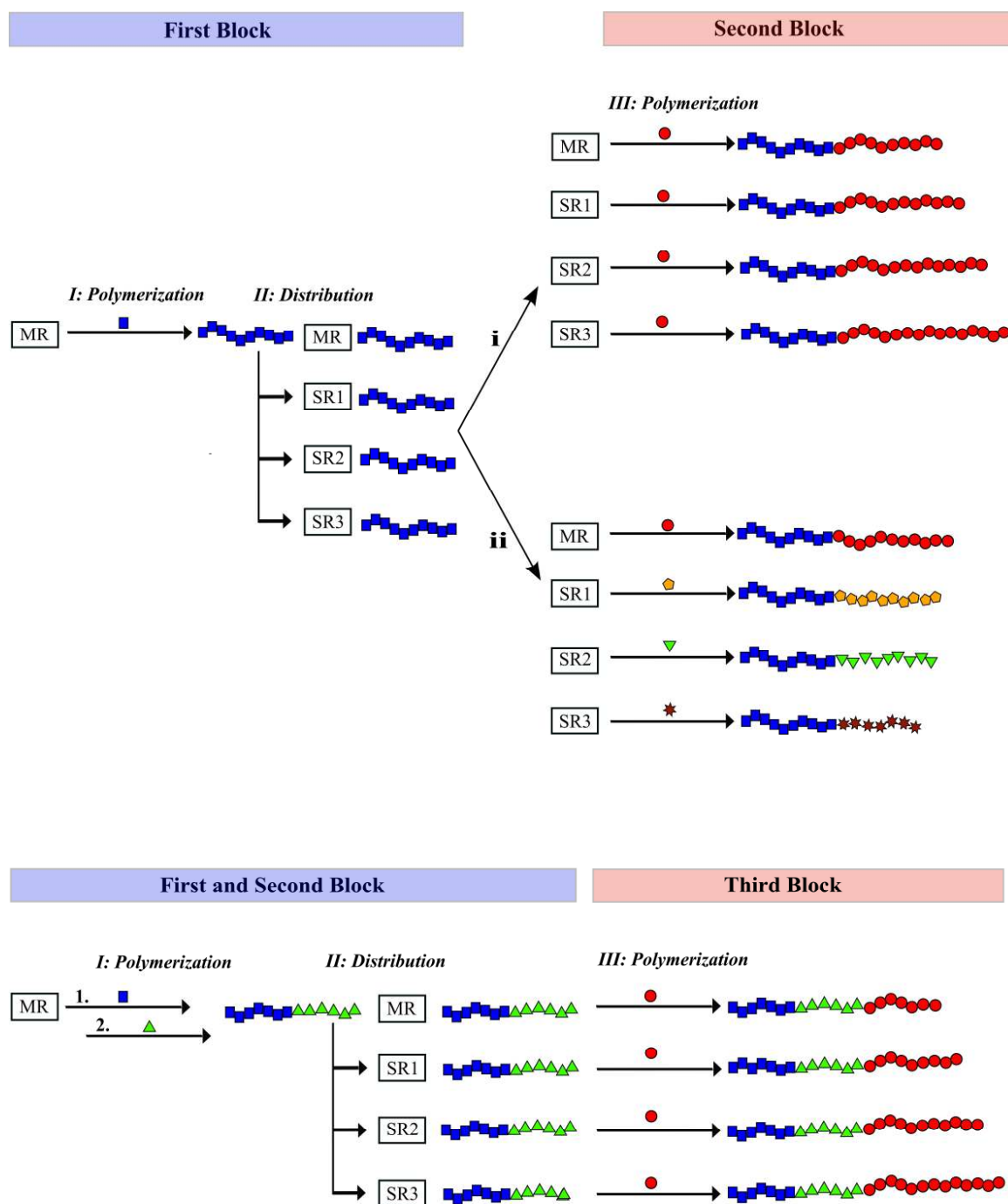
Figure 3.3: Schematic representation of the three steps for the sequential anionic synthesis of AB *(top)* and ABC block copolymer series *(bottom)* as described in this publication *(MR: main reactor; SR 1-3: secondary reactor 1 to 3; I-III: steps in the polymerization procedure; i and ii: possible variants).*

The possibilities to achieve block copolymer architectures can be extended e.g., by using di- or multifunctional initiators (see chapter 5.6). Combinatorial experiments can be also applied to the termination step by using different terminating agents in each reactor. This can open the way to more complex polymer architectures that are based on chain extension and coupling reactions.[54,167]

For example the endcapping could be carried out with a protected alkine or azide function. This would enable the synthesis of more complex block copolymer series by the use of *click* chemistry. Another possibility is to use the combinatorial synthesized block copolymer series as a macroinitiator for a controlled radical polymerization by the use of an appropriate endcapping agent. Thus the anionic polymerization can be transformed into a controlled radical polymerization.[54,168]

3.4   Implementation

In order to test and demonstrate the capabilities of the above described reactor setup, several different block copolymer series were synthesized. Three of these series were selected and reported here to demonstrate the results highlighting different aspects:

- Series **1** consisting of AB diblock copolymers comprising A-blocks of same length and B-blocks of different lengths,

- Series **2** featuring ABC triblock copolymers with identical AB-block and a varying length of the C-block,

- Series **3** are AB diblock copolymers that are based on an identical A-block and vary in the chemical structure of the B-block. The aim was to check if the control over block composition and length was indeed possible.

3.4.1   AB diblock copolymers with variable B-block length

Block copolymer series **1** consists of the four polystyrene-*block*-poly(methyl methacrylate) (PS-PMMA) AB diblock copolymers **1a-1d** with increasing lengths of the PMMA block. All block copolymers were synthesized by sequential anionic polymerization of styrene (S) and methyl methacrylate (MMA) in tetrahydrofuran (THF) with *sec*-butyllithium (s-BuLi) as initiator at -70 °C. Lithium chloride (LiCl) was added as described in literature as an additive to promote the living polymerization of methacrylates with well-defined and narrow molecular weight distributions.[169] After polymerization of the polystyrene (PS) block 1,1-diphenylethylene (DPE) was added to reduce the reactivity of the living styrene anions (see Figure 3.4). This well established method was used to suppress side reactions of the polystyrene chain end with the added methacrylates that would otherwise occur due to high nucleophilicity of the PS anion.[55]
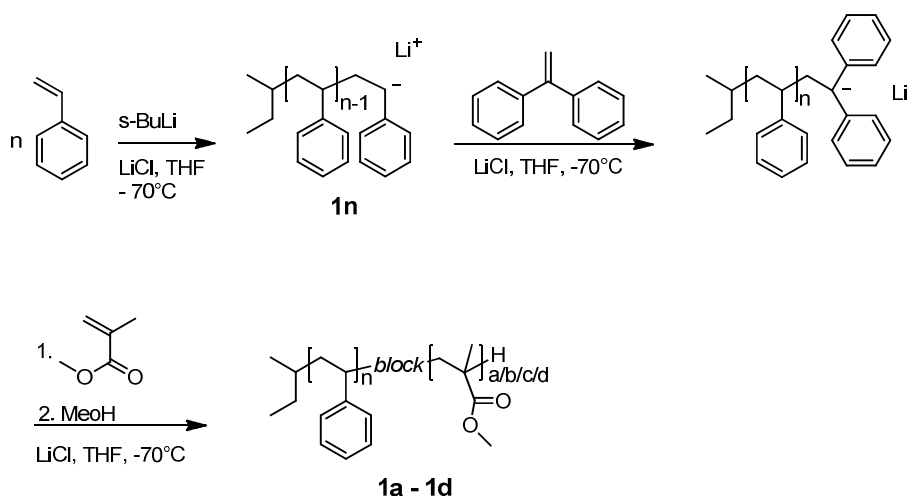
Figure 3.4:   Polymerization of the PS-PMMA diblock copolymer series **1a - 1d.**

In the first step, the PS-precursor **1n** was polymerized in the main reactor (MR) and reacted with DPE. In the second step aliquots of the polymer solution were transferred to the secondary reactors via the temperature controlled vessel and transfer *line 3*. Additionally a sample of the DPE- capped PS-precursor was obtained in the same manner and pumped into a flask with dry methanol via the outlet of *line 3*. In the third step the second block was polymerized in each reactor separately by injecting the appropriate amount of MMA.

Block copolymers batches up to a scale of 10 g were typically obtained in the secondary reactors. Figure 3.5 shows the SEC traces of the four AB diblock copolymers **1a - 1d** and the corresponding PS-precursor **1n**. All four PS-PMMA block copolymers contain an identical PS-block ($M_n = 55.1$ kg/mol). The molecular weight was measured by size exclusion chromatography (SEC) with respect to a polystyrene calibration. The number of average repeating units in the PS-block were determined to be $ru_{PS} = 530$ (**1n**). The molar ratio of A-block to B-block can be calculated by analyzing distinct signals in the ^{1}H-NMR spectra.

Figure 3.5: SEC traces of precursor block **1n** and all AB diblock copolymers **1a - 1d** (RI-Detection; solvent: THF; molecular weight with respect to PS-standards).

The number of repeating units in the B-block were determined for **1a** $ru_{PMMA} = 1430$, **1b** $ru_{PMMA} = 2170$, **1c** $ru_{PMMA} = 2910$ and **1d** $ru_{PMMA} = 4560$. The PS-PMMA block copolymers that cover a molecular weight ranging from $M_n = 167$ kg/mol to $M_n = 509$ kg/mol and exhibit a narrow molecular weight distribution (PDI ≤ 1.06). Due to the rather high molecular weight of the PS-precursor **1n,** minor impurities can result in detectable termination. Small amounts of the PS-precursor **1n** can be detected in the crude

product of **1a - 1d** (see Figure 3.5) and can be quantified via the UV trace in the SEC measurements with respect to the incorporated A-block (**1a:** 3%, **1b:** 5%, **1c:** 4% and **1d**: 7%) The experimentally measured composition is in good agreement with the calculated block copolymer composition (see Table 3.1). Minor deviations are attributed to small variance in measuring the transferred precursor solution volume prior to feeding the SRs. This demonstrates that good control within a series of block copolymers is ensured. PS-PMMA diblock copolymer series are used in block copolymer based lithography.[43] Combinatorial series such as these might be useful to optimize this and other applications.

Table 3.1: Characteristic data of AB diblock copolymer series **1** containing A-block with $ru_{PS} = 530$ and B-blocks with a different length

block copolymer series 1	M_n [a) (kg/mol)	PDI [b)	ru_{PS} [c)	ru_{PMMA} [c)	composition (n:a/b/c/d) calc.[d)	measured[e)
1n	55.1	1.04	530	-	-	-
1a	167	1.05	530	1430	1 : 2.6	1 : 2.7
1b	244	1.04	530	2170	1 : 3.9	1 : 4.1
1c	282	1.04	530	2910	1 : 5.6	1 : 5.5
1d	509	1.06	530	4560	1 : 8.6	1 : 8.6

a) determined by SEC with polystyrene standards, RI-detection; b) polydispersity index; c) average number of repeating units: calculated from block copolymer composition (determined by ^{1}H-NMR) for ru_{PMMA}, with ru_{PS} determined from SEC; values rounded to three significant figures; d) on the basis of the monomer feed; e) determined by ^{1}H-NMR

3.4.2 ABC triblock copolymers with variable C-block length

As mentioned above, this method is not limited to AB diblock copolymers. The second series is based on ABC triblock copolymers, i.e. polystyrene-*block*-poly(2-ethylhexyl methacrylate)-*block*-poly(methyl methacrylate) (PS-PEHMA-PMMA) **2a - 2d**, featuring a constant ratio of the PS and PEHMA blocks and an increasing length of the PMMA block. This series was polymerized similar to the procedure described above for the sequential polymerization of S, MMA and 2-ethylhexyl methacrylate (EHMA) with s-BuLi in THF at -70°C (see Figure 3.6). Again LiCl was used as an additive and DPE for end capping the PS anions. The A-block and the AB-block are polymerized in the first step in the main reactor. After the PS-precursor is polymerized and end capped with DPE, EHMA is injected for the polymerization of the B-block. Aliquots of the living polymer solution are transferred to the secondary reactors and the third block is polymerized in each reactor separately in the last step.
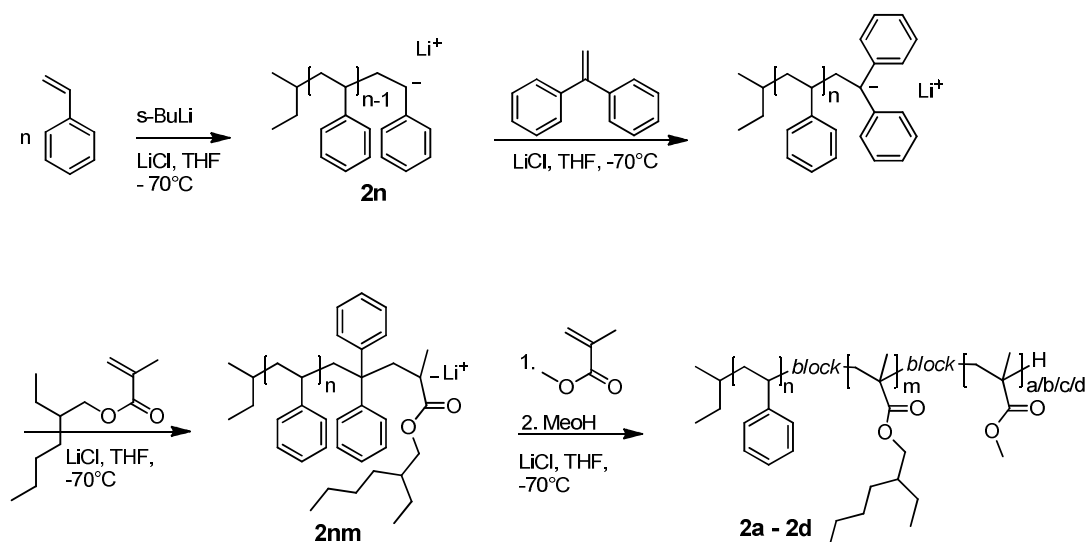
Figure 3.6: Polymerization of the PS-PEHMA-PMMA triblock copolymer series **2a - 2d.**

The SEC curves for block copolymer series **2** including the precursor polymers of the A-block **2n** and the AB-block **2nm** are shown in Figure 3.7. Apparently, all block copolymers could be isolated without contamination of terminated homopolymer **2n** or diblock precursor **2nm**. The signal intensity in the SEC curve of the precursor polymers **2n** and **2nm** is below 1 % in all ABC triblock copolymers indicating that the combinatorial anionic polymerization proceeded without significant termination of the precursors during the process.
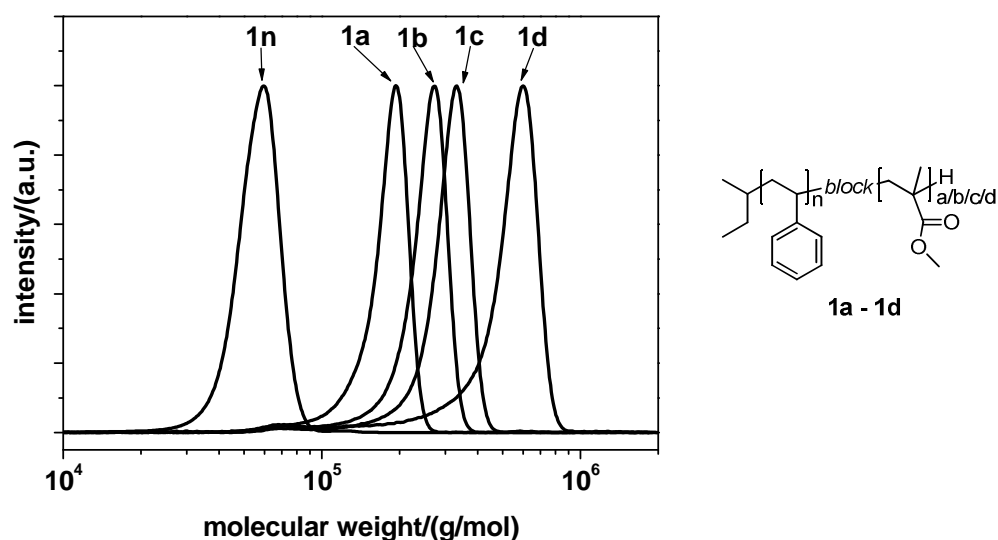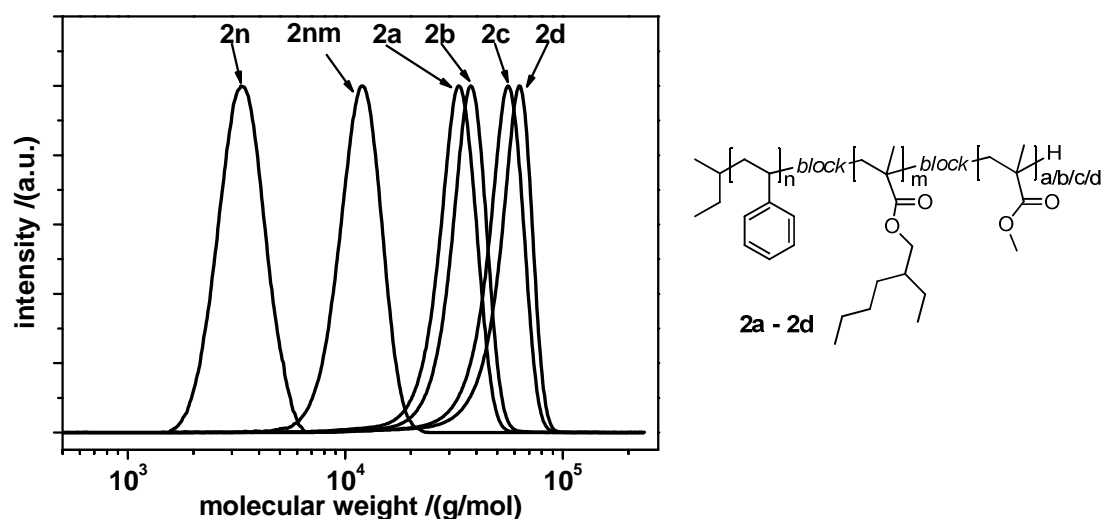

Figure 3.7: SEC traces of precursor blocks **2n** and **2nm** and all ABC triblock copolymers **2a-2d** (RI-Detection; solvent: THF; molecular weight with respect to PS-standards).

44

Characteristic data of the block copolymers of series **2** and its precursors **2n** and **2nm** are given in Table 3.2. The molar ratio of the PS to PEHMA blocks was determined to 1:1.5. The ratio of the PMMA blocks increases from 8.7 to 18.0. The deviation from the ratio calculated from the used monomer feeds compared to the ration determined by ^{1}H-NMR analysis of the block copolymers is minor as already observed in series **1**. The number of repeating units of the A-block **2n** is determined by SEC to be $ru_{PS} = 31$. The numbers of repeating units in the other blocks are calculated using the block ratio determined by ^{1}H-NMR. In the AB diblock **2nm** the repeating units of the B-block are 45. In the ABC triblock copolymers the C-block repeating units are **2a** $ru_{PMMA} = 270$, **2b** $ru_{PMMA} = 320$, **2c** $ru_{PMMA} = 530$ and **2d** $ru_{PMMA} = 560$. The total molecular weight of the ABC triblock copolymers varied from $M_n = 30.7$ kg/mol to $M_n = 53.9$ kg/mol and all polymers exhibit a molecular weight distribution of $PDI \leq 1.06$.

Table 3.2: Characteristic data of ABC triblock copolymer series **2** containing A-block PS_{31}, B-block $PEHMA_{45}$ and C-blocks with a different length

block copolymer series 2	M_n [a] (kg/mol)	PDI [b]	ru_{PS} [c]	ru_{PEHMA} [c]	ru_{PMMA} [c]	composition (n:m:a/b/c/d)	
						calc. [d]	measured [e]
2n	3.2	1.06	31	-	-	-	-
2nm	9.1	1.05	31	45	-	1 : 1.5	1 : 1.5
2a	30.7	1.06	31	45	270	1 : 1.5 : 8.2	1 : 1.5 : 8.7
2b	34.5	1.05	31	45	320	1 : 1.5 : 9.8	1 : 1.5 : 10.4
2c	49.9	1.06	31	45	530	1 : 1.5 : 15.7	1 : 1.5 : 17.2
2d	53.9	1.04	31	45	560	1 : 1.5 : 19.6	1 : 1.5 : 18.0

a) determined by SEC with polystyrene standards, RI-detection; b) polydispersity index; c) composition (determined by ^{1}H-NMR) for ru_{PMMA} and ru_{PEHMA}, with ru_{PS} determined from SEC; values rounded to three significant figures; d) on the basis of the monomer feed; e) determined by ^{1}H-NMR

3.4.3 AB diblock copolymers containing B-blocks with different chemical structures

Finally an AB diblock copolymer series based on the identical precursor A-block and B-blocks with different chemical structures was prepared. Such block polymer series are not accessible by common one reactor setups and techniques. Block copolymer series like this allow the investigation of the influence of the polarity of the end block with respect to an identical A-block. The third synthesized series (**3a-3d**) is composed of P*t*BS as the A-block. Different metharylates were selected as monomers for the B-block, methyl methacrylate, ethyl methacrylate, *n*-butyl methacrylate and *tert*-butyl methacrylate in different amounts. The polymerization procedure is similar as described for series **1**. The

P*t*BS precursor is polymerized and reacted with DPE in the main reactor at -70 °C then aliquot amounts of the living polymer solution are transferred to the secondary reactors. The B-block is polymerized in each reactor separately by injecting the designated monomer yielding the AB diblock copolymer series. The polymerization temperature in the SR3 is set to -45 °C in contrast to the MR, SR1 and SR2 to accommodate the polymerization of *t*BMA.
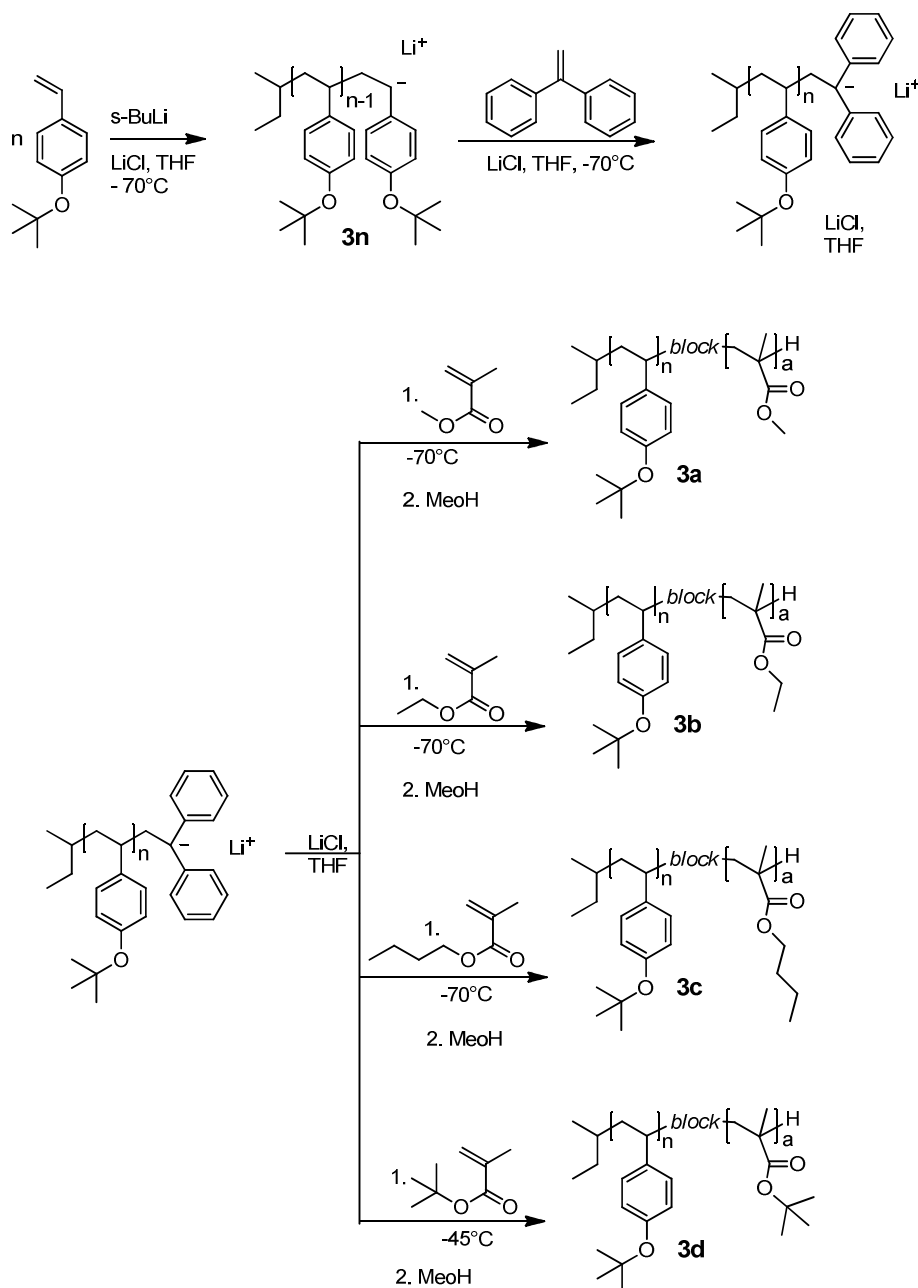
Figure 3.8:   Polymerization of the diblock copolymer series **3** consisting of PS-PMMA (**3a**), PS-PEMA (**3b**), PS-PnBMA (**3c**), PS-PtBMA (**3d**).

One challenge for this polymerization was to provide all purified monomers at the same time. For typical AB diblock copolymers the second monomer was still purified while the first monomer was being polymerized. All monomers had to be kept in liquid nitrogen in the dark to prevent spontaneous polymerization. To accommodate for this issue some of the monomers were purified and distilled one day before the combinatorial polymerization and stored in liquid nitrogen until usage. For the overnight storage the closed vials were set into a disk of foamed polystyrene floating on liquid nitrogen in a high dewar. The vials were placed in holes in the disk in that way that the lower part containing the monomer was immersed in the liquid nitrogen. Thus the monomers were kept at constant temperature although the volume of the refrigerant decreases over night by evaporation.

Figure 3.9 shows the SEC traces of the AB diblock copolymers **3a-3d** and their precursor **3n.** All characteristical data are given in Table 3.3. Termination of the precursor is less than 1% as detected by SEC. The precursor consist of P*t*BS-block **3n** with a molecular weight of $M_n = 5.5$ kg/mol. The molecular weight of the resulting block copolymers is in the range of $M_n = 43.3$ kg/mol (**3d**) to $M_n = 44.0$ kg/mol (**3a**). All resulting diblock copolymers **3a-3d** exhibit a narrow molecular weight distribution (PDI ≤ 1.04), demonstrating that all end block methacrylate monomers could be polymerized in a controlled manner.
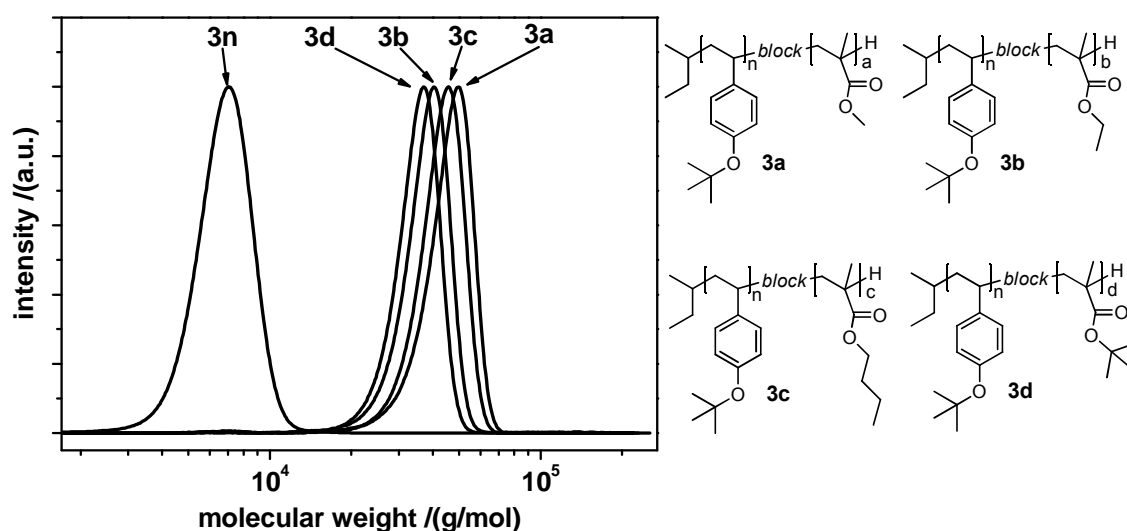
Figure 3.9:   SEC traces of precursor block **3n** and all AB diblock copolymers **3a-3d** (RI-Detection; solvent: THF; molecular weight with respect to PS-standards).

The B-blocks are varied in a molar range from 1:8.9 to 1:13.3 in block composition and the experimentally determined composition was in good agreement with the intended. The block compositions were not intended to be equal for all polymers in this series as one might expect. The resulting different molecular weights were desired to keep the overlay of SEC traces distinguishable. The repeating units were determined in the same way as for series **1** and **2**. It has to be noted the in the case of series **3** the calculation of repeating units from the molecular weight obtained by SEC might not be as accurate as for **1** and **2**. This possible deviation is due to the fact that the molecular weight were given with respect to a polystyrene calibration that might not be exact for poly(*tert*-butxystyrene). Nevertheless the resulting values were commonly in good agreement with the calculated one therefore the polystyrene calibrations was applied also for all poly(*tert*-butxystyrene) based polymers. In the case of series 3 the repeating units were determined to $ru_{PtBS} = 31$, $ru_{PMMA} = 415$, $ru_{PEMA} = 380$, $ru_{PnBMA} = 280$ and $ru_{PtBMA} = 210$.

Table 3.3: Characteristic data of AB diblock copolymer series **3** containing B-blocks with different chemical structures

block copolymer series 3	M_n [a] (kg/mol)	PDI [b]	ru_{PtBS} [c]	ru_{PxMA} [c]	composition (n:a/b/c/d)	
					calc. [d]	found [e]
3n	5.5	1.06	31		-	-
3a	44.0	1.04	31	415	1 : 13.3	1 : 13.3
3b	36.9	1.04	31	380	1 : 9.7	1 : 9.1
3c	41.7	1.04	31	280	1 : 8.6	1 : 8.9
3d	34.3	1.03	31	210	1 : 7.4	1 : 6.7 [e]

a) determined by SEC with polystyrene standards, RI-detection; b) polydispersity index (M_w/M_n); c) average number of repeating units: calculated from block copolymer composition (determined by ^{1}H-NMR) for ru_{PxMA}, with ru_{PtBS} determined from SEC; values rounded to three significant figures; d) on the basis of the monomer feed; e) determined by ^{1}H-NMR

The use of a protected functional monomer such as *t*BOS for the starting block allows for a further functionalization of block copolymers after cleavage of the *tert*-butoxy group.[170] On one hand, the polarity of such a segment is changed considerably resulting in a change of the solution morphologies in certain solvents.[25] On the other hand, the hydroxystyrene allows for its use as a photoresist[41] or the attachment of mesogens or chromophores by a polymer-analogous reaction[171] similar to hydroxyl-functionalized 1,2-polybutadiene[19] and will be discussed in the next chapters.

3.5   Achievements

In this chapter a specially designed reactor setup was presented that can be used for a combinatorial approach to the synthesis of block copolymer series by anionic polymerization. The setup features one main reactor and three secondary reactors to carry out anionic polymerizations on lab scale quantities at low temperatures. The implementation was demonstrated with three series of AB and ABC block copolymers with the identical A-block and AB-block respectively. The B-block in AB diblock copolymers and the C-block in ABC triblock copolymers can be varied with respect to block length or chemical constitution.

4 Azobenzene-containing block copolymers

4.1 Introduction

Homopolymers

Liquid crystalline homopolymers containing laterally attached azobenzene side-groups were first reported by Ringsdorf and Schmidt.[142,143] Eich *et al.* were the first to studying the photoisomerization of azobenzene chromophores and their application as holographic data storage materials.[144] Holographic data storage provides the potential of storing significantly more than one terabyte of information with transfer rates exceeding 1 GB/s and data access time of less than 100 ms. A detailed introduction to holography and holographic data storage is given in chapter 6.1.2.

Until today many different azobenzene-containing homopolymers were synthesized and their photochemistry was investigated.[172–174] Additionally, statistical copolymers with two different azobenzene units[175] as well as copolymers of azobenzene moieties and non-chromophoric mesogens[143,176–178] were investigated in order to improve their performance in holographic experiments (e.g. diffraction efficiency, stability of inscribed information).

Azobenzene-containing polymer materials can be either amorphous or exhibit a liquid crystalline phase. Azobenzene chromophores are shape anisotropic molecules that can act as mesogenic units. In amorphous polymers the stability of the inscribed gratings has been found to depend on the glass transition temperature of the polymer and the type of the azobenzene side-group. Yet, holographically stored information is decaying quickly above this temperature due to the increased thermal relaxation of the photoinduced orientation in the isotropic state.[29,179] Even at room temperature amorphous polymers do not show a pronounced long term stability of the inscribed gratings.

If the azobenzene-containing polymer features a liquid crystalline phase and forms at room temperature a glass with liquid crystalline order, the holographic gratings are expected to be stable at room temperature. Liquid crystallinity also influences several other important parameters like cooperative motion, birefringence, diffraction efficiency and writing time.[28,173] Natansohn and Rochon[173] summarized that the alignment in liquid crystalline polymers is thermodynamically favored in the temperature range of the liquid crystalline phase due to its inherent order. During irradiation with linear polarized light, the director of the liquid crystalline multidomain(s) can be reoriented or -in an initially amorphous quenched film- a liquid crystalline order can be induced. Orientation of the chromophores is easier in the first case whereas the latter is energetically much more demanding.

In a holographic experiment liquid crystalline azobenzene polymers often exhibit an additional increase of the diffraction efficiency after the writing laser is switched off. This "*post-development*" or "*post exposure gain*" is assumed to be due to an increase in orientation of the mesogens along the direction that is given by those chromophores that were pre-aligned during holographic writing process. This effect can be enhanced at elevated temperatures because the increased free volume supports the mesogens thermal movements leading to an faster alignment.[29,177,180]

If azobenzene units are close to each other the photoinduced orientation of the chromophores is stabilized. This "*cooperative effect*" is essential for the stability of the holographically inscribed information.[109,176] Copolymers with azobenzene moieties and non-chromophoric mesogens, as mentioned above, form another class of photoaddressable liquid crystalline polymers. The no-chromophoric, mesogenic groups can undergo cooperative molecular motions with the photooriented azobenzenes, thereby inducing a higher birefringence, and simultaneously stabilizing the orientation. Due to this improved cooperative effect these systems exhibit very good long-term stability.[28,29]

Azobenzene-containing materials for volume holographic data storage

For volume holographic data storage and to achieve high data density, thick films (up to 1-2 mm) are required in order use Bragg-type gratings and to perform angle multiplexing with a high angular selectivity. The films should exhibit a low optical density and no scattering of visible light otherwise the laser beam cannot penetrate the entire sample. Thus the use of homopolymers is precluded since it is difficult for the beam to pass through chromophore-containing thick films because of the large molar extinction coefficient of azobenzene chromophores at the wavelength of the laser beam. Due to this consideration the optical density of the samples has to be adjusted in the range of 0.5 - 0.7. Another issue for the holographic data storage posed by homopolymers is the formation of "*surface relief gratings*" in addition to the desired refractive index modulation upon illumination with a light intensity grating.[174,181] These thin gratings are formed by light induced mass transport and are detrimental to angle-multiplexed inscriptions with high angular sensitivity. Moreover, their diffraction efficiency is usually higher than those of desired phase gratings in the volume. The formation of surface relief gratings is most pronounced on the surfaces of homopolymers and azobenzene-containing molecular glasses.[29,182]

The optical density of azobenzene-containing homopolymers could be reduced by blending the homopolymer with an optical inert polymer. Almost all polymer blends consisting of two or more polymers form macrophase-separated morphologies. These morphologies are in the micrometer range and, therefore, they show bulk light scattering

and are unsuitable for holographic data storage. However, one literature example is known, where this issue was overcome by using a blend, in which both polymers had similar backbones. In this case the multiplexing of 20 holograms could be realized.[183]

If the chromophore content and thereby the optical density is to be diluted another factor has to be considered. In order to efficiently utilize the *trans-cis-trans* isomerization for enhanced writing speeds and improved stabilization, the chromophores have to be close to each other to benefit from the above mentioned cooperative effect. Therefore, diluting the chromophores by statistical copolymerization with an optical inert comonomer is not a viable option since the cooperative effect and, hence, the long-term stability of the inscribed gratings are lost.[184] Ikeda *et al.* reported the formation of holographic gratings in thick films of azobenzene-containing copolymers with non-chromophoric mesogens such as cyanobiphenyl or tolane moieties conserving the cooperative effect. Nevertheless, it has to be noted that scattering issues were apparent that would prohibit the processing of these materials into thicker samples.[178,183] A solution to this issue are azobenzene-containing block copolymers and block copolymer blends discussed in the following.

Azobenzene-containing block copolymers

An elegant concept for controlling the optical density for holographic data storage was first reported by Breiner *et al.*. In this concept the chromophore content is diluted by using azobenzene-containing diblock copolymer systems, as shown in Figure 4.1.[23,29,185] One block is functionalized with the azobenzene chromophores whereas the other segment has to be a transparent optical inert block. Commonly the photoaddressable segment form the minority phase and the optical inert segment forms the matrix. By using a block copolymer approach the optical density of the material can be reduced while maintaining the cooperative effect. As an additional advantage, the use of block copolymers also precludes the formation of surface relief gratings in the holographic writing process. Due to the confinement of the chromophores to the minority phase the solid matrix can prevent the formation of undesired surface relief gratings.[19]
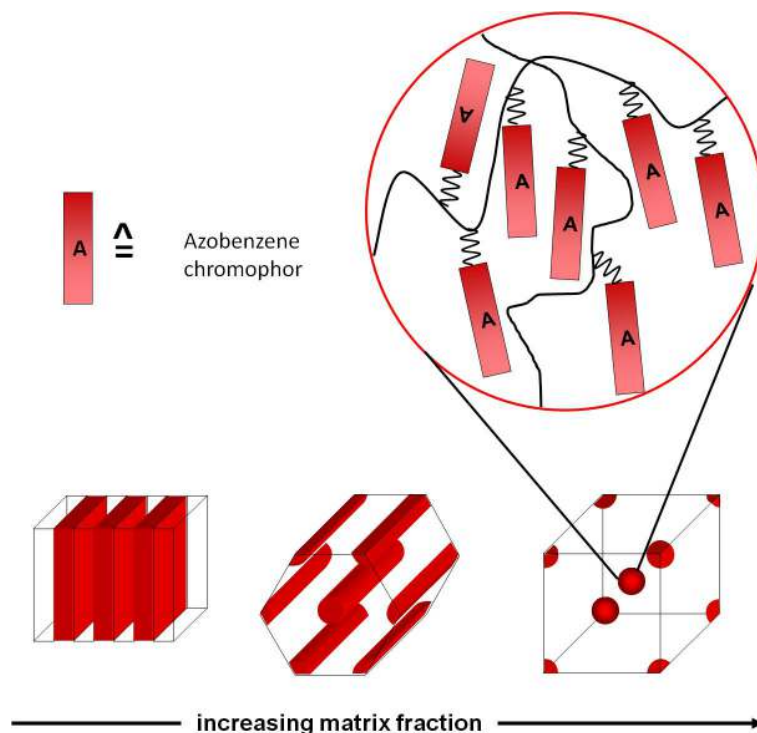
Figure 4.1: Concept for dilution of the optical density in an azobenzene-containing diblock copolymer with increasing matrix fraction while maintaining the cooperative effect in microphase separated confinements.

Azobenzene-containing block copolymer blends

To produce material samples with thickness in the millimeter range, the optical density has to be further diluted. This can be achieved by blending these azobenzene-functionalized diblock copolymers with the homopolymers of the respective optical inert block. The photoaddressable block copolymer is diluted with the matrix homopolymer resulting in a change of morphology from lamellae (via cylinders) to spheres. Upon further increase of homopolymer content the diameter of the sphere stays constant and only the distance between the spheres increases.[23,185] Schmidt *et al.* prepared thick transparent films (1.1 mm) by blending an azobenzene-containing block copolymer with PS homopolymer, allowing angular multiplexing of up to 80 holograms at the same spatial position, which were long-term stable at room temperature.[185]

Synthesis of azobenzene-containing block copolymers

For the synthesis of block copolymers with laterally attached azobenzene side-groups the different synthetic approaches that have been discussed in chapter 1.2.2 for side-group liquid crystalline block copolymers can be utilized. In the following only some examples highlighting the most prominent synthetic methods published in the literature for azobenzene-containing block copolymers are presented.

Up to now several group have been reporting the synthesis of azobenzene-containing block copolymers. In the first reports direct anionic polymerization of an azobenzene methacrylate and styrene was used for the synthesis of side-group liquid crystalline diblock copolymers. [90,91,186] The combination of anionic polymerization of the backbone and polymer analogous attachment of the azobenzene chromophore was reported for hydroxylated polyisoprene-*block*-polystyrene diblock copolymers around the same time.[115,187] More recent work using this approach was based on hydroxylated poly(1,2-butadiene)-*block* polystyrene[19,177] and poly(2-hydroxyethyl methacrylate)-*block*-poly(methyl methacrylate)[23] diblock copolymers functionalized with azobenzene side-groups. Lately the polymer analogous technique was applied in the preparation of an azobenzene-containing ABA triblock copolymer based on polystyrene-*block*-polybutadiene-*block*-poylstyrene.[21] In contrast to the above mentioned example, the polybutadiene segment was not hydroborated and subsequently oxidized. Here the double bonds were first epoxidized and then the attachment of the azobenzene moieties was carried out using amine functionalized chromophores. Azobenzene-containing block copolymers were also synthesized by controlled radical polymerization. Atom transfer radical polymerization (ATRP) is the most widely used technique for the synthesis of azobenzene-containing block copolymers incorporating methacrylic groups containing azobenzene monomers. Examples include diblock copolymers with PMMA segments,[102,188,189] PS segments,[106,190] PEG[83] or PPO[191] segments. Besides diblock copolymers also ABC,[103] ABC$_2$,[192] and ABA triblock copolymers,[193,194] as well as triarm star block copolymers[105] were reported.

4.2   Scope of this chapter

In this thesis novel azobenzene-containing block copolymers that can be block copolymer blends for the production of thick samples for volume holographic data storage were designed, synthesized, processed, and characterized. The aims within this chapter are:

1. implementation of polyhydroxystyrene as a functional monomer to achieve a high glass transition temperatures in resulting functionalized block copolymers,

2. synthesis of functionalizable block copolymers with poly(methyl methacrylate) as well as polystyrene as amorphous, optical inert matrix segments,

3. functionalization of these block copolymers to novel smectic azobenzene-containing block copolymers,

4. investigation of structure-property relations especially with respect to liquid crystalline phases,

5. processing of azobenzene-containing diblock copolymers into thin and thick photo-addressable samples suitable for volume holographic experiments,

6. holographic experiments on selected examples performed in cooperation with the Dr. Hubert Audorff and Prof. Lothar Kador (Bayreuther Institut für Makromolekül-forschung, BIMF) within the framework of SFB481

The azobenzene-containing homopolymers, copolymers for reference experiments and block copolymers were synthesized via the polymer analogous approach, shown in Figure 4.2. The combination of anionic polymerization for the polymer backbone and polymer analogous attachment of the desired side-group is well suited to prepare tailored block copolymers with high molecular weights, narrow molecular weight distributions, and allowing a broad variation of the attached side group. For instance series of block copolymers can be prepared based on the same block copolymer backbone but differing in the attached chromophore allowing to evaluate structure-property relations and to tune the properties. Here an example based on a functionalizable block copolymer with PMMA matrix (**4**) is shown. After anionic polymerization of the backbone and deprotection of the hydroxy function the azobenzene chromophores are attached featuring spacers with different lengths. The block copolymers **6a-6c** exhibit only a single spacer length each whereas **7a-7c** contain a random distribution of two different spacer length in the functional segment.

The respective homopolymer **III** and the copolymers with a random distribution of two different spacer lengths **IV-VI** were prepared as reference materials especially for the mesophase charaterization. The influence of these variations on the resulting mesophase and the holographic behavior were investigated.
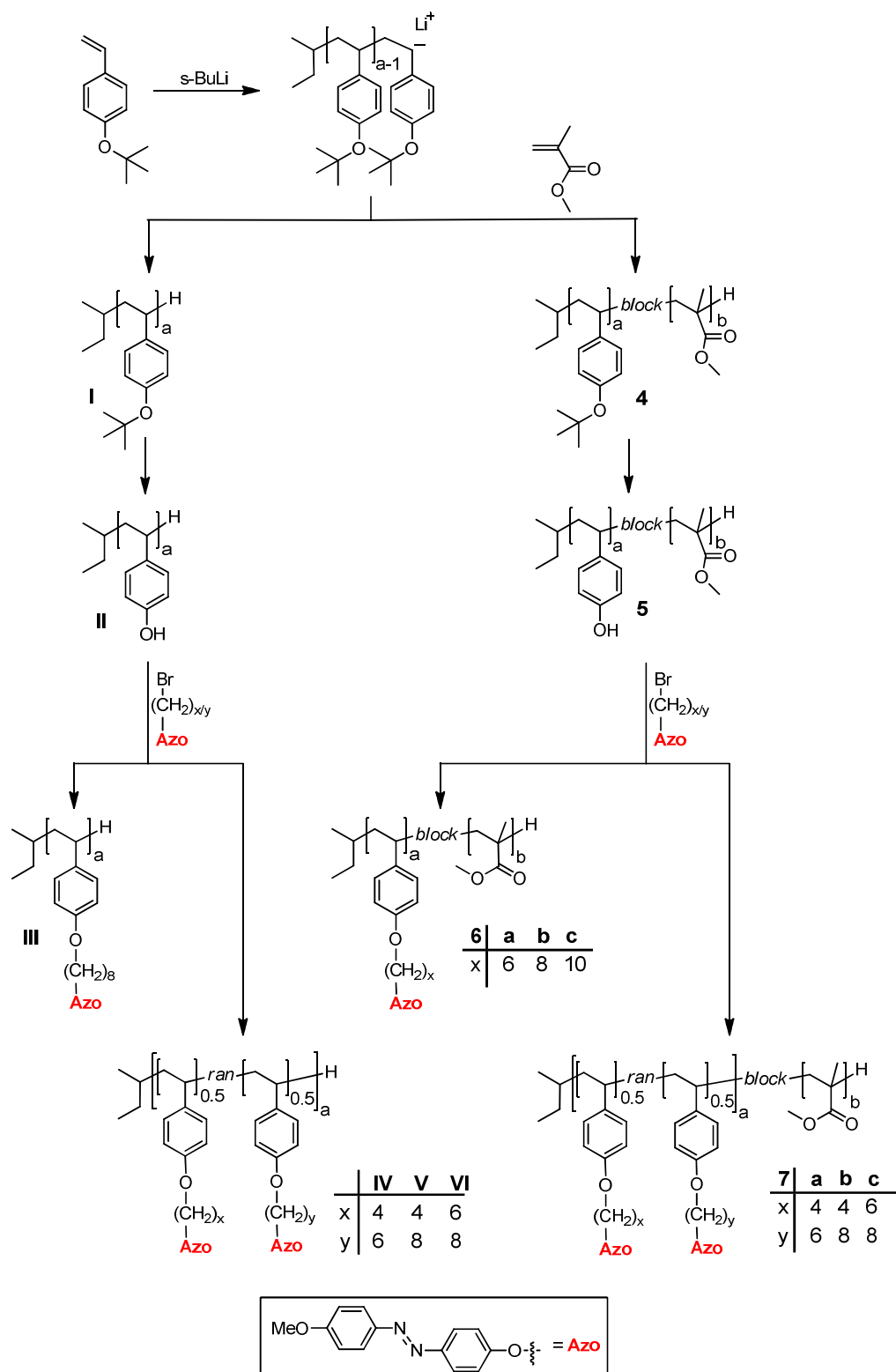
Figure 4.2: Overview of the methoxy azobenzene-functionalized target homo, copolymers and block copolymers that are discussed in this chapter.

III: Azobenzene-functionalized homopolymer and **IV - VI**: azobenzene-functionalized polymers with two different spacer lengths as reference materials for mesophase characterization;

6a - 6c: Azobenzene-functionalized block copolymers;**7a-7c**: azobenzene-functionalized block copolymers with a segment with two different spacer lengths.

57

4.3 Synthesis and characterization of functionalizable homopolymers and block copolymers

Different azobenzene-containing block copolymers were synthesized that are suitable for the block copolymer/homopolymer blend concept to adjust the optical density in thick samples mentioned above. All block copolymers contain a functionalizable segment that can be used for the attachment of the desired chromophore and an amorphous optical inert matrix. Different lengths of this functionalizable block were used throughout the series. For the optical inert matrix block two different monomers were used. One series contains PMMA as second block whereas the second series features a PS matrix. Both, PS and PMMA are known to exhibit good optical transparency making them ideal candidates in order to obtain non-scattering specimens. These two series were intended to be tested in different preparation approaches for holographic data storage materials.

4.3.1 Polyhydroxystyrene

For the synthesis of azobenzene-containing homo- and block copolymers a polymer analogous route is advantageously as described in chapter 1.2.2. For this approach, a functional group has to be present in each repeating unit of the polymer chain to allow further attachment reactions. Hydroxy groups are among others the most commonly used functions for polymer analogous functionalization with azobenzene moieties.[27,174] They allow attachment reactions via esterification or etherification.

A well established monomer for this approach is butadiene or isoprene. Anionic polymerization of butadiene in anhydrous cyclohexane with the use of 1,10-ethane-1,2-diyldipiperidine (DIPIP) results in 1,2-polybutadiene (1,2-PB) that can be further hydroborated and oxidized yielding an alcohol function. Subsequently, the desired side-group can be attached via a polymer analogous esterification.[18,177,195] Poly(2-hydroxyethyl methacrylate) (PEHMA) is another functional polymer used for the synthesis of azobenzene-containing materials.[28,29] Prior to the anionic polymerization it protection is required to avoid termination. For this purpose commonly silyl based protection groups are employed.[23,196] Due to the high reactivity of the protected HEMA derivatives, additives such as alkoxides or LiCl ensure the living character during polymerization.[23]

Within this thesis poly(4-hydroxystyrene) (PHS) was chosen as the functional block. Azobenzene-containing polymers based on this backbone exhibit higher glass transition temperatures (T_g) compared to functionalized polybutadienes. This is advantagously for holographic data storage materials because higher T_gs provide improved stability of the

inscribed gratings. The reactivity of phenolic groups is much higher compared to aliphatic hydroxy groups allowing to conduct a polymer analogous etherification reactions.

As mentioned above hydroxyl functions are unsuitable for direct anionic polymerization. Therefore, a protected hydroxystyrene monomer, namely, *tert*-butoxystyrene (*t*BS) was used. *t*BS can be polymerized in a living fashion resulting in poly(4-*tert*-butoxystyrene) (P*t*BS) without the use of additives.[59,197] Analogously to HEMA different silyl or methoxymethyl protection groups[198] are also possible for anionic polymerization, but *tert*-butoxystyrene has the advantage to be commercially available. The protection group of P*t*BS can be cleaved under acidic conditions yielding PHS.

As shown in Figure 4.3 anionic polymerization of *t*BS can be initiated with s-BuLi in THF at -70 °C and proceeds in a living fashion with in good control over molecular weight and molecular weight distribution.
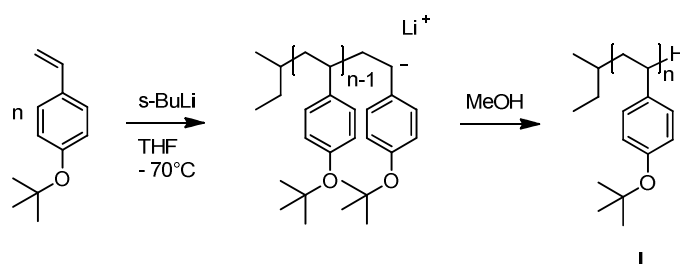
Figure 4.3   Anionic polymerization of *tert*-butoxystyrene resulting in P*t*BS (**I**).

During this thesis several batches of **I** were polymerized. Only few were prepared as a homopolymer batch. Most of the homopolymers were the precursor segments of block copolymers that were isolated prior to the addition of the second monomer. In the following section polymeranalogoues reaction procedures and characterization will be shown exemplarily on a homopolymer batch which resulted in an average number of repeating units of about $ru_{PtBS} = 1860$ (**I**). The determination of molecular weights of P*t*BS was carried out on a SEC setup with THF as eluent. The molecular weights were given with respect to a polystyrene calibration. Comparison of the molecular weights determined by SEC with the theoretical molecular weight calculated from the ratio of initiator and *tert*-butoxystyrene showed a good agreement of both values. Thus, the molecular weights as determined with respect to the polystyrene calibration were used for all further calculations. The average number of repeating units (ru_{PtBS}) was calculated from the number average molecular weight (M_n) determined by SEC.

Deprotection of **I** by acidic cleavage of the *tert*-butoxy group results in PHS (**II**). To this end, the homopolymer **I** was reacted with an large excess hydrochloric acid in THF at reflux over 12 h. Specially care had to be taken during the workup process to avoid crosslinking reactions of the resulting polyhydroxystyrene. In the first step, the acidic solution was precipitated in a very dilute sodium hydroxide solution (0.1 g/L) to neutralize the excess acid. Precipitated polymer was directly transferred into large excess of water adjusted to ph = 5 with pure acetic acid. Otherwise the precipitated polymer would agglomerate while binding a high fraction of water that was difficult to remove. After neutralization of the PHS it could be dried under high vacuum at room temperature. Typically, it was stored at -20 °C until further use. Storage at room temperature resulted in crosslinking.

Direct comparison with the protected precursor and quantification of the deprotection cannot be readily achieved. Determination of the molecular weight by size exclusion chromatography (SEC) measurements is not reliable possible due to the high polarity of the alcohol functions causing the polymer to interact with the column material. Because of the insolubility in CDCl$_3$, ^{1}H-NMR measurements are also impossible that precludes direct comparison with the protected form to confirm the quantitative cleavage of the protection group. Therefore, to quantify the cleavage of the protection group, **II** was reacted with acetyl chloride (Figure 4.4). The resulting polymer **VII** could be analyzed under the same conditions as the protected precursor polymer.
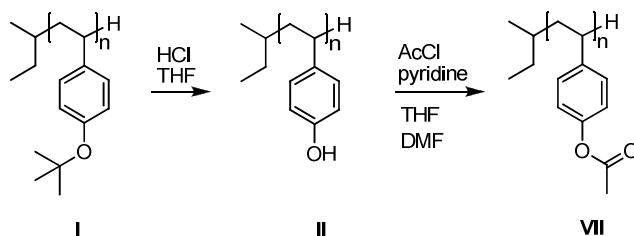
Figure 4.4:   Deprotection of **I** to **II** (PHS) and the acetylation of the hydroxy function yielding **VII**.

^{1}H-NMR traces of **I** and **VII** polymers are depicted in Figure 4.5. The signal for the *tert*-butoxy group at ppm = 1.25 is completely missing in **VII** (ru$_{PAcS}$ = 1860) whereas the signal for the acetoxy group can be detected at 2.25 ppm. Thus, ^{1}H-NMR analysis indicates quantitative conversion for both reactions, namely polymer analogous cleavage and acetylation.
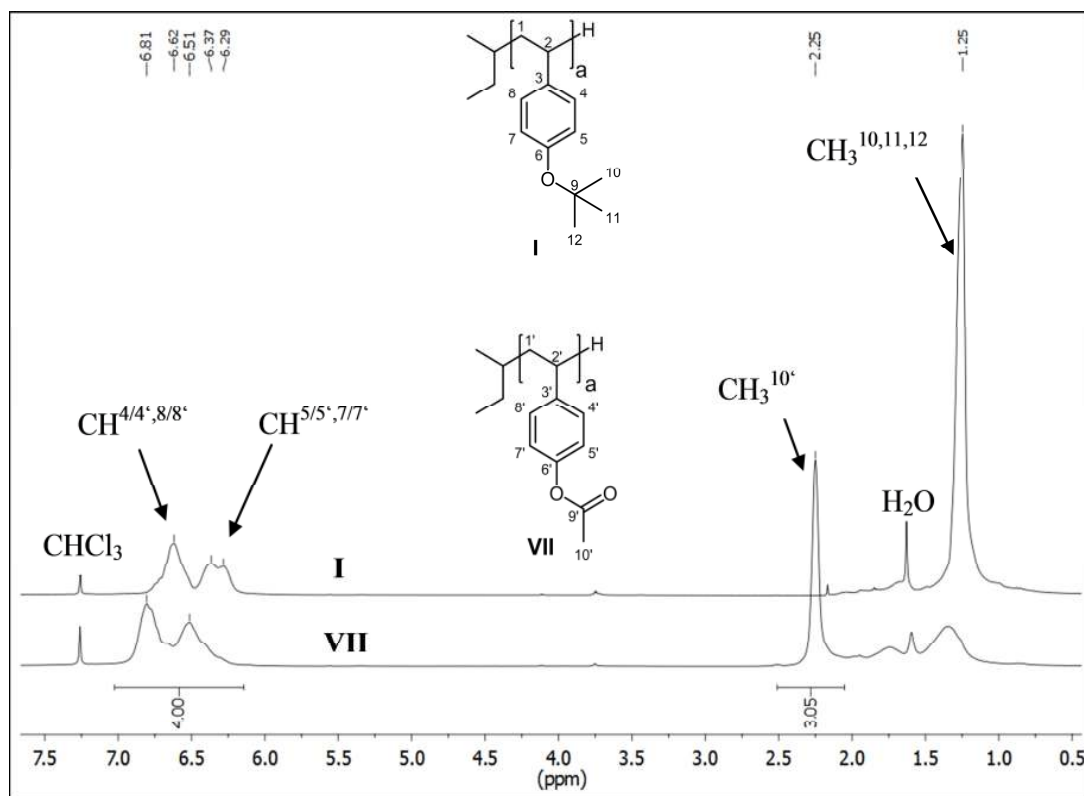
Figure 4.5: ^{1}H-NMR spectra of **I** P*t*BS (upper trace) and **VII** PAcS (lower trace) in CDCl$_3$.

SEC results of acetylated polymer **VII** (M$_n$: 271 kg/mol, M$_w$: 292 kg/mol, PDI: 1.07) revealed a slight reduction of molecular weight compared to **I** (M$_n$: 310 kg/mol, M$_w$: 333 kg/mol, PDI: 1.07). This might be attributed to the lower molecular weight and, therefore, to a lower hydrodynamic volume of the polymer.

Thermal analysis of all three polymers was conducted by differential scanning calorimetry (DSC) at a heating rate of 10 K/min under N$_2$ (Figure 4.6). The protected homopolymer **I** exhibit a glass transition at 105 °C and the hydroxyl functionalized homopolymer **II** a much broader and higher glass transition at around 133 °C. It should be noted that this transition shifts to higher temperatures with each heating cycle which might indicate an increased intermolecular formation of hydrogen bonds or side reactions. The glass transition of the acetylated homopolymer **VII** at 124 °C is shifted to higher temperature compared to **I** and is better defined than for **II**.
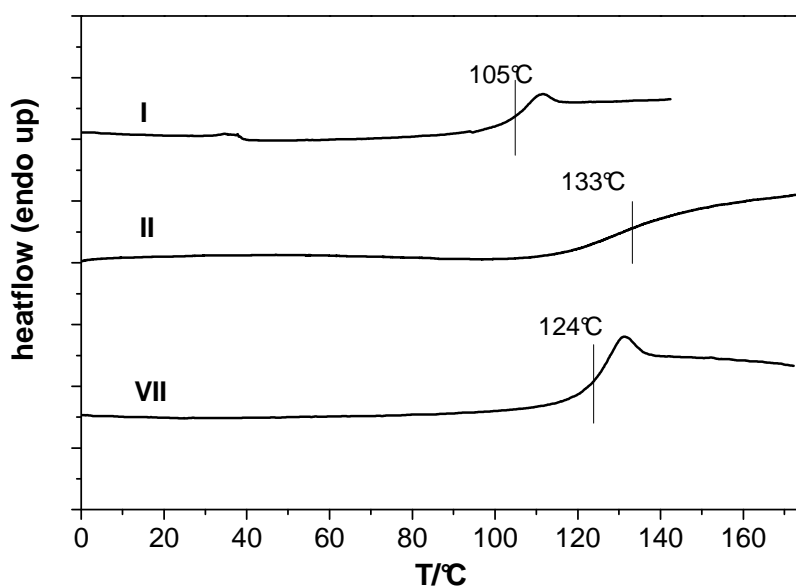
Figure 4.6:   Second heating thermograms of homopolymers **I**, **II** and **VII** at a heating rate of 10 K/min under N_2.

4.3.2   Synthesis and characterization of functionalizable block copolymers with PMMA matrix

All P*t*BS-PMMA block copolymers were prepared by sequential anionic polymerization of *t*BS and MMA in THF at -70 °C using s-BuLi as initiator (see Figure 4.7). LiCl was used as an additive to reduce side reactions of the ester group of the MMA during polymerization and 1,1-diphenylethylene (DPE) was added to reduce the reactivity of the P*t*BS anions. The polymerization reactor and the polymerization procedure described in chapter 3.4.3 were used. Typically, batches up to 50 g of diblock copolymer were prepared. A sample of each P*t*BS precursor **I** was isolated and terminated in dry methanol prior to the addition of MMA. The homopolymers **I** can be used to prepare azobenzene-functionalized homopolymers.
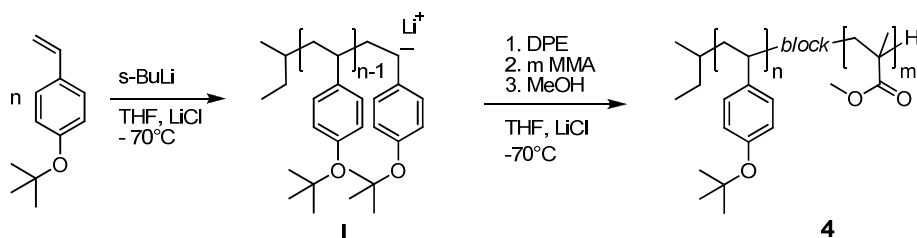
Figure 4.7:   Synthetic pathway to AB diblock copolymer P*t*BS-PMMA **4a - 4c** via precursor **I**.

Three different P*t*BS-PMMA block copolymers were prepared (**4a - 4c**). Their characteristic data are given in Table 4.1. The overall molecular weight of these polymers ranges from about $M_n = 28$ kg/mol for **4a** to $M_n = 128$ kg/mol for **4c** featuring an increasing length of both, the functionalizable block as well as the matrix block. The length of the functional segment increase from $M_n = 3.36$ kg/mol, ($ru_{PtBS} = 19$), for **Ia** in **4a** to $M_n = 43.13$ kg/mol, ($ru_{PtBS} = 245$), for **Ic** in **4c**. The different block length of the PMMA block were chosen to be tested for compatibility with the commercially available PMMA grades used for the later blend experiments (see chapter 4.7.2). All block copolymers exhibit a narrow molecular weight distribution (PDI ≤ 1.07). **4c** contains fractions of homopolymer **I** that was terminated during the addition of the styrene resulting the broadest molecular weight distribution (PDI $= 1.07$). This contamination can be removed after the deprotection step and will be discussed in the synthesis of the block copolymer series **6** (see chapter 4.5.3).

Table 4.1: Characteristic data of block copolymers **4a-4c** and their P*t*BS precursors **Ia-Ic**

block copolymer series 4	$M_n{}^{a)}$	$M_w{}^{a)}$	$PDI^{b)}$	$ru_{PtBS}{}^{c)}$	$ru_{PMMA}{}^{c)}$	$w_{PtBS}{}^{d)}$	$w_{PMMA}{}^{d)}$
	kg/mol					%	%
4a	28.3	29.3	1.04	19	241	12.2	87.8
precursor Ia	3.4	3.6	1.07	19	-	-	-
4b	72.9	76.0	1.04	61	455	11.8	88.2
precursor Ib	10.7	11.1	1.04	61	-	-	-
4c	128.3	137.0	1.07	245	878	32.1	67.9
precursor Ic	43.1	44.37	1.03	245	-	-	-

a) determined by SEC with polystyrene standards, RI-detection; b) polydispersity index (M_w/M_n); c) average number of repeating units determined by SEC and ^{1}H-NMR d) weight fraction determined by ^{1}H-NMR

The block copolymers **4a** and **4b** exhibit nearly the same block copolymer composition with a weight fraction of the functionalizable block of $w_{PtBS} \approx 12$ % but the block length of the latter polymer is three times higher. Therefore these polymers are expected to exhibit the same morphology after functionalization. The functionalizable block copolymer **4c** is used for most functionalization reactions with methoxy azobenzene chromophores. It contains a weight fraction of 32% of the functionalizable block. Functionalization of this segment with azobenzene chromophores will result in a weight fraction as high as 50%. This large segment with a total number of 245 repeating units should be beneficial for the holographic properties of thick samples prepared from blends of the azobenzene-functionalized block copolymer **6** with PMMA homopolymer (see

chapter 4.7). Due to this long azobenzene-containing block the spheres resulting from the blending should feature a larger radius favoring the cooperative effect of the chromophores (see chapter 4.1). The thermal properties were exemplarily determined for the diblock copolymer **4c** via DSC with a heating rate of 10 K/min exhibiting a glass transition temperature for the P*t*BS block of $T_{g(PtBS)} = 111°C$, which is a very similar value compared to the homopolymer, and $T_{g(PMMA)} = 129°C$ for the PMMA block, a value as it can be expected for anionically synthesized PMMA.

Synthesis and characterization of a functionalizable triblock copolymer with PMMA matrix

Poyl(*tert*-butoxystyrene)-*block*-poly(2-ethylhexyl methacrylate)-*block*-poly(methyl methacrylate) (PtBS-PEHMA-PMMA) triblock copolymer **9** was synthesized by the sequential anionic polymerization of *t*BS, EHMA and MMA in THF. LiCl was used as an additive for the controlled polymerization of the methacrylates and 1,1-diphenylethylene (DPE) was added to reduce the reactivity of the PtBS anions. The polymerization reactor and the polymerization procedure described in chapter 3.4.2 were used.
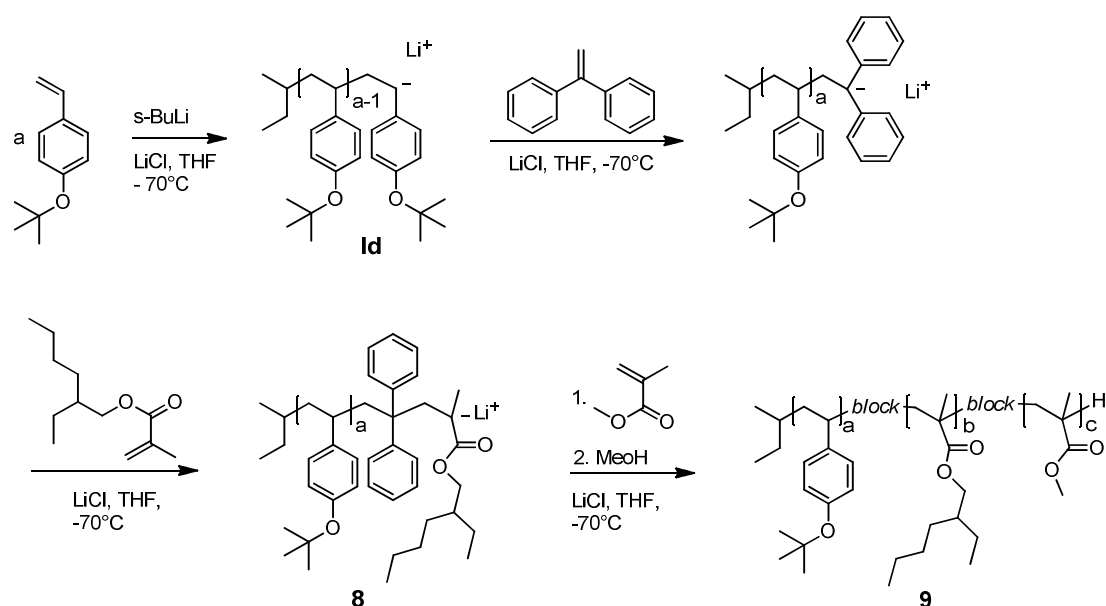
Figure 4.8:   Synthetic pathway to AB triblock copolymer **9** (P*t*BS-PEHMA-PMMA).

The triblock copolymer was characterized by SEC and the molecular weight was determined to $M_n = 54.3$ kg/mol with a PDI of 1.06. The repeating units in each segment were determined from the ^{1}H-NMR analysis to ru$_{PtBS} = 16$, ru$_{PEHMA} = 65$ and ru$_{PMMA} = 469$. This corresponds to the molar fractions of PtBS:PEHMA:PMMA 1:4.1:29.5.

4.3.3 Synthesis and characterization of functionalizable block copolymers with PS matrix

PtBS-PS block copolymers (**10**) were prepared by sequential anionic polymerization of *tert*-butoxystyrene and styrene in THF at -70 °C using s-BuLi as initiator (see Figure 4.9). The polymerization reactor and the polymerization procedure described in chapter 3.4.1 were used. A sample of each PtBS precursor (**I**) was isolated and terminated in dry methanol. Typically batches resulted up to 70 g of block copolymer.
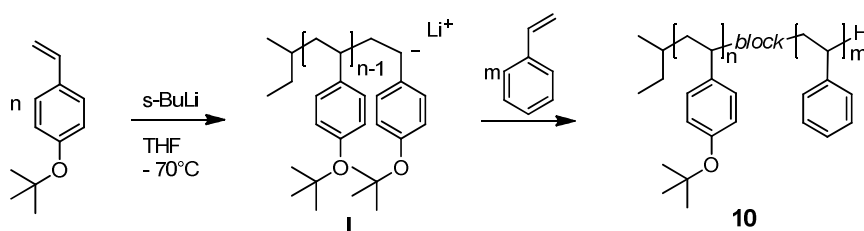
Figure 4.9:   Synthesis of PtBS-PS diblock copolymers **10a – 10e**.

Block copolymer **10a** was polymerized in a single reactor batch and features a long PtBS block (**Ie**) and was used for the preparation of thick samples by blending with PS homopolymer after functionalization with the azobenzene chromophores (see 4.7.2). As mentioned for **4c**, the long PtBS block was chosen to result in larger spheres in blending experiments.

One block copolymer series (**10b-10e**) was prepared with increasing length of the PS segment using the combinatorial approach as described in chapter 3.4.1. Exemplary, thermal characterization of **10a** revealed only one glass transition in the range of 106 °C. Since the glass transitions temperature of both blocks are expected to be in the same range (105°C-111°C) one can assume that they are superimposed.

Table 4.2: Characteristic data of P*t*BOS-PS block copolymers **10a-10e** and their P*t*BS precursors **Ie** and **If**

block copolymer series 9	M_n [a] kg/mol	M_w [a] kg/mol	PDI [b]	ru_{PtBS} [c]	ru_{PS} [c]	w_{PtBS} [d] %	w_{PS} [d] %
10a	99.2	102.7	1.04	188	651	32.8	67.2
precursor Ie	*33.1*	*34.1*	*1.03*	*188*			
10b	158.6	162.7	1.03	48	1407	5.5	94.5
10c	143.4	147.1	1.02	48	1340	5.7	94.3
10d	92.2	94.9	1.03	48	630	11.5	88.5
10e	66.8	69.2	1.04	48	445	15.4	84.6
precursor If	*8.5*	*8.8*	*1.04*	*48*	*-*	*-*	*-*

a) determined by SEC with polystyrene standards, UV-detection; b) polydispersity index (M_w/M_n); c) average number of repeating units determined by SEC and ^{1}H-NMR d) weight fraction determined by ^{1}H-NMR

4.4 Synthesis of reactive azobenzene chromophores

Two different types of mesogenic azobenzene chromophores were used in the syntheses of photo-addressable polymers. The first derivatives **Azo1-4** consists of methoxy azobenzene derivatives with variable spacer length which open the possibility to be attached to the polymer backbone via an ether linkage. The mesogenic methoxyazobenzene chromophores **Azo1-4** were chosen because the resulting homopolymers are known to exhibit smectic mesophases when attached to a polystyrene based backbone.[87] Furthermore, only spacer with an even number of methylene units were used because the resulting side-group liquid crystalline polymers are known to exhibit the higher phase transition temperatures compared to the odd-membered ones.[87] The second chromophore type is a cyanoazobenzene derivative **Azo5** that was attached via an ester linkage to the polymer backbone.

Azo	1	2	3	4
x	4	6	8	10
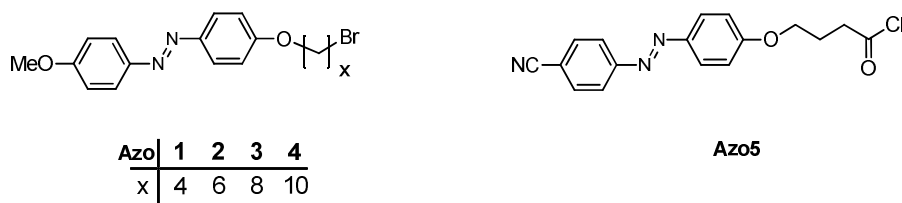
Figure 4.10:   Azobenzene mesogens **Azo1-4** and **Azo5** used in this thesis.

Holographic properties of these liquid crystalline azobenzene-containing polymers should be investigated as part of this work. The methoxy functionalization of the azobenzene

core is much more chemically and thermal stable compared to the cyano group in **Azo5**. Especially the thermal stability is advantagous during the annealing processes that are required during the preparation of holographic samples (details are given in chapter 4.7).

The alkyl dibromide spacer that result in ether linkages to the chromophore as well as the polymer were chosen because of its commercial availability in different lengths allowing an easy variation of the spacer length. The respective azobenzene-containing block copolymers were used to reveal structure-property relations with respect to the influence of the spacer length on the holographic performance.

The cyano derivative **Azo5** was chosen because these chromophores are known to result in high refractive index modulation in the holographic experiments.[184] On the other hand the cyano group is prone to side reaction at elevated temperatures under basic conditions during the synthesis. Therefore, the chromophores synthesis and spacer attachment had to be optimized. **Azo5** is attached to the PHS block via an esterification reaction utlizing the reactive acid chloride that is known to result in a high degree of conversion in the polymer analogous reaction.[19,29]

The synthesis of the azo chromophores **Azo1-4** was carried out similar to the procedure described by Imrie *et al.*[87] whereas the synthesis of **Azo5** was carried out according to procedures as developed in our group.[199] A schematic overview of the synthetic pathway is given in Figure 4.11. The series **Azo1-4** was prepared in a two step synthesis. The first step is an azo coupling of phenol with the diazotized 4-methoxy aniline resulting in the hydroxy functionalized chromophor **Azo1a**. The second step is the introduction of the bromine functionalized spacer in the chromophore via a Williamson ether synthesis. Utilizing a large excess of the dibromo-compound reduces the probability of the spacer to react with two azobenzene chromophores. Due to phenolic hydroxy function potassium carbonate is sufficient as a base for the deprotonation. In this series excess alkyldibromide had to completely removed, otherwise coupling reactions between the polymer chains during the polymer analogous reaction can occur.

The synthesis of **Azo5** starts in a similar manner with the azo coupling yielding the cyano functionalized azo chromophor **Azo5a** and the attachment of the butyric acid ethyl ester spacer. After subsequent saponification of **Azo5b** the carboxylic acid derivative **Azo5c** is converted into the acid chloride **Azo5**. The specific reaction conditions of the saponification, e.g. the solvent mixture (ethanol/THF/water) and stirring at room temperature ensure that the formed potassium salt of the carboxylic acid precipitates and, thus, protects the product from further side-reactions, e.g. the hydrolysis of the cyanogroup into an aromatic acid. The chromophor **Azo5** is connected to the polymer backbone via a polymer analogous esterification.
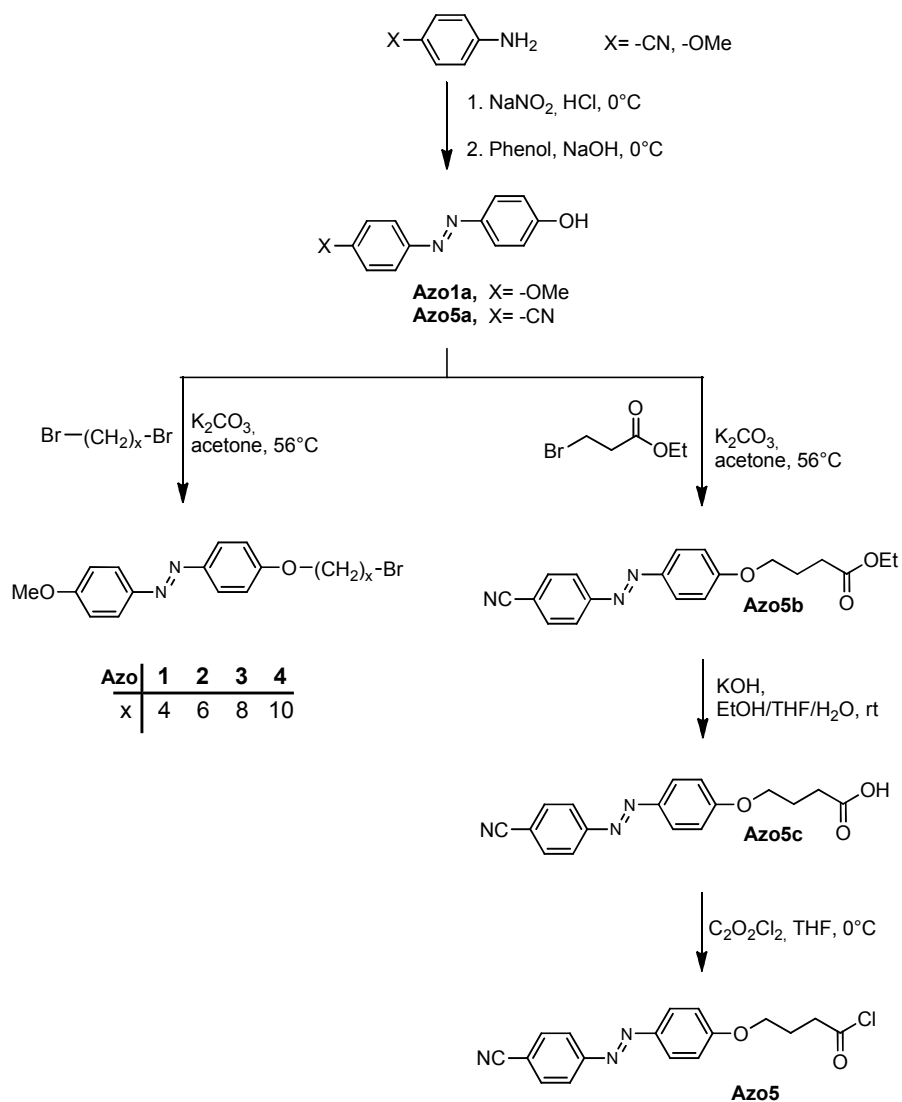
Figure 4.11:   Synthetic pathway for azobenzene chromophores **Azo1 - Azo5.**

68

4.5 Azobenzene-functionalized homopolymers, copolymers and block copolymers

4.5.1 Synthesis and characterization of methoxy azobenzene-functionalized homopolymer

All methoxy azobenzene-containing polymers were functionalized using the same procedure. Therefore the synthesis and polymer characterization is described and discussed in detail using **III** as a typical example. For the characterization of the polymers a set of polymer analytic techniques was used. Molecular weight and molecular weight distribution was analyzed by SEC. The degree of conversion was determined by IR spectroscopy and ^{1}H-NMR.

The azobenzene-functionalized homopolymer **III** was prepared as a reference material for the mesophase characterization of the respective block copolymers. It was synthesized via a two step polymer analogous reaction of the anionically synthesized polymer **Ic** (Figure 4.12). The homopolymer **Ic** was deprotected by acidic cleavage of the *tert*-butoxy group according to the procedure described in chapter 4.3.1. The azobenzene chromophore **Azo3** was attached to the polymer backbone **IIc** in a polymer analogous etherification reaction yielding **III**.
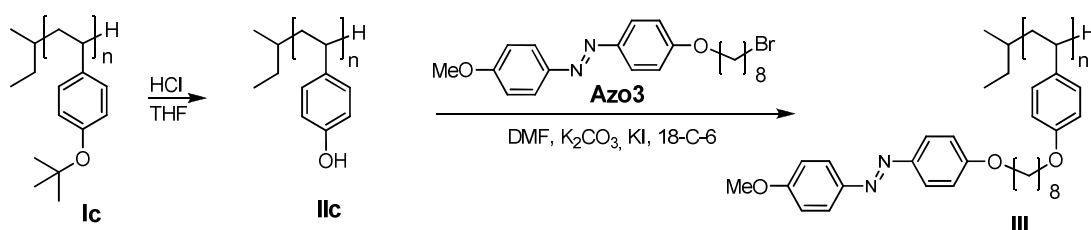
Figure 4.12:   Polymer analogous deprotection of **Ic** and attachment of chromophore **Azo3** to the precursor **IIc** via etherification resulting in methoxy azobenzene-containing homopolymer **III**.

The Williamson ether synthesis was carried out in anhydrous N,N-dimethylformamide (DMF) at 110 °C with potassium carbonate as base and potassium iodine and 18-crown-6 as catalyst.

In an ether synthesis, as a S_N2 reaction, the reactivity is enhanced when carried out in polar, aprotic solvents. Aceton is commonly employed as demonstrated in chapter 0 for the attachment of the spacers to the azobenzene units. Here it turned out to be unsuitable, which is attributed to the insufficient solubility of the resulting polymers **III**. Therefore N,N-dimethylformamide DMF was used at a reaction temperature above 100 °C. The reaction was carried out under inert atmosphere and in anhydrous solvents, otherwise an extensive darkening of the solvent was observed and hard to remove side products in the

oligomeric range were detected. The reactivity of the alkyl bromides was enhanced by the addition of a catalytic amount of KI and 18-crown-6 whereas the latter acts as a phase transfer catalyst. KI undergoes a halide exchange with the bromide of the chromophores yielding a more reactive iodide. Potassium carbonate was sufficient as a base due to the phenolic alcohol function as already mentioned for the synthesis of the chromophores. Typically reaction times about 24 h were used. Determination of an endpoint of the polymer analogous attachment proved difficult because the molecular weights determined by SEC did not necessarily correspond to the degree of conversion in a linear fashion thus, the reaction could not be monitored directly. The only viable solution was a micro work up of every sample drawn during the reaction and determination of the degree of conversion by ^{1}H-NMR.

After stopping the reaction, a first precipitation of the functionalized polymer **III** in water was performed in order to remove the inorganic salts. Further purification was achieved by repeated precipitating a 10 wt% polymer solution in methanol. Typically, this procedure resulted in a rest chromophore content of less than 2% as determined by SEC measurements (UV-trace).

SEC traces of **III** and the precursor **Ic** performed on the SEC setup with 0.25 wt% of an electrolyte are given in Figure 4.13. **III** showed a molecular weight of $M_n = 120$ kg/mol and a molecular weight distribution of $M_w/M_n = 1.05$ based on polystyrene standards. The molecular weight of the functionalized polymer is nearly threefold compared to its precursor polymer **Ic** ($M_n = 43$ kg/mol) and thus in the expected range. The monomodal and narrow molecular weight distribution confirmed that the polymer analogous reaction proceeded without significant coupling between polymer chains (Figure 4.13).
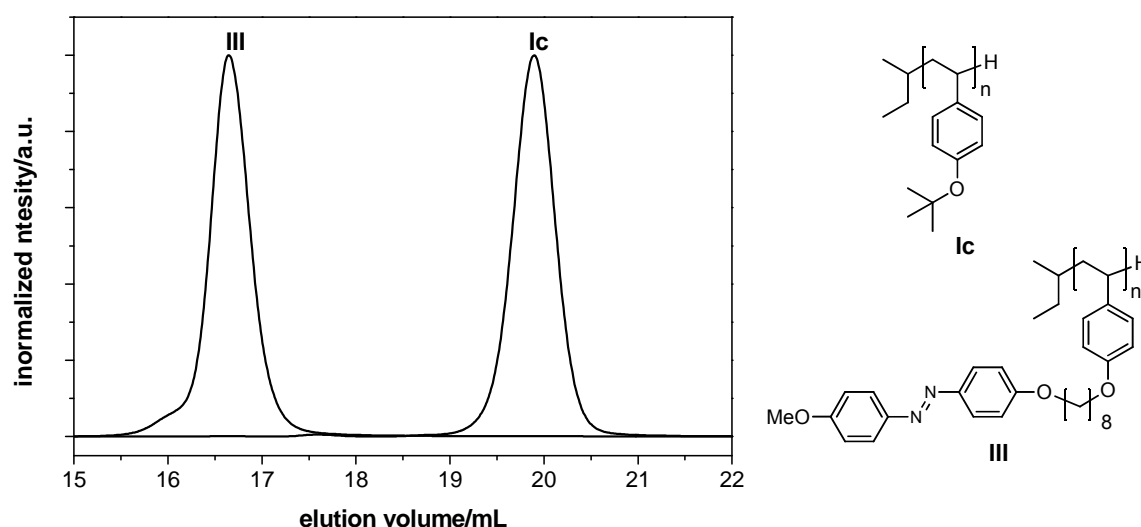
Figure 4.13: SEC traces of methoxy azobenzene-containing homopolymer **III** and its precursor polymer **Ic** (eluent: THF + 0.25 wt% tetrabutylammonium bromide).

Determination of degree of conversion

The FT-IR-spectra provide a first indication on the degree of conversion (DC). In Figure 4.14 the spectra of **III** and the deprotected precursor **IIc** are presented. The hydroxy functionalized polymer **IIc** shows a broad signal corresponding to the phenolic $\tilde{v}$(O-H) at a wavenumber 3295 cm^{-1}. In the azobenzene-functionalized homopolymer **III** this signal is no longer apparent indicating a high degree of conversion within the error margins. Other specific signals can be compared as well, although it has to be noted that both spectra cannot be normalized on one common signal. Thus, the intensity in the specific signals is difficult to determine. The strong signal at 1250 cm^{-1} for the **III** originates from the (C-O) stretching vibrations of the arylalkyl ethers of the spacer connections to the backbone as well as the chromophore. The intensity of the (C-H) stretching vibrations of the alkyl bonds at 2930-2830 cm^{-1}, the (C=C) stretching vibrations of the aryl bonds at 1600 cm^{-1} as well as a signal at of 841 cm^{-1} indicating a 1,4-disubstituted benzene ring are increased due to the attachment of the chromophore.
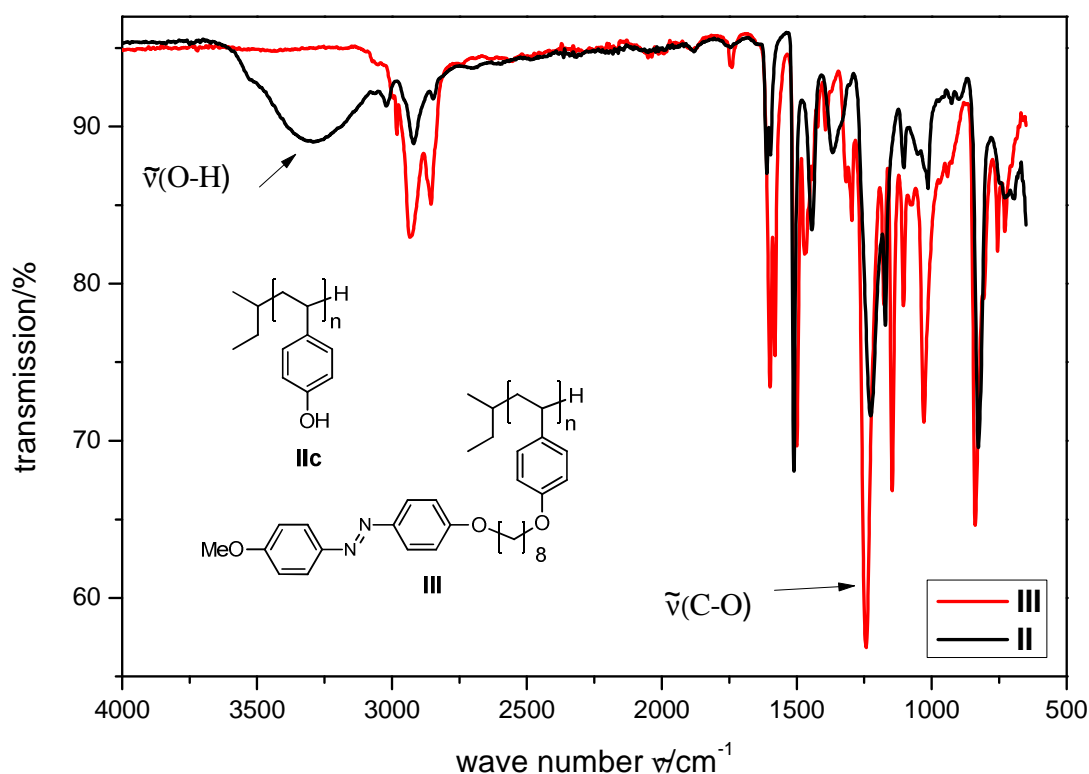
Figure 4.14: Infrared (IR) spectra of methoxy azobenzene-containing homopolymer **III** (red) and hydroxyl functionalized precursor **IIc** (black).

^{1}H-NMR spectra of the functionalized polymer were recorded using CDCl$_3$ as solvent (Figure 4.15). Sometimes 1-3 drops of DMF-d$_7$ had to be added to ensure full solubility

of the polymer. The degree of conversion was determined using the integrals of the aromatic protons of the azo moiety (CH$^{1-4}$) compared to the integrals of the aromatic protons (CH^{a,b}) of the backbone. Signals in polymer ^{1}H-NMR spectra tend to broaden, therefore the specific signal cannot always be separated.
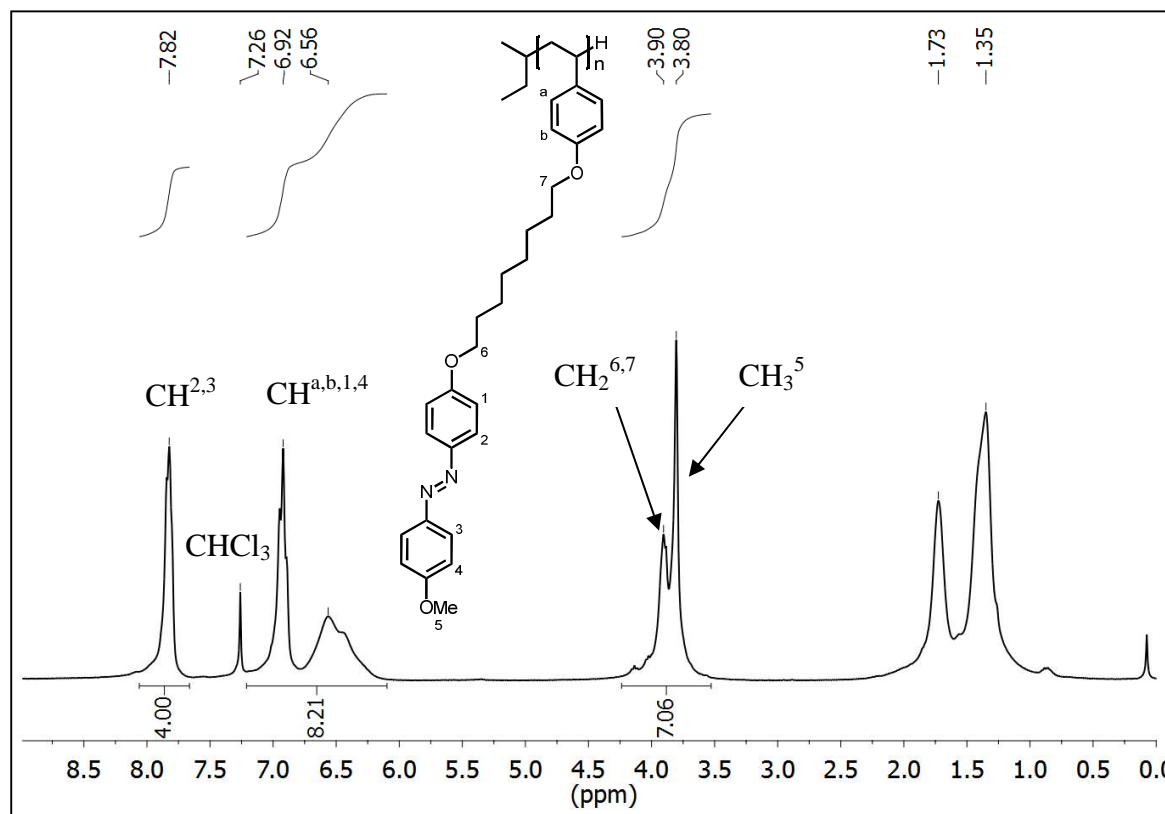
Figure 4.15: ^{1}H-NMR spectra of methoxy azobenzene-containing homopolymer **III** in CDCl$_3$ with signals used for calculation of degree of conversion.

In homopolymers like **I** the signal of CH$_3^{5}$ + CH$_2^{6,7}$ can be used as a distinct signals sole for the attached chromphore and amounts to an integral of I(CH$_3^{5}$+CH$_2^{6,7}$) = 7H. In contrast, for the block copolymers with PMMA matrix discussed later, this signal is not separated from the O-CH$_3$ signal of the PMMA, therefore another set of signals has to be used.

The aromatic protons CH^{2,3} near to the azo-group are normally detected without any overlap with signals arising from the backbone. Therefore this integral was used as reference [^{1}H-NMR (CDCl$_3$-d$_1$): δ(ppm)= 7.6-8.0 (m, 4H, CH^{2,3})]. The signals of the other four aromatic protons of the azobenzene [^{1}H-NMR (CDCl$_3$-d$_1$): δ(ppm)= 7.2-6.7 (m, 4H, CH^{1,4})] partly cover with signals of the aromatic protons of the backbone [^{1}H-NMR (CDCl$_3$-d$_1$): δ(ppm)= 6.8-6.1 (m, 4H, CH^{a,b})] forming the integral [I(CH^{1,4}+CH^{a,b})] which is needed for the determination of the degree of conversion. Assuming the integral

for a 100 % conversion $[I(CH^{1,4}+CH^{a,b})_{100}]$ have to yield a value 8H, the degree of conversion (DC) can be calculated with Equation (4.1).

$$DC = \frac{I(CH^{a,b})_{100}}{I(CH^{1,4}+CH^{a,b})-4H} \cdot 100 \qquad (4.1)$$

In the case of **III** the conversion was determined as

$$DC = \frac{4H}{8.21-4H} \cdot 100 \approx 95\ \% \qquad (4.2)$$

The degree of conversion determined with this method is not overly exact. Small deviations in the limits of the integrals result in significant changes in the calculated degree if conversion.

4.5.2 Synthesis and characterization of methoxy azobenzene copolymers with two different spacer lengths

As will be discussed in chapter 4.6, the azobenzene-containing homopolymer **III** shows a smectic mesophase with a high degree of order. This high order is on the one hand envisioned to be beneficial to the stability of holographically inscribed gratings but on the other hand might be detrimental to the writing time. To disturb the packing of the mesogens and thus to lower the order of the resulting mesophase, azobenzene-containing polymers with a random distribution of two different spacer lengths were prepared (Figure 4.16). It has been shown that in functional polymers where the chromophores contains spacers of varying lengths, the clearing temperatures were lowered with respect to the values of the respective polymers with a single spacer length. Thus, the degree of order of the smectic phase should be lowered.[87]

The syntheses were performed in a similar manner as described for the functional polymer **III** (see Figure 4.16). Apart from the polymeric educt **Ic** (ru$_{PtBS}$ = 245), the homopolymer **Ie** (ru$_{PtBS}$ = 188) was functionalized as well. Both polymers were deprotected under acidic conditions. For the polymer analogous attachment of the chromophores a 1:1 feed ratio of the two different spacers was used. For all spacer length the same reactivity is to be expected and an attachment equal to the feed ratio can be assumed. The composition cannot be determined since the spacers differ only in the number of methylene units. Applying ^{1}H-NMR analysis, the respective signals of those cannot be clearly distinguished. Three combinations of chromophore mixtures were utilized to obtain functional polymers **IV-VI** featuring a random distribution of chromophores with varying spacer lengths (x/y) along the backbone, namely **Azo1** and

Azo2 (4 and 6 methylene units), **Azo1** and **Azo3** (4 and 8 methylene units), and **Azo2** and **Azo3** (6 and 8 methylene units).
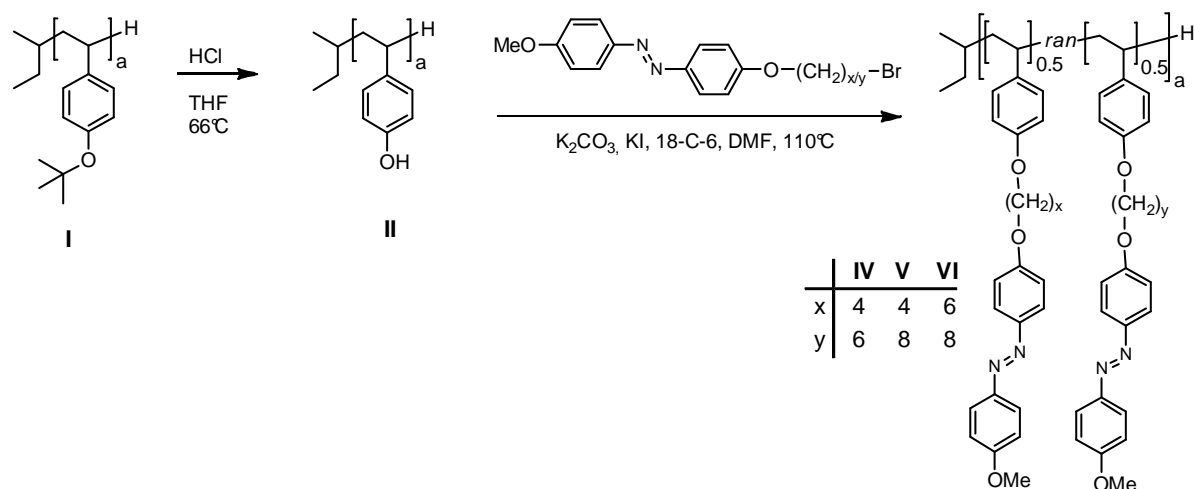
Figure 4.16: Synthesis of methoxy azobenzene-containing polymers with random distribution of two different spacers **IV-VI**.

The characteristic data of the functionalized polymers **III - VI** are summarized in Table 4.3. The degree of conversion (DC) is 85 % with the exception of **VI**. For this polymer a DC of only 75% was determined. The theoretical molecular weights (M_n(th)) were calculated using the repeating units determined for the precursor polymers **I**, the degree of conversion and the molecular weight of an average functionalized repeating unit. It is evident that the polystyrene calibration results in an apparent molecular weights that overestimates the molecular weight by a factor 1.2-1.8. The polymers with the random distribution of two different spacers exhibit a noticeable higher molecular weight than the polymer **III** featuring a single spacer length. The highest deviation to the theoretical value is exhibited by the functionalized homopolymer **VI** with the lowest degree of conversion and the highest fraction of remaining hydroxyl functions, respectively. For the polymers based on the same homopolymer **Ic** ($ru_{PtBS} = 245$) **III, IV** and **VI** the molecular weight, as determined by SEC, ranges from $M_n = 120$ kg/mol for **III** to $M_n = 161$ kg/mol for **VI**. The molecular weight of the functionalized polymer is three- to fourfold compared to its precursor polymer **Ic** ($M_n = 43$ kg/mol). The lower molecular weight of **V** is due to the homopolymer **Ie** ($ru_{PtBS} = 188$, $M_n = 33$ kg/mol) used for this polymer. All functional polymers (**III – VI**) show a narrow molecular weight distribution (PDI ≤ 1.06) indicating that side reactions did not occur. It has to be noted that **IV** contains significant amount of contamination with low molecular weight chromophore (5.8 % UV-signal intensity in SEC) that could not be removed regardless of the purification procedure.

Table 4.3: Characteristic data of methoxy azobenzene-containing copolymers with two different spacer
lengths **IV-VI** compared to **III**

homo-polymer	$x^{a)}$	$y^{a)}$	$DC^{b)}$	$M_n^{c)}$	$M_w^{c)}$	$PDI^{d)}$	$M_n(th)^{e)}$	$ru_{PtBS}{}^{f)}$
			%	kg/mol			kg/mol	
III	8	-	95	120	126	1.05	95.6	245
IV	4	6	85	123	131	1.06	91.2	245
V	4	8	86	87	92	1.06	72.8	188
VI	6	8	75	161	169	1.05	89.0	245

a) number of methylene units in spacer; b) degree of conversion, determined by ^{1}H-NMR; c) determined by SEC (eluent: THF + 0,25 wt% electrolyte), molecular weight with respect to narrowly distributed polystyrene standards, UV-detection; d) polydispersity index; e) theoretical molecular weight calculated from repeating units and degree of conversion; f) average number of repeating units determined for respective homopolymer **I**

4.5.3 Synthesis of functionalized block copolymers with PMMA matrix

Similar to the aforementioned homopolymers, the azobenzene-containing block copolymers were designed to be used in holographic experiments unveiling structure property relationships, e.g. the temporal evolution of refractive index modulation with the spacer length. Likewise, only chromophores with spacers with an even number of methylene units were used in this series but increasing from x= 6 to x= 10 (**Azo2** to **Azo4**). PHS was used as a functionalizable block instead of poly(1,2-butadiene)[19,177] or poly(2-hydroxy-ethyl-methacrylate)[23,185] to achieve a higher glass transition temperature and a smectic mesophase of the azobenzene-containing block.

Figure 4.17 shows the reaction sequence yielding the functionalized diblock copolymers with PMMA matrix. The diblock copolymer **4c** (PtBS$_{245}$-b-PMMA$_{878}$; M_n = 128 kg/mol; M_n = 137 kg/mol; PDI = 1.07, described in chapter 4.3.2) was deprotected under similar conditions as described in chapter 4.3.1. The resulting diblock copolymer **5c** was functionalized in a polymer analogous etherifications with the methoxy azobenzene chromophore series **Azo2-4** resulting in the diblock copolymers **6a-6c**. Compared to the synthetic procedure for the polymer analogous attachment of the mesogens for the homopolymer **III** (described in detail in chapter 4.5.1) for block copolymer systems the reaction time had to be increased. Due to the difficulties in monitoring the reaction progress discussed chapter 4.5.1 the optimal reaction times had to be determined experimentally. Typically 24 h to 48 h to were used because for longer reaction times no increase in the degree of conversion could be determined although the molecular weight distribution tended to broaden with increasing reaction time.

As discussed for the azobenzene-containing homopolymers mixtures of two different spacer lengths were used to disturb the packing of the mesogens resulting in a lower ordered mesophase. The same combinations as in chapter 4.5.2 were chosen for the

functionalized block copolymers with PMMA matrix yielding the diblock copolymers **7a-7c**.
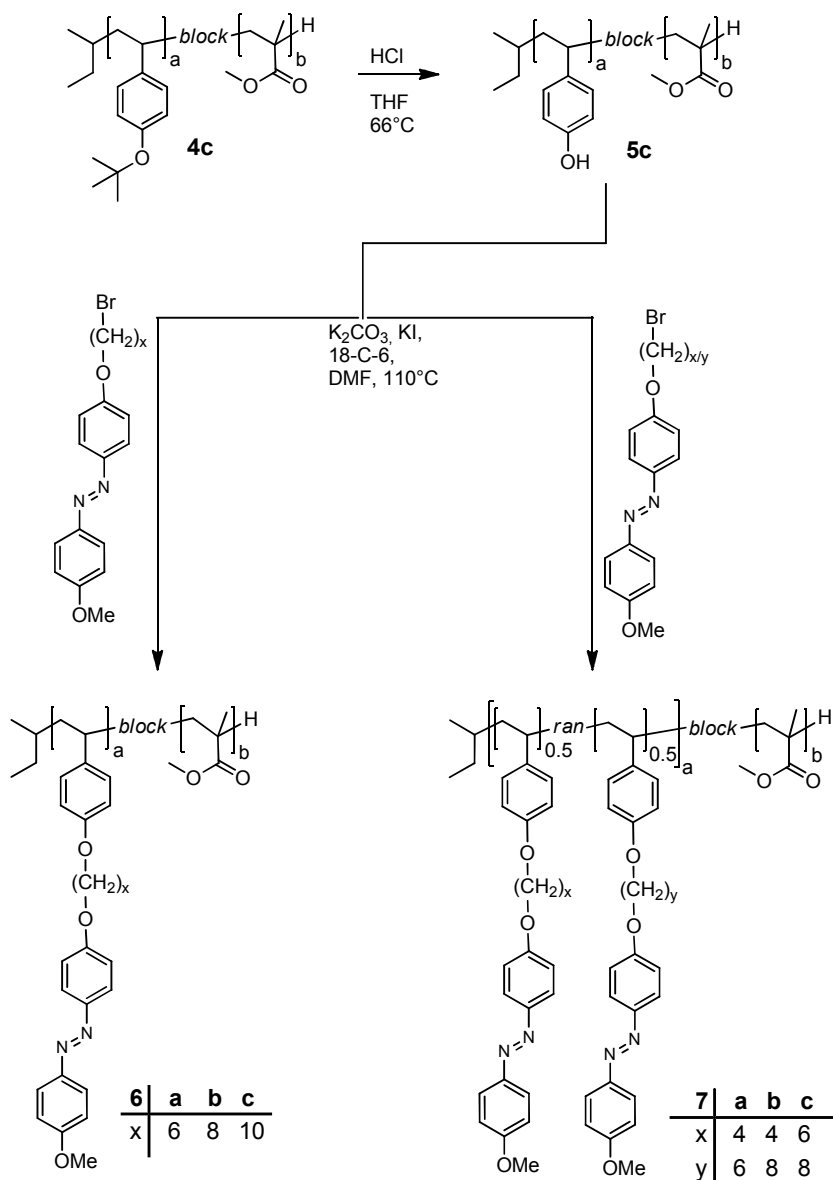
Figure 4.17:   Synthesis of the methoxy azobenzene-containing diblock copolymer series **6** and **7**.

An exemplary SEC curve is given in Figure 4.18 for the functionalized diblock copolymer **6a** with the respective diblock copolymer **4c** and the precursor homopolymer **Ic**. It is evident that the functionalized block copolymer **6a** exhibits a narrower molecular weight distribution than **4c.** As mentioned in chapter 4.3.2 the block copolymer **4c** contains a fraction of homopolymer **Ic** or block copolymer with a shorter PMMA block that might be due to termination during the addition of the MMA. This undesired contamination could be removed or at least drastically reduced after the deprotection of the hydroxy group. Due to its higher polarity the homopolymer **II** (PHS) is much better soluble in MeOH compared to the block copolymer **5c** with the non-polar PMMA

segment. Thus the purification was achieved by repeated precipitation of the deprotected block copolymer **5c** in MeOH.
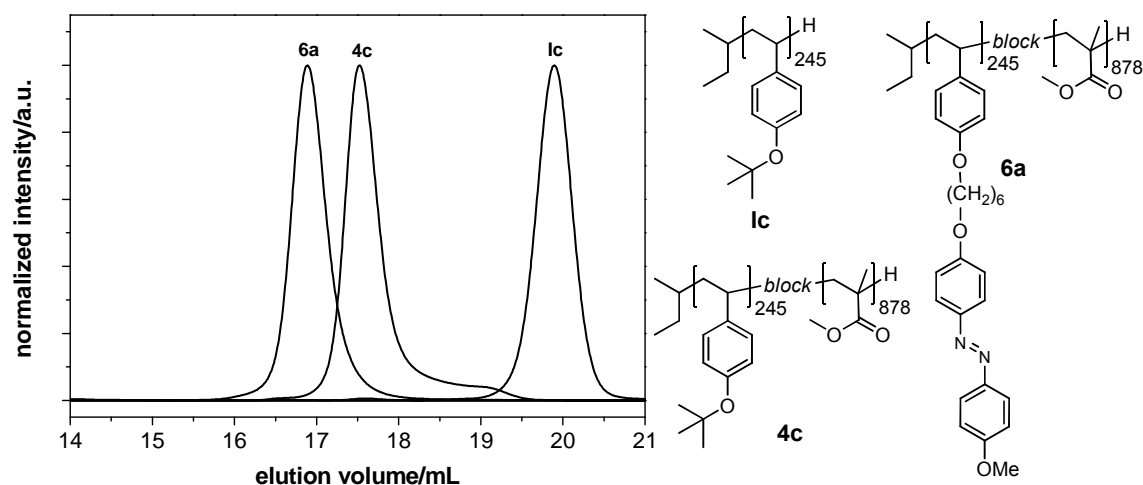
Figure 4.18:   SEC elugrams of the methoxy azobenzene-containing diblock copolymer **6a** and the precursors **4c** and **Ic**.

Characteristical data of all block copolymers in series **6** and **7** are given in Table 4.4. All functionlized block copolymer exhibit a narrow molecular weight distribution (PDI $\leq$ 1.07). This indicates that the polymer analogous attachment of the side-groups proceeded without a significant amount of side reactions causing inter chain crosslinking. In the series **6a-6c** the molecular weight increases with increasing spacer length from $M_n = 249$ kg/mol for **6a** to $M_n = 293$ kg/mol for **6c**. The degree of conversion in this series is similar for all three members (DC $\geq$ 86 %). Series **7a-7c,** with a mixture of different spacer lengths, shows a slightly decreased degree of conversion (82 % $\leq$ DC $\leq$ 84 %) and the molecular weight is in the range of $M_n = 291$ kg/mol for **7a** to $M_n = 300$ kg/mol for **7b.** The slightly higher molecular weight of **7b** might be due to detectable amount of inter chain coupling reactions that are evident in the broader molecular weight distribution. Overall, for the series **7a-7c** higher molecular weights are determined than expected from the results of **6a-6c**. The determination by SEC results in higher molecular weights compared to the theoretical molecular weights (M_n(th)) by the factor 1.3-1.5 for series **6** whereas it is slightly higher for series **7** with a factor of 1.6-1.7. This observation might be due to the increased hydrodynamic radius that might arise from the mixing of different spacers. The same trend was also observed for the respective homopolymers (see chapter 4.5.1). This observation cannot be explained. Compared to the diblock copolymer **4c** ($M_n = 128$ kg/mol) the increase in apparent molecular weight ranges from 1.9 fold for **6a** to 2.5 fold for **7b**. The weight fractions of all diblock copolymers in series **6** and **7** are in the range of 50 – 54 wt%. Similar weight fractions are

expected because for all of these polymers the same precursor block copolymer **4c** was used and differences are only due to the spacer length of the attached chromophores and the degree of the polymer analogous attachment.

Table 4.4: Characteristic data of methoxy azobenzene-containing block copolymer series **6** and **7** with PMMA matrix based on **4c** ($PtBS_{245}$-$PMMA_{878}$)

block copolymer series 6 and 7	x^a	$y^{a)}$	$DC^{b)}$	$M_n{}^{c)}$	$M_w{}^{c)}$	$PDI^{d)}$	$M_n(th)^{e)}$	$w_{Azo}{}^{f)}$	$ru_{Azo}{}^{g)}$	$ru_{PMMA}{}^{g)}$
			%	kg/mol			kg/mol	%		
6a	6	-	90	249	261	1.05	186	53	245	878
6b	8	-	86	266	282	1.06	187	54	245	878
6c	10	-	86	293	306	1.04	193	54	245	878
7a	4	6	82	291	304	1.04	177	50	245	878
7b	4	8	84	300	322	1.07	181	51	245	878
7c	6	8	84	297	309	1.04	184	52	245	878

a) x,y: number of methylene units in spacer; b) degree of conversion, determined by ^{1}H-NMR; c) determined by SEC (eluent: THF + 0,25 wt% electrolyte), molecular weight with respect to narrowly distributed polystyrene standards, UV-detection; d) polydispersity index; e) theoretical molecular weight calculated from repeating units and degree of conversion; f) weight fraction of the azobenzene-containing block, determined by ^{1}H-NMR; g) average number of repeating units determined for diblock copolymer **4c**

4.5.4 Synthesis of functionalized block copolymers with PS matrix

In addition to the methoxy azobenzene-functionalized block copolymers with PMMA matrix containing different spacer length (**6**), analogous polymers based on the diblock copolymer **10a** ($PtBS_{188}$-PS_{651}; M_n = 99 kg/mol; M_n = 102 kg/mol; PDI = 1.04, described in chapter 4.3.3), a block copolymer with a PS matrix, were synthesized yielding **12a** and **12b** (see Figure 4.19). In this case only spacer length of eight and ten methylene units were used (**Azo 3**, **Azo4**). The polymer analogous functionalization was carried out in the same manner as described and discussed in chapter 4.5.1. The protection group of the diblock copolymer **10a** was cleaved under acidic conditions yielding the hydroxy functionalized block copolymer **11a.** The attachment of the methoxy azobenzene chromophores **Azo3** and **Azo4** was carried out via a polymer analogous etherification reaction.
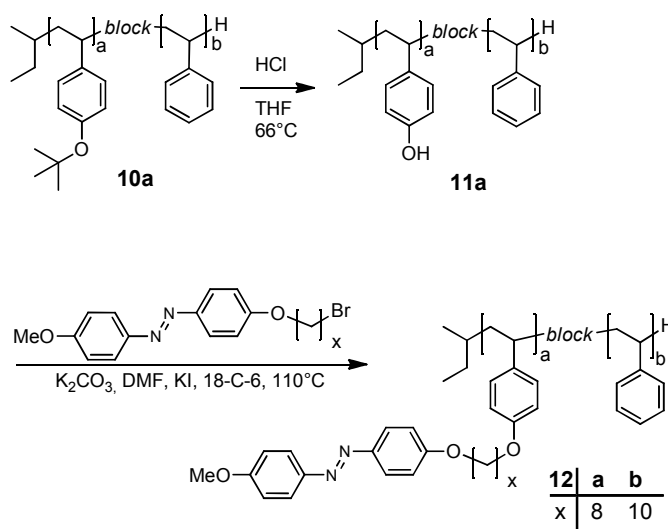
Figure 4.19:   Synthesis of methoxy azobenzene-containing diblock copolymer **12a** and **12b**.

The determined molecular weights are $M_n = 234$ kg/mol for **12a** and $M_n = 243$ kg/mol for **12b** and both block copolymers exhibit a narrow molecular weight distribution (PDI = 1.04). The difference in molecular weight is due to the different spacers used and in the expected range. This is contrast to the degrees of conversion determined by ^{1}H-NMR. Although the degree of conversion for **12b** is lower (63 %) than for **12a** (87 %) the molecular weights exhibit the expected difference. In comparison to the theoretical molecular weights (M_n(th)) the values determined by SEC are overestimated by a factor 1.8 for **12a** and 2.2 for **12b**. The resulting weight fraction of the azobenzene-containing block is again around 50 wt% for both polymers and therefore similar to the results obtained for the diblock copolymer series **6**. The higher calculated weight fraction of the azobenzene-containing block for **12a** arises from the lower degree of conversion determined for **12b**.

Table 4.5: Characteristic data of methoxy azobenzene-containing AB diblock copolymers with PS matrix based on **10a** (PtBS$_{188}$-PS$_{651}$)

block copolymer series 12	x	DC$^{a)}$ %	M_n $^{b)}$	M_w $^{b)}$	PDI $^{c)}$	M_n(th)$^{e)}$	w_{Azo} $^{f)}$	ru_{Azo} $^{g)}$	ru_{PS} $^{g)}$
			kg/mol			kg/mol	%		
12a	8	87	234	244	1.04	146	54	188	651
12b	10	63	243	253	1.04	134	51	188	651

a) number of methylen units in spacer; b) degree of conversion, determined by ^{1}H-NMR; c) determined by SEC (eluent: THF + 0,25 wt% electrolyte), molecular weight with respect to narrowly distributed polystyrene standards, UV-detection; d) polydispersity index; e) theoretical molecular weight calculated from repeating units and degree of conversion; f) weight fraction of the azobenzene-containing block, determined by ^{1}H-NMR; g) average number of repeating units determined for diblock copolymer **10a**

4.5.5 Synthesis and characterization of cyano azobenzene-containing block copolymers

Cyano azobenzene-containing block copolymers with PMMA matrix

Cyano azobenzene-functionalized block copolymers **13** were prepared based on the functionalizable diblock copolymers **4a** (PtBS$_{19}$-b-PMMA$_{241}$; $M_n = 28.3$ kg/mol; $M_n = 29.3$ kg/mol; PDI $= 1.04$) and **4b** (PtBS$_{61}$-b-PMMA$_{455}$; $M_n = 72.9$ kg/mol; $M_n = 76.0$ kg/mol; PDI $= 1.04$). As described in chapter 4.3.2 theses two block copolymers feature nearly the same block ratio but different number of repeating units. Prior to the attachment of the chromophores the block copolymers **4a** and **4b** were converted into the hydroxy functionalized block copolymers **5a** and **5b** by acidic cleavage of the *tert*-butoxy group. The chromophore **Azo5** was chosen because cyano azobenzene derivatives showed promising results in previous holographic experiments regarding their maximum refractive index modulation, writing times and stability of the inscribed gratings.[29] The chromophore attachment was carried out in a polymer analogous estherification yielding the functionalized block copolymers **13a** and **13b** (see Figure 4.20). These reactions using activated acid chloride normally proceed in very high yields.[19,29,117] The reaction was carried out in anhydrous THF while using pyridine as scavenger for the resulting HCl.
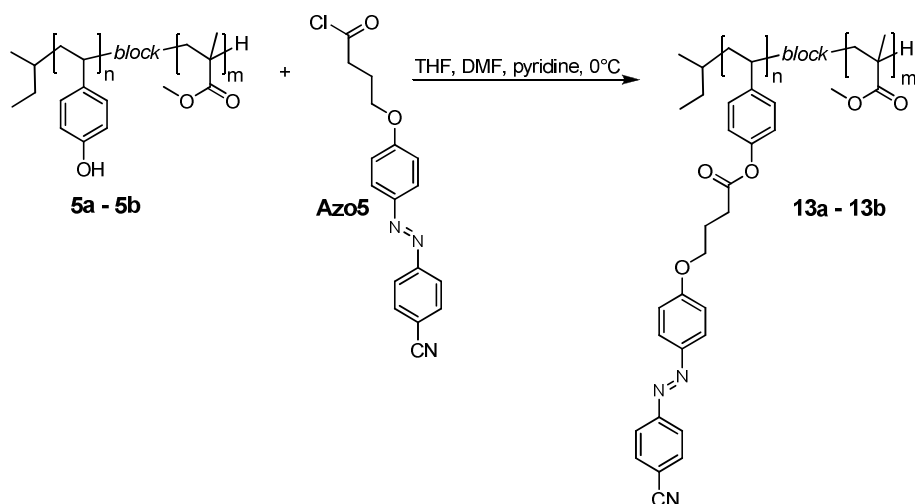
Figure 4.20: Reaction scheme for the synthesis of cyano azobenzene-containing diblock copolymer **13a** and **13b.**

The characteristic data of **13** are given in Table 4.6. The resulting molecular weights are $M_n = 31$ kg/mol for **13a** and $M_n = 79$ kg/mol for **13b** while both block copolymers exhibit a narrow molecular weight distribution (PDI ≤ 1.1). These molecular weights determined by SEC are in good agreement with the theoretical values. It has to be noted that the

molecular weight distribution is broader compared to results obtained for the other block copolymers where the chromophores were attached to the polymer backbone via an ether bond (see chapter 4.5.3). If an esterification reaction is used for the attachment of the chromophores, typically a coupling of polymer chains to a certain degree is observed. Therefore the respective molecular weight distributions are not as narrow as determined for the polymers functionalized by a polymer analogous etherification (compare Table 4.4). Because of these results the polymer analogous etherification reaction was the preferred attachment reaction in this thesis.

Table 4.6: Characteristic data of cyano azobenzene-containing AB diblock copolymers **13** with ester linkage and PMMA matrix

block copolymer series 13	$DC^{a)}$	M_n $^{b)}$	M_w $^{b)}$	PDI $^{c)}$	$M_n(th)^{e)}$	w_{Azo} $^{f)}$	ru_{Azo} $^{g)}$	ru_{PS} $^{g)}$
	%	kg/mol			kg/mol	%		
13a	89	30.6	33.6	1.10	32.1	23	19	241
13b	84	78.7	84.1	1.07	84.46	22	61	455

a) determined by SEC, molecular weight with respect to polystyrene standards, UV-detection; b) polydispersity index; c) degree of conversion of polymer analogous reaction, determined by ^{1}H-NMR; d) weight fraction of azobenzene-containing block; e) average number of repeating units determined for precursor polymer **5a** and **5b**

Cyano azobenzene-containing triblock copolymer with a PEHMA middle block and a PMMA matrix

The cyano azobenzene-functionalized triblock copolymer **15** is based on **9**. The protection group of the precursor was removed via hydrolysis prior to the attachment of the chromophores. Due to the very low weight fraction of the P*t*BS segment a higher excess of hydrochloric acid had to be used than usual to yield an acid concentration in the reaction mixture that resulted in cleavage of the protection group.

The activated acid **Azo5** was used in a polymer analogous esterification yielding the azobenzene-functionalized polymer **15** (see Figure 4.21). The synthesis was carried out as described for **12**.
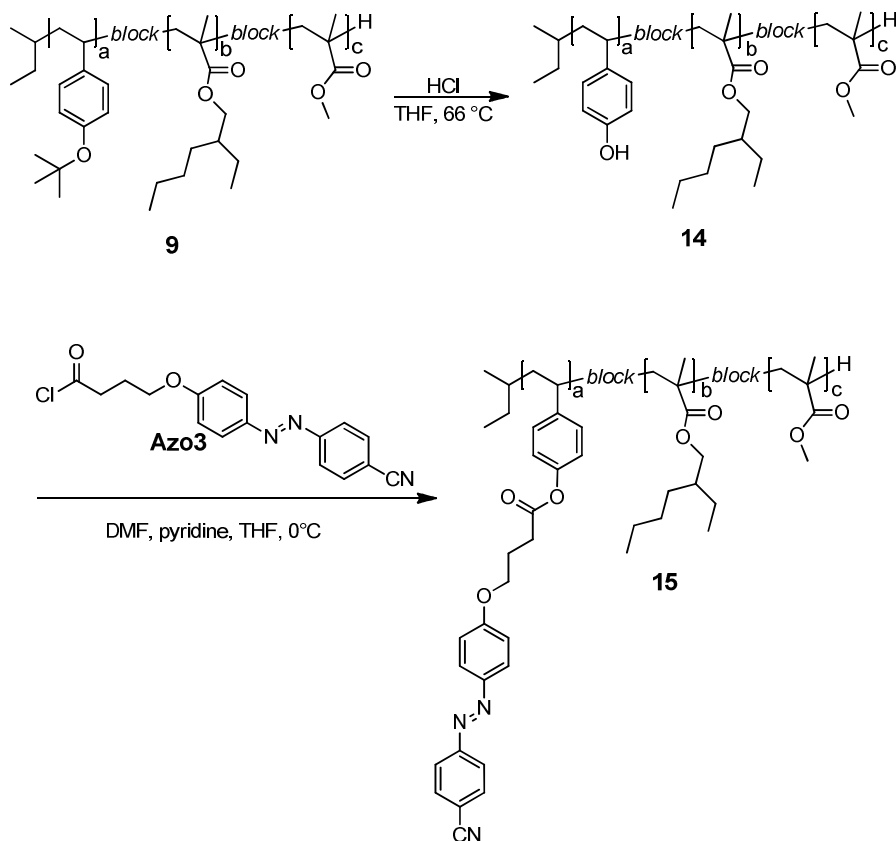
Figure 4.21:   Synthesis of cyano azobenzene-containing triblock copolymer **15**.

The molecular weight of **15** was analyzed by SEC and determined to $M_n = 51.2$ kg/mol with a molecular weight distribution of PDI = 1.08. Thus no increase in the molecular weight is apparent compared to the precursor block copolymer **9** ($M_n = 54.3$ kg/mol). The negative deviation of **15** compared to **9** is within the uncertainty of measurement of the SEC setup.

The degree of conversion was determined to DC = 46 % by ^{1}H-NMR. It has to be noted that the determination of the degree of conversion for this polymer is nearly impossible (i.e. the error is high) due to the low molar fraction of the polyhydroxy segment respectively the of the azobenzene segment. Because of the low functional content the integral in the 1H-NMR spectra carry a low signal to noise ratio. The weight fraction of the azobenzene-containing block was calculated to 6.4 wt%. This determination is strongly dependent on the degree of conversion and therefore carries the same inherent error.

4.6   Solid state properties of azobenzene-containing polymers

The azobenzene-containing homopolymers, copolymers and block copolymers with laterally attached azobenzene-containing side-groups were analyzed regarding their thermal behavior. Thermogravimetric analysis (TGA) was performed to evaluate the thermal stability of the upper compounds, which is mainly necessary to determine the temperature range in which phase transitions by differential scanning calorimetry (DSC) can be investigated. DSC was conducted at a scanning rate of 10 K/min under N_2 atmosphere up to 190 °C.

The glass transition temperatures (T_g) given were determined at the temperature of half heights of the respective transition. The liquid crystalline to isotropic transition temperature (clearing temperature T_{cl}) represent the peak maximum of the transition.

In addition to DSC experiments, liquid crystalline mesophases were also investigated by polarized optical light microscopy (POM) and X-ray diffraction (XRD). In the latter a temperature controlled Guinier diffractometer system with Cu-Kα ($\lambda = 1.541$ Å) was used. Powder diffractogramms were recorded using capillary tubes with a diameter of 1.5 mm or 2.0 mm. The samples were first heated 10-20 °C above T_{cl} for 1 h and afterwards annealed for 1 h at $T_g < T < T_{cl}$ prior to the measurements.

4.6.1   Methoxy azobenzene-containing homopolymer III
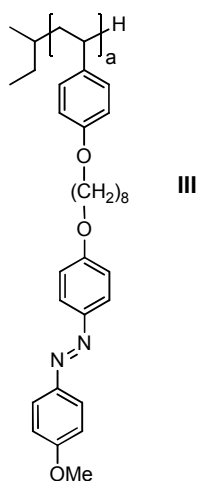
The thermal behavior of homopolymer **III,** as analyzed by DSC, exhibits two detectable transitions (Figure 4.22). Upon heating the polymer undergoes from a glassy state ($T_g = 92$ °C) into a liquid crystalline phase with a clearing transition at $T_{LC-i} = 156$ °C. The enthalpy of the LC to isotropic transition is $\Delta H = 15.5$ J/g. Upon cooling the isotropic-liquid crystalline transition shows a small supercooling of 7 °C and the glass transition is

shifted by 5 °C. This shift in the transition temperatures is very low for side-group liquid crystalline polymers, often much higher temperature differences are observed.[195]
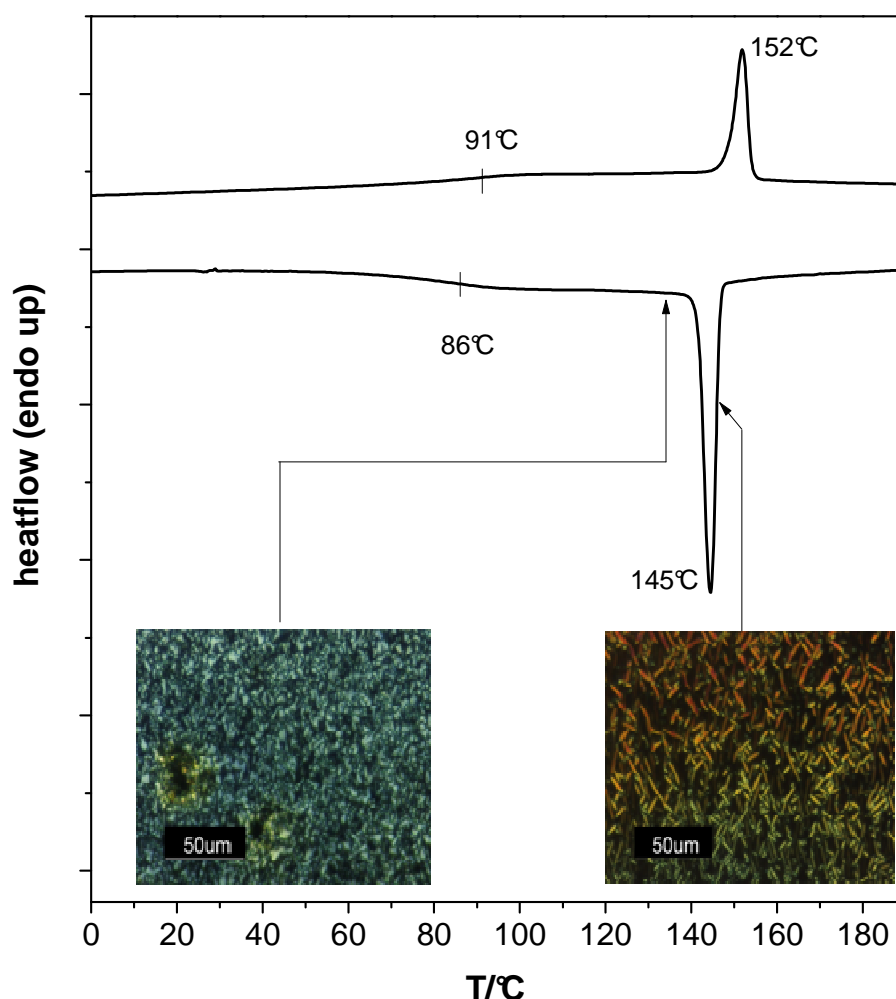
Figure 4.22:   DSC traces of second heating and cooling at 10 K/min under N_2 with insets of POM images between crossed polarizers of methoxy azobenzene-containing homopolymer **III** on cooling from the isotropic phase. *right*: bâtonnets; *left*: Schlieren texture.

Further confirmation of the liquid crystal phase was established through polarized optical light microscopy (POM). On cooling from the isotropic phase, that appeared black, birefringent textures became apparent. For **III** at first bâtonnets formed that developed into Schlieren textures on further cooling (Figure 4.22). The latter texture did not change upon further cooling and was still apparent after cooling below the glass transition temperature. Thus a glass with a liquid crystalline order was obtained.

In general, the Schlieren texture cannot be clearly attributed to a specific liquid crystalline phase, i.e. nematic as well as smectic mesophases may exhibit this structure. In contrast

the development of bâtonnets at the beginning of texture formation is a proof for a smectic mesophase. A nematic mesophase is expected to exhibits initially a droplets.[200]

Powder X-ray diffraction (XRD) pattern of **III** was recorded in the liquid crystalline state at a temperature of 120 °C using a Guinier setup to gain further information on the liquid crystalline phase. In this case, the powder was first heated above the clearing temperature (170 °C) for 1 h to densify the material in the sample tube. Prior to the XRD measurement the samples was annealed for another hour above the glass transition temperature at 120 °C at which the measurement was conducted.

In the wide angle range the diffractogram shows, a broad halo around $\theta = 10°$ that is attributed to the amorphous polystyrene backbone. At small angles two reflection are detected. A sharp reflection at $\theta = 1.48°$ followed by a stronger reflection at $\theta = 2.95°$. These signals can be attributed to the first-order and second-order reflection of a smectic layer distance because they match equation (4.3) that is the necessary condition for the existence of a smectic mesophase.

$$\theta_{100} : \theta_{200} \approx 1 : 2 \tag{4.3}$$

The layer spacing (d) that corresponds to these reflections can be calculated using the Bragg equation (4.4) and is determined to 29.9 Å.

$$\lambda = 2d_{hkl} \sin\theta \tag{4.4}$$
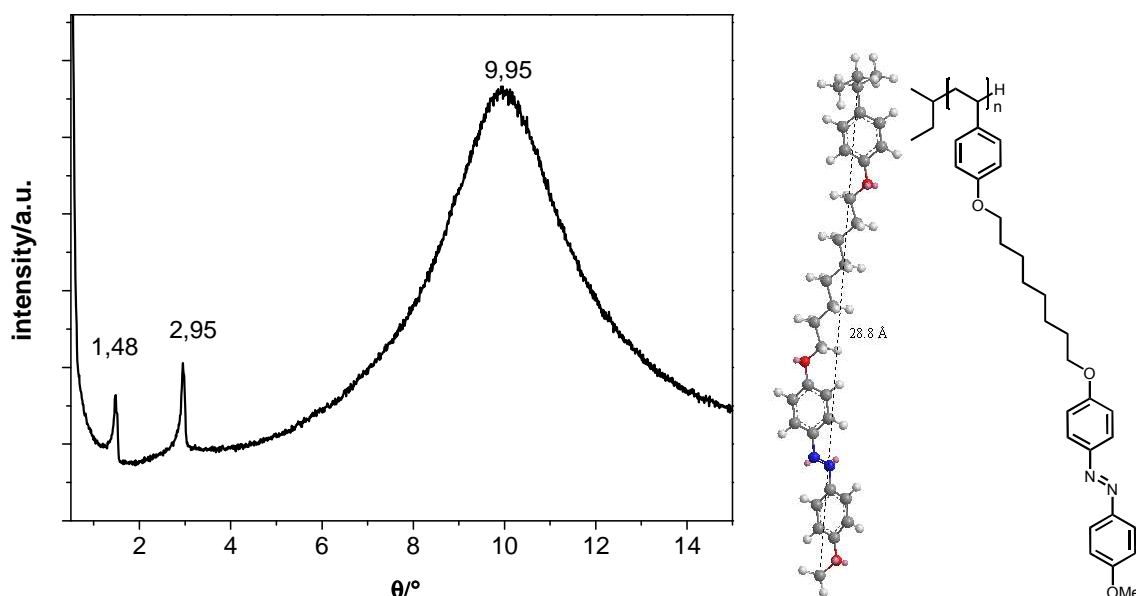
Figure 4.23: XRD diffractogram of methoxy azobenzene-containing homopolymer **III** at 120 °C (*left*); model and chemical structure of **III** (*right*).

For side-group liquid crystalline polymers several possibilities for the formation of a smectic A mesophase exist.[86,201] Figure 4.24, *right* shows four possible structures. The polymer backbone can be confined between the smectic layers (a and c), or can be randomly distributed and is only partially affected by the smectic order (b and d). In the first case the polymer backbone has to be taken into account for the calculation of length of the mesogenic side group, in the latter case the backbone is excluded. The mesogenic side-groups can be partially (c and d) or fully (a and b) interdigitated depending on the polar end groups of the mesogen.
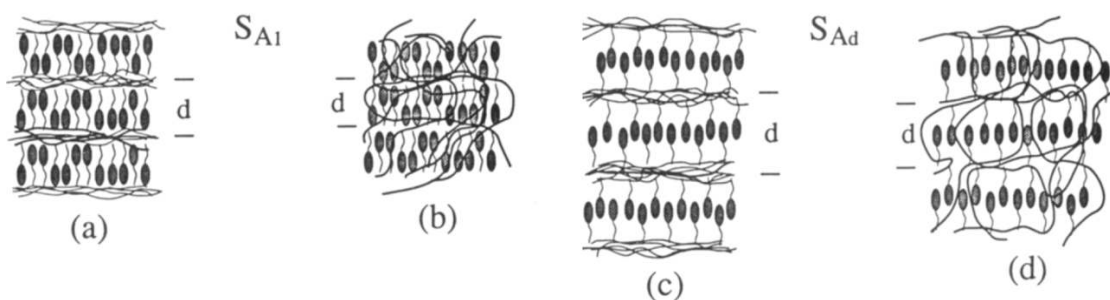
Figure 4.24:   Smectic A phases exhibited by side-group polymers.[201]

Polymers with methoxy substituted mesogenic units tend to show a grater overlap in the interdigitated smectic phases than cyanobiphenyl containing polymers that are known to form partially interdigitated smectic phases.[201] For **III** the estimated length of the mesogenic side-group with polymer backbone is $l = 28.8$ Å or without polymer backbone $l_b = 23.2$ Å. Considering the layer distance determined by XRD (d = 29.9 Å) and a fully interdigitated SmA phase with the polymer backbone confined between the smectic layers (Figure 4.24, a) seem reasonable as well as partially interdigitated SmA phase with an isotropic polymer backbone structure (Figure 4.24, d).

This characterization is in agreement with results reported by Imrie *et al.* on a analogous azobenzene-functionalized homopolymer.[87] They described the phase behavior as g 76 SmA 145 i. The increased transition temperatures (g 91 SmA 152 i) found in this work for homopolymer **III** might be due to the higher molecular weight of this homopolymer. While the polymer reported in literature exhibited a molecular weight of $M_n = 37$ kg/mol the molecular weight of **III** is more than three-fold ($M_n = 120$ kg/mol).

4.6.2 Methoxy azobenzene-containing polymers with two different spacer lengths

	IV	V	VI
x	4	4	6
y	6	8	8
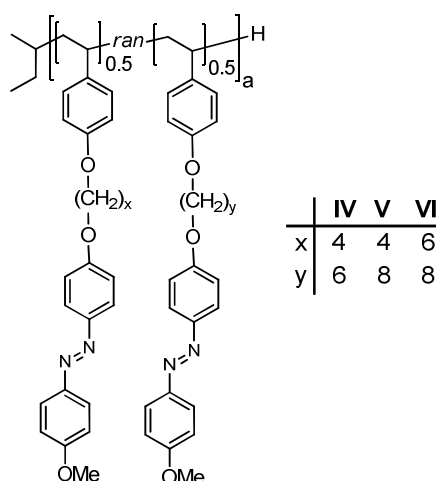
The azobenzene-functionalized polymers **IV-VI** contain two different spacer lengths each. The mixture of spacer lengths was used to disturb packing of the mesogens and to reduce the order of the mesophase. Thermal characterization by DSC revealed a glass transition as well as a liquid crystalline to isotropic transition for each copolymer in this series. Second heating DSC traces are shown in Figure 4.25 in comparison to the above described homopolymer **III**. The detected clearing temperatures were 156 °C (**IV**), 152 °C (**V**) and 142 °C (**VI**). These temperature decrease with increasing average number of methylene units in the mixed spacers thus, **IV** (x = 4; y = 6) has the highest T_{cl} whereas **VI** (x = 6; y = 8) exhibits the lowest T_{cl}. The glass transition temperature shows the same decreasing trend ranging from 105 °C for **IV** to 92 °C for **VI.** The heat capacity change in these (second order) phase transitions is very low. The inset in Figure 4.25 is an exemplary magnification of the glass transition of **IV**. The parallel lines are used to determine the height of the glass transition. Glass transition temperatures given resemble have heights of this step. The decrease of the glass transition temperature with increasing average spacer length for the homopolymers is attributed to an internal plasticization effect of the side chain on the polymer backbone of side-group liquid crystalline polymers which is commonly found.[77,79,86] The LC-isotropic transition enthalpy of varies from 5.8 J/g for **VI** to 15.5 J/g for **III**. No trend is apparent in these values but all of these transition enthalpies are in the range of smectic to isotropic transitions. However, for a nematic-isotropic transition lower values would be expected.
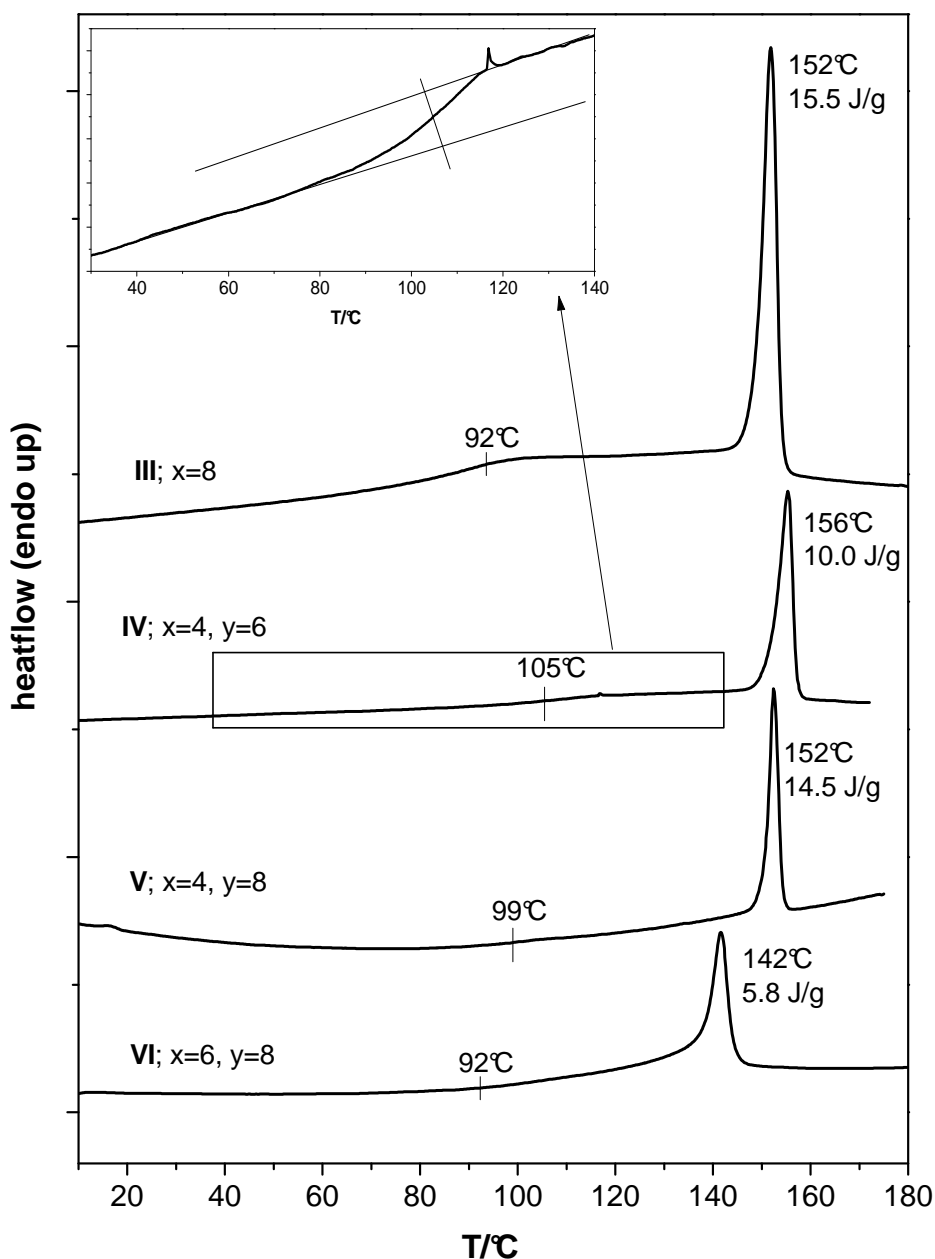
Figure 4.25: DSC traces of second heating of methoxy azobenzene-containing polymers **III** and **IV-VI** at 10 K/min under N_2 with inset magnified glass transition step of **IV**. The parallel lines should indicate how the glass transition temperature at half heights of the transition is determined.

The optical characterization of **IV-VI** (see Figure 4.26) revealed the same characteristic Schlieren texture as observed for **III** albeit it is much finer structured and as not fully developed. In contrast to **III** in the series **IV-VI** no bâtonnets were observed upon cooling from the isotropic to liquid crystalline phase. Similar as described for the functional polymer **III**, the Schlieren textures were apparent even at room temperature, below the glass transition temperature of the polymer. No conclusion concerning the mesophase

could be drawn from the POM images alone, although it is reasonable to assume the same smectic mesophase for all functionalized homopolymers **III-VI**.
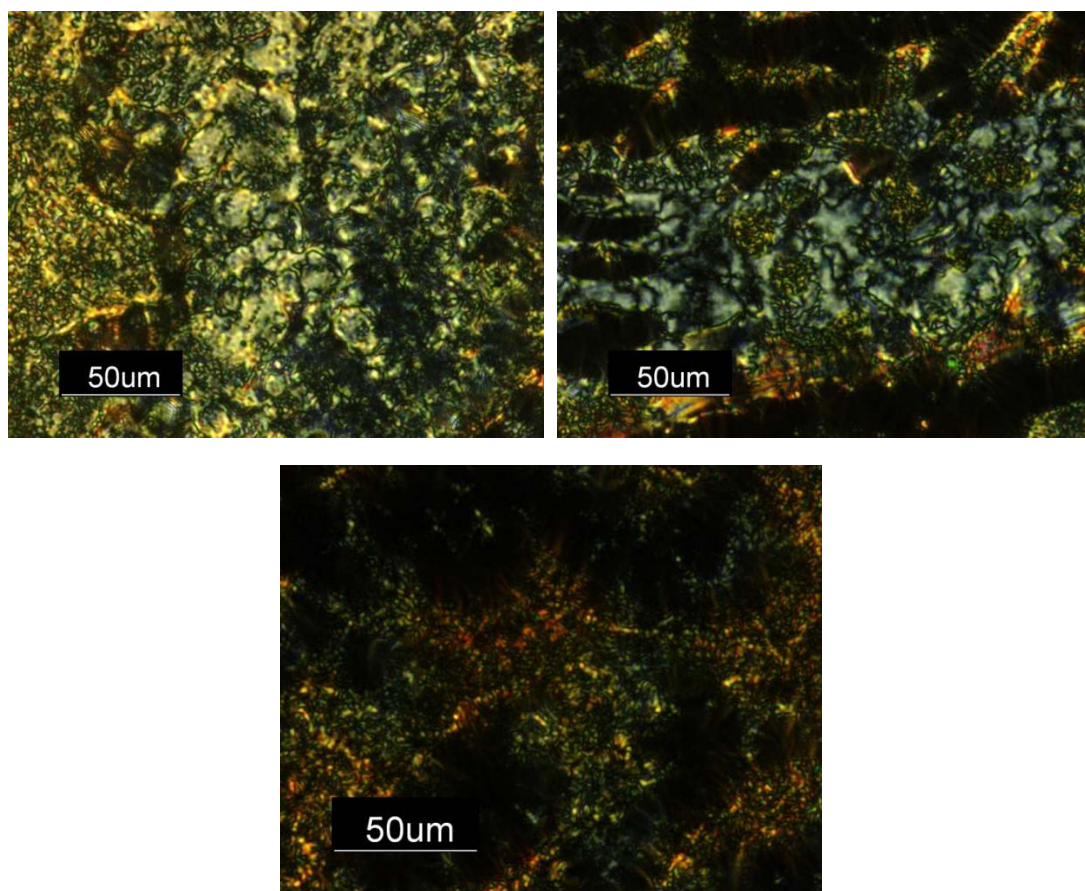
Figure 4.26:   Light microscopic images taken between crossed polarizers of the methoxy azobenzene-containing polymers **IV** (*top left*), **V** (*top right*) and **VI** (*bottom middle*) at 120 °C.

To gain further information about the mesophase of **IV-VI** XRD pattern were recorded in the liquid crystalline phase at 120 °C utilizing samples similarly prepared as described above for functional polymer **III**. In Figure 4.27 the diffraction patterns of **IV-VI** in comparison to **III** are shown. Significant reflections and the respective calculated layer distances are given in the inset.

The typical reflection in the small angle region, indicating the first order (100) and second order (200) of the layer distance as described for **III,** confirm the existence of a smectic mesophase for the azobenzene-containing polymers **IV-VI**. The smectic layer distance increases with increasing average number of methylene units in the mixed spacers from 24.6 Å for **IV** (x = 4; y = 6) to 27.6 Å for **VI** (x = 6; y = 8) in this series. As expected **VI** with the longest spacer combination exhibits the highest layer distance.

	x	y	(100)	(200)	d /Å
III	8	-	1,48	2.95	29.9
IV	4	6	1.79	3.59	24.6
V	4	8	1.72	3.46	25.6
VI	6	8	1.60	3.21	27.6
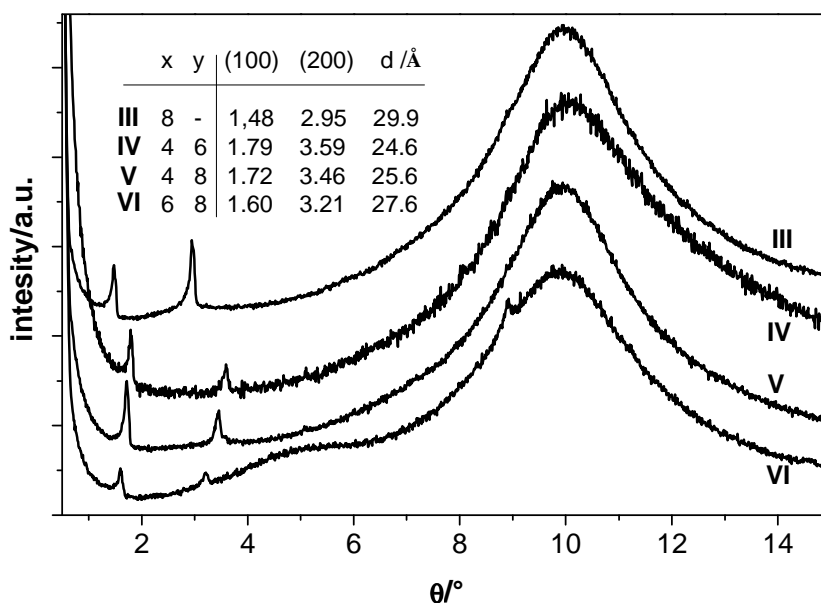
Figure 4.27:   Stacked XRD diffractograms of methoxy azobenzene-containing polymer **III** and **IV-VI** at 120 °C.

The results obtained for **V** and **VI** are in agreement with results reported by Imrie *et al.* on a analogous azobenzene-functionalized copolymer.[87] They reported series of azobenzene-functionalized copolymers with mixtures of eight-membered spacers while varying the other from y = 3 to y = 12. For the combination x = 4 and y = 8, comparable to **V**, and x = 6 and y = 8, comparable to **VI**, they described the phase behavior as g 76 SmA 137 i and g 78 SmA 144 i. As discussed for the functionalized homopolymer **III** the polymers described in literature exhibit partially lower transition temperatures compared to the copolymers in this work **V** (g 99 SmA 152 i) and **VI** (g 92 SmA 142 i). Again this observation is attributed to the much higher molecular weight of the copolymers presented here (**V**: $M_n = 87$ kg/mol; **VI**: $M_n = 161$ kg/mol) compared to the polymers described by Imrie *et al.*(x = 4, y = 8: $M_n = 37$ kg/mol; x = 6, y = 8: $M_n = 42$ kg/mol).

4.6.3   Methoxy azobenzene-containing block copolymers with PMMA matrix

The methoxy azobenzene-containing diblock copolymer of series **6** consists of three polymers with the spacer length x = 6 (**6a**), x = 8 (**6b**) and x = 10 (**6c**).

6	a	b	c
x	6	8	10
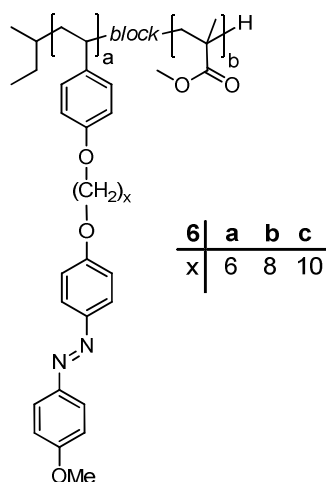
The thermal behavior of all diblock copolymers was examined by DSC under the same conditions as for the homopolymers. Second heating DSC traces are shown in Figure 4.28. All diblock copolymers of series **6** exhibit a clearing temperature of the functionalized azo block (T_{cl}(Azo)) in the range of 142 °C (**6c**) to 152 °C (**6a**). The T_{cl}(Azo) of the homopolymer **III** (T_{cl}(Azo) = 152 °C) is 10 °C higher than for the respective diblock copolymer **6b** with the same spacer length (x = 8), featuring the same number of repeating units (ru = 245). The low T_{cl} might be due to the lower degree of conversion of **6b** (DC = 86 %) compared to **III** (DC = 95 %) or the confinement effect imposed by the microphase separation in the diblock copolymer. Positive as well as negative deviations in the liquid crystalline to isotropic transitions temperatures have been observed in azobenzene-containing homopolymers and their respective block copolymers.[90,115,193] Another explanation might be the significant overlap of the glass transition of the functionalized block with the glass transition of the PMMA segment that might cause the shift to higher temperatures.

In the series of the diblock copolymers **6**, the temperature of the liquid crystalline to isotropic transition decreases with increasing spacer length as observed for the polymers **IV-VI**. The clearing transition enthalpy increases slightly with the spacer length thus, a rising order of the respective mesophase might be indicated. Ultimately, the value of the transition enthalpy is an indication for a smectic phase as described for the homopolymers **III-VI**. Mostly two glass transitions were detected for the functionalized diblock copolymers **6**, although the determination is not always possible (as in **6b**) due to the similar glass transition temperature range of both segments that results in a significant overlap. The glass transition of the azobenzene-functionalized block (T_g(Azo)) could be

detected in all block copolymers. The decrease of the glass transition temperature with increasing spacer length for the block copolymers is attributed to the plasticizing effect of the side chain on the polymer backbone of side chain liquid crystalline polymers, as it was observed for the homopolymers **III-VI**.[77,79,86] The glass transition of the PMMA block (T_g(PMMA)) is detected at T_g= 127 – 128 °C and is in good agreement with the T_g observed for anionically polymerized PMMA This value is higher due its syndiotactic content compared to PMMA obtained from free radical polymerization.
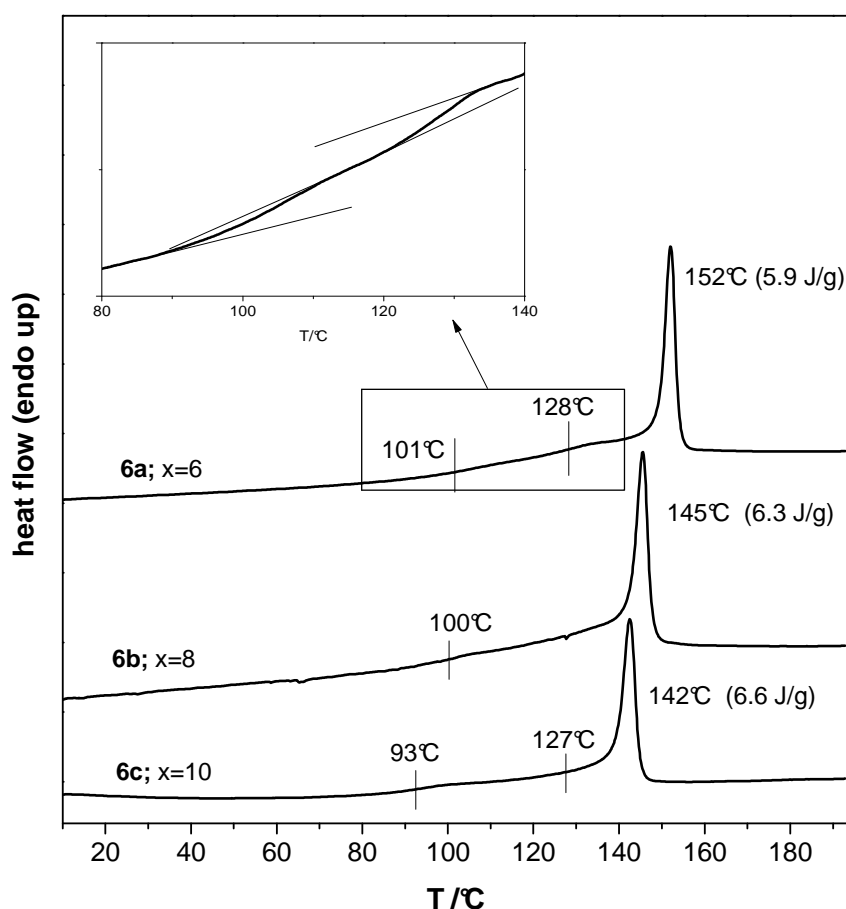
Figure 4.28:   Second heating DSC traces at a heating rate of 10 K/min under N_2 of methoxy azobenzene-containing diblock copolymer series **6.**

All block copolymers **6a-c** exhibited birefringence below the clearing point when examined under the polarized optical microscopy. In contrast to the homopolymers **III** and **IV-VI**, the block copolymers **6a-c** failed to produce an identifiable liquid crystalline texture upon cooling or annealing below the clearing temperature. This is attributed to the confinement effectin the phase separated block copolymers and the higher viscosity of the block copolymers compared to the homopolymer originating from the MMA block.

XRD diffractograms of the functionalized block copolymers **6a-6c** recorded at 120 °C are shown in Figure 4.29. Values of the (100) and (200) reflections as well as the respective layer distances are shown in Figure 4.29. In the wide angle range the block copolymers show the previously described halo around $\theta = 10°$, that is caused by the polyhydroxystyrene backbone. In addition, a second halo was found at $\theta = 7°$ that can be attributed to the amorphous PMMA block.[202] **6a** and **6b** exhibit two signals at small angles corresponding to the first (100) and second order (200) of the smectic lattice distance although the intensity decreased compared to the homopolymer **III** as a consequence of the overall lower concentration in the block copolymer. For **6c** the first order signal is not clearly detected because it is already superimposed by the tail of the primary beam thus the layer distance was calculated only from the (200) signal. The corresponding layer distance increases as expected with increasing spacer length of the block copolymers as shown in Figure 4.29 from 26.3 Å for **6a** (x = 6) to 34.0 Å for **6c** (x = 10). The layer distance for **6b** (x = 8) is 30.6 Å and thus slightly higher than for the respective homopolymer **III** (29.9 Å) but within the measurement accuracy.
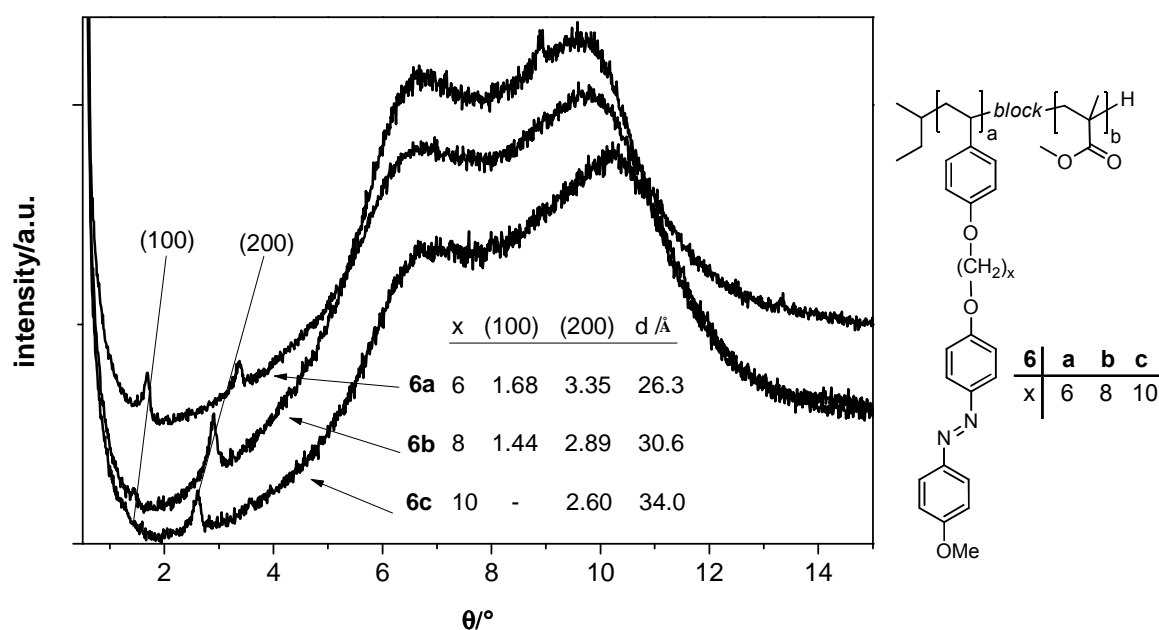
Figure 4.29: XRD diffractograms of the methoxy azobenzene-containing diblock copolymers **6a - 6c** at 120 °C.

The weight fraction of the azobenzene-containing block in all block copolymers is in the range of w_{Azo} = 50 to 54 wt%. Due to the fact that the whole series **6** is based on the functionalizable block copolymer **4c** the different weight fraction are only based on the degree of conversion and the spacer length of the attached chromophores.

The bulk morphology of the functionalized block copolymers was investigated by transmission electron microscopy (TEM). Samples for TEM measurements were obtained by dissolving the block copolymers in THF at a concentration of 7 wt%, filtering the solution through a PTFE filter (0.5 µm) into a glass vial and slow evaporation of the solvent over one week. The polymer films were dried under vacuum (approx. 10^{-3} mbar) for one day at room temperature. Subsequently the films were annealed in the liquid crystalline phase at 140 °C and 130 °C for 12 h each before slowly cooling to room temperature within 6 h. Thin cuts of the sample (50 nm) were prepared with a microtome and placed on carbon grids. The cutting of the samples was conducted in the facilities of Bayreuther Zentrum für Kolloide und Grenzflächen (BZKG) by Carmen Kunert. The thin cut samples were stained with ruthenium tetroxide (RuO_4) vapor for 15 min to increase the contrast between the two different blocks. The azobenzene-containing block was stained preferentially, resulting a dark image, while the unstained PMMA segment remains bright.[23]

TEM measurements were performed by André Gröschel (Department of Macromolecular Chemistry II), images for **6a-c** are shown in Figure 4.30. These micrographs show cross-sections of lamellar structures that are a cut perpendicular to the lamellae. The slight blurring in the micrograph results from the partial degradation of the PMMA segment due to radiation damage from the electron beam during the measurements.[23,203] Due to this effect also the lamellar dimensions obtained from the micrographs might not reflect the actual values. Nevertheless, the average thickness of the lamellae was determined by averaging multiple points of dark and bright lamellae each. The determined average thicknesses of the lamellae were 31-34 nm for the PMMA lamellae and 21-23 nm for the azo block lamellae in the three diblock copolymers **6a-6c**. Thus all diblock copolymers of series **6** exhibit the same morphology with nearly identical feature size. The azobenzene-containing lamellae show a lower diameter compared to the PMMA lamellae with a difference of ~8 nm. The weight fractions do not equal the volume fractions that control the origin of the microphase separated feature size. The density of the azobenzene-containing segment is expected to be higher than for the PMMA segment, therefore one might assume a resulting lower volume fraction of the azobenzene-containing segment compared to the PMMA segment.
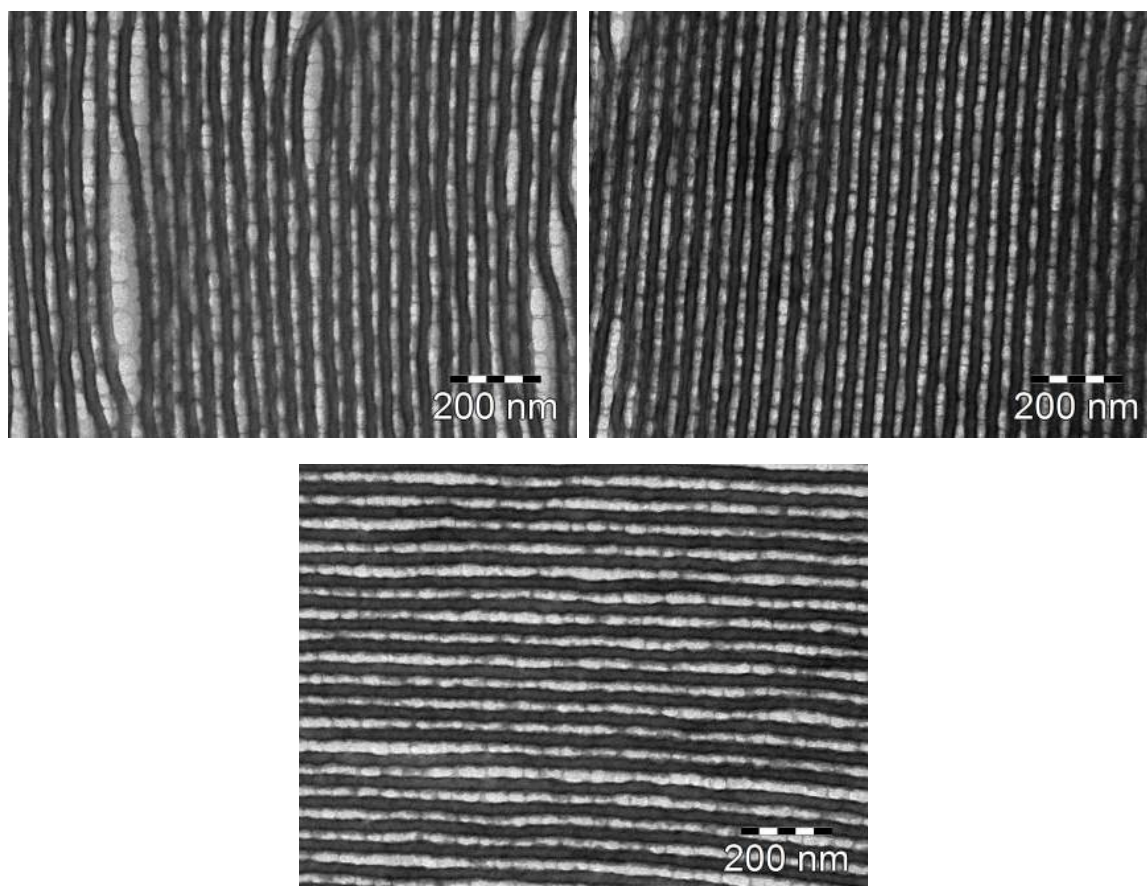
Figure 4.30:   TEM micrographs of methoxy azobenzene-containing diblock copolymers **6a** (*top left*), **6b** (*top right*) and **6c** (*bottom*) annealed at 140 °C for 12 h and 130 °C for 12 h, stained with RuO$_4$; the black part corresponds to the azobenzene-containing block.

Block copolymer series **7** is based on a PMMA segment and a polyhydroxsytrene segment which is functionalized with methoxy azobenzene chromophores with two different spacer lengths each.

7	a	b	c
x	4	4	6
y	6	8	8
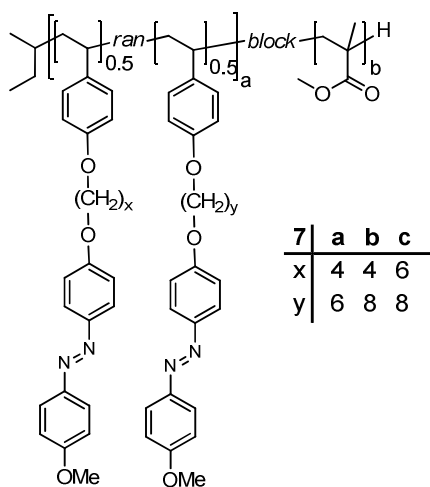
In Figure 4.31 the second heating DSC thermograms are shown. To visualize the glass transitions of **7a**, the inset shows a magnification of the temperature range around the

expected transitions. Generally, in this series two glass transitions, one for each block, and a liquid crystalline to isotropic transition are expected.

The block copolymers with mixed spacers (**7a-7c**) do not show the clear trend as it was observed for the respective homopolymers. In this series both transition temperatures of the functionalized block (T_g(Azo) and T_{cl}(Azo)) do not continuously decrease with the increasing averaged number of methylene units of the different spacers. **7a** exhibits the highest transition temperatures (T_g(Azo) = 107 °C, T_{cl} = 150 °C)) as it was also observed for the transitions of the respective homopolymer **VI**. However, **7b** features the lowest transitions (T_g(Azo) = 100 °C, T_{cl} = 135 °C. This unexpected behavior might be due to a possible deviation from the desired 1:1 ratio of the two different spacers.

All members of the series **7a-7c** should exhibit the glass transition of the PMMA segments (T_g(PMMA)) as described for **6a** and **6c**. However only for **7a** this transition was detectable at T_g(PMMA) = 130 °C. In case of **7b** and **7c** this transition is already superimposed by the comparable lower transition temperatures of liquid crystalline to isotropic transition.

All block copolymers **7** exhibited birefringence below the isotropic to liquid crystalline transition when examined under the polarized optical microscopy. In contrast to the homopolymers **III** to **VI**, the block copolymers **7** an identifiable liquid crystalline texture upon cooling or annealing below the clearing temperature cannot be found for the block copolymers **7**. As discussed for the block copolymers of series **6** this is attributed to the confinement and the higher viscosity of the block copolymers compared to the homopolymer originating from the MMA block. Exemplary POM image taken between crossed polarizers shown in the inset of the Figure 4.31 for **7c** illustrating the isotropic phase above the clearing temperature and the birefringence below the isotropic to liquid crystalline transition.
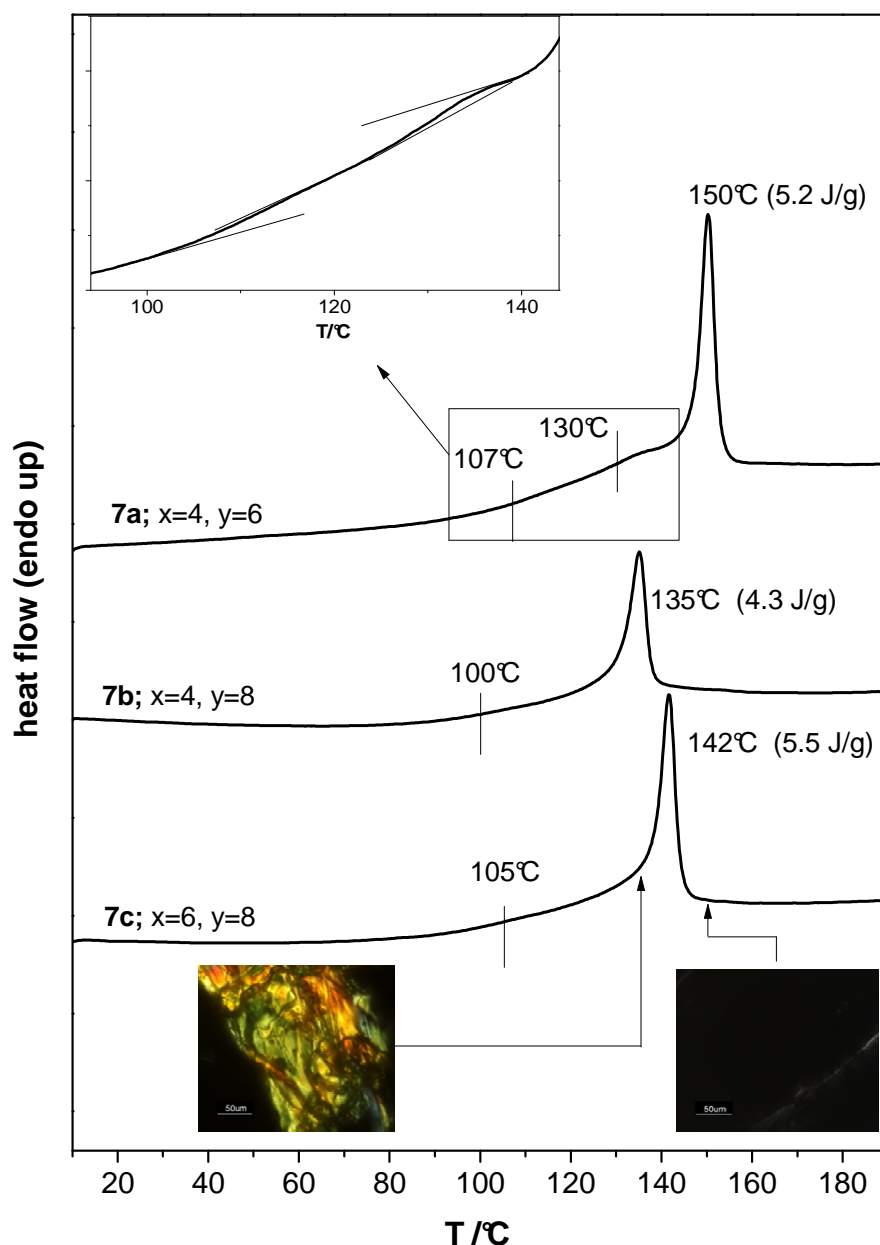
Figure 4.31:   Second heating DSC traces at a heating rate of 10 K/min under N_2 of methoxy azobenzene-containing diblock copolymer series **7** with POM images taken between crossed polarizers for **7c** at 135 °C (*left*) and at 150 °C (*right*).

The XRD diffractograms of the block copolymers **7a-7c,** the significant reflection as well as the resulting layer distances are given in Figure 4.32. As observed for the block copolymer series **6** two distinct reflections at small angles as well as two halos at wide angles are observed. The halos can be attributed to the PMMA segment ($\theta = 6.5°$) and the polystyrene based backbone ($\theta = 10°$). The block copolymers **7a-7c** exhibits the same trend as observed for the respective homopolymers **IV-VI**, i.e. the smectic layer distance increase with increasing length of the spacers. The values range from 24.6 Å for **7a** (x = 4

and y = 6) to 28.7 Å for **7c** (x = 6 and y = 8). The absolute values determined for the layer spacing of the smectic polymers slightly differ for the respective members of the homopolymer series **IV-VI** and the block copolymer series **7a-7c**. Whereas **IV** exhibits the same layer distance as the respective block copolymer **7a**, the layer distances for **V** and **VI** are by ~1 Å shorter compared to the respective block copolymers **7b** and **7c**.

	x	y	(100)	(200)	d /Å
7a	4	6	1.79	3.60	24.6
7b	4	8	-	3.34	26.5
7c	6	8	1.54	3.08	28.7
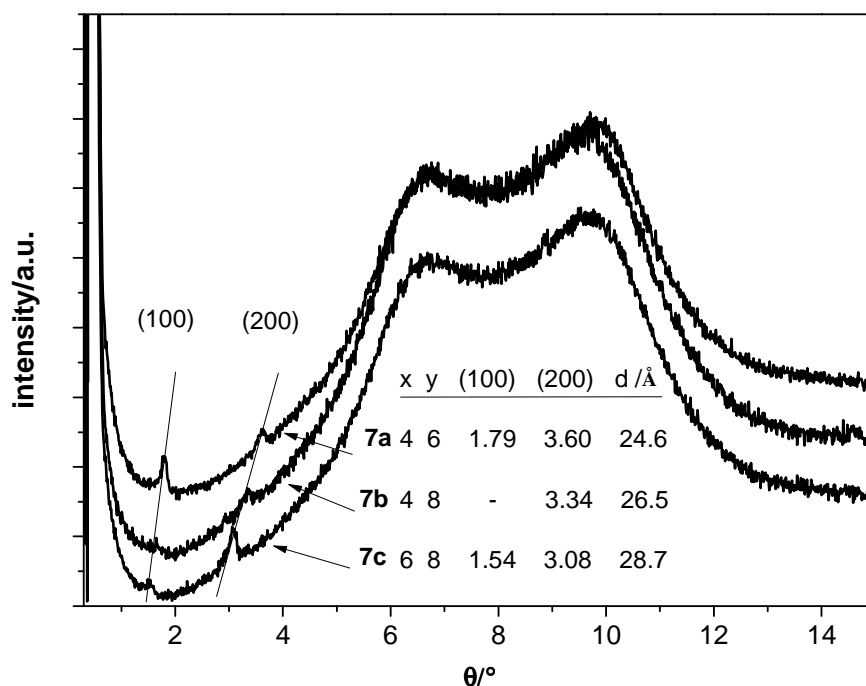
Figure 4.32:   XRD diffractograms of the methoxy azobenzene-containing diblock copolymers **7a-7c** at 120 °C.

The weight fraction of the azobenzene-containing block in all block copolymers **7a-c** is in the range of w_{Azo} = 50 – 52 wt%. The small differences arise from the degree of conversion and the composition of different spacer length of the side-groups in the three block copolymers. Regarding the results obtained for block copolymer series **6,** which features similar weight fractions, a lamellar mircophase separation is expected for series **7** as well. Exemplary, a micrograph of transmission electron microscopy (TEM) investigations for **7c** is given in Figure 4.33. The sample for this was prepared in the same way as described for the block copolymers of series **6**. As expected a lamellar bulk morphology was found. The average thickness of the dark lamellae, corresponding to the azobenzene-containing segment, was 22 nm whereas the thickness of the bright lamellae, corresponding to the PMMA segments, was 34 nm. These values coincide with the thicknesses obtained in diblock copolymer series **6**. As observed in series **6** the lamellae of the azobenzene-containing segment show a lower diameter although the weight

fractions are nearly identical. This observation is might be attributed to the higher density of the azobenzene-containing segment and thus featuring a reduced volume fraction.
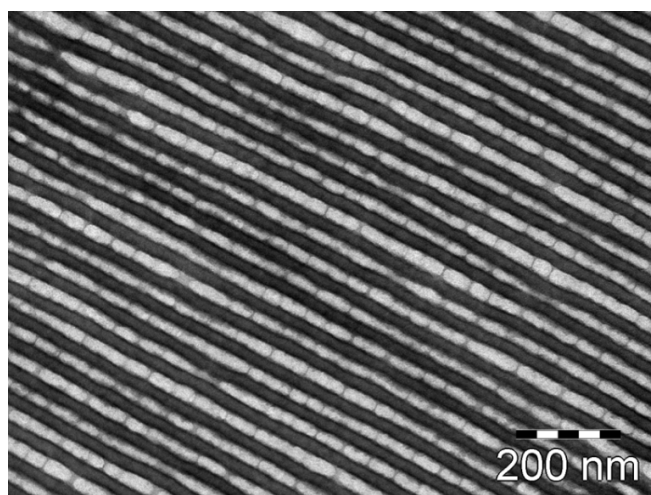
Figure 4.33:   Exemplary TEM micrographs of the methoxy azobenzene-containing diblock copolymer **7c** annealed at 140 °C and 130 °C for 12 h each, stained with RuO_4; the black part corresponds to the azobenzene-containing block.

4.6.4   Methoxy azobenzene block copolymers with PS matrix
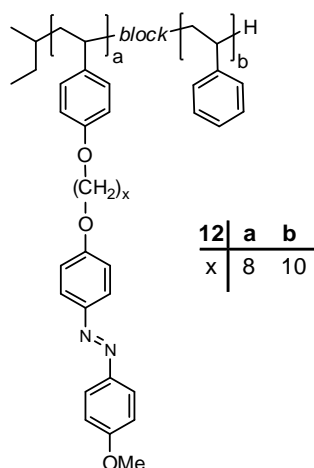
12	a	b
x	8	10

The diblock copolymes **12a, b** are diblock copolymers with PS matrix and a functional PS segment containing azobenzene chromophores with the spacer lengths of x = 8 (**12a**) and x = 10 (**12b**), respectively. Second heating traces of the DSC analysis of the methoxy azobenzene-containing diblock copolymers **12** are shown in Figure 4.34. In contrast to the diblock copolymer series **6** and **7,** only one broad glass transition is detected. Taking into account the results obtained for the diblock copolymers **6a-6c**, it is reasonable to assume that the only one glass transition is detected because the T_gs of the azobenzene-containing segment (T_g(Azo)) and the PS matrix (T_g(PS))are superimposed. For the azobenzene-containing block in **6b** and **6c** the T_g(Azo) of the functionalized block were 93 °C (**6c**)

and 101 °C (**6b**) respectively and commonly polystyrene homopolymers exhibit a glass transition T_g(PS) around 100 °C. Since the functional segment of diblock copolymers **6b** to **6c** with PMMA matrix are similar, the detected clearing temperatures for **12a** and **12b** can be compared. The value of **12a** (T_{cl} = 143 °C) is in good agreement with the clearing temperature obtained for **6b** (T_{cl} = 145 °C), whereas **12b** (T_{cl} = 135 °C) is shifted by ~7 °C to lower temperatures. This deviation as well as the broad liquid crystalline to isotropic transition peak can be explained by the moderate degree of conversion that is 63 % for diblock copolymer **12b** and thus, significantly lower than for **6c** with a degree of conversion of 86 %.
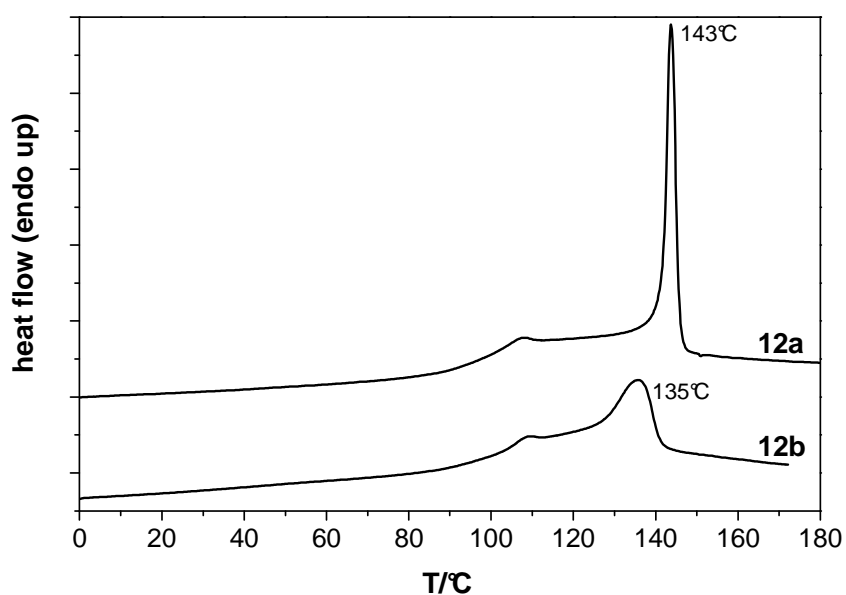
Figure 4.34:   Second heating traces from DSC at a heating rate of 10 K/min under N_2 of methoxy azobenzene-containing diblock copolymer series **12**.

The XRD diffractograms of both methoxy azobenzene-containing diblock polymers with PS matrix **12** are given in Figure 4.35 together with the values of the detected reflection as well as the respective layer distances. Both diblock copolymers show the broad halo around θ = 10° that is caused by the amorphous polystyrene segments as well as the polystyrene based backbone of the functional segment. **12a**, the block copolymer with an eight-membered spacer, exhibits two distinct reflections in the small angle region that correspond layer distance of 29.6 Å. This distance is in agreement with the distance determined for the respective homopolymer **III** (29.9 Å) with the same spacer length. In contrast, **12b** shows only one reflection in the small angle region. If the signal is interpreted as a first order signal the respective lattice distance could be calculated to 19.6 Å. This uncharacteristically low value might originate from the low degree of conversion (DC = 63 %) that might not result in fully extended mesogenic side-groups.

100

The formation of smectic mesophase with a tilt angle of the mesogens may also explain this observation.
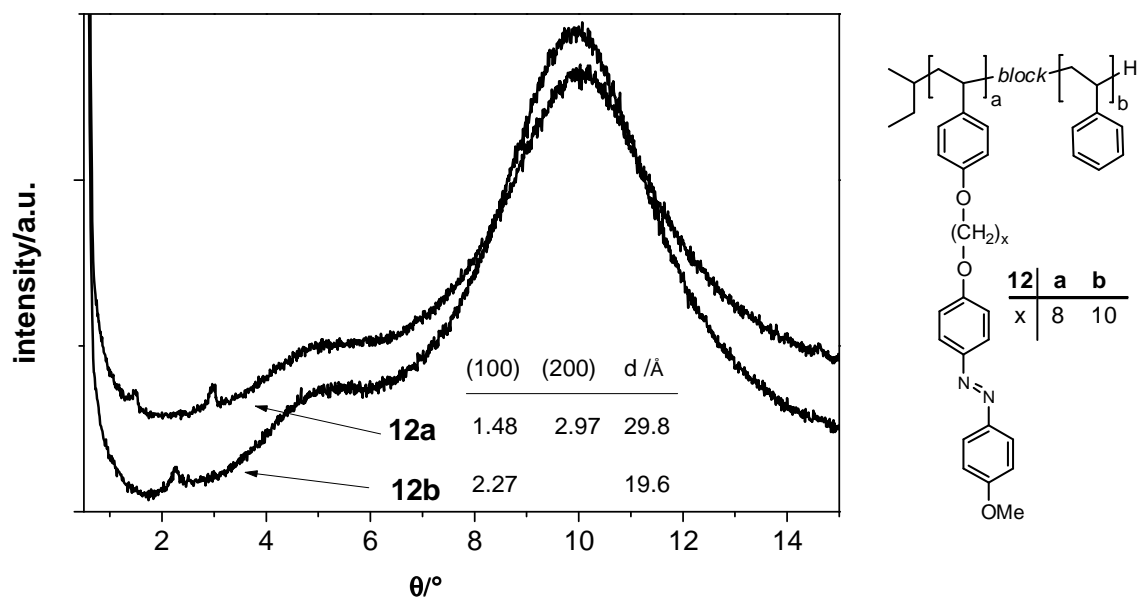
Figure 4.35:   XRD diffractograms of the methoxy azobenzene-containing diblock polymers with PS matrix **12a** and **12b** at room temperature.

Comparison of all methoxy azobenzene-containing polymers

For easier reference and as summary the thermal and mesophase properties of all methoxy azobenzene-containing homopolymers, copolymers and block copolymers are given in Table 4.7.

Table 4.7: Thermal data of all methoxy azobenzene-containing homopolymers, copolymers and block copolymers

samples	$x^{a)}$	$y^{a)}$	$T_g(Azo)^{b)}$	$T_g(PMMA)^{c)}$	$T_{cl}(\Delta H)^{d)}$	$d(SmA)^{e)}$
			°C	°C	°C (J/g)	Å
homopolymers and copolymers						
III	8	-	92	-	152 (15.5)	29.9
IV	4	6	105	-	156 (10.0)	24.6
V	4	8	99	-	152 (14.5)	25.6
VI	6	8	92	-	142 (5.8)	27.6
block copolymers						
6a	6	-	101	128	152 (5.9)	26.3
6b	8	-	100	n.f.	145 (6.3)	30.6
6c	10	-	93	127	142 (6.6)	34.0
7a	4	6	107	130	150 (5.2)	24.6
7b	4	8	100	n.f.	135 (4.3)	26.5
7c	6	8	105	n.f.	141 (5.5)	28.7
	$x^{a)}$	$y^{a)}$	$T_g(Azo)^{b)}$	$T_g(PS)^{c)}$	$T_{cl}(\Delta H)^{d)}$	$d(SmA)^{e)}$
			°C	°C	°C (J/g)	Å
12a	8	-	106	106	143 (7.4)	29.8
12b	10	-	104	104	135 (4.9)	19.6

a) number of methylen units in spacer; b) glass transition temperature of the functionalized block; c) glass transition temperatureof the PMMA or PS block, n.f.: not found; d) T_{cl}: clearing temperature, ΔH: transition enthalpy, determined from second heating thermograms by DSC with a scan rate of 10 K/min under nitrogen; e) distance of the smectic layer spacing determined by XRD

4.6.5 Cyano azobenzene-containing block copolymers

13a - 13b
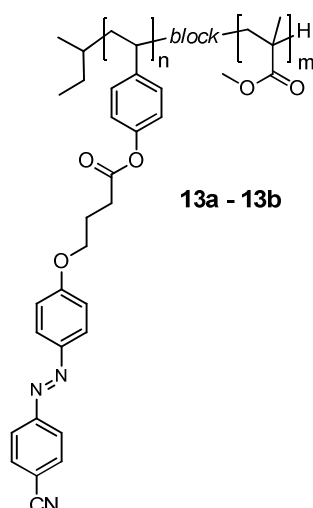
The diblock copolymers **13a** and **13b** contain a cyano azobenzene chromophore that is attached to the polymer backbone via an ester linkage. Both polymer have the same chemical structure and block composition (see chapter 4.5.5) but differ in molecular weight. **13b** is used for the following discussion.

DSC traces of second heating and cooling are shown in Figure 4.36. The insets show POM images taken between crossed polarizers at a temperature of 155 °C (right) and 122 °C (left), respectively. On heating as well as cooling only one broad transition can be observed. The heating thermogram might be interpreted as a glass transition temperature of an aged sample as indicated by the "excess peak" at 135 °C, which would result in Tg ≈ 130 °C. However, the POM images have to be taken into account. At temperatures below 130 °C a birefringent phase is evident that is significantly reduced in brightness upon heating above 135 °C, even though the images did not become dark at elevated temperatures. This effect might be attributed to a shear induced birefringence that did not relax fully due to the high viscosity of the sample. The observation, that the possible clearing transition is hardly detectable as well as the glass transition of the functionalized block (T_g(Azo)) cannot be determined might be attributed to low weight fraction of the functionalized block which is only 22 wt% for **13b**.

Considering this observation, it is reasonable to interpret the transition observed in the DSC traces as a superimposition of the glass transition of the matrix, expected around 127 °C, and a liquid crystalline to isotropic transition of the azobenzene-containing segment with a maximum about $T_{cl} = 135$ °C.

Figure 4.36:   Second heating and cooling DSC traces at a heating rate of 10 K/min under N_2 of cyano azobenzene-containing diblock copolymer **13b.** Insets are POM images between crossed polarizers of **13b** at 155 °C (*right*) and at 120 °C (*left*).

The XRD measurement at 120 °C, i.e. in the temperature range of the liquid crystalline phase, is given in Figure 4.37. The sample was heated to 140 °C for 1h and annealed at 120 °C for 1 h prior to the measurement at the same temperature. No distinct signal is visible in the small angle region thus rendering a smectic mesophase improbable. Two superimposed broad halos can be detected around $\theta = 6.5°$ and $\theta = 9°$. These signals are caused by the PMMA matrix ($\theta = 6.5°$) and the polystyrene based backbone of the functionalized segment ($\theta = 9°$). The higher intensity of the former halo compared to the diffractograms obtained for diblock copolymer series **6** and **7** is caused by the higher weight fraction of the PMMA segment in the case of **13b**.

Based on the above described results, **13b** is assigned to a nematic phase because no indication for a smectic mesophase was evident.
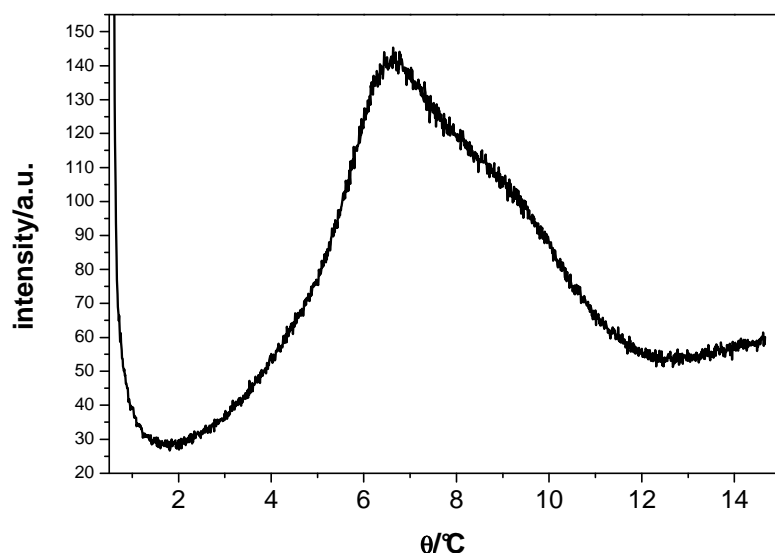
Figure 4.37: XRD diffractogram of the cyano azobenzene-containing diblock polymers with PMMA matrix **13b** at 120 °C.

The morphology of the diblock copolymers **13** was investigated via TEM analysis, both contain a 22-23 wt% of an azobenzene-containing block. The thin cut samples were prepared and stained with RuO_4 to increase the contrast between the two segments as reported for the TEM images of the diblock copolymer series **6** and **7**. The only difference was the annealing temperature which was set to 120 °C for 24 h. The resulting images are shown in Figure 4.38. For the block copolymer with the higher molecular weight **13b** ($M_n = 84.1$ kg/mol, $ru_{Azo} = 61$, $ru_{PMMA} = 455$) a cylindrical morphology can be clearly identified. Areas of cylinders cut perpendicular to the long axis that form a hexagonal packing are visible. Cylinders cut along the long axis are also found. In contrast for the diblock copolymer with the lower molecular weight **13a** ($M_n = 33.6$ kg/mol, $ru_{Azo} = 19$, $ru_{PMMA} = 241$) the morphology cannot be clearly identified. Nevertheless, the formed structures seem to exhibit smaller dimensions compared to **13b**. Unfortunately, no images with a higher magnification could be obtained for this sample due to significant blurring caused by radiation damage. However it is reasonable to assume the same morphology is present that was found for **13b**.
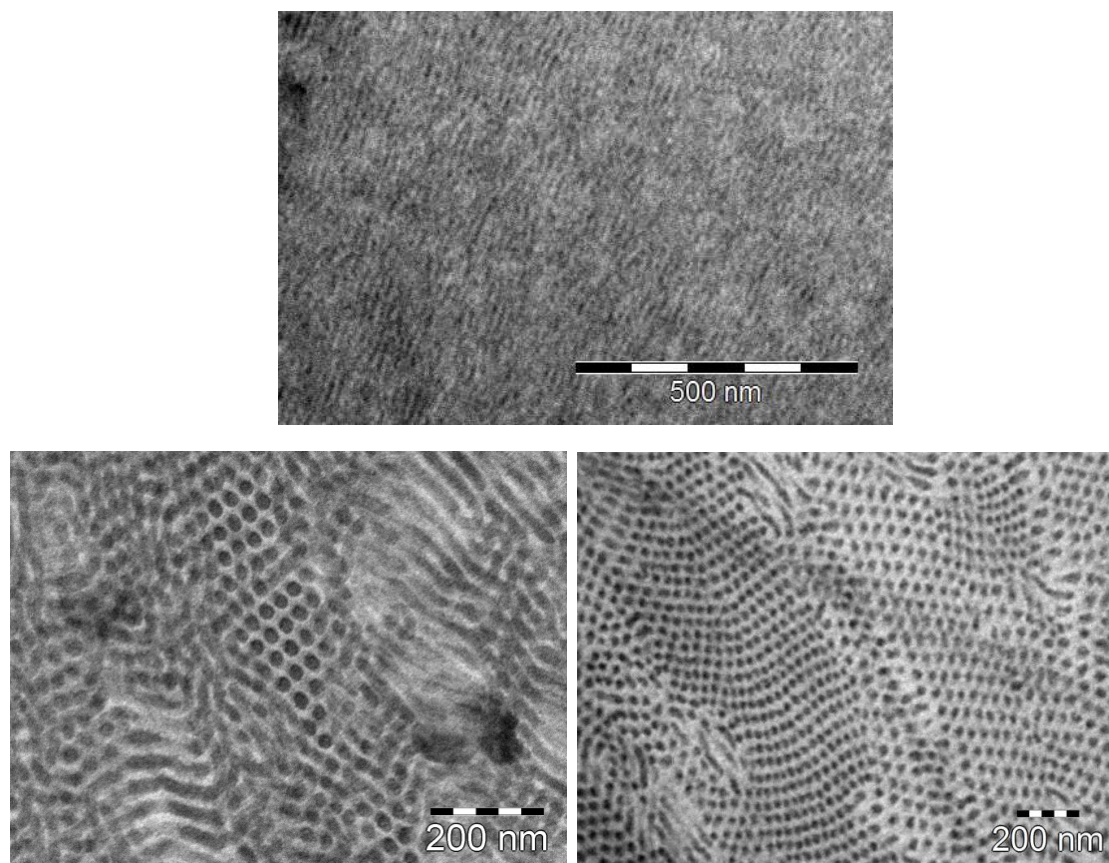
Figure 4.38:   TEM images of **13a** (top) and **13b** (bottom left and right) annealed at 120 °C for 24 h, stained with RuO$_4$; dark areas correspond to the azobenzene-containing segment, bright areas to the PMMA.

The triblock copolymer **15** contains a azobenzene-containing segment, a PEHMA middle block and a PMMA matrix. From the precursor **14** the repeating units were determined to ru$_{PtBS}$ = 16, ru$_{PEHMA}$ = 65 and ru$_{PMMA}$ = 469.
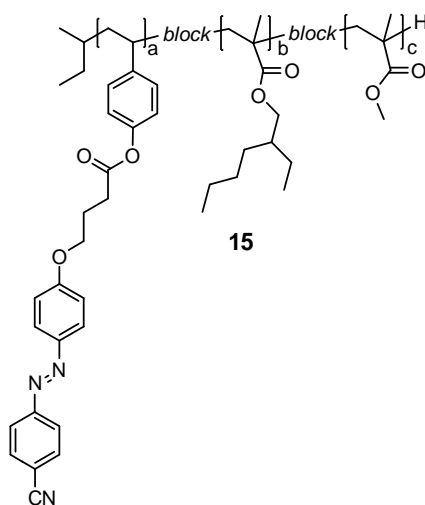
Analysis of the thermal properties via DSC (see Figure 4.39) revealed only the glass transition of the PMMA matrix at a temperature of 126 °C on heating. This is not

unexpected considering the block copolymer composition (A:B:C = 1:4.1:29.5). The fractions of the functionalized segment as well as the PEHMA middle block are much to minor to be detectable in the thermograms.
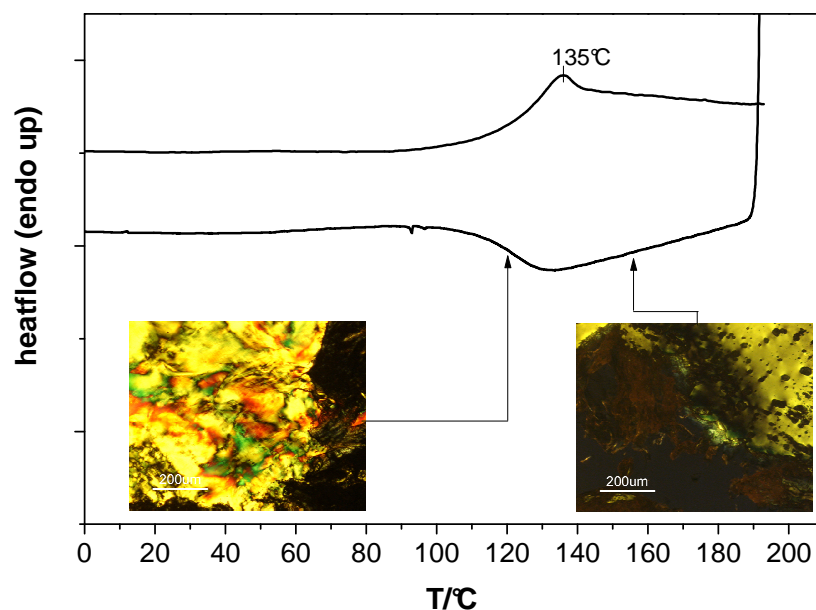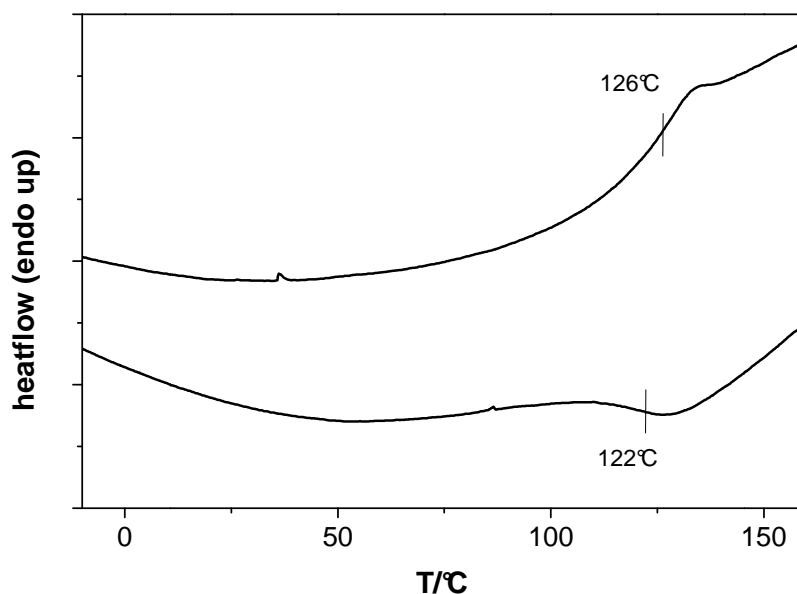

Figure 4.39:   Second heating and cooling DSC traces at a heating rate of 10 K/min under N_2 of cyano azobenzene-containing triblock copolymer **15.**

The cyano azobenzene-containing triblock copolymer with a PEHMA middle block and a PMMA matrix **15** was analyzed via TEM. An example of the resulting images is given in Figure 4.40. The present bulk morphology is not easily identified. On the basis of the obtained images a cylindrical morphology of the azobenzene-containing block is assumed. The PMMA and the PEHMA segment cannot be distinguished therefore no conclusion can be drawn if the PEHMA form a shell around the cylinders or if any kind of other possible morphology is present.
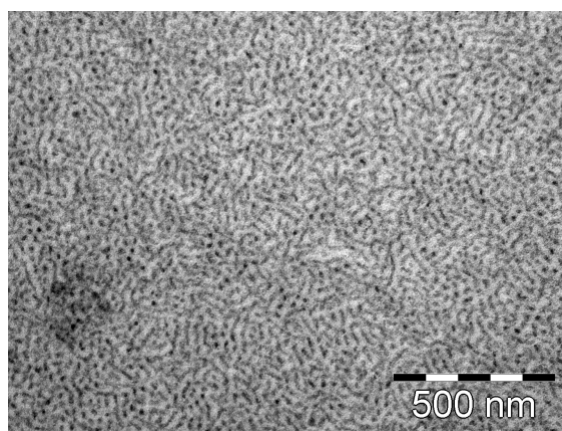
Figure 4.40:   TEM images of **15** annealed at 120 °C for 24 h, stained with RuO_4; dark areas correspond to the azobenzene-containing segment.

4.7   Holographic experiments

Holographic measurements were performed by Dr. Hubert Audorff at the Bayreuth Institute of Macromolecular Research (BIMF) in the framework of the Collaborative Research Center 481 (Sonderforschungsbereich (SFB) 481) by the German Research Council (Deutsche Forschungsgemeinschaft, DFG).

Two s-polarized plane waves at 488 nm with an intensity of each 1 W/cm^2 are brought to interference in the plane of the sample. Due to the s:s-polarization a light-intensity grating is generated in the material. Reading was performed at 685 nm, which is well outside of the absorption of the azobenzene chromophore. From the holographic experiment, the diffraction efficiency is obtained. The refractive index modulation, n_1, was calculated according to Kogelniks theory. For details see experimental part, chapter 6.1.1.

In Figure 4.41 a typical temporal evolution of the refractive index modulation is shown. An important parameter determining the speed of the writing process is the slope near $t = 0$s. This maximal slope is proportional to the sensitivity of the azobenzene-containing material (see 6.1.1). Other important parameters are *a)* is the maximum refractive index modulation (n_{1max}) that is reached at the time t_{max}, commonly the writing laser is switched off at this point; *b)* is the 90% value of n_{1max} and corresponds to the time $t_{90\%}$; *c)* is the value of n_1 after initial relaxation ($n_{1(rel)}$), this value is used to determine the evolution of n_1 after writing laser switch off. For further details see chapter 6.1.1.
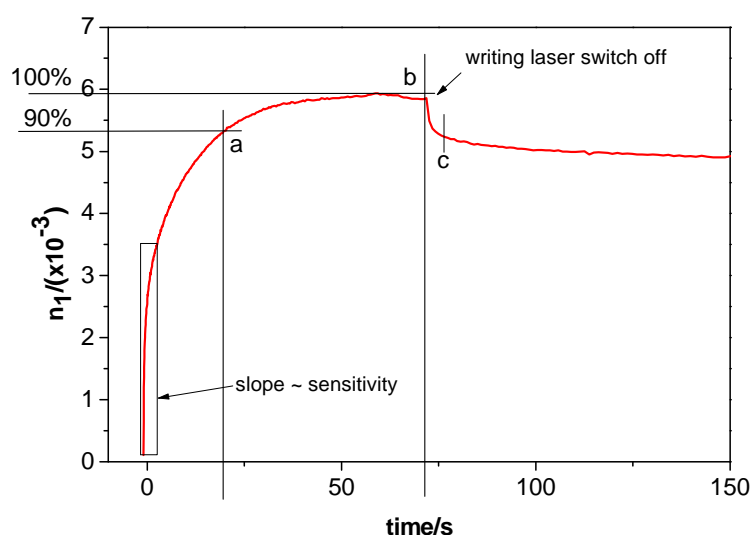
Figure 4.41:   Typical temporal evolution of the refractive index modulation at room temperature with indication of obtained values.

4.7.1 Holographic experiments on thin samples of methoxy azobenzene-containing polymers

In this chapter the following questions will be addressed using azobenzene-containing polymers:

1. influence of sample preparation (annealing vs. quenching) on holographic behavior,

2. temperature dependency of the holographic writing process and stability of the holographic gratings,

3. influence of spacer length on holographic behavior.

4.7.1.1 Influence of sample preparation of methoxy azobenzene-containing homopolymer
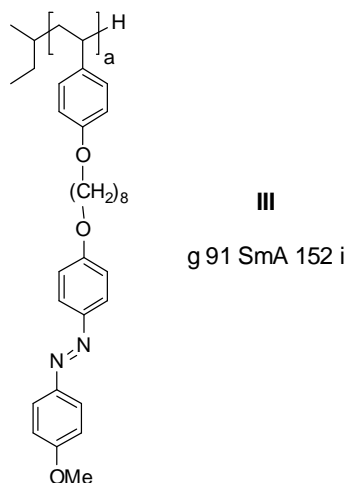
In the first set of holographic experiments the influence of the smectic mesophase order on the holographic behavior was investigated. Considering the inherent order of the smectic mesophase it can be assumed that the orientation of the chromophores requires a higher amount of energy than in a non isotropic sample (see chapter 4.1). To study this influence samples were prepared in two different ways denoted as (i) and (ii). For this thin film of the azobenzene-containing homopolymer **III** were prepared by spin coating a 7 wt% solution in THF at 2000 rpm onto a cleaned glass slide. The resulting films typically featured a thickness of 0.6-1.6 µm. For every hologram, the film thickness was measured with a profilometer (Veeco Dektak 1500).[147] To remove residual solvent the thin films were annealed at 80 °C for 1h. The procedures for the subsequent sample preparation are shown schematically in Figure 4.42.

(A) Smectic samples featuring multidomains were prepared by heating the films into the isotropic phase ($T > T_{LC\text{-}iso}$) for 15 min and subsequent annealing of the samples at $T_g < T < T_{LC\text{-}iso}$. In the case of azobenzene-containing homopolymer **III** annealing was carried out at 150 °C for 1h and at 120 °C for 2h.

After cooling to room temperature this procedure yielded glassy samples with smectic order, from now on denoted as "annealed". Formation of the smectic phase was confirmed via POM. Images between crossed polarizers showed the expected Schlieren texture as described in chapter 4.6.1.

(B) Amorphous samples were prepared by heating up to the isotropic phase ($T > T_{LC\text{-}iso}$) for 15 min. The formation of the smectic mesophase was precluded by rapidly cooling the samples below the glass transition temperature of the polymer. This was achieved by placing the slides on a copper cylinder (r= 5 cm, h= 25 cm) standing in liquid nitrogen. Thus amorphous samples were obtained that appeared dark between crossed polarizers. These samples are denoted "quenched".

isotropic melt

(**A**) annealing T = T$_{iso-LC}$-5°C   (**B**) rapid cooling below T$_g$

smectic phase   isotropic glass

200um   200um
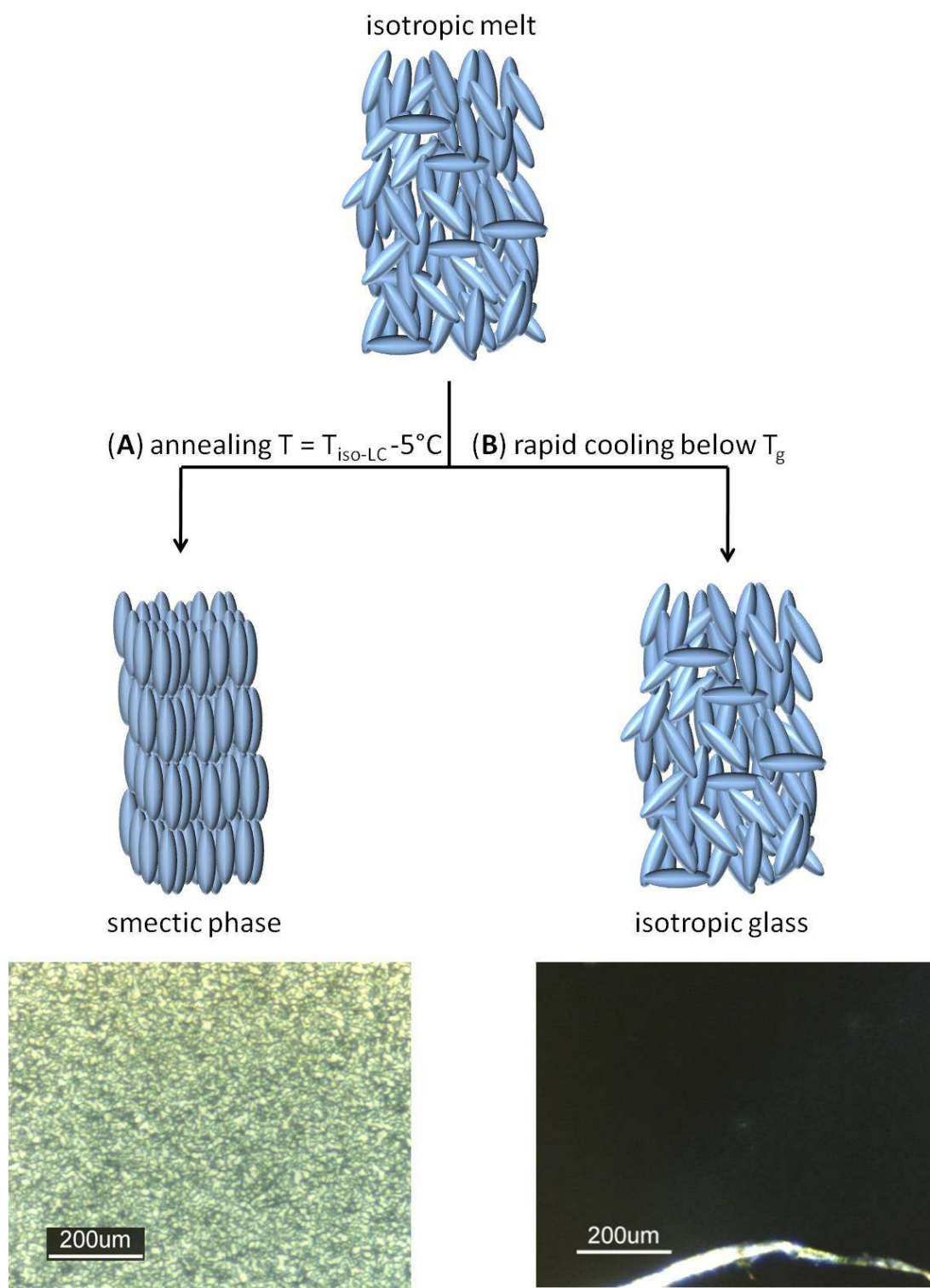
Figure 4.42:   Schematic representation of the preparation of smectic samples of III as well as amorphously quenched samples. Below: POM images between crossed polarizers of samples of the methoxy azobenzene-containing homopolymer **III.** *left:* annealed at 130 °C for 1 h (d = 0.69 µm); *right:* amorphous quenched sample (heated to 170 °C, rapidly cooled below T$_g$ on copper bock in liquid N$_2$, d = 0.69 µm).

The temporal evolution of the refractive index modulation was recorded for annealed and quenched samples of **III** at room temperature. The respective curves are given in Figure 4.43. The writing beam was switched of when the maximum refractive index modulation ($n_{1(max)}$) was reached. The refractive index modulation of both curves is zero at t=0. The fact that the curve for the annealed samples starts at $n_1 = 2.2 \times 10^{-3}$ is caused by the experimental setup whereby the recording starts at $t = 0.5$ s, yielding an initial n_1 which is higher than zero.

If the order of the mesophase hinders the reorientation of the azobenzene chromophores in the sample, the sensitivity of the smectic samples should be lower compared to the amorphous sample.

The sensitivity is proportional to the slope of the temporal evolution of the refractive index modulation near t=0. From the inset in Figure 4.43 the area of interest can be compared. The initial slope of both curves is nearly identical thus the sensitivity in an early stage of both samples does not differ to a great extend. This result indicates that the mesophase of the smectic sample does not have an influence on the holographic behavior of the azobenzene-containing polymer.

However, the absolute values of the maximum refractive index modulation as well the respective time to reach these values are indeed depended on the inherent order of the azobenzene chromophores. The annealed sample exhibits a higher maximum refractive index modulation ($n_{1(max)} = 8 \times 10^{-3}$) compared to the quenched sample ($n_{1(max)} = 6 \times 10^{-3}$). On the other hand the writing time until this maximum is reached is more than double the time for the annealed sample ($t_{max} = 202$ s) compared to the quenched sample ($t_{max} = 71$ s). A much greater difference in is expected if prealigned liquid crystalline sample are be used. In a monodomain the director exhibits a macroscopic orientation thus, the reorientation in the irritated area would result in a very high diffraction index difference between the irradiated and non-irradiated areas. Although in the initial sample multidomains were present that do not normally show an overall director orientation, the domain size might be high enough to explain the increased refractive index modulation in the sample.
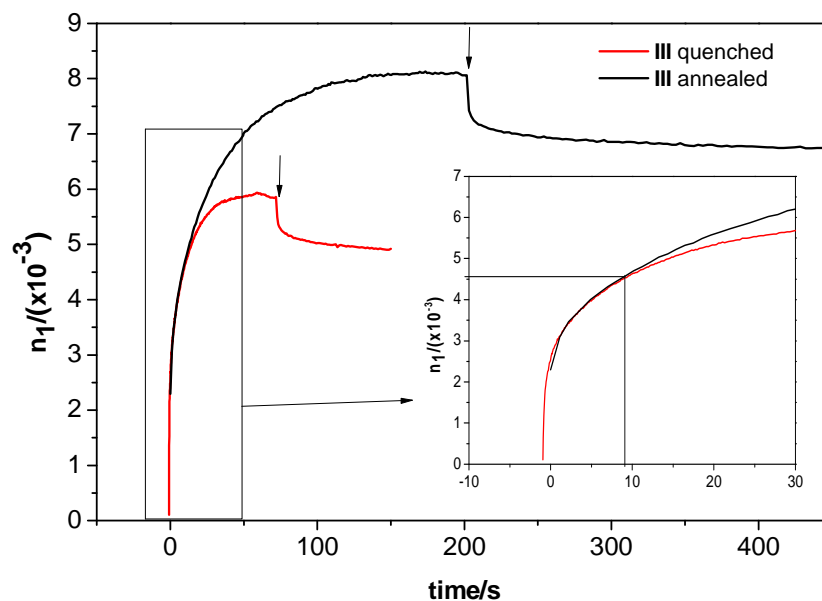
Figure 4.43:   Temporal evolution of the refractive index modulation at room temperature for annealed (130 °C for 2 h) samples (left) and a amorphously quenched samples (heated to 170 °C, rapidly cooled below T_g on copper bock in liquid N_2) of the methoxy azobenzene-containing homopolymer **III**. Time of writing laser switch off is indicated by arrows.

4.7.1.2 Influence of writing temperature for methoxy azobenzene-containing homopolymer

Stumpe *et al.*[204] investigated the temperature dependence of the laser induced birefringence in smectic polyacrylate based copolymers with mixtures of cyano azobenzene chromophores and cyanobiphenyl or N-(4-methoxybenzylidene)-4-butylaniline mesogens. In contrast to a holographic experiment in this kind of experiment only one laser beam is used to photoorient the chromophores in a sample thus, no overexposure is possible and the expected refractive index difference between irradiated and non-irradiated area is higher. An increase of photoorientation at writing temperatures above the glass transition temperature was found as well as an increase in photo-induced birefringence. The photo induced birefringence increased above T_g with a maximum at a temperature ~20 °C below the clearing temperature and decreased again until the clearing temperature was reached. Notably, for all polymers the orientation was not stable and decayed after the irradiation was stopped. Above the glass transition temperature full thermal relaxation occurred within 50 sec.

Wendorff *et al.* [205] presented a nematic (g 28 SmA 96-98 N 130-134 I) polyacrylate with an ethoxy azobenzene chromophores as well as the respective cholesteric (g 27 SmA 83-85 N* 127-128 I) copolymer with a mixture of the azobenzene chromophore and a cholesteryl-based mesogen. They studied the influence of the light intensity as well as the writing temperature in a holographic experiment. A significant increase in the diffraction

efficiency with increasing temperature from 80 to 120 °C was found. Nevertheless in both polymers the inscribed gratings vanished in a matter of seconds due to thermal relaxation in the system although liquid crystalline phases were present. The rate of relaxation also increased with increasing temperature.

Ikeda *et al.*[206] investigated the holographic behavior of nematic poly(meth)acrylate based copolymers with mixtures of nitro azobenzene chromophores with tolane or cyanobiphenyl mesogens. Higher diffraction efficiency and very low writing times were observed at writing temperatures above the glass transition temperatures. The thermal relaxation occurred on the same time scale thus no stable gratings were obtained in the liquid crystalline temperature range.

Smectic photoaddressable block copolymer systems based on a methyrylate segment with a cyano azobenzene chromophore and a PMMA matrix were investigated by Alcalá *et al.*.[188] As observed by the other groups for homopolymers and copolymers they found an increase of photo-induced birefringence with increasing temperature up to 70 °C, i.e. ~16 °C above T_g of the azobenzene-containing segment. At 90 °C no birefringence could be induced although the clearing temperatures were determined around 150 °C.

The low refractive index modulation obtained at room temperature indicates that the photo induced orientation of the chromophores is insufficient. The mobility of azobenzene units should increase with temperature and a faster photo-orientation should be achieved (faster birefringence growth rate) at higher temperatures.

To investigate the influence of the writing temperature on the holographic properties the temporal evolution of the refractive index modulation was recorded at different temperatures from 20 to 120 °C in steps of 20 °C (Figure 4.44). The maximum refractive index modulation increases with increasing temperature up to 100 °C from $n_{1max} = 0.01$ (20 °C) to $n_{1max} = 0.03$ (100 °C). From 100 °C to 120 °C n_{1max} decreases significantly and resulting in a lower n_{1max} than recorded at 20 °C. A radical change in the holographic behavior is evident in the temperature range around 80 °C. Below 80 °C the refractive index modulations drops slightly immediately after switching off the writing beam due to relaxation processes. At a temperature of 80 °C and higher, refractive index modulations exhibits postdevelopment (i.e. the refractive index modulation increases although the writing laser is switched off). In the temperature range up to 80 °C the writing process was stopped at 500 s without reaching the maximal value. For 100 °C a significant reduction of the writing time can be observed, whereby n_{1max} is already reached after 40 s. At 120 °C t_{max} lowered to 10 s but also the n_{1max} is lower by the factor of six compared to writing at room temperature.

These results indicate that a substantial orientation of the chromophores is achieved by writing at a temperature around 80 °C. The resulting postdevelopment indicates an increased order into mono-domain like structures (only liquid crystalline azobenzene-containing polymers exhibit postdevelopment, see chapter 4.1). The local heating resulting from the laser beams is estimated to be in the range of 10 to 15 °C.[207] If this effect is taken into account the resulting temperature (i.e. 90-95 °C) is in good agreement with the determined glass transition temperature of **III** ($T_g = 92$ °C).
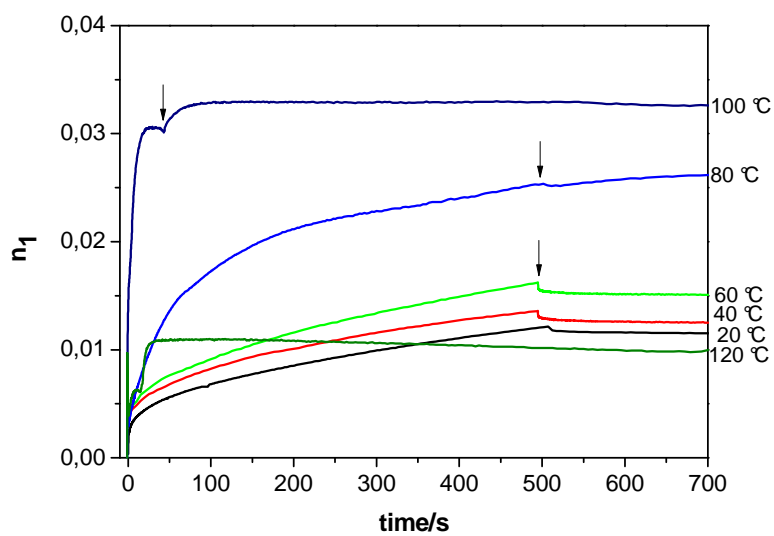
Figure 4.44: Temporal evolution of refractive index modulation at different temperatures for thin films ($d = 0.69 \, \mu m$) annealed at 120 °C for 2 h of the methoxy azobenzene-containing homopolymer **III**. Arrows indicate writing laser switch off.

In previous studies the chromophores of amorphous azobenzene-containing polymers could be oriented in the solid state and the stability of the inscribed gratings decreases when the glass transition temperature is reached.[29] In contrast, liquid crystalline azobenzene-containing polymers show an increase of the chromophore orientation with increasing temperatures even above the glass transition temperature as described for literature discussed above. This trend is also observed in this thesis for investigations on homopolymer **III**. In contrast to most of the studies the holographic gratings inscribed in thin smectic films of homopolymer **III** exhibited a high stability and even a postdevelopment in the liquid crystalline temperature range.

Results obtained for the homopolymer **III** indicated that in this smecitc azobenzene-containing polymer system significant chromophore reorientation only occurs when the writing temperature is in the range of the glass transition temperature of the polymer. In a temperature range above the glass transition temperature and below the clearing

temperature rapid formation of holographic gratings can be achieved that exhibit postdevelopment at the given temperature.

4.7.1.3 Influence of spacer lengths of methoxy azobenzene-containing block copolymers

6	a	b	c
x	6	8	10

6a: g 101 SmA 152 i
6b: g 100 SmA 145 i
6c: g 93 SmA 142 i
T_g(PMMA)= 127-130°C

7	a	b	c
x	4	4	6
y	6	8	8

7a: g 107 SmA 150 i
7b: g 100 SmA 135 i
7c: g 105 SmA 141 i
T_g(PMMA)= 127-130°C
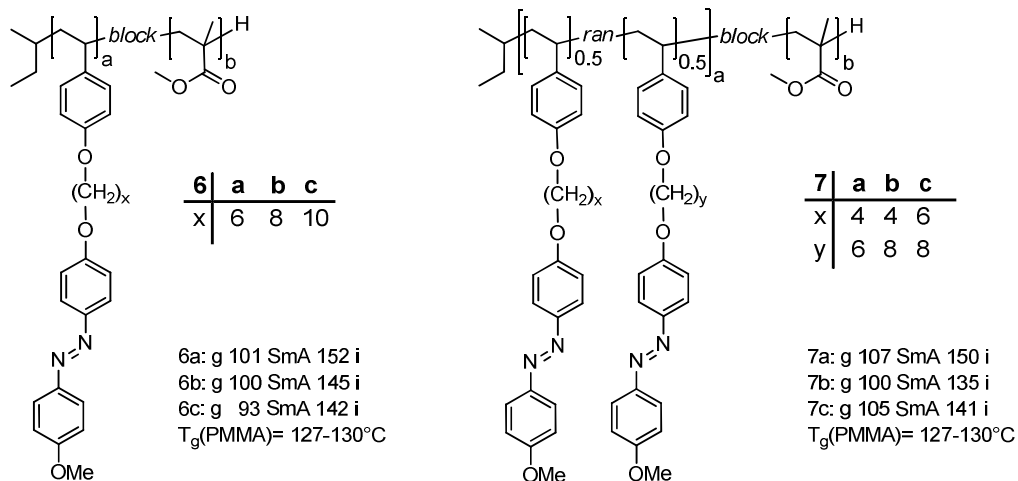
The influence of the spacer connecting the azobenzene chromophore to the polymer backbone was studied by holographic experiments. Thin films were prepared via spin coating followed by annealing the samples for 2 h at 10 °C below the clearing temperature of the respective polymer. In order to obtain more reliable results, the samples were measured several times (depending on the variance three to eleven times) and the average of the experiments was calculated (see Table 4.8).

The high order in the smectic mesophase is attributed to be responsible for the longer writing times to reach the maximum of the temporal evolution of the refractive index modulation and the stability of the inscribed gratings. Therefore, the holographic properties of annealed smectic thin films and thin films quenched to an amorphous state were compared. The same procedures were used that are described before. Initially amorphouse polymer films were prepared by heating the samples above the clearing temperature (T_{cl}(Azo)) and subsequent rapid cooling (quenching) below the glass transition temperature (T_g(Azo)) on a copper block standing in liquid nitrogen. By holographic illumination with two polarized light beams, it might be possible to induce a liquid crystalline mesophase in the initially amorphous samples,[173] similar to results reported for the low-molecular-weight compounds.[199] For the annealed diblock copolymers the maxima of the $\pi\pi^*$-transitions were located in the range of 346 nm to 346 nm as listed in Table 4.8, whereas the quenched samples show a small red shift. This can

be explained by the reduced formation of the molecular aggregates in the liquid-crystalline phase. Compared to the results obtained for thin films of **III** described above this also confirms an amorphous phase in the quenched sample.[19]

All samples of the investigated block copolymers exhibited good stability of the inscribed holographic gratings, i.e. the refractive index modulation did not decrease significantly after the initial relaxation. The respective holographic results as well as the thickness of each film are given in Table 4.8.

Table 4.8: Results of the holographic experiments on thin films of methoxy azobenzene-containing diblock copolymer series **6** and **7** at room temperature

block copolymer	max. $\pi\pi^*$ transition nm	max. $n\pi^*$ transition nm	$t_{90\%}$ s	$n_{1(90\%)}$ 10^{-3}	$n_{1(4000s)}/n_{1max}$ %	$n_{1(60000s)}/n_{1(rel)}$ %	d µm
6a (a)	344	405	1368±988	6.7±1.5	100	103	1.09
6b (a)	345	407	1856±625	7.4±1.3	97	96	1.23
6c (a)	346	408	8929±3680	7.1±1.4	100	98	0.98
7a (a)	341	409	112±11	6.6±0.7	100	97	0.91
7b (a)	345	403	136±31	6.8±0.3	100	104	0.90
7c (a)	346	404	1027±694	10.3±1.7	100	103	0.68
6a (q)	346	408	13±5.6	3.4±0.5	93	nm	1.09
6b (q)	347	409	37±18.7	2.8±0.2	98	nm	1.25
6c (q)	347	407	688±67	6.3±1.6	100	102	0.93
7c (q)	348	415	180±117	7.3±4.7	104	113	0.67

(a): sample annealed 2h 10°C below T_{cl}; (q) amorphous quenched sample, heated above T_{cl} and rapidly quenched below T_g samples (left)

For easier comparison in the Figure 4.45 the writing time to reach 90% of the maximum refractive index modulation ($t_{90\%}$) for all diblock copolymers are plotted. The writing time $t_{90\%}$ in this series of diblock copolymers increases from **6a** to **6c**. With increasing spacer length, the tendency of the azobenzene chromophores to move independently from the back bone rises and the anisotropy of the side group increases. This might cause an increase in the degree of order of the smectic phase becomes more stable as can be seen chapter 4.5.3. This leads to longer writing times and an increase of the refractive index modulations of the annealed diblock copolymers as shown in Figure 4.45.

The maximum refractive index modulation is not significantly influenced by the length of the spacers and, thus, the degree of order of the smectic phase. All annealed samples of the block copolymers exhibit a $n_{1(max)}$ in the range of 6.6×10^{-3} to 10.3×10^{-3} with no apparent dependency on the spacer length.

Figure 4.45: Time to reach 90 % of the maximum refractive index modulation (*left*) and respective 90 % of the maximum refractive index modulation (*right*) for methoxy azobenzene-containing diblock polymers **6a–7c** for holographic experiment at room temperature. (a): sample annealed (1h at 150 C, 2h at 120 °C).

Amorphous quenched samples were only investigated for the block copolymers **6a-6c** and **7c**. In Figure 4.46 the writing times and refractive index modulation for these measurements are given. Comparing the results in the series **6** the writing time until 90 % of the refractive index modulation is reached ($t_{90\%}$) exhibits the same trends as observed for the smectic samples although the absolute values are significantly reduced. The reduction in writing times is higher for the poloymers with shorter spacers. Thus, the reduction by the factor 12 is observed for **6c** whereas the writing time is reduced by the factor 100 for the azobenzene-containing block copolymer with the four-membered spacer **6a**. The block copolymer containing a mixture of two spacer lengths **7c** also exhibits a reduced writing time although it is only lower by the factor 6 compared to the smectic sample.

The 90 % values of the maximum refractive index modulation are lower in the amorphous quenched samples compared to the smectic samples as also observed for the homopolymer **III**. No dependency on the spacer lengths can be observed. Nevertheless the difference to the smectic samples is lower for the ten membered spacer **6c** and block copolymer **7c** with the mixture of six and eight membered spacers.

All samples of initially amorphous quenched azobenzene-containing block copolymers exhibit good long-term stability. For **7c** a slight postdevelopment effect can be observed. This might indicate the formation of a liquid crystalline phase induced in the initially amorphous samples. As shown in Figure 4.47, POM images between crossed polarizers of the irradiated sample show birefringence only in the irradiated region, a possible indicating for the formation of a liquid crystalline mesophase due to the photo-orientation.
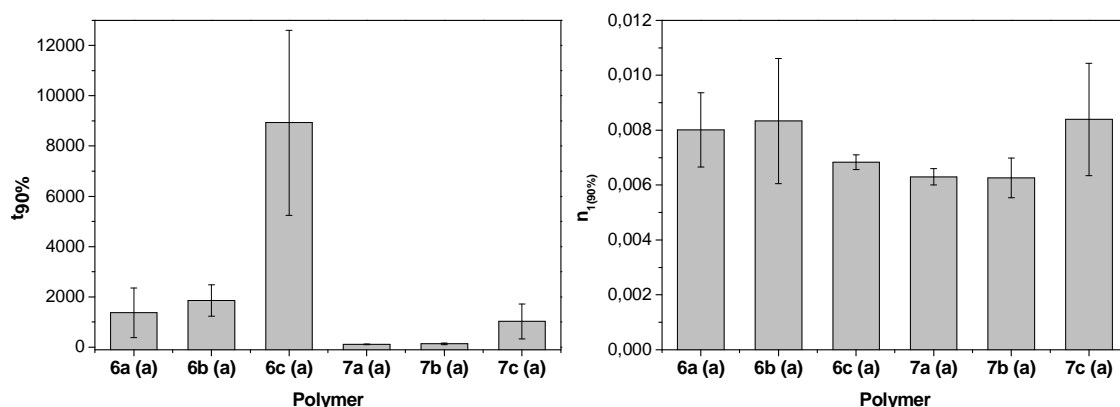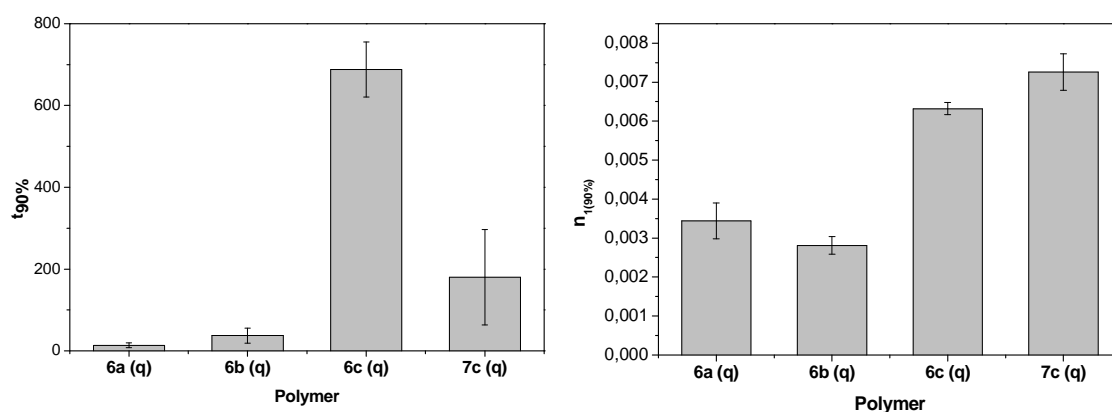
Figure 4.46.   Time to reach 90 % of the maximum refractive index modulation (*left*) and respective 90 % of the maximum refractive index modulation (*right*) for methoxy azobenzene-containing diblock polymers **6a–6c** and **7c** for holographic experiment at room temperature. (q) quenched sample, (heated to 170 °C, rapidly cooled below T_g on copper bock in liquid N_2).
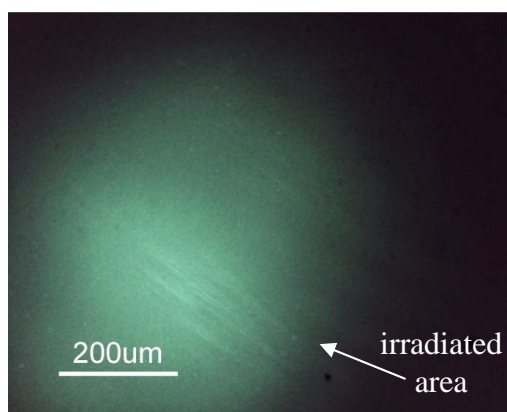
Figure 4.47:   POM images between crossed polarizers of an amorphous quenched sample (heated to 170 °C, rapidly cooled below T_g on copper bock in liquid N_2) of the methoxy azobenzene-containing block copolymer **7c** after irradiation at room temperature. The irradiated area appears bright.

In conclusion, a liquid-crystalline phase can be induced by the holographic light grating and stable holographic gratings can be inscribed. In the initially amorphous sample, the reorientation occurs faster leading to writing times one order of magnitude shorter as compared to the annealed sample, whereas the refractive index modulation does not change so strongly. Therefore, the sensitivity to light increases in the quenched samples.

4.7.1.4 Influence of the writing temperature on thin films of methoxy azobenzene-containing block copolymer 7c

7c

g 105 SmA 141 i
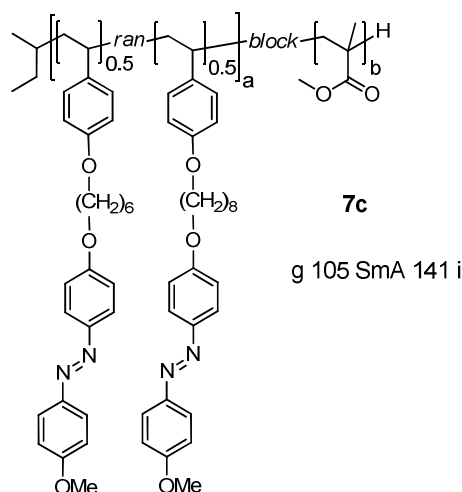
The influence of the writing temperature depending on the sample preparation on the holographic behavior was investigated on azobenzene-containing block copolymer **7c**. The diblock copolymer **7c** featuring a mixture of a six-membered and an eight-membered spacers. This block copolymer exhibits a smectic mesophase between 105 °C and 141 °C.

As described above smectic annealed samples and amorphous quenched samples were prepared. The temporal evolution of the refractive index modulation for a smectic annealed thin film of **7c** at different temperatures (20 °C to 100 °C) is shown in Figure 4.48. On the left side the temporal evolution up to 4000 s is shown to accommodate the exceptionally long writing time until the maximum refractive index modulation is reached at room temperature. Both values are very high compared to the measurements at elevated temperatures but well within range of the variance discussed above. At temperatures above 23 °C the writing time as well as the maximum refractive index modulation are significantly reduced thus on the right side the relevant magnification is shown. For easier comparison the relevant values are extracted and plotted in separate graphs (Figure 4.50, Figure 4.51, and Figure 4.52). From Figure 4.48 it can be seen, that the sensitivity at an early stage increases with increasing writing temperature and, thus, the system becomes faster.
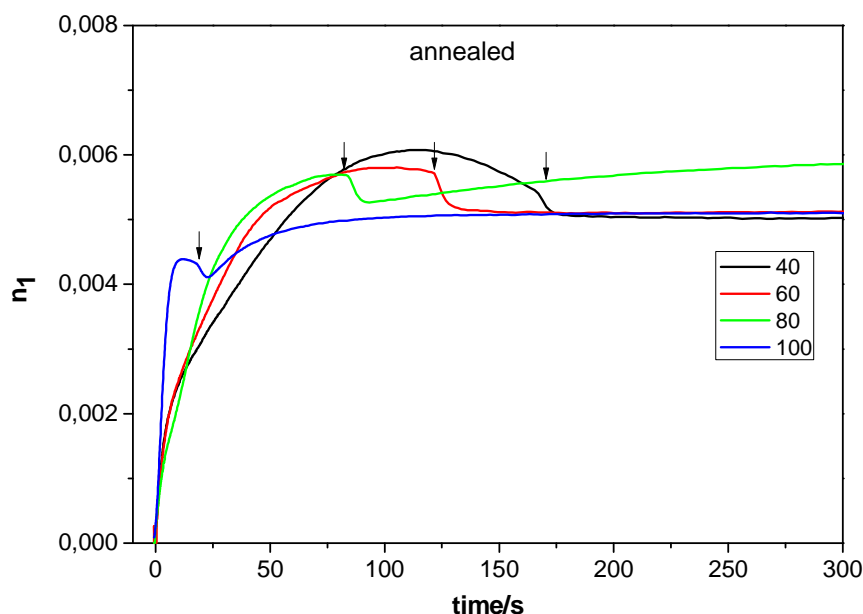
Figure 4.48:   Temporal evolution of the refractive index modulation of an annealed (150°C for 1h and at 130°C for 2h) thin film (d = 0.67 µm) of **7c** at different writing temperatures. Arrows indicate writing laser switch off.

To compare the influence of sample preparation the temporal evolution of the refractive index modulation for a for initially amorphously quenched thin film (quenched) of **7c** at different temperatures (40 °C to 100 °C) is shown in Figure 4.49. The times were the writing laser was switched off are indicated by arrows. For this sample the differences between measurements at room temperature and at elevated temperatures are not as drastic as described for the annealed sample. In the following the extracted significant values are compared to the results obtained for the annealed sample (Figure 4.50 ($t_{90\%}$), Figure 4.51 ($n_{1(90\%)}$), Figure 4.52($n_{1(4000s)}/n_{1(rel)}$)). For the amorphous quenched sample an increase in sensitivity is observed as described for the smecitc annealed sample.
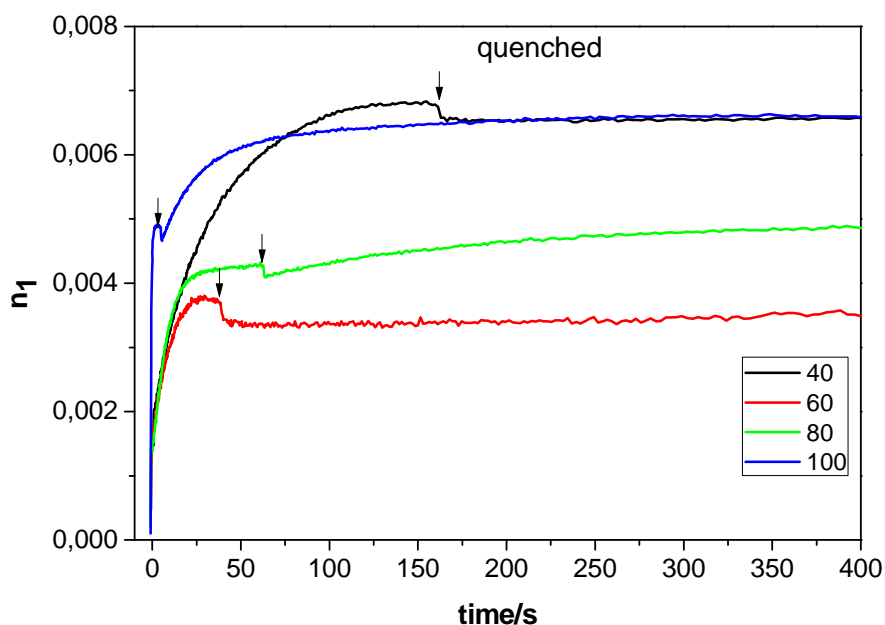
Figure 4.49:   Temporal evolution of the refractive index modulation of a quenched thin film
               (d = 0.96 µm; heated to 170 °C, rapidly cooled below T_g on copper bock in liquid N_2) of **7c**
               at different writing temperatures. Arrows indicate writing laser switch off.

As presented before, writing times at which 90 % of the maximum refractive index
modulation were reached ($t_{90\%}$) were compared and discussed. Figure 4.50 reveals the
pronounced temperature-dependence of the writing time t_{90} on a logarithmic scale. With
increasing temperature from (40 °C to 100 °C), the $t_{90\%}$ decreased by two orders of
magnitude for the annealed as well as the quenched sample. At 100 °C the quenched
sample reaches a $t_{90\%}$ of 1 s whereas the writing time of annealed sample amounts for 6 s.
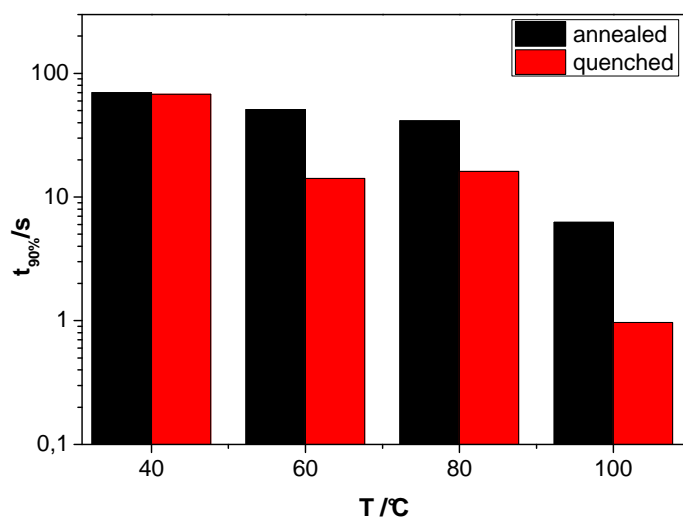
Figure 4.50:   Temperature dependence of time to reach 90 % of $n_{1(max)}$ of inscribed holographic gratings
               for amorphous quenched (heated to 170 °C, rapidly cooled below T_g on copper bock in
               liquid N_2) and annealed (1h at 150 C, 2h at 130 °C) samples of the methoxy azobenzene-
               containing diblock copolymer **7c.**

122

In contrast to the writing time the results for the temperature dependence of the 90 % value of the refractive index modulation ($n_{1(90\%)}$) do not show a clear trend. For 40 °C and 100 °C the $n_{1(90\%)}$ of the quenched sample is higher than for the annealed sample. It can be noted that for the smectic annealed the $n_{1(90\%)}$ decreases with increasing temperature. For the quenched sample a local minimum at 60 °C is apparent although theses minor differences in $n_{1(90\%)}$ might be attributed to the variance in the experimental results. For this sample the 90 % value of the refractive index modulation is reduced by a factor 0.6 when the writing temperature is increased from 40°C to 100°C.
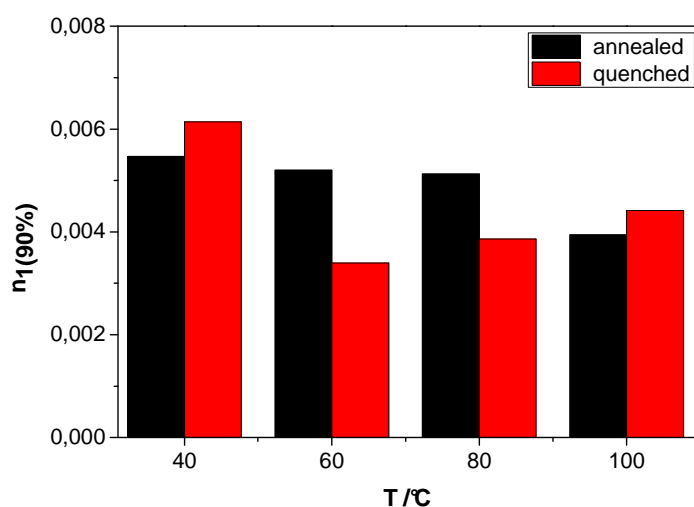
Figure 4.51:   Temperature dependence of the refractive index modulation ($n_{1(90\%)}$) of inscribed holographic gratings for amorphous quenched (heated to 170 °C, rapidly cooled below T_g on copper bock in liquid N_2) and annealed (1h at 150 C, 2h at 120 °C) samples of **7c.**

The temperature dependence of the temporal evolution of the refractive-index modulation after writing laser is switched off ($n_{1(4000s)}/n_{1(rel)}$) is presented in Figure 4.52. For the annealed sample the inscribed gratings are stable at room temperature. A slight postdevelopment is observed with increasing temperature, reaching a maximum value of 122 % at a temperature of 100 °C. The amorphous quenched samples shows approximately the same trend, an increase of postdevelopment with increasing temperature, although at 60 °C a negative deviation is apparent that might be attributed to variance in the measurement. In this sample the postdevelopment reaches 136 % at a temperature of 100 °C. From Figure 4.48 and Figure 4.49 it can be seen that the refractive index modulation increases directly after the initial relaxation for temperatures 80 °C and 100 °C. The rate of the postdevelopment is higher at 100 °C for both samples.
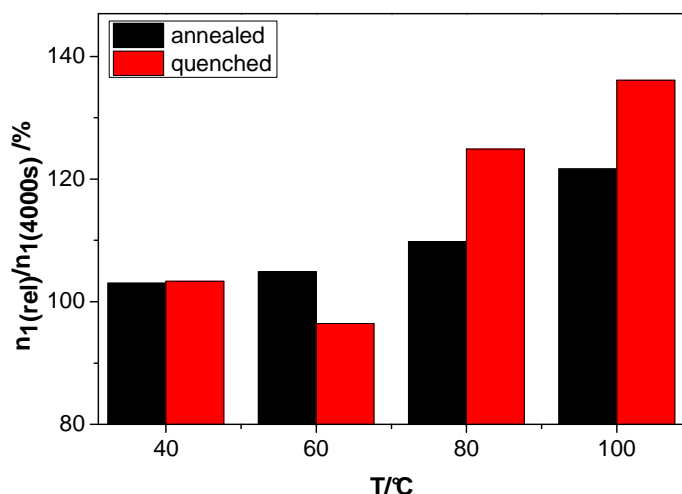
Figure 4.52:   Temperature dependence of refractive index modulation of inscribed holographic gratings 4000 s after writing laser switch off for amorphous quenched (heated to 170 °C, rapidly cooled below T_g on copper bock in liquid N_2) and annealed (1h at 150 C, 2h at 120 °C) samples of **7c**.

The above described results for the azobenzene-containing diblock copolymer indicate that the orientation process of the chromophores induced by the holographic experiment is facilitated by elevated temperatures. Thus the writing times are drastically reduced as well as the postdevelopment is amplified with increasing temperatures. The increased thermal relaxation at elevated temperatures and thus a decrease of the refractive index modulation after writing laser switch off that was reported by other groups[188,204–206] could not be observed in this work.

Different results were obtained for the azobenzene-containing homopolymer **III** compared to the block copolymer **7c**. While both showed improvement in writing times and postdevelopment at elevated temperatures with significant performance increases around the glass transition temperatures, the observed trend for the refractive index modulation are. For the homopolymer **III** an increase of the refractive index modulation is observed that is in agreement with the result in literature for the block copolymer **7c** a decreasing trend was observed.

The results of holographic experiments on thin films for methoxy azobenzene-containing polymer can be summarized as follows.

1. *Influence of the sample preparation (smectic vs. amorphous quenched):*
    In quenched samples the writing times as well as the refractive index modulation is reduced while the postdevelopment is slightly enhanced. The sensitivity in the early stage of the smectic and the amorphous quenched samples does not differ significantly.

2. *Influence of the writing temperature on thin films:*

   The sensitivity sensitivity in the early stage increases at elevated temperatures. Writing times decrease and postdevelopment is amplified with increasing temperatures. Refractive index modulation increases with temperature for homopolymer **III** and decreases for block copolymer **7c**. Significant faster orientation is achieved at writing temperatures in the range of the glass transition of the photoaddressable segment.

3. *Influence of spacer length:*

   Writing times increase with increasing spacer length due to higher order of the smectic mesophase. Mixing of two different spacer length results in lower order of the mesophase, and also lower writing times. No influence on the refractive index modulation is apparent.

4.7.2 Holographic experiments on thick samples of block copolymer blends

In this chapter the following questions will be addressed using azobenzene-containing polymers:

1. preparation of thick samples based on blends of azobenzene-containing block copolymer and PMMA by different approaches,

2. investigation of stability of inscribed holographic gratings in these samples,

3. suitability of these samples for holographic angular multiplexing.

Volume holographic data storage with exceptional high data density requires thick samples (>100 µm). Thick films allows one perform angle multiplexing of Bragg-type gratings with a high angular selectivity. Due to the high optical density of the azobenezene at the writing wavelength a diluting concept is necessary, where the beneficial cooperative effect of the chormophores is maintained. This can be achieved by blending azobenzene-functionalized diblock copolymers with the homopolymers of the respective optical inert and transparent block as shown in Figure 4.53. Dilution of photoaddressable block copolymer with the matrix homopolymer results in a change of morphology from lamellae via cylinders to spheres. Upon further increasing the homopolymer content the diameter of the sphere remains constant and only the distance between the spheres increases.[23,185] By blending an azobenzene-containing block copolymer with PS homopolymer Häckel *et al.* prepared transparent samples with a thickness of 1.1 mm, in which angular multiplexing of 80 holograms at the same spatial position was demonstrated.[185] The use of PMMA as optical inert matrix in these blend has not been successfully demonstrated yet.

increasing matrix fraction by addition of matrix homopolymer
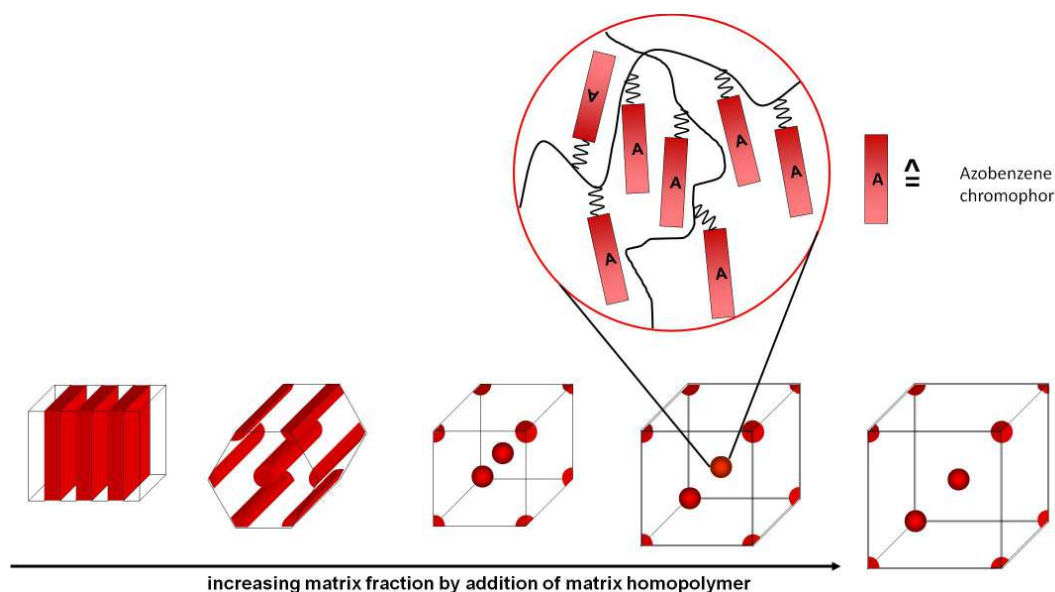
Figure 4.53:   Schematic representation of a concept for the dilution of an azobenzene-containing diblock copolymer with optical inert homopolymer maintaining the cooperative effect in the microphase separated confinements.

126

Sample preparation methods

Several processes were investigated to produce thick samples. As discussed in chapter 1.3 the optical density of the thick samples can be adjusted by diluting the azobenzene content in a blend of the photaddressable block copolymer with the homopolymer of the matrix (PS or PMMA). These azobenzene-containing blends have to be processed into a medium for holographic data storage. The desired thickness of theses samples is within the millimeter range. Typically samples produced in this work were aimed to have a thickness of about 1.1 mm to 5 mm. Several polymer processing techniques will be discussed that can be applied to produce the desired samples For all approaches the azobenzene-containing block copolymers have to contain a matrix that compatible with the homopolymer used in the blend process. Characteristic data of the utilized homopolymers are summarized in Table 4.9.

Table 4.9: Characteristic data of commercial homopolymers used in the blend experiments

	$M_p{}^{a)}$	melt volume flow rate	T_g
	kg/mol	cm^3/10 min	°C
PMMA (Röhm) 8N	114	$3.0^{b)}$	117
PMMA (Röhm) 7H	80	$1.4^{b)}$	112
PS (BASF AG) 165 H	165	$3.4^{c)}$	90

a) molecular weight of peak maximum, determined by SEC (eluent: THF) with respect to polystyrene standards; b) 230 °C, 3.8 kg; c) 200 °C, 5 kg

Three approaches were used: the hot pressing (A), cell cast process (B) and injection molding (C). The injection molding and parts of the cell cast experiments were conducted by C. Löffler.

(A) *Hot-pressing* is a preparation process for polymer films at a low-strain-rate using high by simultaneous application of high pressure and temperatures.

(B) *Cell casting* is a method normally used for creating PMMA sheets. A solution of PMMA/MMA is prepared by dissolving PMMA resin in liquid MMA monomer. A thermal radical initiator is added and this mixture is the poured between two flat sheets of toughened glass sealed with a rubber gasket and heated for polymerization. PMMA is better suited for the cell cast process because for PS the resulting specimens usually contain bubbles and inhomogeneities that are detrimental to the optical quality of the sample.

(C) *Injection molding* of a thermoplastic polymer performed by feeding the polymer into a heated barrel, melting, mixing, and pressing into a colder mold cavity where it cools and

hardens to the configuration of the mold cavity. PS is more widely used this process than PMMA due to lower viscosity of the respective melt. Injection molding of blend of azobenzene-containing block copolymer and PS have successfully been demonstrated. [185] However, injection moldable PMMA grades are commercially available (e.g. 7H Röhm; 80N Asahi Kasei) and were used in this work.

Blending experiments:

For *hot pressing* only experiments a blend containing functionalizable block copolymer and PMMA was prepared. The blend was prepared by precipitating a solution comprising 98.5 wt% of PMMA (7H) and 1.5 wt% diblock copolymer **4c** (PtBS$_{245}$-b-PMMA$_{878}$, M$_n$ = 128 kg/mol, PDI = 1.07) in THF into MeOH. The polymer was thoroughly dried under vacuum (~10 mbar) at 70 °C for 24 h. Thick films were prepared in a hot press (Carver 25-12-2HC). The powder was melted in the press at 170 °C for 3 min before pressure (0.2 bar) was applied for 5 min. The pressed film was transferred into a press at ambient conditions and allowed to cool under slight pressure to avoid deformation of the sample. The sample thickness was adjusted by stacking the pressed films and repeating the pressing process.

These processing conditions were not suited to produce thick films with a high optical quality. An example is shown in Figure 4.54.

Figure 4.54:   Image of a thick film (1.5 mm) of a blend of PMMA (7H) with 1.5 wt% of diblock copolymer **4c** prepared in hot press.

For the *cell casting* process several parameters had to be taken into account and were optimized to obtain samples with high optical quality. The optical quality of the samples was reduced by the formation of bubbles. These can be caused by the N$_2$ emitted by the

initiator 2,2-azobis(isobutyronitrile) (AIBN) or can be formed at to high temperature by the evaporation of MMA. In turn the half life time of the initiator is also depended on the temperature. Thus, the amount of the initiator as well as the polymerization temperature influenced the amount of bubbles formed in the sample. Besides this bubble formation the samples often exhibited turbidity or scattering. The origin of this issue could not be determined but might be due to residual traces of solvents or phase separation between the block copolymer and the PMMA, although TEM results were inconclusive. A careful optimization of the parameters yielded the following typical procedure:

MMA was destabilized by filtering through a short column of basic alumina oxide A mixture comprising 33 wt% of PMMA (7H) and 66 wt% MMA was stirred over 3d until the polymer was fully dissolved. 2 wt% of cyano azobenzene-containing diblock copolymer **13b** were added with respect to the mixture and incorporated by vigorous stirring. 0.25 mol% AIBN with respect to the amount of MMA was added, the mixture was homogenized and then polymerized in a silicon oil bath at 50 °C for 16 h. The polymerization was completed at 80 °C for 24 h. Using this optimized procedure the resulting thick sample did not exhibit bubbles or turbidity (see Figure 4.55).
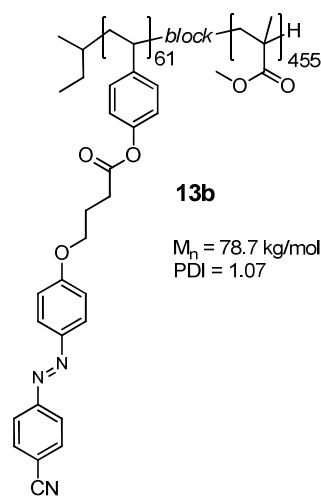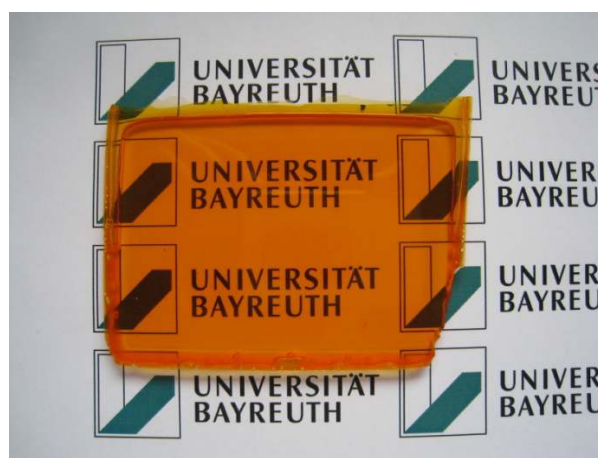
Figure 4.55:   Typical images of a thick sample prepared by cell cast with 2 wt% **13b** in PMMA.

Cyano azobenzene-containing diblock copolymer **13b** as well methoxy azobenzene-containing diblock copolymer **6b** based block copolymers were tested in combination with PMMA (7H) for the cell cast process. The molecular weights of the PMMA segments and the PMMA homopolymer seemed to be close enough to prevent a macrophase separation.

Large samples could easily be prepared with this cell cast process. Although it was demonstrated that cell casting is in general suited to prepare thick samples, the cell cast process did not yield fully reproducible samples and samples were therefore not pursued

for the holographic experiments that require a high optical quality of the data storage material.

For the i*njection molding* process, blends based on PMMA as well as PS matrices were used. PMMA grades 7H and 8N were tested for their suitability for the injection molding process. 7H provided better processability despite a lower melt volume-flow rate than 8N and was used for further experiments. Blends containing 8N were also prepared but this PMMA grade requires higher temperatures during the processing thus imposing a higher thermal stress on the azobenzene-containing polymer. Methoxy azobenzene-containing diblock copolymer **6b** was selected for the blending process because of the appropriate MW of the PMMA segment. Only a methoxy azobenzene-containing polymer was used because of the inferior thermal stability of the cyano azobenzene derivatives (see chapter 4.5.5).

Different approaches were tested for the preparation of **6b**/PMMA mixtures that were used for the injection molding. Powder-powder mixtures were prepared in a powder mixer or by grinding the polymers with by mortar and pestle. These mixtures were subsequently homogenized in polymer melt mixer (DSM High Shear Twin Screw Mixer) at 240 °C. Alternatively, **6b** and PMMA were dissolved in THF and precipitated in MeOH yielding **6b**/PMMA that were dried and directly used for the injection molding. The preparation of the mixtures significantly influenced the optical quality of the resulting injection molded specimen.

Thick samples were prepared by injecting the polymer blend into a surface-polished mold with a diameter of 25 mm and a thickness of 1.1 mm using a DACA MicroInjector. The optimized process conditions were:

4 min melting at 240 °C, Step 1: 8 bar, 5 s; Step 2: 16 bar, 2 s; Step 3: 16 bar, 8 s; dwell pressure: 12 bar, mold temperature: 70 °C

PS 165 H was used in combination with methoxy azobenzene-containing diblock copolymer **12a** using the same equipment and parameters as described above but at a temperature of 210 °C instead of 240 °C.

Process temperatures were lowered from the values given in the data sheets to reduce the thermal stress on the functionalized polymers while maintaining the required melt flow properties thus the optimized temperatures are ~10 °C lower than specified. The high processing temperatures caused polymer degradation on some samples characterized by black Schlieren.

Typical examples of the thick polymer samples based on PMMA and PS are given in Figure 4.56.

Figure 4.56:   Images of the injection molded samples: PMMA (7H) with 0.75 wt% (*top left*) and 1.5 wt% (*bottom left*) of methoxy azobenzene-containing diblock copolymer **6b** as well as PS (165 H) with 0.75 wt% methoxy azobenzene-containing diblock copolymer **12a** (*top right*) prepared by powder-powder mixtures.

One disadvantage of the injection molding process is the shear stress and flow orientation that induces birefringence in the polymer samples.[185] This shear birefringence is detrimental to the holographic experiments but can be reduced by annealing the samples inside the a polished mold for 20 h at 135-140 °C under vacuum. This procedure is sufficient to reduce shear birefringence to a large extent as shown in Figure 4.57. Two samples of injection molded PMMA 7H are compared. On the left is the sample without annealing as it was prepared by injection molding. This sample exhibits high birefringence. On the right is an annealed sample that shows a significantly reduced birefringence. This annealing process and the related characterization were conducted by Dr. K. Kreger.

Figure 4.57:   Images between crossed polarizers of injection molded samples of PMMA 7H before (*left*) and after (*right*) the annealing process (20 h at 135-140 °C under vacuum).

The quality of the samples prepared by injection molding was analyzed using a micro-haze *plus* (BYK Gardner) to determine the transmission, haze and clarity. While haze is defined as the percentage of light that is deflected more than 2.5° from the incoming light direction (wide angle scattering) clarity is defined as the percentage of light that is deflected less than 2.5° (small angle scattering). While the transparency was reduced for all samples with azobenzene-containing block copolymer, the preparation conditions influenced the haze and clarity values. Additionally, both parameters were influenced by minor coarseness of the mold resulting in a reduced optical quality of the samples. Analysis of all samples prepared under different conditions revealed that powder–powder-mixtures prepared in the MicroInjector exhibited the best optical properties. All results are given in details in the experimental part, chapter 6.6.

Due to these results and the macroscopic appearance the annealed samples with 1.5 wt% **6b** and sample with 0.75 wt% **6b** were used for further experiments.

Control of optical density

For the holographic experiments the optical density (OD) of the material at the wave length of the writing beam has to be sufficient low to allow the beams to penetrate the whole sample. Specimens with a thickness of 1.1 mm containing concentrations of 0.75 wt% and 1.5 wt% of methoxy azobenzene-containing diblock copolymer **6b** and 99.25 wt% homopolymer PMMA and 98.5 wt% homopolymer PMMA respectively, were prepared. The relevant region of the UV-Vis spectra is shown in Figure 4.58. At the wave length of the writing laser beam (488 nm) the sample containing 1.5 wt% **6b** exhibits an OD of 0.85 whereas the sample with a concentration of 0.75 wt% has an OD of 0.37. The latter value is sufficiently high enough for the following holographic experiments therefore samples with 0.75 wt% **6b** were used for the preliminary holographic experiments on thick samples. The optimal optical density should be about 0.7 for holographic data storage materials. Holographic experiments are usually performed at a writing wavelength of 488 nm.
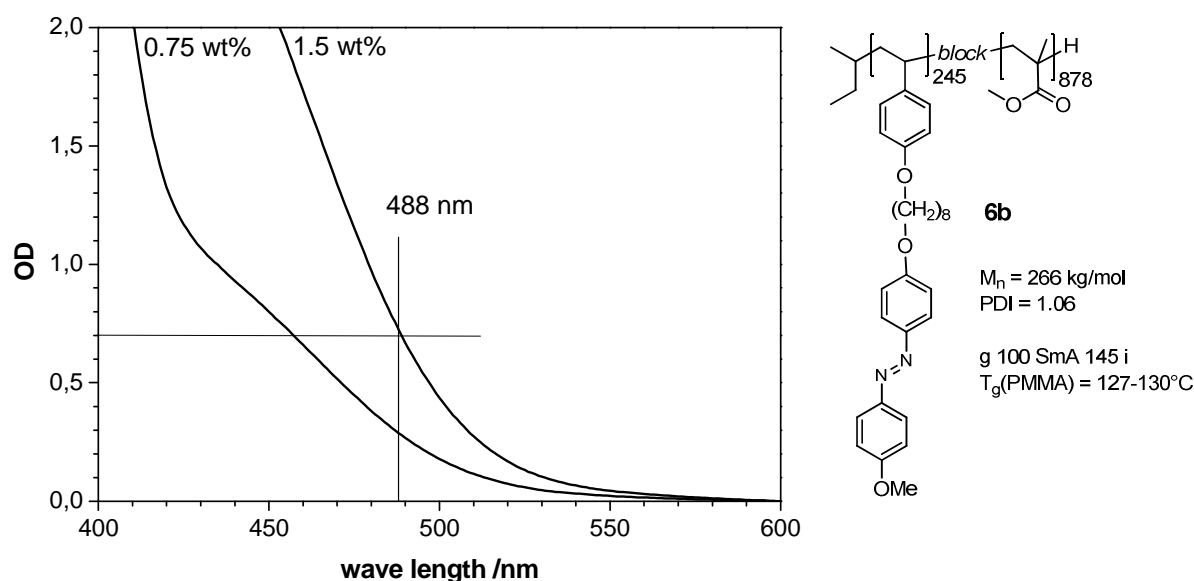
Figure 4.58: Optical density at the writing wave length of the holographic experiments of injection molded polymer blend samples (d = 1.1 mm) with different concentrations of methoxy azobenzene-containing diblock copolymer **6b** (measurements were performed by K. Kreger). The region of OD that can be used for holographic experiments as well as the writing wave length are indicated.

Temporal evolution of diffractive index modulation

At first single holographic gratings were inscribed at room temperature to investigate the temporal evolution of the diffractive index modulation in thick samples prepared of PMMA based blends with 0.75 wt% of the methoxy azobenzene-containing diblock copolymer **6b**. The temporal evolution of the refractive index modulation at room temperature is given in Figure 4.59. On the left side the timescale until $n_{1(max)}$ is reached is magnified, this writing time is comparable to values obtained for thin films of **6b**. Directly after writing laser switch off n_1 relaxes slightly to $n_{1(rel)}$ over a period of 100 s. This decrease of n_1 was also observed in holographic experiments on thin films at room temperature and might be due to the thermal relaxation of an unwanted *cis*-population grating. In Figure 4.59 (right) the postdevelopment is evident over 17 hours. This evolution of the refractive index modulation is very promising.

In previously published results on thick samples non-chomophoric mesogens in the azobenzene-containing block had to be used to increase the stability in the sphere morphology. Nevertheless, the refractive index modulation decreased slightly with time.[185,208] In contrast, in the system described in this thesis the inscribed gratings were stable and exhibited an increase in refractive index modulation. This observation also indicates that a liquid crystalline mesophase is present in the nano-confined azobenzene-containing minority phase otherwise no postdevelopment effect would occur.

133

Confirmation of the existence and nature of a liquid crystalline phase in the nano-confined domains is not easy to achieve due to the very high dilution.
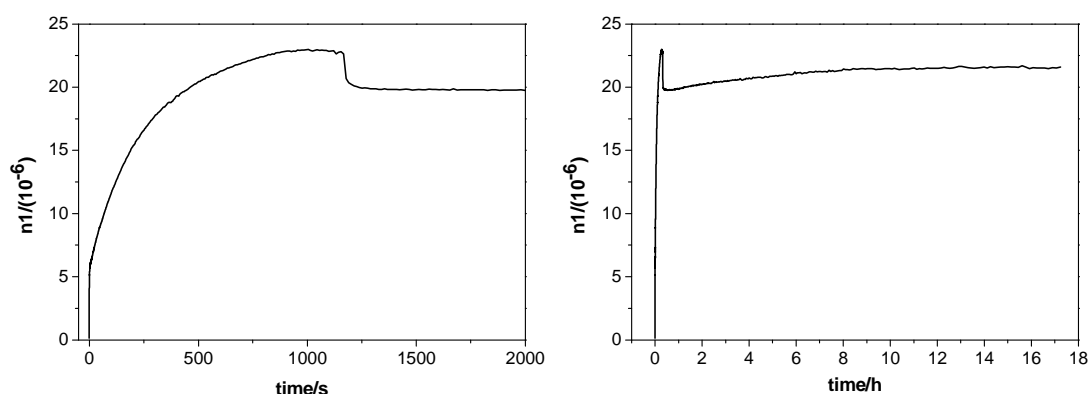
Figure 4.59:   Temporal evolution of the refractive index modulation at room temperature of an injection molded PMMA blend sample (d = 1.1 mm) with 0.75 wt% methxy azobenzene-containing diblock copolymer **6b** (annealed at 150 °C for 24 h prior to the experiment) for the first 2000 s (*left*) and the long term evolution of the refractive index modulation over 18 h (*right*).

This demonstrates principle performance of azobenzene-containing block copolymer blends in thick samples. The influence of the writing temperature on the holographic properties obtained for the thick samples was not investigated to date. This would be interesting whether the results received from the thin films were applicable for the thick samples as well.

Angular multiplexing

In holographic data storage the storage density can be significantly increased by using several multiplexing techniques that allow the storage of multiple holograms in the same volume element.[137] One approach that can be used for intensity holograms is the angular multiplexing. With this technique several holograms are written in the same volume element under different angles of the incident beams. In the experimental setup used, this is achieved by rotating the sample (see Figure 4.60).
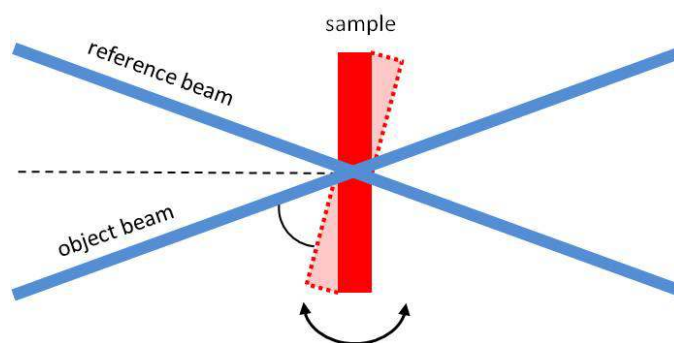
Figure 4.60:   Schematical representation of angular multiplexing in a holographic experiment by rotating the sample.

If multiple holograms are written at different angles in the same volume element of azobenze-containing polymer blends, the maximum achievable refractive index modulation $n_{1(max)}$ is shared between the single gratings; thus, n_1 of each individual grating is much lower than $n_{1(max)}$ measured in a single grating experiment. As a result, an increased number of inscribed holograms lead to an increased the signal-to-noise ratio.

Angular multiplexing of holographic intensity gratings in 1.1 mm thick injection-molded samples was investigated at room temperature on annealed samples of PMMA blend containing 0.75 wt% of the methoxy azobenzene-containing block copolymer **6b.** Five gratings were subsequently writing at the same volume element of one sample. The refractive index modulation was subsequently recorded over the angular range of +3 ° to - 3 ° after the completion of the writing process yielding a representation of all inscribed gratings shown in Figure 4.61. The five gratings were inscribed 1 °, 0 °, -1 °, -2 °, and 2 °. The signal intensity (i.e. the refractive index modulation) of an intensity grating is reduced by the writing of the next grating in the same volume element. By each photo-orientation process under a distinct angle, fractions of the previously oriented chromophores are reoriented, thus reducing the intensity of the previous holographic grating. Therefore, the refractive index modulation of the last grating is always distinctly higher than that of the previously inscribed if all gratings were recorded with the same intensity of the incident beams. This causes a decay in the direction 1-5 as shown in Figure 4.61. By this experiment it has been principally demonstrated that angular multiplexing is possible in injection molded samples of blends of azobenzene-containing block copolymer with PMMA.
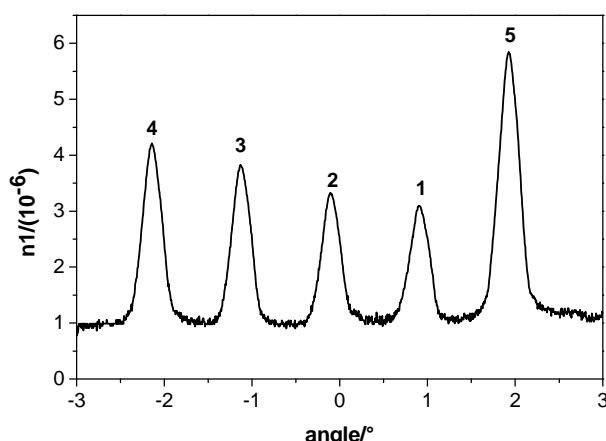
Figure 4.61:   Five angular multiplexed holographic intensity gratings in an injection molded PMMA blend sample (d = 1.1 mm) with 0.75 wt% methxy azobenzene-containing diblock copolymer **6b**.

Achievements

In this chapter azobenzene-containing homopolymers, copolymers and block copolymers with PMMA or PS matrix were synthesized and characterized. Polyhydroxystyrene was introduced as the functionalizable segment that resulted in liquid crystalline polymers with a high glass transition temperature after polymer analogous attachment of the mesogenic side-groups. Most of the block copolymers were designed to investigate structure-property relations regarding their thermal and mesophase behavior as well as to their application as materials for holographic data storage. The structure-property relation of the resulting mesophase was investigated in functionalized block copolymers as well in the respective homopolymer that were used as reference materials. Holographic experiments were conducted on selected examples of the prepared azobenzene-containing polymers and several influences on the holographic behavior were investigated. At writing temperatures of 100 °C in amorphous quenched samples the writing times could be significantly reduced while the refractive index modulation decreased only slightly. Thick samples (1.1 mm) were prepared by injection molding with blends of this photoaddressable block copolymer and PMMA or PS. Preliminary results confirmed the stability of holographic inscribed gratings and angular multiplexing of holographic volume gratings was demonstrated.

136

5   Cyanobiphenyl-functionalized ABA block copolymers as gelators for liquid crystals

5.1   Introduction

A gel is a soft, solid or solid-like material that contains at least two different components: A solvent as the majority component and a gelator that forms the gelating network as a minority component.

ABA triblock copolymers have been extensively studied as gelators for isotropic liquids based on the principle of selected solubility.[209–215] A frequently used polymer system is polystyrene-*block*-polyisoprene-*block*-polystyrene   (SIS).   Hydrocarbons   such   as tetradecane and *n*-heptane can be used as selective solvent for the polyisoprene B-block.[210–215]

In this chapter functionalized ABA triblock copolymers are presented that can be used as gelators for low molecular weight liquid crystals. As previously described in chapter 1.4, Kornfield *et al.* introduced ABA triblock copolymers comprising of a functional B-block and two polystyrene A-blocks suitable to gel the low molecular weight liquid crystal 5CB.[118,119] The gelation is based on the selective solubility of the A-blocks and B-block in a nematic solvent leading to the formation of a physical network as illustrated in Figure 5.1. Both, A and B segments are soluble in the isotropic liquid. However, in the liquid crystalline phase only the functionalized B-block remains soluble. Due to microphase separation, the polystyrene A-blocks self assemble into nodes that create the thermoreversible physical network.

Typically, the solubility of amorphous polymers, for example, the A-blocks in the ABA triblock copolymers, in common solvents is a monotonic function of the temperature; thus, the quality of the solvent changes gradually. In contrast, *liquid crystalline solvents cause an abrupt change in solvent quality due to their first-order transition from the isotropic into the liquid crystalline phase*. While the polymer can be soluble in the isotropic phase the long range order in liquid crystalline phase significantly decreases the solvent quality.[216–218] In general, dissolution of the end blocks in a liquid crystal is unfavorable because it decreases the entropy of the dissolved polymer. In contrast, side-group liquid crystal polymers have been reported to be soluble in liquid crystalline solvents due to their mesogenic side-groups which may render them compatible.[216,218–220]

Important features of gels based on block copolymers described in the following are: The *gelator* forms a thermoreversible network inside the solvent. The A-blocks form the physical crosslinking points or solid *nodes*. The length of the functionalized B-block determines the *network span,* the distance between the nodes. The *gelation temperature* is

the temperature at which a space filling thermoreversible network is formed and gelation of the solvent is achieved. The *critical concentration* is minimal gelator concentration at which gelation occurs.
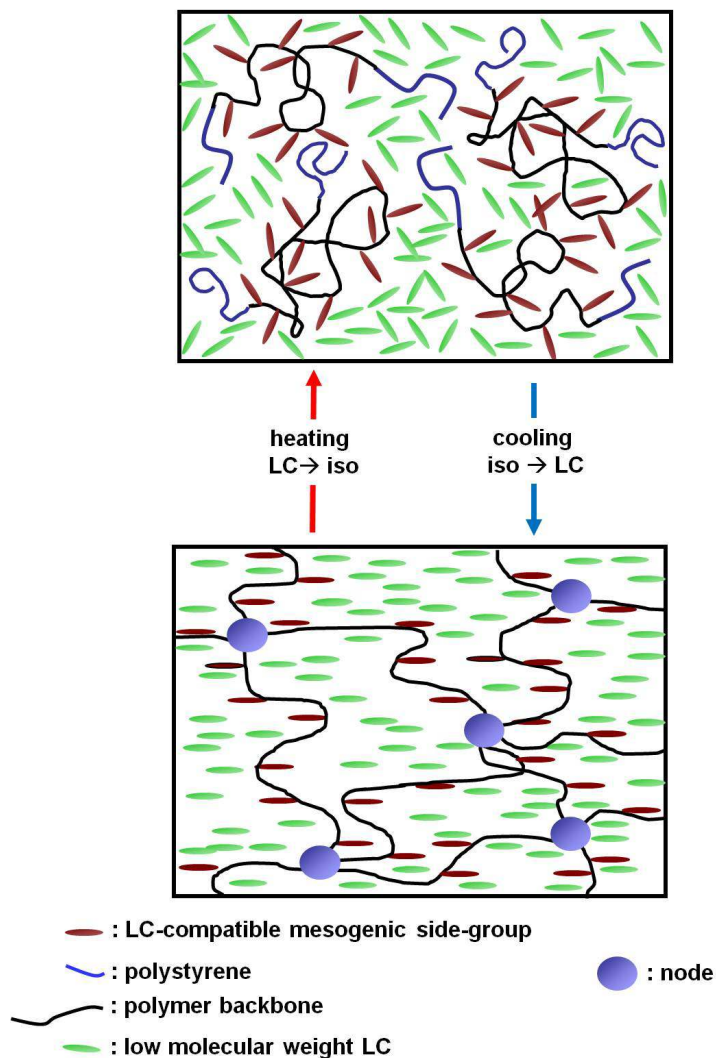
Figure 5.1:   Schematic illustration of model of a thermoreversible LC physical gel using ABA triblock copolymer gelators in a nematic solvent.

5.2   Scope of this chapter

In this chapter novel cyanobiphenyl-functionalized block copolymers are designed, synthesized and characterized that can be used as gelators for low molecular weight liquid crystals. The objectives of this chapter are:

a)   synthesis and characterization of cyanobiphenyl-functionalized homopolymers and their structure-property relations with respect to the solubility in 5CB

b)   anionic polymerization of ABA triblock copolymers comprising functionalizable B-blocks with very high degree of polymerization

c)   synthesis and characterization of novel cyanobiphenyl-functionalized ABA triblock copolymers

d)   preparation of liquid crystalline gels based on 5CB using these block copolymer gelators

e)   investigation of the influence of the polymer backbones of the gelators on the gelation of 5CB by rheological methods

f)   investigation of gelation by electro-optical methods in cooperation with Dr. Maxim Khazimullin and Prof. Ingo Rehberg (Experimental Physics V) within FOR608

In the following, the concept of this study and the design of the polymers are discussed. The ABA triblock copolymers presented in this chapter consist of two polystyrene A-blocks and a B-block based on poly(4-hydroxystyrene) functionalized with 4-cyanobiphenyl moieties (Figure 5.2). The block copolymers were prepared using two different approaches via anionic polymerization and subsequent polymer analogous reactions. For this, the functionalizable B-block is deprotected and functionalized with cyanobiphenyl moieties. Using this approach series of gelators were prepared with variations in the B-block length, the A-block lengths and the polymer architecture. A comprehensive study was conducted to investigate the structure-property relation regarding the gelation of the low molecular weight liquid crystal 5CB.
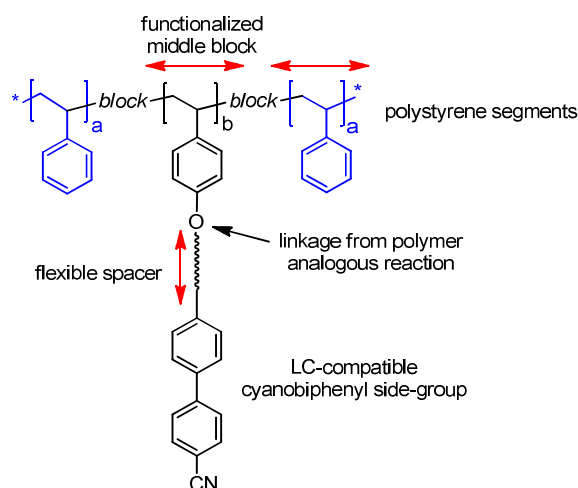
Figure 5.2: Schematic representation of the targeted ABA triblock copolymers with the variations in block length and spacer length as indicated by red arrows.

In Figure 5.3 schematically structures of three different ABA block copolymers with varying lengths of the single segments and the corresponding schematic illustration of physical LC gels are shown. Considering ABA block copolymers composed of a LC compatible side-group functionalized B-block and polystyrene A-blocks at concentrations where gels are formed, different lengths of the blocks and block copolymer compositions will affect the network structure such as network span, network density and size of the physical nodes. The network span and, hence, the network density are determined by the length of the functionalized B-block. As a result, the critical gelator concentration, that is the minimal concentration at which a sample filling network is formed, depends on the length of the B-block. Theoretically, a higher degree of polymerization of the B-block should result in lower critical gelator concentration. In Figure 5.3 (left) an ABA triblock copolymer gelator is shown with A-blocks and a long B-segment. The resulting thermoreversible gel network is assumed to contain large physical nodes and a low network density due to the high network span of the functionalized B-block. This should yield a stable gel due to the large nodes but a weak gel due to low number of nodes. In a simplistic model the radius of the polystyrene spheres that form the nodes due to the phase separation equals the maximal length of the extended PS chain. If the lengths of the polystyrene A-blocks are decreased (Figure 5.3, middle), the size of the physical nodes is expected to decrease while the network density is unchanged. This should result in a less stable gel due to the smaller nodes. If the length of the functionalized B-block is decreased (Figure 5.3, right), the network span is reduced and the network density is expected to increase. The resulting gel should be harder than the two previous due to the increased number of nodes and the stability of the network should be the same as in the previous example.
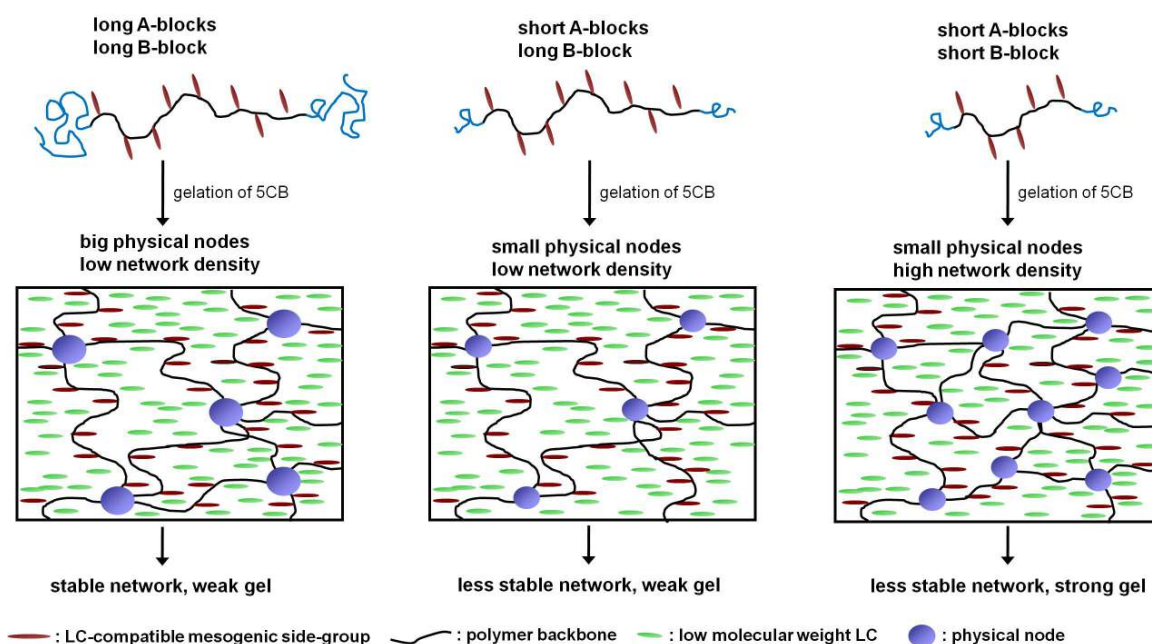
Figure 5.3: Schematic illustration of the assumed influence of variations in the block lengths of the ABA triblock copolymer gelator on the resulting gel network.

5.3 Synthesis and characterization of cyanobiphenyl-containing homopolymers

If the functionalized ABA triblock copolymers were used as gelators for the liquid crystal 4-cyano-4'-(pentyl)biphenyl (5CB), the functionalized B-block requires good solubility in the nematic phase of this solvent. Side-group liquid crystal polymers have been reported to be compatible with LC solvents in both the nematic and the isotropic phases if the laterally attached mesogenic side-groups are structurally very similar. As reference materials and to investigate the structure-property relationship with respect to meosphases and the solubility in 5CB the structurally analogous cyanobiphenyl-containing homopolymers were prepared and studied.

Regarding cyanobiphenyl-containing liquid crystalline side-group polymers that were based on a polyhydroxystyrene backbone were reported by Imrie et al..[221] They prepared polymers with spacers featuring three to twelve methylene units (x). PHS (M_n = 30 kg/mol, ru_{PHS} = 250) was functionalized with bromo-functionalized mesogens in a polymer analogous attachment reaction using a procedure described by Crivello et al..[122] In this report PHS and the mesogens were reacted in a water/toluene (1:4) mixture under reflux using NaOH and tetra-n-butylammonium bromide as a phase transfer catalyst. From a spacer length of x = 3 upwards all functionalized polymers were liquid crystalline and a SmA phase was reported.

In contrast, here the functionalizable polymer backbone with a high degree of polymerization was prepared by anionic polymerization. The functional segments in this

chapter exhibit a much higher degree of polymerization, about ten-fold, compared to the polymers reported by Imrie and to polymers that have been described in chapter 4. After the polymerization the block copolymers were deprotected. The mesogenic cyanobiphenyl side-groups were prepared with different spacer lengths bearing a ω-bromo function. In the last step the functional polymers were prepared in a polymer analogous attachment reaction of the mesogens to the polymer backbone.

Synthesis of the cyanobiphenyl moieties

The cyanobiphenyl (CB) unit was chosen as mesogenic side-group due to its structural similarity to 5CB. Even membered flexible spacers containing from four to ten methylen units (x) were used for the connection of the mesogenic unit to the polymer backbone. The spacers were attached to the CB unit via an ether linkage for enhanced flexibility and chemical stability. As shown in Figure 5.4, **CB1-4** were prepared in a one step reaction from the hydroxyl functionalized CB moiety and the α,ω-dibromoalkanes. The same reaction conditions were used for the Willimason ether synthesis as in chapter 4.5 for the azobenzene chromophores. The usage of potassium carbonate in the absence of water precludes the attack on the cyano function that might be promoted by a stronger base (see chapter 4.5 for details). The purity of the CB moieties **CB1-4** was determined by ^{1}H-NMR and SEC using an oligomeric column set. The absence of excessively used alkyldibromide had to be ensured to avoid coupling reactions during the polymer analogous attachment of the CB units to the polymer backbone.

CB	1	2	3	4
x	4	6	8	10
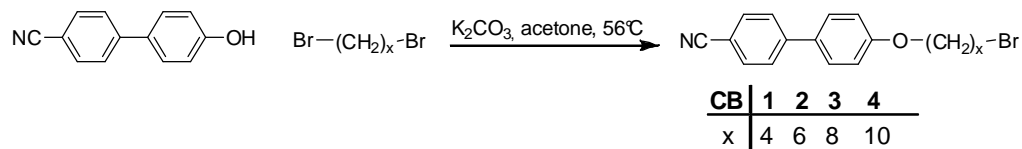
Figure 5.4: Synthesis of the cyanobiphenyl meosgenic units **CB1-4** via Willimason ether reaction.

Synthesis of cyanobiphenyl-containing homopolymers

Cyanobiphenyl-containing homopolymers were prepared by functionalizing polyhydroxystyrene (PHS) **II** with the above mentioned mesogenic moieties **CB1-4** as illustrated in Figure 5.5. The polymer backbone was prepared by anionic polymerization of the protected monomer *tert*-butoxystyrene resulting in poly(tert-butoxystyrene) **I** ($M_n = 470$ kg/mol, PDI = 1.06 (eluent: THF, UV-detection) $ru_{PtBS} = 2670$). Details and discussion concerning the anionic polymerization of the homopolymers and block copolymers in this chapter will be given in 5.4. The protection groups were cleaved under

acidic conditions yielding **II** by reacting the homopolymer I with an excess of hydrochloric acid in THF under reflux as described in detail in chapter 4.3.1. The attachment of the mesogenic side-groups was carried out in the last step.

At first, the polymer analogous functionalization reported by Imrie *et al.*[221] was tested. During this thesis this procedure failed to yield the desired polymers. On the one hand if the rather strong base NaOH was used side reactions of the cyano group seemed to take place as evident from thin layer chromatography (TLC) and ^{1}H-NMR. On the other hand the described solvent mixture turned out to be not suitable to properly dissolve the precursor polymer as well as the product. This might be due to the fact that the polymers used in this thesis exhibited a much higher molecular weight compared to those described Imrie *et al.*.

Therefore, similar reaction conditions as reported in the previous chapter for polymer analogous attachment of the azobenzene moieties were used. To this end the attachment of the cyanobiphenyl moieties was carried out in anhydrous DMF, using potassium carbonate as base, potassium iodide as catalyst and 18-crown-6 as phase transfer catalyst. The reaction was conducted at 110 °C over at least 24 h to 48 h.

x	IX	X	XI	XII
x	4	6	8	10
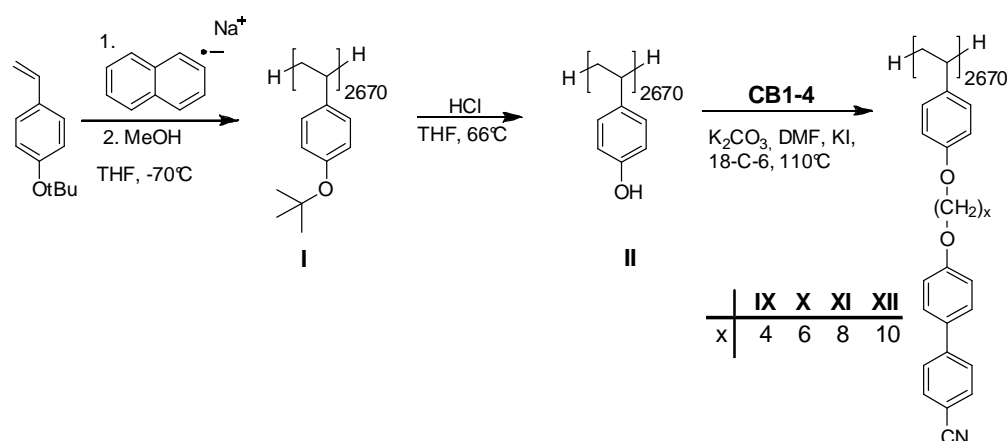
Figure 5.5:   Anionic polymerization of **I**, deprotection and synthesis of the cyanobiphenyl-functionalized homopolymers **IX-XII.**

The degree of conversion of the polymer analogous attachment of the side-groups was monitored with IR spectroscopy and determined with ^{1}H-NMR as already described for the azobenzene containing polymers in chapter 4.5.1. In Figure 5.6 the ^{1}H-NMR spectrum of **XI** in CDCl$_3$ with indication of the relevant integrals is shown. Although signals of the different proton pairs of the cyanobiphenyl group are commonly broad and no splitting can be resolved, for **XI** the splitting can be seen. Often DMF-d$_7$ had to be added to break aggregation and increase the solubility. For the determination of the degree of conversion of the attachment reaction specific integrals were used. The integrated area for the ^{1}H NMR peaks corresponding to the CH[1,2,3] of cyanobiphenyl group at 7.6 - 7.4 ppm were

143

compared to the signal of the $CH^{a,b}$ of the polystyrene backbone at 6.7 – 6.1 ppm. Often the signal of CH^4 overlaps with this signal and has to be taken into account. Using these integrated areas the degree of conversion can be calculated for **XI** to DC = 99 %. The homopolymer **IX** (DC = 97 %) exhibit nearly the same degree of conversion whereas **XII** and **X** show a slightly decreased value of DC = 87-89 %.
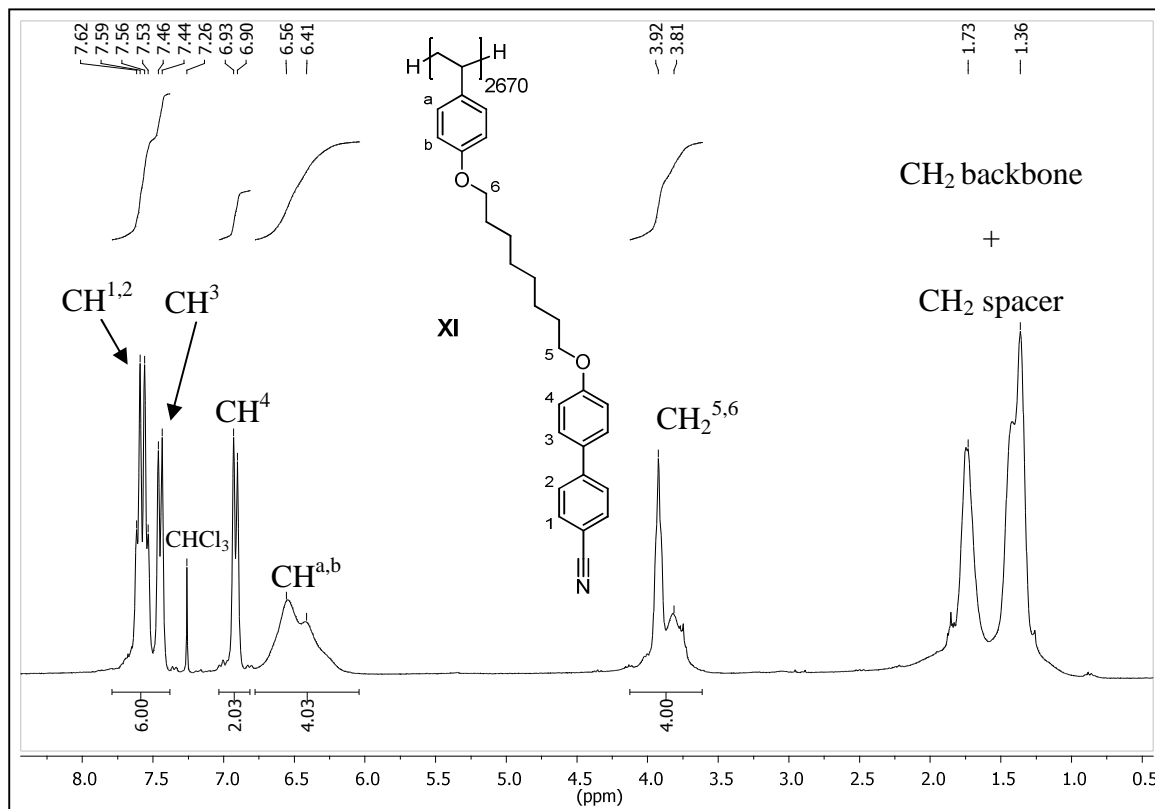
Figure 5.6: ^{1}H-NMR spectrum in CDCl$_3$ of cyanobiphenyl-functionalized homopolymer **XI**. The integrals used for determination of the degree of conversion are marked.

The molecular weight of all functionalized polymer was determined with the SEC setup using THF with 0.25 wt% electrolyte as eluent. Measurement of the SEC with pure THF as eluent resulted in extreme broadening of the resulting curves as well as unrealistic high molecular weights. This behavior was attributed to aggregation of the side-groups of the functionalized polymers. This aggregation can be avoided by using the electrolyte tetrabutyl ammonium bromide. The molecular weights are reported here with respect to polystyrene standards. The theoretical molecular weights (M_n(th)) were calculated using the repeating units determined for the precursor polymer, the degree of conversion and the molecular weight of an average functionalized repeating unit. Characteristic data of the resulting cyanobiphenyl-containing homopolymers **IX-XII** are given in Table 5.1. From comparison of M_n(th) and M_n determined by SEC it is evident that the polystyrene

144

calibration results in apparent molecular weights that overvalue the molecular weight by a factor of 1.6. Nevertheless, the determined molecular weights can be used for relative analysis of molecular weight trends and molecular weight distributions. In the following only the molecular weights determined by SEC will be discussed.

The molecular weight ranges from $M_n = 1600$ kg/mol for **X** (x = 6) to $M_n = 1865$ kg/mol for **XII** (x = 10). These molecular weights are very high and are at least ten times the values determined for the azobenzene-containing homopolymer and copolymers in chapter 4.5.

One might expect an increase in molecular weight with increasing length of the attached spacers, **IX** (x = 4) to **XII** (x = 10). This trend is observed here with the exception of **X** (x = 6). This might be due to its lower degree of conversion (DC = 89 %) compared to **IX** and **XI**. The PtBS homopolymer **I** ($ru_{PtBS} = 2670$) that is the precursor of **17d**, was used for the synthesis of the cyanobiphenyl-containing homopolymers **IX-XII**. The molecular weight of the protected precursor **I** was determined using the SEC using THF with 0.25 wt% electrolyte as eluent for better comparison to $M_n = 532$ kg/mol with a PDI of 1.07. The apparent molecular weight of cyanobiphenyl-containing homopolymers **IX-XII**, as determined with respect to polystyrene standards, increased by the factor 3 to 3.5 compared to the functionalizable homopolymer **I**. The increase expected from the theoretical molecular weights is in the range of a factor 2.0 to 2.6.

Table 5.1: Characteristic data of all CB containing hompolymers **IX - XII** and the precursor **I**

homo-polmyers	$x^{a)}$	$M_n^{b)}$	$M_w^{b)}$	$PDI^{c)}$	$DC^{d)}$	$M_n(th)^{e)}$	$ru^{f)}$
		kg/mol			%	kg/mol	
IX	4	1637	1898	1.16	97	1013	2670
X	6	1600	2128	1.34	89	1027	2670
XI	8	1732	2176	1.26	99	1174	2670
XII	10	1865	2099	1.12	87	1148	2670
I *	-	*532*	*570*	*1.07*	-	*470*	*2670*

a) spacer length in methylene units; b) determined by SEC (eluent: THF + 0.25 wt% electrolyte); molecular weight with respect to polystyrene standards, UV-detection; c) polydispersity index, M_w/M_n; d) degree of conversion of polymer analogous reaction, determined by ^{1}H-NMR; e) theoretical molecular weight calculated from repeating units and degree of conversion; f) average number of repeating units determined for respective functionalizable homopolymer **I**; * the homopolymer batch **I***l* was used

The SEC traces of the cyanobiphenyl-containing polymers **IX-XII** are shown in Figure 5.7 in comparison to the functionalizable homopolymer **I** that they are based on. Compared to the functionalizable homopolymer **I** a broadening of the molecular weight distribution can be observed for all functionalized homopolymers. Commonly, the

fraction of side reactions increased if the purity of the educts was not sufficiently high. Prolonging of the reaction time also caused a broadening of the molecular weight distribution; thus, an optimum had to be found that ensured a high degree of conversion without significant increase of intermolecular reactions. Reaction control of the polymer analogous attachment proved difficult because the molecular weight determined by SEC did not necessarily correspond linear to the degree of conversion. The only viable solution was a micro work up of every sample drawn during the reaction and determination of the degree of conversion by ^{1}H-NMR.

In Figure 5.7 exemplary SEC traces for the cyanobiphenyl-containing triblock copolymers with the shortest spacers **IX** (x = 4) and the longest spacer **XII** (x = 10) as well as the functionalizable homopolymer **I** are shown. The molecular weight distribution of **X** is the broadest in this series of functionalized homopolymers with a PDI = 1.34. Homopolymer **XII** (PDI = 1.12), **IX** (PDI = 1.16) and **XI** (PDI = 1.26) show narrower molecular weight distributions. Taking into account the exceptional high molecular weight of these polymer the determined molecular weight are quite reasonable. Additional shoulders in the SEC traces indicated the occurrence of coupling reaction during the mesogen attachment to a minor degree.
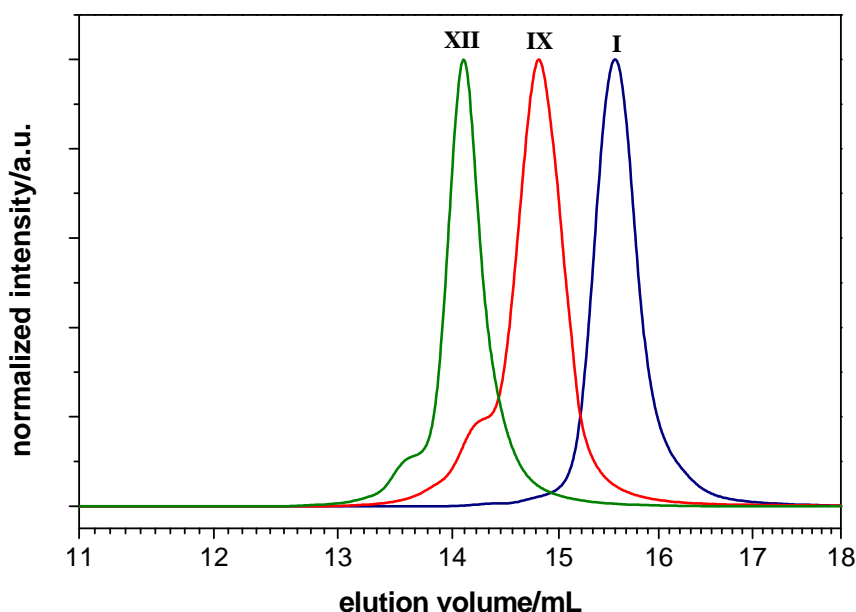

Figure 5.7:   SEC traces of cyanobiphenyl-containing homopolymers **IX** with shortest spacer (x = 4), **XII** shortest spacer (x = 10), and the functionalizable homopolymer **I** (eluent: THF + 0.25 wt% tetrabutylammonium bromide, UV detection).

.

5.3.1 Solid state characterization of cyanobiphenyl homopolymers

Possible liquid crystalline phases of the cyanobiphenyl-functionalized polymers are relevant for their miscibility in the nematic solvent.[216,219] Thus their thermal properties were analyzed by DSC under N_2 with a heating rate of 10 K/min. The thermal stability in the investigated temperature range was confirmed via thermo gravimetric analysis (TGA) prior to thermal investigation by DSC.

The second heating thermograms are given in Figure 5.8. In addition, POM images taken between crossed polarizers for **IX-XII** above and below the liquid crystalline to isotropic transition are shown as well as magnifications in the range of the glass transitions for **XI** and **XII**. The glass transitions that were detected in this series were quite broad and contained a low heat capacity. The reported temperatures mark the middle of the transition.

Homopolymer **XI** (x = 8) exhibits the highest clearing temperature at 112 °C and a glass transition around 62 °C. For the cyanobiphenyl-functionalized homopolymer **XII** with the longest spacer (x = 10) a glass transition is detected at 68 °C as well as a sharp clearing transition at 105 °C. These two cyanobiphenyl-containing homopolymers can be clearly described as liquid crystalline. In contrast, the DSC curves for the polymers **X** (x = 6) and **IX** (x = a) are less obvious. For **X** a glass transition can be detected around 63 °C that is partially superimposed with a liquid crystalline to isotropic transition with a maximum at 90 °C. Compared to the homopolymers **XI** and **XII** this transition is very broad. For the cyanobiphenyl-containing homopolymer **IX** (X = 4) only one broad transition is detected around 80 °C. This might be attributed to a glass transition; although, a clearing transition with low heat capacity might be a superimposed. The general trend for **X-XII** of the clearing transitions corresponds to reports in literature on analogous polymers, although here the temperatures are decreased compared to these reported.[201,221]

The formation of a mesophase seems to increases with increasing spacer length. The liquid crystalline to isotropic transition gets sharper with increasing spacer length and the enthalpy of this transition increases slightly. For the glass transition one would expect decreasing temperatures with increasing length of the spacer as discussed for azobenzene-containing homopolymers and block copolymers in chapter 4.5, nevertheless in the series **IX-XII** they were all found in the same temperature range. This might be due to the different degrees of conversion in the series **IX-XII**, because the transition temperatures are influenced by the degree of attachment of the mesogens.[20,88]

Further investigation of the liquid crystal clearing behavior of the cyanobiphenyl-functionalized homopolymers was established by means of polarized optical microscopy (POM). Microscopic images of **IX**-**XII** between crossed polarizers are inset in the second heating thermograms in Figure 5.8. For the homopolymers **XII** (x = 10) and **XI** (x = 8)

these images appear black above the clearing temperatures and exhibited birefringence below the isotropic to liquid crystalline transition that was persistent at room temperature. Textures obtained for **XII** in the liquid crystalline temperature range might be identified as Schlieren texture. Polymer **X** also exhibited birefringence on heating below the assumed clearing temperature, although the images did not turn completely black above this transition. This observation might be attributed to remaining shear induced birefringence. For polymer **IX** with the four-membered spacer birefringence could be induce at temperatures of 80 °C. On heating these birefringence developed into a texture that might be seen as Schlieren textures as shown in Figure 5.8 until a temperature of 95 °C. Upon further heating the textures collapsed and the intensity of the birefringence decreased but did not result in a completely black image. On cooling increase in birefringence was observed over a broad temperature range starting at about 95 °C without resulting reaching the level that was observed on heating. Commonly **IX**-**XII** failed to produce identifiable liquid crystalline textures upon cooling into or annealing in the liquid crystalline temperature range. This observation as well as the persistent birefringence above the clearing temperatures are attributed to the high viscosity of these polymers due to their high molecular weight.
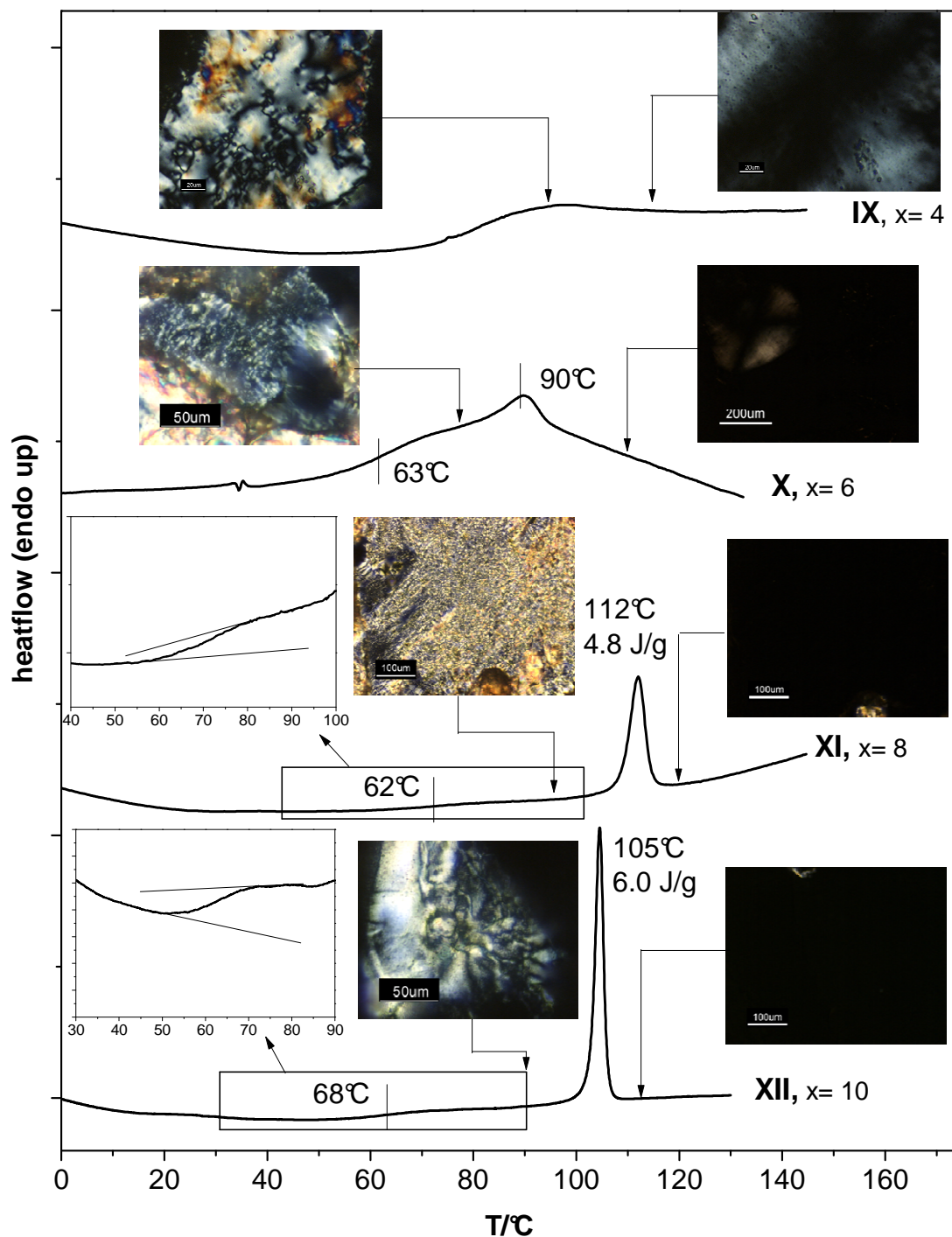
Figure 5.8:   DSC traces of second heating of cyanobiphenyl-containing homopolymer **VIII-XI** at 10 K/min under N_2 with insets are microscopic images between crossed polarizers for polymers **X-XII**. Temperatures were images were taken are marked with lines.

X-ray diffraction (XRD) pattern of homopolymers **IX-XII** were performed using a Guinier setup to gain further information on the liquid crystalline phases. For **X-XII** the diffractograms (Figure 5.9) were recorded below the respective clearing temperatures and for **IX** the diffractogram at 70 °C. Generally, the results on the XRD analysis of the

polymer **IX-XII** did not change significantly when measured at room temperature or close to the clearing temperatures in the liquid crystalline phase. All cyanobiphenyl-containing homopolymers show a broad halo around $\theta = 10$ that is attributed to the amorphous polymer backbone. The polymer with the longest spacer **XII** (x = 10) shows a reflex in small angle region of the diffractogram at $\theta = 2.05$. **XI** also exhibits this distinct reflex at $\theta = 2.26$ albeit with a much lower intensity. For the polymers **X** and **IX** no such distinctive reflexes in the small angle region are evident.
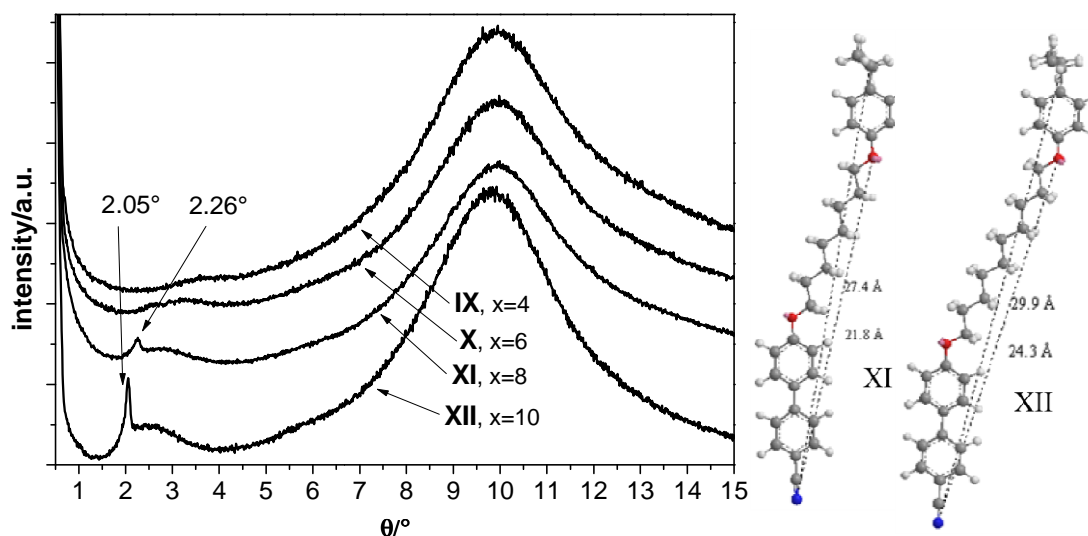
Figure 5.9: XRD diffractograms of cyanobiphenyl-functionalized homopolymers **IX** (70 °C), **X** (70 °C), **XI** (80 °C) and **XII** (90 °C) and models for **XI** and **XII**.

It is not obvious if the detected reflection correspond to the (100) or (200) of a smectic layer spacing. Estimation of the lengths of the mesogenic side-groups with polymer backbone (*l*) yields **XI** $l = 27.4$ Å and **XII** $l = 29.9$ Å. The lengths without the polymer backbone (l_b) are estimated to **XI** $l_b = 21.8$Å and **XII** $l_b = 24.3$ Å (see Figure 5.9, right). If the small angle reflections for **XI** and **XII** are interpreted as first order reflection of a smetic layer spacing the corresponding layer distances can be calculated using the Bragg equation (equation 4.4) to $d = 19.5$ Å (**XI**) and $d = 21.5$ Å (**XII**). These distances are lower than the length of the mesogenic side-group without polymer backbone (l_b). Thus, no SmA phase can be present because this would require the ration of the determined and the calculated distance (d/l_b or d/l) to be equal or above 1 as shown in Figure 5.10. Therefore, a tilted smectic mesophase (SmC) might be assumed. For a tilted phase the expected layer distance would also be below the length of the mesogenic side-group. This assumption is in contrast to the literature on similar side-group liquid crystalline polymers that report partially interdigitated smectic A phases.[201,221] The reflections also might be interpreted as second order reflections (200) assuming the (100) reflections are already

150

superimposed by the primary beam. For **XII** at $\theta \approx 1$ a very weak reflex might be identified. The corresponding layer distances are **XI** d = 39.1 Å and **XII** d = 43.0 Å. The ratios of these values to calculated length of the mesogenic side-groups are between above 1 and, thus, a partially interdigitated smectic A phases would be possible.

Based on this data **XI** and **XII** can be assigned to a smectic mesophase without further identification whereas the mesophase of **X** cannot be assigned but is expected to coincide with **XI** and **XII**. In contrast, for **IX** only the POM analysis indicated a liquid crystalline phase of unknown nature.

SmA	SmA	SmC
partially interdigitated	fully interdigitated	fully interdigitated
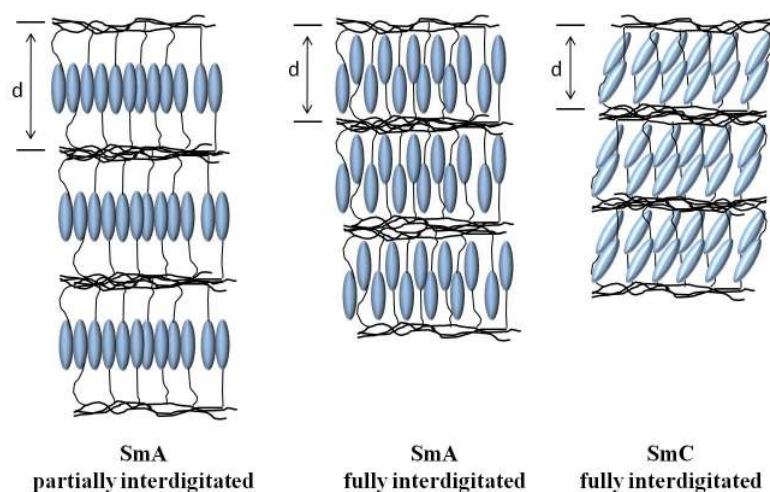
Figure 5.10:   Examples of smectic phases exhibited by side-group polymers.

These results differ from the material properties reported previously by Imrie *et al.*.[201,221] This group found all SmA phases for all cyanobiphenyl-containing homopolymers with the spacer lengths x = 4, 6, 8 and 10. The mesophase was identified by the formation of focal conic textures and from the enthalpies of the clearing transitions. The reported phase behaviors were g 77 SmA 107 i (x = 4), g 60 SmA 120 i (x = 6), g 39 SmA 123 i (x = 8) g 18 SmA 118 i (x = 10). XRD results were only reported for the polymer with the four-membered spacer but the diffractograms did not exhibit significant reflection indication a smectic phase. This observation was attributed to the high viscosity of the system. However, these results are difficult to compare to the cyanobiphenyl-functionalized polymers in this work. Unfortunately Imrie *et al.* reported only the molecular weight of the functionalizable homopolymer PHS (M_n(PHS) = 30000 g/mol, ru_{PHS} = 250) without its molecular weight distribution and no details on the functionalized polymers were reported. The CB functionalized homoplymers **IX-XII** presented in this thesis, have a much higher (about ten-fold) degree of polymerization (ru_{CB} = 2670). The higher resulting viscosity of the polymer melt might be detrimental to the mesophase formation.

Deviations in the thermal behavior can also arise from the different degrees of conversion in the different polymer systems as well as the different molecular weights. Imrie *et al.* reported a quantitative mesogen attachment (determined by elementary analysis) while the polymers in this thesis exhibit a non-quantitative degree of conversion that certainly influences the thermal properties.

5.4   Polymerization of functionalizable triblock copolymers

For chemical LC gels it has been shown that the rubbery as well as the electro-optical properties depend on the crosslinking density.[152,222] In ABA triblock copolymers the network density and network span is dependent on the polymer backbone. The critical gelator concentration, i.e. the minimum polymer concentration necessary to form a gel, is in turn dependent on network span. The length of the functionalized B-block largely determines the network span and a lager span should result in a lower critical gelator concentration.

Depending on the gelator concentration the block copolymers can adopt different conformations in the solvent as shown in Figure 5.11. For low concentrations the probability that a ABA triblock copolymer gelator will form loops is high. In this configuration both A-block self-assemble in the same polystyrene sphere. If more than one polymer chain loops back to one sphere the configuration can be called flower-like. With increasing concentration the probability that a gelator chain forms a bridge configuration increases. In this case the functionalized backbone is connected to two different polystyrene spheres. With increasing concentrations this configuration leads to the formation of a gel network.[223]

Kornfield *et al.* assumed that the tendency to form loops is dependent on the rigidity of the geator backbone.[118,119] Flexible polymer backbones tend to form more loops with both A-blocks self-assembled in the same node. Thus, these loops do not contribute to the network formation. More rigid backbones are expected to form less loops and, hence, decrease the critical gelator concentration. Therefore, the polymer backbone of the B-block is an important factor for affecting the rheological and electro-optical properties of a LC gel.
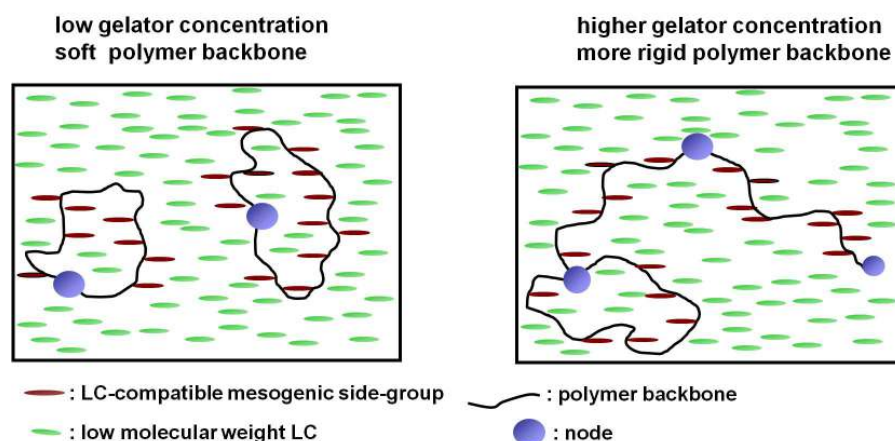
Figure 5.11:   Configuration of the functionalized ABA triblock copolymer gelator in 5CB depending on the gelator concentration or rigidity of the polymer backbone. *Left*: ring or flower configuration at low gelator concentrations or with soft polymer backbone of the B-block; *right*: partially bridge conformation at higher gelator concentrations or with gelators with a more rigid backbone.

In this work, poly(4-hydroxystyrene) was selected as the functionalizable backbone for the middle block. As already described in chapter 4 4-*tert*-butoxystyrene (tBS) was used as the protected monomer for the anionic polymerization. An advantage is the phenolic functionality that allows subsequent polymer analogous etherification that is used to attach the mesogenic moieties. Furthermore, it is known that poly(4-hydroxystyrene) result in relatively high glass transition temperature (T_g) even if mesogenic side-groups are attached.[87,122]

To investigate the influence of the polymer backbone composition and length of the ABA block copolymers on the gel properties several functionalizable ABA block copolymers were synthesized. One aim was the preparation of a very long B- block with a high degree of polymerization ($DP_{PtBS} > 2000$), that increase the network span and, therefore, lowers the critical concentration of the gelator in 5CB. For the synthesis of the polymer backbone two different routes have been employed that are presented in Figure 5.12.

For *route A* a bifunctional initiator, sodium naphthalene, was used for the anionic polymerization of *t*BS forming the B-block. Sodium naphthalene was one of the first initiators utilized in anionic polymerization and acts as an electron transfer agent.[48,49] The radical anion that is formed in the reaction of sodium with naphthalene transfers an electron onto the *tert*-butoxystyrene (*t*BS) monomer. Two of these styrenic anion radicals form a dianionic dimer yielding the effective bifunctional initiator. Prior to the addition of styrene, an aliquot of the P*t*BS (**I**) block was isolated and terminated. These PtBS homopolymers were required for characterization and were also used for the synthesis of the functionalized homopolymers **IX-XII**. Subsequently, styrene was added for the polymerization of the symmetric A-blocks.

For the *route B* a monofunctional initiator for the sequential polymerization of (1) styrene, (2) tert-butoxystyrene and (3) styrene was employed (see Figure 5.12). For the preparation of ABA triblock copolymers containing a B-block with a high degree of polymerization the sequential polymerization a commercial monofunctional initiator (e.g. s-BuLi, 1.3 M in pentane) was used. Here, practical issues have to be considered due to the restrictions imposed by the reactor size and equipment (see chapter 3). The degree of polymerization can be calculated using equation (5.1) for a given amount of monomer. If the first A-block, polystyrene, should feature a lower degree of polymerization (e.g. $DP_{PS} \approx 500$) and the following B-block, poly(*tert*-butoxystyrene), should be much longer (e.g. $DP_{PtBS} > 2000$) the required volume of initiator or the volume of the first monomer (styrene) must be very low because the overall amount of monomer is limited by the reactor size.

$$DP = \frac{m(monomer)}{n(initiator) \times M(monomer)} \tag{5.1}$$

Initiator volumes of less than 0.1 mL are difficult to handle and the error while measuring and transferring is significant. For instance the dead volume of the utilized syringe is in the range of 0.4 mL. This issue can be overcome by diluting the initiator with a dry, inert solvent that effectively increase the volume to be injected and, thus, reduces the risk of faulty initiator amounts. Another approach to circumvent this issue is to start the polymerization with considerable amount of styrene and initiator yielding the desired first block with the required low molecular weight but at higher concentration in the reactor. Subsequent disposing a larger fraction of the living polystyrene solution and adding fresh dry solvent allows one to add an appropriate amount of *t*BS. That is required for the large middle block, without facing the issues associated with a non-manageable viscosity in the reactor.
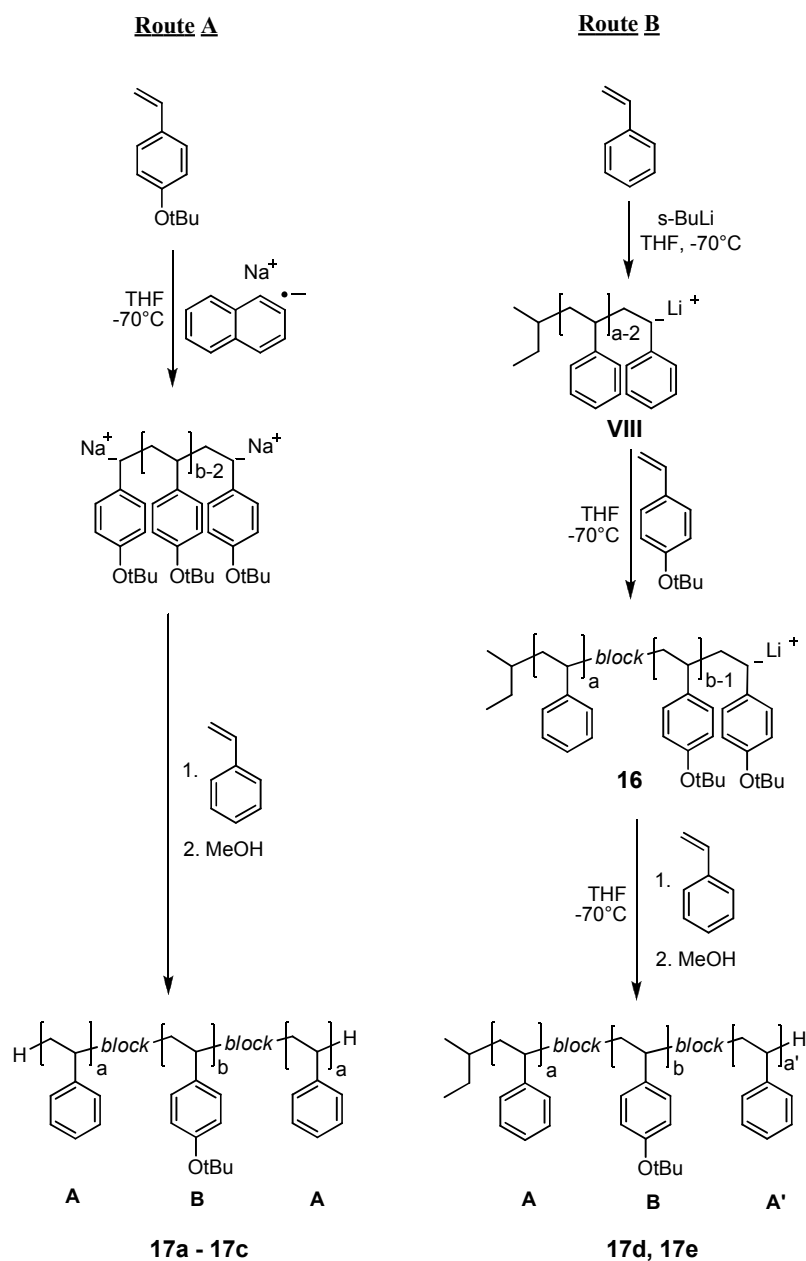
Figure 5.12:   Synthetic pathways to the functionalizable ABA and ABA' triblock copolymers **17a-17e** using two different routes. Route A uses a bifunctional initiator resulting ABA' triblock copolymers and route B uses a monofunctional initiator.(THF: tetrahydrofuran, s-BuLi: sec-butyl lithium).

The use of the route B also allowed the preparation of ABA triblock copolymers, which in part features a star-shaped architecture (PS-P*t*BS-PS)$_y$ **24** (y = 1-3). This was achieved by using a coupling agent after the sequential polymerization of the triblock copolymer **17d** that will be discussed in chapter 5.6.

Both approaches have their distinct advantages. In case of *route A*, the use of a bifunctional initiator ensures that the lengths of both A-blocks are identical and, therefore, one might assume that phase separation occurs more easily. In addition, this initiator also allows the relatively easy preparation of high molecular weight B-blocks that cannot be obtained in the same fashion as with a monofunctional initiator due to the practical issue discussed above. Disadvantageously is the fact that the initiator solution necessitates the absence of excessively used sodium. If this solution contained two different initiating species the resulting molecular weight distribution would be broadened.

In case of *route B* where a monofunctional initiator is used, the required amount of styrene for the third block has to be carefully calculated since the previously disposed amount has to be taken into account. Advantageously, this approach typically yielded narrower molecular weight distributions compared to the bifunctional initiator. The resulting triblock copolymers are inherently ABA' triblock copolymers because it is unlikely that the length of the end blocks will be identical.

Characteristic data of all ABA and ABA' triblock copolymers **17** prepared by both routes as well as their respective precursor blocks are given in Figure 5.12. The triblock copolymers are listed according to the used routes and ordered with increasing B-block lengths. Block copolymers prepared by route A are **17a-c** whereas **17d** and **17e** were synthesized using route B.

As described in chapter 4.3.1, the molecular weights of all PS and PtBS precursors were determined on a SEC setup with THF as eluent with respect to a polystyrene calibration. The molecular weights determined by SEC were in good agreement with the theoretical molecular weight calculated from the ratio of initiator and *tert*-butoxystyrene. Thus, the molecular weights as determined with respect to the polystyrene calibration were used for all further calculations. The average number of repeating units (ru$_{PtBS}$) was calculated from the number average molecular weight (M_n) determined by SEC and were rounded to 10 units.

The ABA triblock copolymers **17a** contains the shortest B-block in the ABA series with ru$_{PtBA} \approx 930$. The A-blocks is about half the length (ru$_{PS} \approx 490$). The overall molecular weight of $M_n = 306$ kg/mol with a PDI of 1.10. ABA' triblock copolymer **17d** features an overall molecular weight of $M_n = 124$ kg/mol with a B-block length (ru$_{PtBA} = 680$) comparable to **17a.** In this case the A-blocks are not equal in length (ru$_{PS} = 190, 120$).

The B-block of ABA triblock copolymer **17b** (ru$_{PtBA} = 1860$) is about two times the length of the preceding polymers **17a**. The A-block lengths (ru$_{PS} = 430$) are about the same length while the molecular weight ($M_n = 403$ kg/mol). **17c** features a long B-block (ru$_{PtBA} = 2670$) and A-blocks (ru$_{PS} = 360$) comparable in length to **17b**. The molecular weight of this ABA triblock copolymer is determined to $M_n = 528$ kg mol. The member

of series **17** with the highest molecular weight (M_n = 1000 kg/mol) and the longest B-block (ru_{PtBA} = 3740) is the ABA' triblock copolymer **17e**. The molecular weight distributions in series **17** are in the range of 1.03 (**17d**) to 1.10 (**17a**). Generally the molecular weight distribution was broader for the block copolymers that were prepared using route A.

Table 5.2: Characteristic data of PS-P(*t*BS)-PS triblock copolymer series **17**

block copolymer series 17	route[a]	M_n[b]	M_w[b]	PDI[c]	$A_aB_bA_a$		
		kg/mol			ru_A[d]	ru_B[d]	ru_A[d]
17a	A	278	306	1.10	490	930	490
precursor Ij		*163*	*171*	*1.05*	*-*	*930*	*-*
17b	A	403	436	1.08	430	1860	430
precursor Ik		*327*	*345*	*1.07*	*-*	*1860*	*-*
17c	A	528	558	1.06	360	2670	360
precursor Il		*470*	*499*	*1.06*	*-*	*2670*	*-*
	route[a]	M_n[b]	M_w[b]	PDI[c]	$A_aB_bA'_{a'}$		
					ru_A[d]	ru_B[d]	$ru_{A'}$[d]
17d	B	124	125	1.03	190	680	120
A-block precursor 16a		*112*	*115*	*1.03*	*190*	*680*	*-*
AB-block precursor VIIIa		*20.1*	*20.8*	*1.04*	*190*	*-*	*-*
17e	B	1000	1120	1.06	530	3740	550
A-block precursor 16b		*912*	*953*	*1.05*	*530*	*3740*	*-*
AB-block precursor VIIIb		*55.4*	*57.0*	*1.03*	*530*	*-*	*-*

a) route used for anionic polymerization: A: bifunctional initiator, B: monofunctional initiator; b) determined by SEC (eluent: THF + electrolyte); molecular weight with respect to polystyrene standards, UV-detection; c) polydispersity index, M_w/M_n; d) average number of repeating unit, rounded to 10 units, calculated from M_n for first block in polymerization sequence, calculated from block ratio determined by ^{1}H-NMR for other block(s)

5.5 Polymer analogous reaction to cyanobiphenyl-containing triblock copolymers

The cyanobiphenyl-functionalized block copolymers **19-22** are based on the precursor block copolymers **17a-17e**, thus the letter indicates the polymer backbone whereas the number denotes the spacer length: **19a-19e** (x = 4), **20** (x = 6), **21** (x = 8) and **22** (x = 10).

The functionalization of the ABA and ABA' triblock copolymers **17** with the cyanobiphenyl mesogenic units **CB1-4** was carried out similar to the procedure described for the functionalized homopolymers **IX-XII**. Each block copolymer of the series **17** was deprotected under acidic conditions yielding the respective hydroxyl functionalized block copolymer **18**. Attachment of the **CB1-4** units to B-blocks of the triblock copolymers was achieved by polymer analogous reaction using a Williamson etherification. The reaction conditions were the same as for the CB homopolymers **IX-XII** (see chapter 5.3), although the reaction time had to be increased for the block copolymers. The solvent as well as all other components had to be thoroughly dried beforehand otherwise the fraction of crosslinking during the polymer analogous reaction would drastically increase and result in a broad molecular weight distribution. This factor has to be especially important since in this block copolymer series **19-22** the molecular weight of the functionalizable block copolymers was very high. Therefore, the probability of crosslinking reactions is statistically increased.
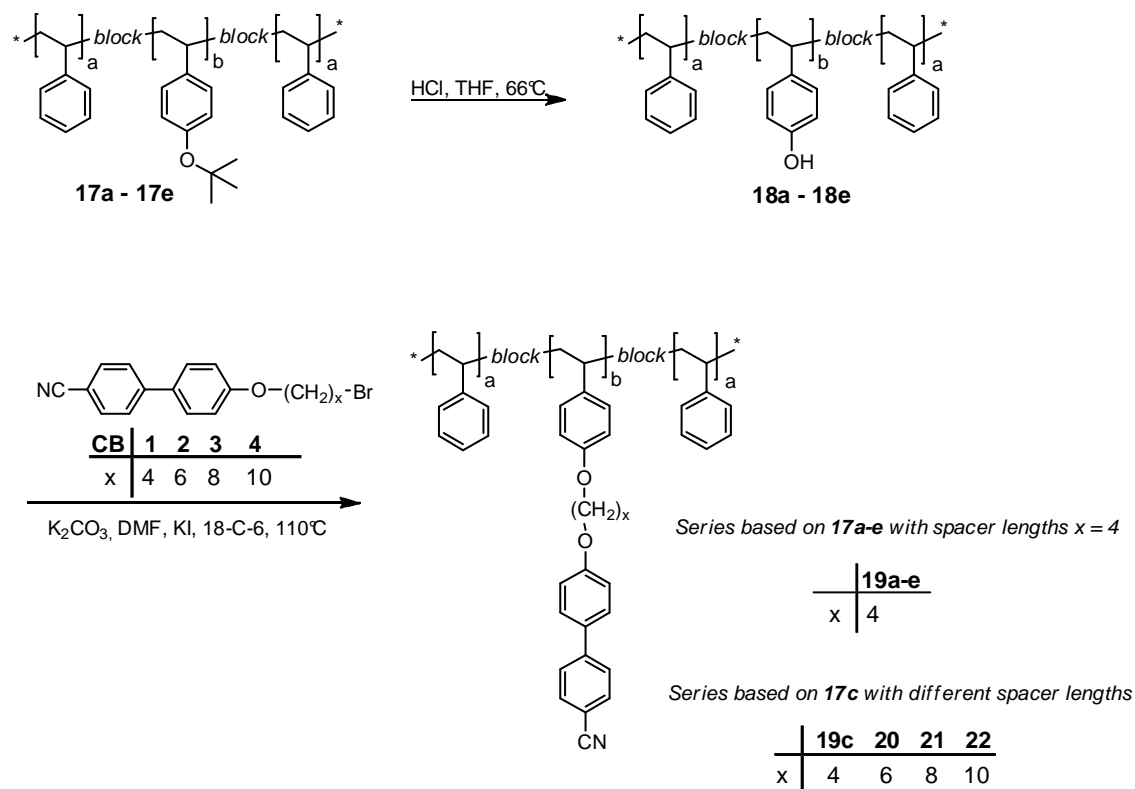

Figure 5.13: Synthesis of cyanobiphenyl functionalized ABA triblock copolymers **19-22**.

The degree of conversion (DC) of the polymer analogous attachment of the side-groups was monitored with IR spectroscopy and determined by ^{1}H-NMR as already described for the cyanobiphenyl-functionalized homopolymers in chapter 5.3. The integrated area of the ^{1}H NMR peaks at 7.6 - 7.4 ppm corresponds to six protons of cyanobiphenyl group and were compared to the integrated area at 7.2 – 6.1 ppm. Commonly in this area the remaining two protons of the cyanobiphenyl group as well as the aromatic protons of the PtBS and PS backbone show significant overlap and thus were integrated as one signal. By knowing the integral values from the precursor block copolymers **17,** the degree of conversion could be calculated. In gelator series **19** the degree of conversion is in the range of 78-88 % with the exception of **19e** where the DC was found to be 59 %.

The number average molecular weights, M_n, of the different blocks of the gelators were determined by SEC with respect to polystyrene standards. Therefore the given molecular weights can only be treated as relative values to be compared within the series, as discussed in chapter 5.3. The total molecular weight increases in series **19** (x = 4) from $M_n = 601$ kg/mol for gelator **19a** up to $M_n = 2460$ kg/mol for block copolymer **19e**. It has to be noted that these values are already about the molecular weight of the cut off volume of the SEC setup and, thus, have to be seen as orientation values that do not represent absolute molecular weights. Therefore, comparison of the number average molecular weights determined by SEC with the theoretically calculated ones also show that the molecular weights by SEC are overestimated by the factor 1.6 to 2.2.

Compared to the functionalizable triblock copolymers **17a-c** all gelators **19-22** exhibit broader molecular weight as observed by SEC. The determined values were in the range of PDI = 1.05 for **19d** to PDI = 1.30 for **19c**. The broadening in molecular weight distribution may be due to small intermolecular coupling reactions during the attachment of side groups. With increasing length of the functionalized block the probability of inter-chain side reactions increases statistically. Thus, the dependence on the middle block length can be seen in block copolymer series **19a-e**, the PDI of the members with a longer middle block tend to increase more during the polymer analogous reaction (see Table 5.3). Nevertheless the PDI of the gelators is quite narrow for having such a high molar mass side-group functionalized segment.

The resulting weight fraction of the CB functionalized middle block ranges from 76 wt% for **19a**, thus containing the highest weight fraction of polystyrene end blocks, up to 93 wt% for block copolymer **19d** containing the lowest fraction of polystyrene end blocks.

Table 5.3: Characteristic data of block copolymer gelators **19-22**

block copolymer	spacer $x^{a)}$	$M_n{}^{b)}$	$M_w{}^{b)}$	$PDI^{c)}$	$DC^{d)}$	$w_{CB}{}^{e)}$	$M_n(th)^{f)}$	$A_aB_bA_a$		
		kg/mol			%	%	kg/mol	$ru_A{}^{g)}$	$ru_B{}^{g)}$	$ru_A{}^{g)}$
19a[h]	4	894	947	1.06	88	76	415	490	930	490
19b[h]	4	1409	1713	1.22	78	87	673	430	1860	430
19c[h]	4	1560	2107	1.30	83	92	947	360	2670	360
19d[i]	4	601	630	1.05	87	86	261	190	680	120
19e[i]	4	2460	3052	1.24	59	91	1112	530	3740	550
20[h]	6	2068	2560	1.24	70	92	883	360	2670	360
21[h]	8	1954	2348	1.21	80	93	1047	360	2670	360
22[h]	10	1812	2184	1.21	84	94	1142	360	2670	360

a) number of methylene units in spacer; b) determined by SEC (eluent: THF + 0.25 wt% electrolyte), molecular weight with respect to polystyrene standards, UV-detection; c) polydispersity index; d) degree of conversion of polymer analogous reaction, determined by ^{1}H-NMR; e) weight fraction of the cyanobiphenyl-containing segment f) theoretical number average molecular weights, calculated from repeating units; g) average number of repeating units: calculated from ^{1}H-NMR and SEC **17a-c**; h) route A (ABA-triblock copolymer); i) route B (ABA' triblock copolymer) used for polymerization of the respective functionalizable block copolymer **17d, e**

5.5.1 Solid state characterization of cyanobiphenyl-functionalized triblock copolymers

At first the *influence of the spacer length is demonstrated* for the block copolmyers **19-22** based on the same polymer backbone **17c** ($ru_A = 360$, $ru_B = 2670$, $ru_A = 360$). In the following the cyanobiphenyl-functionalized triblock copolymers **19c** (x = 4), **20** (x = 6), **21** (x = 8) and **22** (x = 10) were compared.

	19c	20	21	22
x	4	6	8	10
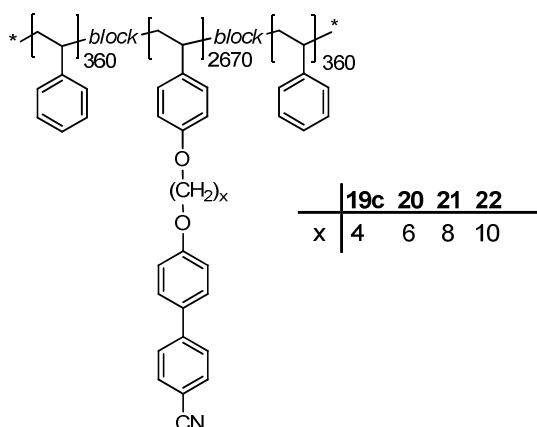
The thermal properties of the selected functionalized block copolymers were analyzed by DSC under N_2 with a heating rate of 10 K/min. The thermal stability in the investigated temperature range was confirmed via thermo gravimetric analysis (TGA) prior to thermal investigation by DSC. The second heating thermograms are given in Figure 5.14. The inset showing POM images taken between crossed polarizers above and below the clear

transition temperature. For all functionalized block copolymers based on the functional triblock copolymer **17c** the glass transition of the polystyrene blocks cannot be observed due to the very low weight fraction of the PS segments. For **19c** (x = 4) and **20** (x = 6) one broad transition is detected that might be assigned to the glass transition of the functionalized block that is superimposed with a clearing transition. This behavior was already observed for the respective homopolymers **IX** (x = 4) and **X** (x = 6). The half heights of these transitions are 80 °C for **19c** and at 74 °C for **20**. A glass transition is observed for **22** at 70 °C while it cannot be clearly determined for **21**. The detected transitions for **19c** and **22** are in the same temperature range as found for the respective homopolymers, while **20** exhibits a higher T_g than its respective homopolymer **X** ($T_g = 62$ °C) that might be attributed to different degrees of conversion. Liquid crystalline to isotropic transitions are only clearly detected for **21** (x = 8) and **22** (x = 10). While for **21** this transition is broad with a maximum at 94 °C it is much narrower for the cyanobiphenyl-functionalized triblock copolymer with the longest spacer **22** with a maximum at 97 °C. The enthalpy of the clearing transition cannot be easily compared because the broad peak for **21** makes a neat determination difficult. The clearing temperatures are lower than the temperatures found for the relevant homopolymers **XI** (x = 8, $T_{cl} = 112$ °C) and **XII** (x = 10, $T_{cl} = 105$ °C). This might be caused by the lower degree of conversion of the cyanobiphenyl-functionalized triblock copolymer **21** and **22** compared to the cyanobiphenyl-functionalized homopolymers **XI** and **XII**.

When viewed between crossed polarizers polymer **19c** and **20** exhibited shear induced birefringence that did relax slowing on heating over a wide temperature range. On cooling the birefringence increased but did not return to the state prior to heating. For **21** and **22** birefringent structures were apparent below the isotropic to liquid crystalline transition. On heating these structures darkened significantly at the clearing temperatures although shear induced birefringence was still observed comparable to **19c** and **20** (compare insets in Figure 5.14). This is attributed to the high viscosity of the block copolymer melts that is caused by the very high molecular weights and, thus, causing the issues with the shear induced birefringence. Neither of the functionalized triblock copolymers exhibited a characteristic liquid crystalline texture. As discussed for the azobenzene containing block copolymers in chapter 4.6.3 this is attributed to the confinement in the microphase separated morphology and the high viscosity of the polymer systems.
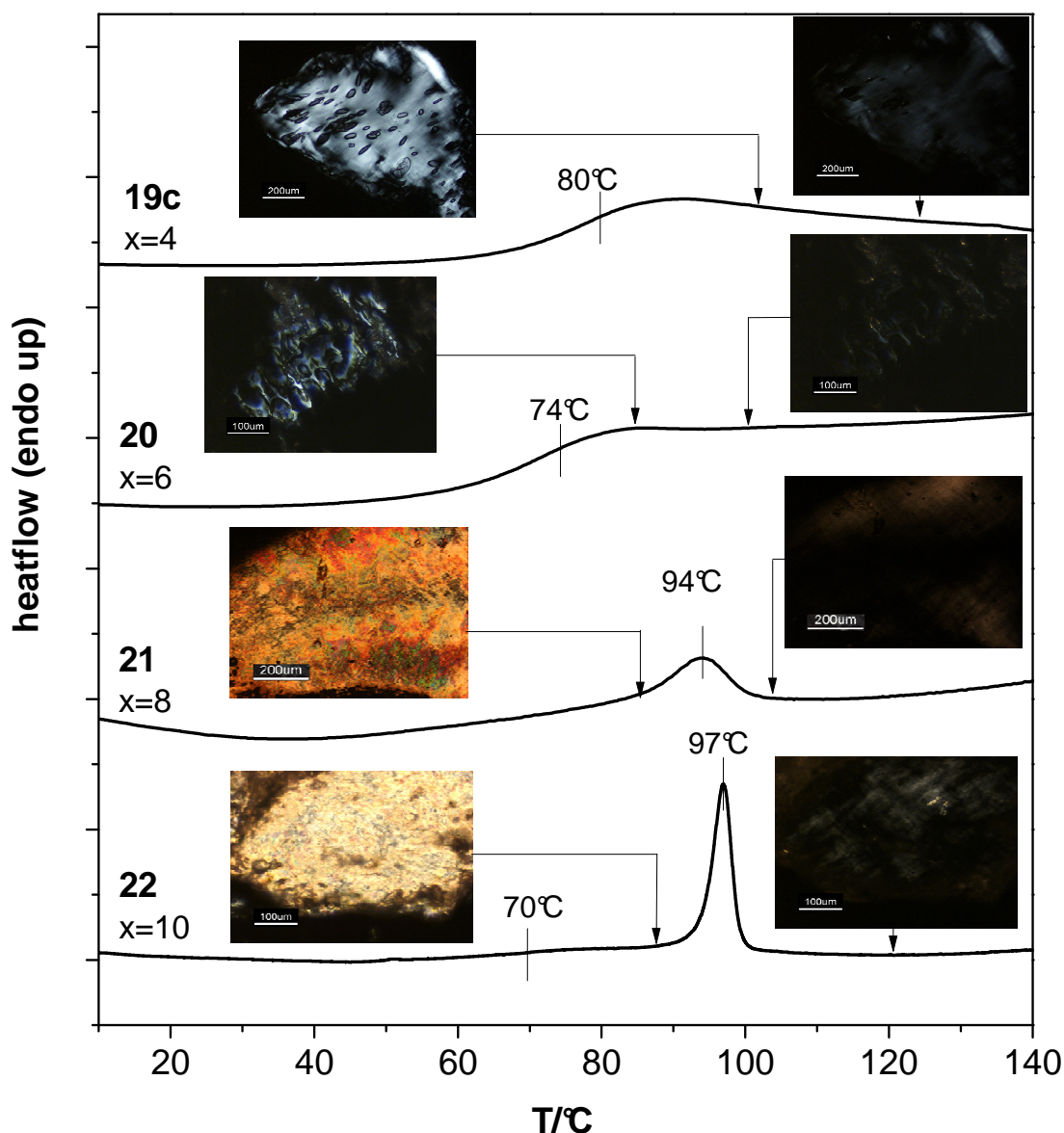
Figure 5.14:   DSC traces of second heating of cyanobiphenyl-containing ABA triblock copolymers **19c**, **20**, **21** and **22** at 10 K/min under N_2. Insets are POM images between crossed polarizers for polymers with markings for the temperature at which an image were taken (on cooling).

X-ray diffraction (XRD) pattern of the cyanobiphenyl-containing triblock copolymers **19c, 20, 21,** and **22** were recorded below their respective clearing temperature using a Guinier setup (Figure 5.15). In addition, for the polymers **19c** (x = 4) and **20** (x = 6) measurements were performed at room temperature as well as at 80 °C but no significant differences were observed. Thus, only the measurements at 80 °C are shown in Figure 5.15. All cyanobiphenyl-containing triblock copolymers show a broad halo around $\theta = 10$ that is attributed to the amorphous polymer backbones as observed for all other polystyrene based polymers in this thesis. Only the block copolymer with the longest spacer **22** (x = 10) exhibits a clear reflection in the small angle region at $\theta = 2.05$

162

indication a layered structure. For the respective homopolymer **XII** with the same spacer length an identical reflection was found. For all other cyanobiphenyl-containing triblock copolymers **19c, 20,** and **21** no indication of a smectic mesophase was evident in the XRD patterns. The sharp reflection in the small angle region for **22** is superimposed with a broad signal of lower intensity. This signal can be observed for all other block copolymers. With decreasing spacer length it shifts to higher angles and the intensity decreases.
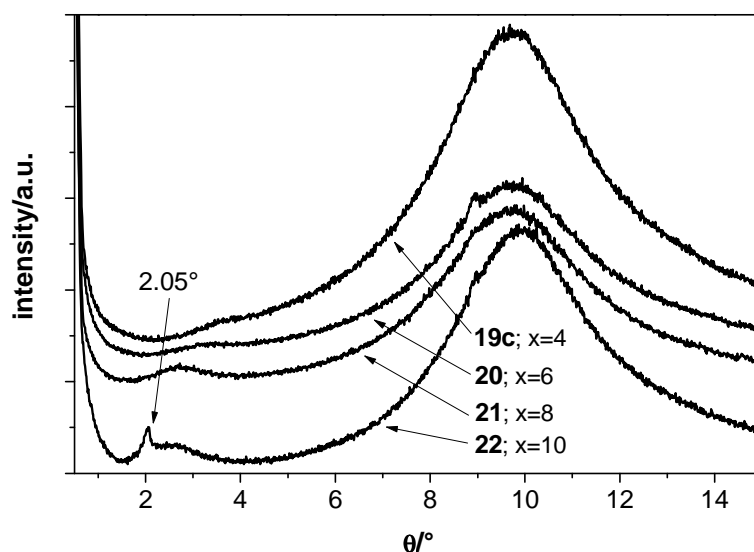
Figure 5.15: XRD diffractogram of cyanobiphenyl-containing ABA triblock copolymer **19c** at 80 °C, **20** at 80 °C, **21** at 80 °C and **22** at 90 °C.

Based on the characterization discussed above the cyanobiphenyl-containing triblock copolymers **22** with the longest spacer (x = 10) is assigned to a smectic mesophase. **21** (x = 8) did not exhibit the significant reflections in the XRD analysis but it is reasonable to assume that it features the same smectic mesophase as displayed by its respective homopolymer **XI** and the analogous block copolymer **22**. No indication of a smectic phase was found for the in the block copolymers **20** (x = 6) and **19c** (x = 4). These results are promising for the intended applications of the functionalized block copolymers as gelators of the liquid crystal 5CB. While smectic polymers (**21** and **22**) are not expected to be soluble in a nematic liquid, crystal the block copolymers (**19c** and **20**) might be soluble to some degree and were used for the following experiments.

The *influence of the polymer backbone composition* on the thermal properties is investigated using the members of series **19**, the cyanobiphenyl-containing triblock copolymers with a four-membered spacer. The detected differences between the polymers in series **19** were minor and, thus the block copolymers with the lowest (**19a**, $w_{CB} = 76$ wt%) and highest weight fraction (**19c**, $w_{CB} = 92$ wt%) of the cyanobiphenyl-functionalized block were chosen exemplarily.

	19a	19c
a	490	360
b	930	2670
a	490	360
w_{CB}	76	92
w_{PS}	24	18
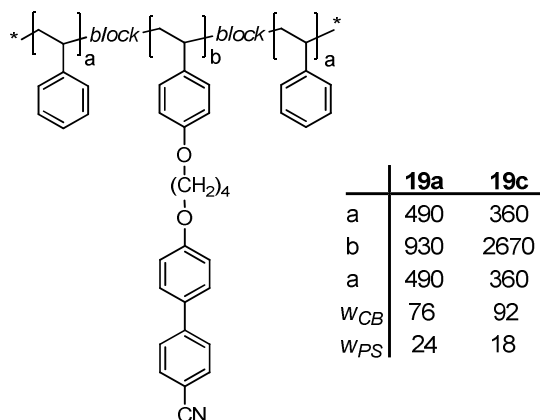
The thermal properties were characterized in the same way as described before for the cyanobiphenyl-containing homopolymers **IX-XII**. Figure 5.16 the second heating thermograms at a scan rate of 10 K/min under N_2 of **19a** compared to **19c** are given. The thermal behavior of **19c** ($w_{CB} = 92$ wt%) was already described above and shows only a broad transition around 80 °C that is presumably the glass transition of the functionalized block. In contrast for the functionalized ABA triblock copolymers **19a** with the highest weight fraction of polystyrene segments ($w_{PS} = 24$ wt%, $ru_{PS} = 490$) two transitions can be detected. The T_g at 109 °C is in the temperature range as detected for polystyrene homopolymers of similar molecular weight, hence it can be attributed to the polystyrene segments of the ABA triblock copolymer **19a**. The glass transition of the functionalized segment is observed around 87 °C. This shift to higher temperatures compared to **19c** might be cause by the overlap with the adjacent T_g of the polystyrene blocks.

Analysis under POM and by XRD did not show any influence by the different compositions of the block copolymer backbone for the functionalized block copolymer with the four-membered spacer **19a** and **19c**.
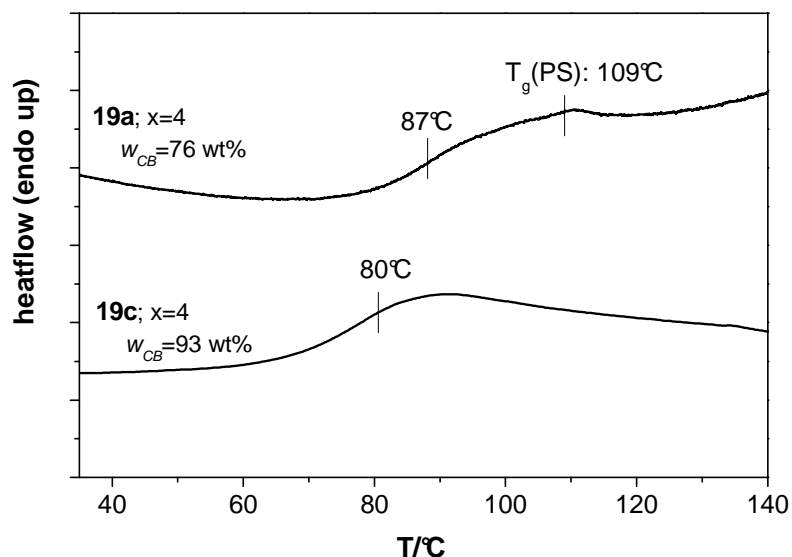
164

Figure 5.16:   DSC traces of second heating of cyanobiphenyl-containing ABA triblock copolymers **19a** and **19c** at 10 K/min under N_2.

5.6   Synthesis and characterization of cyanobiphenyl-containing star-shaped block copolymer

The cyanobiphenyl-functionalized triblock copolymers in this thesis were designed as gelators for the low molecular weight liquid crystal 5CB. The network nodes or crosslinking points of the physical gel network are formed by the phase separated polystyrene A-blocks. In a linear ABA triblock copolymer each polymer can be connected to two different nodes, i.e. if no loop back occurs and both A-blocks are in the same physical crosslinking point. If the architecture of the block copolymer is changed from linear to a star architecture the number of network nodes will be increase. A schematic representation of such architecture is shown in Figure 5.17 compared to a linear triblock copolymer gelator. In the case of a three arm star block copolymers with each arm consisting of a linear triblock copolymer the number of outer physical crosslinking points is increased to three and a new chemical crossslinking point is introduced connecting the three arms. The inner core of the star-shaped block copolymer where polystyrene A-blocks are covalently connected can also serve as a physical crosslinking point in the network created by the gelator in the low molecular weight liquid crystal 5CB. This increase of crosslinking points should result in a higher network density and thus a more rigid network.
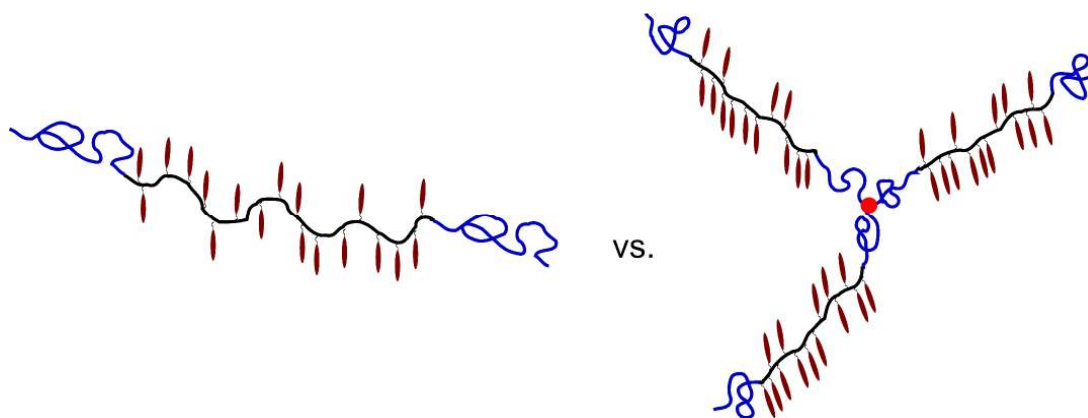
Figure 5.17:   Schematical illustration of a linear triblock copolymer gelator (left) compared to a three arm star-shaped block copolymer gelator with each arm containing an ABA triblock copolymer. Chemical crosslinking point connecting the arms of the star is indicated by a red dot. *Blue:* polystyrene A-blocks; *black*: B-block polymer backbone; *red*: mesogenic side-groups attached to the B-block polymer backbone.

For the synthesis of the star-shaped block copolymer precursor a combination of linear sequential anionic polymerization to an ABA' triblock copolymer and the use of a coupling agent was employed. Among the several coupling agents for anionic polymerchains that are described in literature (see for example ref[224,225]), tetrachlorosilane was used. It is known that poly(styry1)lithium does not undergo complete reaction with stoichometric amounts of tetrachlorosilane due to steric hindrances.[224] A distinct amount of the coupling agent was added to the living polymer chains and was allowed to react over 20 h at first at -70 ° and later at room temperature. The high reaction time as well as the temperature were required to achieve a high coupling rate. Quantiative formation of three arm stars was precluded to the steric hindrance and the high molecular weight of the ABA' block copolymers. Linear ABA' triblock copolymers were used for each arm and, therefore, even non-coupled ABA' block copolymers (unimers) or dimers are suited as gelators in the intended application.

The synthesis of the star block copolymer precursor **23** is shown in Figure 5.18 followed by its deprotection and functionalization with the cyanobiphenyl moieties **CB1** or **CB3** yielding the gelators **25a** and **25b**. The ABA' triblock copolymer **17d** that was prepared using route A (see chapter 5.4) was the precursor used for the synthesis of the star block copolymer **23**. After complete polymerization of **17d** the coupling was carried out with a solution of tetrachlorosilane in dry THF.
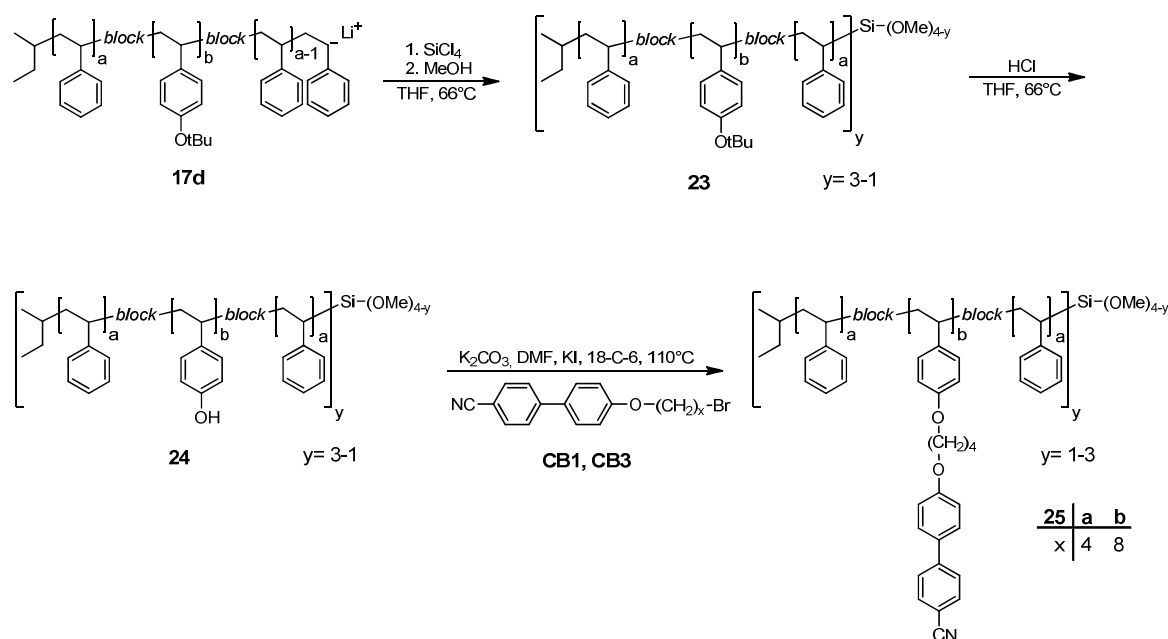
Figure 5.18: Synthesis of star-shaped block copolymer **23** and the functionalization with cyanobiphenyl moieties **CB1** or **CB3** yielding gelator **25a** and **b**.

As mentioned above, the coupling reactions did not proceed quantitatively and resulted in a block copolymer mixture. The fractions of each component were determined by SEC via the integral area of the UV detector signal. The relevant SEC traces of **24** and its precursors are given in Figure 5.19. The resulting mixture contained 25 % of ABA triblock copolymer **17d** (y = 1), 35 % of the respective dimer (y = 2) and 40 % of a three-arm star block copolymer (y = 3) where each arm consists of **17d**. For simplicity this mixture will be denoted star block copolymer **24** from now on. Functionalization with cyanobiphenyl side groups was carried out in the same manner as described for the linear ABA triblock copolymer gelators **19-22.** The star block copolymer **23** was deprotected under acidic conditions resulting in the hydroxyl functionalized block copolymer **24**. Only the cyanobiphenyl moieties with four (**CB1**) and eight methylene units (**CB3**) were used for the functionalization via polymer analogous etherification reaction.

167

Figure 5.19:   SEC traces of star-shaped block copolymer mixture **23** and its precursors **17d**, **16a** and **VIIIa** (eluent: THF, UV detection).

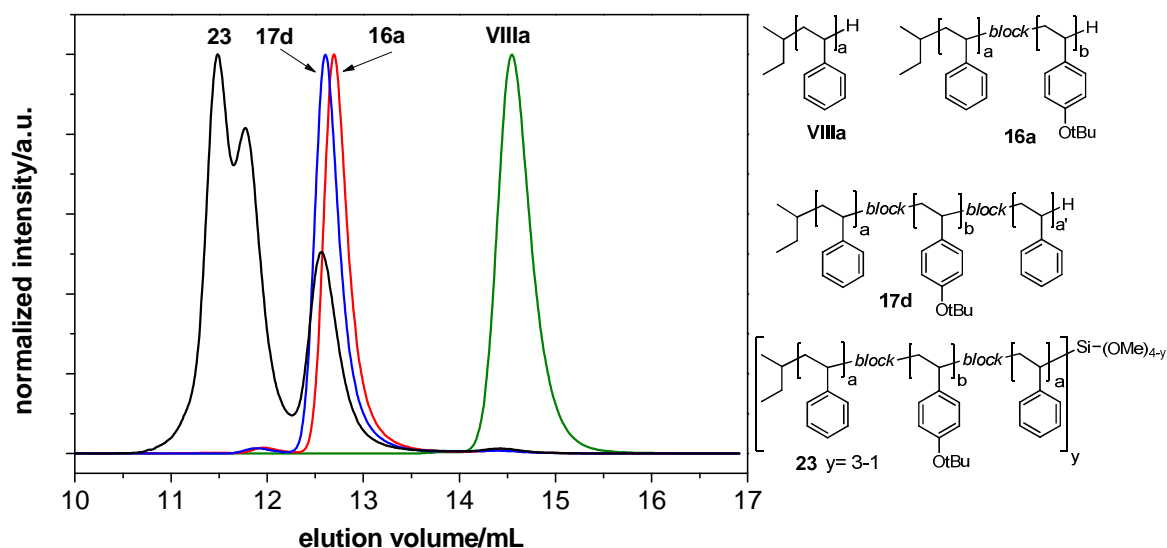Characteristic data of the gelators **25a** and **25b** as well as all of the functionalizable block copolymer **23** and its precursors are given in Table 5.4. The molecular weights and molecular weight distributions obtained by SEC for the mixture of star-shaped block copolymers and linear block copolymers **23** are of limited use. The signal of the unimer, dimer and three arm star cannot be separately analyzed because of their significant overlap. Thus, no M_n or M_w values could be obtained for each fraction. The averaged molecular weight of $M_n = 239$ kg/mol with a distribution of 1.24 was obtained for the mixture containing unimer, dimer and three arm star. Significant values that could be obtained were the peak maxima of the molecular weights for each fraction: unimer (**17d**) $M_p = 134$ kg/mol; dimer $M_p = 291$ kg/mol and $M_p = 400$ kg/mol for the three arm star.

For the cyanobiphenyl funtionalized block copolymers **25a** and **25b** degrees of conversion were determined to 75 % and 69 % which is in the range described for the linear triblock copolymers discussed above. The averaged molecular weights were determined using an SEC setup with THF and an electrolyte as eluent to $M_n = 850$ kg/mol for **25a** and an increased number average molecular of $M_n = 900$ kg/mol for **25b**. The respective molecular weight distributions are PDI = 1.22 for **25a** and PDI = 1.22 for **25b**. The resulting weight fractions of the functionalized blocks are virtually the same with $w_{CB} = 85\text{-}85$ wt% because the block copolymer **25b** with the longer spacer exhibits the lower degree of conversion.

Table 5.4: Characteristic data of star-shaped block copolymer gelators **25** and the functionalizable star-shaped block copolymer mixture **23** as well as the block copolymer **17d**

block copolymer	spacer $x^{a)}$	$M_n^{b)}$	$M_w^{b)}$	$PDI^{c)}$	$DC^{d)}$	$w_{CB}^{e)}$	$A_aB_bA'_{a'}$		
		kg/mol			%	%	$ru_A^{f)}$	$ru_B^{f)}$	$ru_{A'}^{f)}$
25a	4	850	1035	1.22	75	85	190	680	120
25b	8	900	1155	1.28	69	86	190	680	120
23	-	*239*	*298*	*1.24*	-	-	*190*	*680*	*120*
17d	-	*124*	*125*	*1.03*	-	-	*190*	*680*	*120*

a) number of methylene units in spacer; b) determined by SEC (eluent: THF, for **25a,b** THF + 0.25 wt% electrolyte), molecular weight with respect to polystyrene standards, UV-detection; c) polydispersity index; M_w/M_n d) degree of conversion of polymer analogous reaction, determined by ^{1}H-NMR; e) weight fraction of the cyanobiphenyl-containing segment f) average number of repeating units: calculated from ^{1}H-NMR and SEC of **17d**

5.7 Physical gelation of 5CB

To evaluate, whether the cyanobiphenyl-containing block copolymers are suited as gelators for the low molecular weight nematic liquid crystal 5CB homogeneous mixtures were prepared first. In the following the sample preparation is discussed.

Sample preparation

In the pioneering work of Kornfield *et al.* a solvent based technique for the homogenization of the 5CB/block copolymer mixture were employed to prepare thermoreversible physical gels. 5CB as well as the predetermined amount of gelator were dissolved in dichloromethane (DCM) as cosolvent to achieve homogenization. The solvent DCM was subsequently slowly evaporated under reduced pressure.[119]

This preparation method was not used in this thesis because the complete absence of the DCM after evaporation is difficult to verify and residual solvent might influence the sample properties. Thus, a thermal dissolution technique was used. 5CB and the respective polymer were placed in a 1 mL vial. The capped vial was heated well above the clearing temperature of 5CB. Homogenization was achieved by rotating the samples in a tumble mixer at 50 °C (for polymer addition of ≤ 5 wt%) or 70 °C (for higher polymer concentrations) for 48 h. Mass concentrations (wt%) are given as $wt\% = \dfrac{m(5CB)}{m(polymer)} \cdot 100$. Mixtures of functionalized homopolymers and block copolymers were prepared over a concentration range of 0.2 wt% up to 20 wt% in 5CB. For easier comparison of the different gelator and gel properties mostly samples prepared with a weight fraction of 5 wt% gelator in the nematic solvent will be discussed in this chapter.

Miscibility of 5CB and cyanobiphenyl-functionalized homopolymers

The solubility of the side-group functionalized homopolymers in 5CB with respect to the spacer length was tested using the series of cyanobiphenyl-containing homopolymers **IX-XII**. Mixtures of 5CB with 5 wt% of the respective homopolymers were prepared. The concentration of 5 wt% was chosen because this was the typical concentration used also for the gelation experiments later on. The above described procedure for the sample preparation failed to result in homogeneous mixtures of 5CB with 5 wt% of the functionalized homopolymer with longest spacer (x = 10) **XII**. In these samples macroscopical demixing was observed, that was attributed to the smectic phase of **XII**. Thus, this polymer was not used for the following tests.

The mixtures containing 5CB with 5 wt% of the respective homopolymers were analyzed by DSC. The heating rate was 1 K/min under N_2, which is the typical heating rate used in

the temperature dependent rheology experiments discussed later. The second heating and cooling traces of the different mixtures in comparison to pure 5CB are given in Figure 5.20. For the mixture containing **IX** (x = 4) only one liquid crystalline to isotropic transition, comparable to pure 5CB ($T_{cl} = 35.8$ °C, $T_{iso-LCl} = 35.5$ °C), was detected on heating ($T_{cl} = 35.7$ °C) as well as on cooling ($T_{iso-LCl} = 35.3$ °C). In contrast for the mixtures with **X** and **XI** two different transitions were detected, a strong peak at the clearing temperature of pure 5CB (**X**: $T_{cl} = 35.8$ °C, **XI**: $T_{cl} = 35.9$ °C) and an additional signal at higher temperature of much lower intensity. Both transitions are detected on heating an on cooling. For a homogeneous mixture only a single clearing transition is expected. The additional signals in DSC curves of the mixtures containing **X** and **XI** are attributed to clearing (respective isotropic to liquid crystalline) transitions of the side-group liquid crystalline homopolymers.
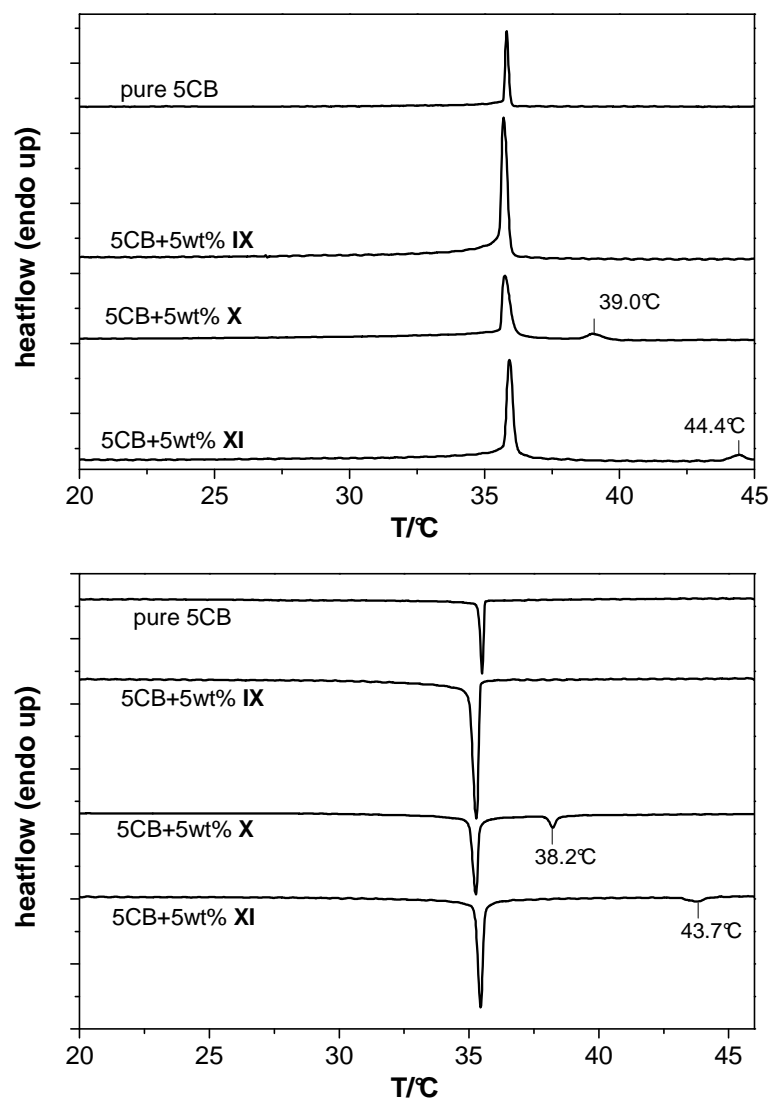

Figure 5.20:   Stacked DSC second heating (*top*) and second cooling (*bottom*) traces at a heating and cooling rate of 1K/min under N_2 of pure 5CB and 5CB mixtures with 5wt% of **IX-XI.**

171

These transition are significantly shifted to lower temperatures (5CB+**X**: T_{cl} = 39.0 °C; 5CB + **XI**: T_{cl} = 44.4 °C) compared to transitions of the pure liquid crystalline homopolymers (**X**: T_{cl} = 90 °C; **XI**: T_{cl} = 112 °C). This observation proofed the formation of a second phase, besides the nematic phase, consisting of homopolymer plasticized by the low molecular weight liquid crystal.[219] In this second plasticized phase the transition temperatures of the homopolymers are reduced.

The DSC measurements on mixtures of 5CB with 5 wt% of the side-group functionalized polymers revealed that only the homopolymer with the four-membered spacer **IX** forms a homogeneous phase with the nematic solvent whereas for smectic homopolymers **X** and **XI** phase separation occurs.

Although it has to be noted that for the pure cyanobiphenyl-containing homopolymer **IX** no liquid crystalline phase was evident in the DSC and, thus, no additional signal in the DSC of the mixture with 5CB might be expected. To further confirm the homogeneity of the phase in the mixture of 5CB and **IX** the thermal behavior was analyzed by POM. Images between crossed polarizers on cooling are shown in Figure 5.21. The left images shows the isotopic phase at 35.0 °C very close to the isotropic to liquid crystalline transition. In the right image the resulting texture just below this transition at 34.4 °C is shown. Only one phase transition was observed on cooling as well as on heating. From the formation of the liquid crystalline phase down to room temperature no additional textures or black spots were visible that might indicate a phase separation. [219]

Because of these results triblock copolymers bearing a four-membered spacer, as in the homopolymer **IX**, were chosen for the gelation experiments.
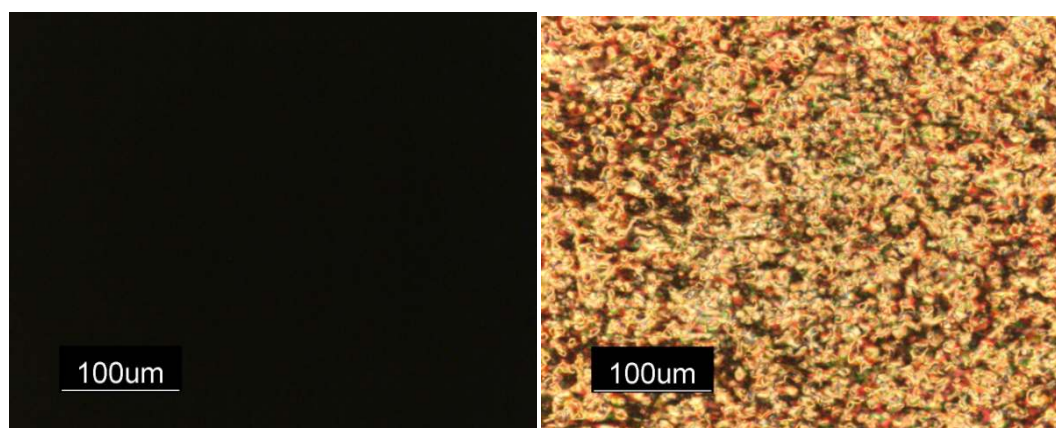

Figure 5.21:   POM images taken between crossed polarizers for a mixture of 5CB with 5 wt% of the cyanobiphenyl-functionalized homopolymer **IX** at 35.0 °C above the clearing temperature (*left*) and at 34.4 °C (*right*).

5.7.1 Rheology investigation of the liquid crystalline gels

The definition of the term gel has been subject to extensive debates in literature and is not always used in the same sense.[226,227] In this thesis a definition and description is used that seems to be widely accepted:[227] A gel is a soft, solid or solid-like material that contains at least two different components. From the rheological point of view, the storage modulus (G') of a gel should exhibit a pronounced plateau extending over three decades of frequencies (ω) while being higher than the loss modulus (G'') in a frequency depending oscillating experiment.

The gelation point, a characteristic value of a thermoreversible physical gel which denotes the transition of the soft solid into a liquid is preferably determined by rheological experiments. In physical gels, the gelation point is extracted from a temperature-dependent oscillating experiment at that point, where the storage modulus (G') crosses the loss modulus (G'').

A detailed description of the rheology involved is given in the experimental part in chapter 6.1.2.

Liquid crystalline gels were prepared using the block copolymer gelators with a four-membered spacer **19a-e** and **25a** in 5CB as described above and were characterized by rheological methods. Oscillatory rheological measurements were performed, using an Anton-Paar MCR301 rheometer. The measurement setup used was a cone-plate geometry with a diameter of 50 mm featuring an angle α of 1°. The temperature was adjusted by Peltier devices in the plate. Representations of the rhemoter and the geometry are given in Figure 5.22.
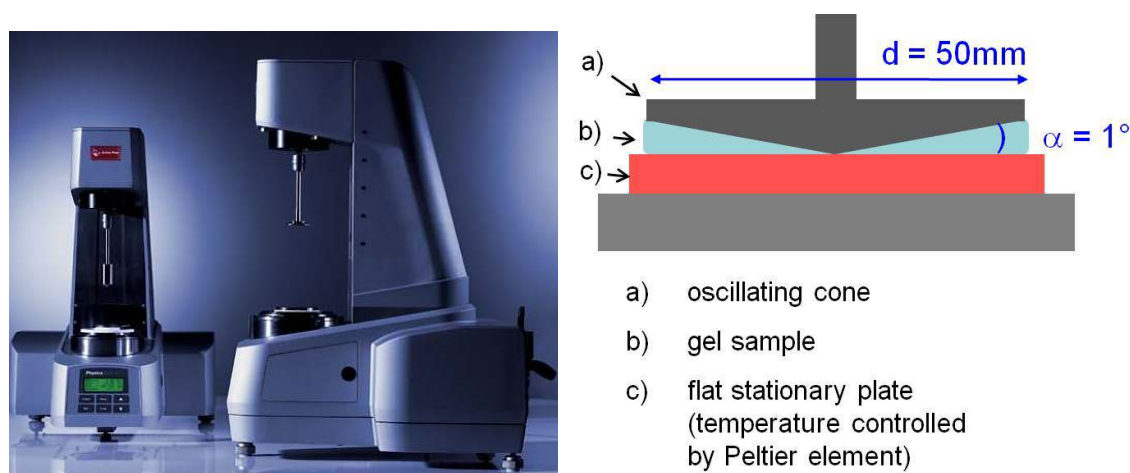

Figure 5.22:   Image of the Anton-Paar MCR301 rheometer[228] (*left*) and schematical representation of the cone-plate rheomter geometry (*right*).

Prior to sample loading the plate as well as the sample were heated to 50 °C. The 5CB/block polymer mixture was transferred in the liquid isotropic state onto the plate with a syringe and the cone was lowered to the measurement position. Prior to every measurement, the sample was kept at the respective temperature for one hour. For temperature-dependent measurements a heating/cooling rate of 1 K/min was applied and an oscillation frequency of f = 1 Hz (6.28 rad/s). Here, the measurements on heating are shown. All measurements were performed within the linear viscoelastic regime, which was determined by strain-dependent measurements of the dynamic shear storage modulus G' and loss modulus G''. Typically, strain in the range of 0.1 % or 1 % deformation was applied depending on the concentration and temperature of the solution. It should be noted that only mixtures were examined that exhibited macroscopically gel-like behavior, i.e. vials filled with the 5CB/block polymer mixtures could be turned and placed on upside down over a long period of time without observing flow. In Figure 5.23 a photo of a macroscopically gelled sample (left) in contrast to liquid reference (right) is shown.
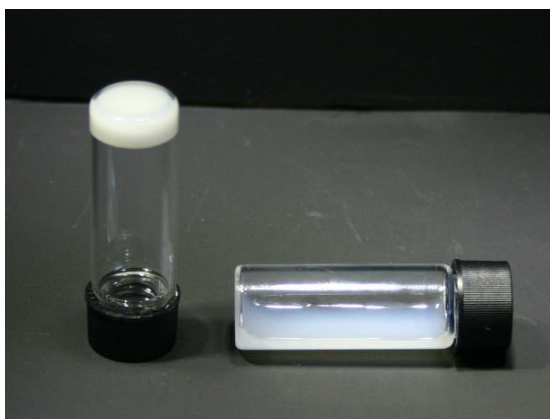

Figure 5.23: Photograph of a gel sample (*left*) using 5CB + 5 wt% **25a** compared to the nematic liquid crystal 5CB (*right*) at room temperature.

5.7.2   Influence of gelator concentration

At first the influence of gelator concentration on the gelation and the rheological properties of the gelled samples were investigated using the functionalized triblock copolymer **19c**.
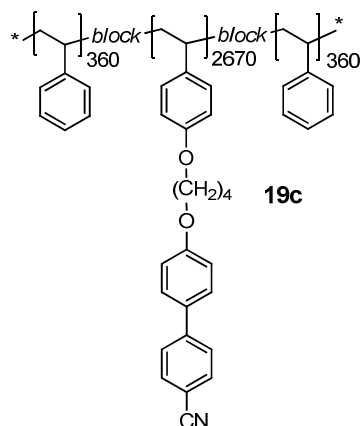
Representative results of frequency-dependent rheological experiments of **19c** in 5CB at 25 °C in a double logarithmic plot are given in Figure 5.24. The storage modulus (G') and loss modulus (G'') against angular frequency (ω) are plotted for the concentrations of 3.0, 5.0 and 10.0 wt%. Over a wide frequency range G'(ω) is higher than G''(ω) indicating a rubbery, i.e. gel-like state. All samples show a crossing of G'(ω) with G''(ω) at higher ω. This crossing point shifts to higher ω with increasing gelator concentration from 20 rad/s for 3 wt% to around 100 rad/s for 10 wt%. Above this frequency the mixtures exhibit a viscous liquid-like behavior. Both moduli show a weak dependence on the frequency that increases with decreasing gelator concentration, so the sample can be termed as a gel. G'(ω) and G''(ω) as well as the gap between them increase with the increasing gelator concentration, indicating a higher elasticity as well as a more rigid network.

Figure 5.24: Linear dynamic viscoelastic curves at 25 °C for different mass concentrations of **19c** in 5CB.

To study the effect of the gelator concentration of the gelation temperature and to investigate the rheological behavior of the gel around this 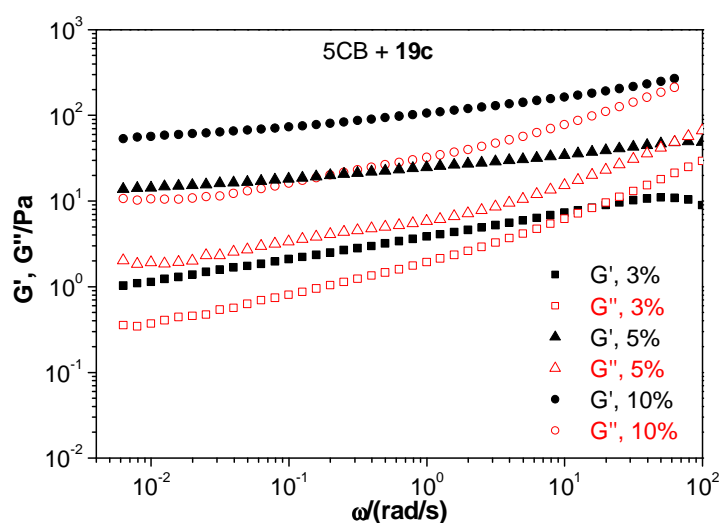point, temperature-dependent measurement were carried out at a heating rate of 1 K/min and a frequency of 1 Hz. The logarithmic plot of the storage modulus (G') and loss modulus (G'') against temperature for 3.0, 5.0 and 10.0 wt% concentrations of **19c** in 5CB on heating are given in Figure 5.25. Below a certain temperature all mixtures show gel-like behavior. G' is higher than G'' for all mixtures and both moduli increase with increasing gelator concentration, as already discussed for the frequency-dependent investigation in Figure 5.24. Above a certain temperature the mixture exhibit characteristics of a viscous liquid, G'' is higher than G'. The temperature at which G' crosses G'' can be termed the gelation temperature. In these heating curves this temperature indicates the disassembly of the gelnetwork. For 10 wt% and 5 wt% concentrations this temperature is 32.8 °C while for 3 wt% it is slightly lowered to 31.8 °C. These determined gelation temperatures show a negative deviation from the clearing temperature of 5CB which was determined to 35.8 °C at a heating rate of 1 K/min. The deviation seems to increase with decreasing gelator concentration. Up to now, no explanation can be given for this observation. The complex viscosity (η^*) is proportional to the sum of the storage and loss modulus as shown in equation (5.2).

$$\eta^* = \frac{G^*}{i\omega} = \frac{G' + iG''}{i\omega} \tag{5.2}$$

From this relation is apparent to assume that the complex viscosity of the 5CB/gelator mixture in the liquid state (i.e. above ~33 °C) increases with increasing weight fraction of the gelator. For the mixture containing 3 wt% and 5 wt% of the gelator **19c** the storage modulus exhibits an unexpected alteration around 35 °C from the evolution observed at a concentration of 10 wt%. For the 5 wt% sample it might be described as step (34.0 °C to 34.4 °C) during the sharp decrease in G' while for 3 wt% it can be described as a local maximum in G' in the range of 34.5 °C to 35.4 °C. The behavior is observed at a temperature where the system can be described as a viscous liquid. This local increase of G' might be attributed to the known contribution of liquid-liquid interfaces to the elasticity of two-phase liquids.[229] Thus, formation of a biphasic region in this temperature range may be assumed.

Figure 5.25:   Temperature dependence of linear dynamic viscoelastic behavior of gel samples with concentrations of **19c** of 3 wt%, 5 wt% and 10 wt% in 5CB on heating with a heating rate of 1 K/min (arrows indicates direction of sweep).

To identify differences in the gelation behavior on heating compared to the cooling process the above shown heating curves (G': black, G'': red) are shown together with the respective cooling curves (G': blue, G'': green) a rate of 1 K/min in Figure 5.26. For an easier comparison only the samples with 3 wt% and 10 wt% are shown. Both samples show only a very small hysteresis. The gelation temperature is shifted to lower temperature by 0.7 °C for the samples with 19 wt% **19c**, while the shift for the sample with 3 wt% is about 0.1 °C.

For both concentrations the moduli show nearly the same plateau values. A distinct difference is the behavior of the storage modulus of the 3 wt% sample around 35 °C. On cooling the unexpected increase in G' is much more pronounced compared to the heating curve and the maximum is shifted by 0.4 °C to 34.4 °C.

This comparison shows that on heating as well as on cooling the gelation temperature is similar to the transition from the isotropic to the nematic phase of the solvent 5CB.
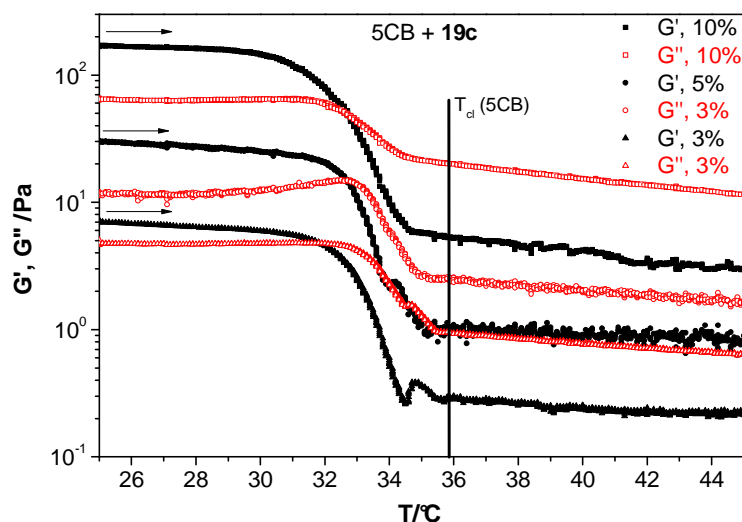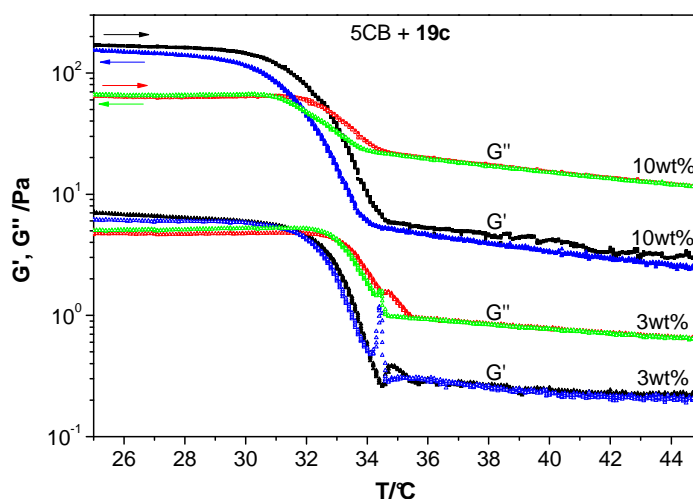
Figure 5.26:   Temperature dependence of linear dynamic viscoelastic behavior of gel samples with concentrations of **19c** of 3 wt% and 10 wt% on heating (G': black, G'': red) and cooling (G': blue, G'': green) with a rate of 1 K/min (arrows indicates direction of sweep).

These measurements confirm that the elasticity of the gel increases with increasing gelator concentration. In a gel the storage modulus (G') has to be higher than the loss modulus (G''). With decreasing concentration the gap between the G' and G'' in the gel state decrease and, thus, the gel weakens. For a gelator concentration of 3 wt% G' is only marginally higher than G''. Hence, it is reasonable to assume that the critical gelator concentration is slightly below 3 wt%. The gelation temperature shows a negative deviation from the isotropic to liquid crystalline transition which increases with decreasing gelator concentration.

5.7.3   Influence of block copolymer backbone

In contrast to the aforementioned concentration behavior, the influence of the different backbones of the block copolymer gelators on gel behavior was investigated as well. Dynamic oscillatory rheology experiments were performed for all 5CB/gelator mixtures at a constant gelator concentration of 5 wt%. Additionally, the thermal behavior of all gel samples was investigated by DSC with a heating rate of 1 K/min that is the same as used in the temperature-dependent rheology measurements. In the following figures the rheology measurements are shown together with the second heating DSC curves to provide a better comparison of the behavior around the transition temperature. The gelators of series **19** were divided in pairs for convenient evaluation of specific influences.

Length of polystyrene A-blocks

At first the impact of the polystyrene A-block lengths on the gelation properties was analyzed. A strong dependence on the lengths of the A-blocks is to be expected since the immiscibility between the polystyrene segments and the unfavorable solvent, e.g. 5CB in the nematic phase, are a function of the degree of polymerization.

	19a	**19d**
a	490	190
b	930	680
a	490	120
w_{CB}/wt%	76	86
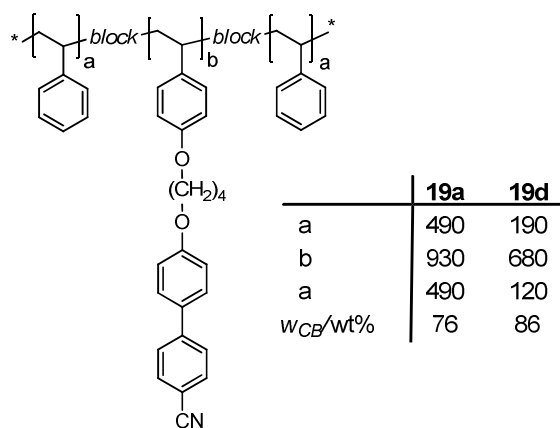
Therefore, the cyanobiphenyl-functionalized ABA triblock copolymers **19a** and **19d** were compared. Both gelators feature the lowest number of repeating units of repeating units in the functionalized B-block ($ru_{CB} = 680$, 930) in series **19** but the PS A-blocks in **19a** ($ru_{PS} \approx 490$) are about two times the length as in **19d** ($ru_{PS} = 190$, 120).

The double logarithmic plot of the storage modulus (*G'*) and loss modulus (*G''*) against angular frequency (ω) for 5CB with 5 wt% of **19a** and **19d** at different temperatures, are given Figure 5.27. The sample containing **19a** shows gel-like characteristic over the whole frequency range, G'(ω) is always higher than G''(ω). The storage modulus shows only a weak dependence on ω at higher frequencies. Both moduli show a dependence on the temperature, G'(ω) decreases in the range from 25 °C to 34 °C and, thus, the elasticity of the sample decreases. In contrast the sample containing **19d** does not qualify as a gel at a mass concentration of 5 wt%, because G'(ω) in normally higher than G''(ω). Both moduli show a strong dependence on the frequency as well as the temperature. That means 5 wt% is below the critical gelator concentration of **19d**.
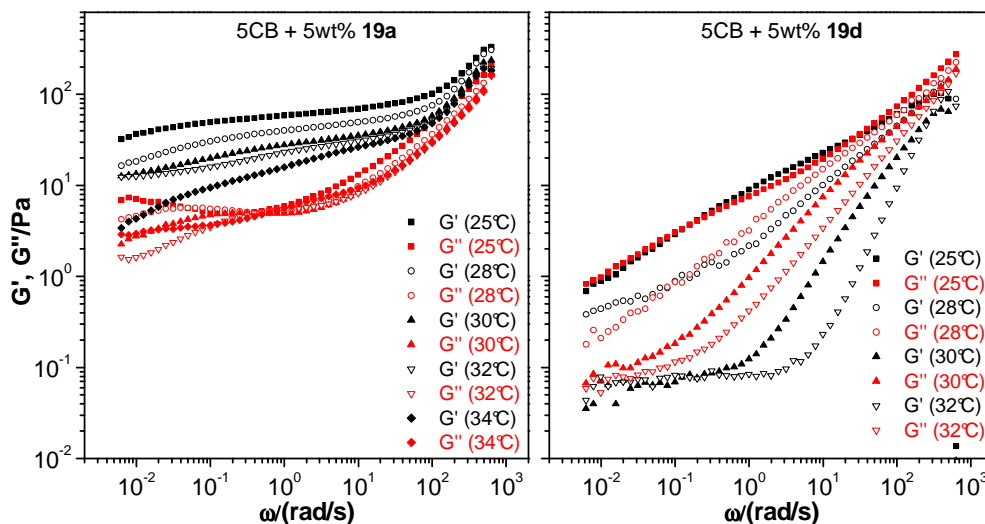
Figure 5.27: Linear dynamic viscoelastic curves for 5CB gel samples with 5 wt% of **19a** (*left*) and **19d** (*right*). Measurements were performed at different temperatures.

The temperature dependency on heating of the linear dynamic viscoelastic behavior for both samples is shown in Figure 5.28. The sample with gelator **19a** shows a plateau in both moduli from 25 °C up to 34.5 °C while G' is higher than G'' indicating a rubbery, i.e. gel-like, behavior. The temperature dependency of **19a** can be described as ideal in terms of gelation model discussed in chapter 5.1. G' is significantly higher than G'' in the gel state and the crossover temperature range is very narrow with a sharp decline in both moduli that ends with a very low storage modulus in the liquid state. Thus, the resulting viscosity of the liquid state is low. The gelation point coincides with the clearing temperature determined by DSC. In this DSC scan only a single sharp transition is detected.

In contrast, the sample with gelator **19d** cannot really be termed a gel because it does not fulfill the required criteria. G' equals G'' in the temperature range of 25 °C to 26 °C and directly above a viscous liquid state is observed. Below the crossing point of G' and G'' at 25.8 °C the sample is a viscous liquid as shown above. In the second heating DSC curve the clearing transition is significantly broadened and an additional shoulder is detected at lower temperature. The storage modulus exhibits the above described local increase in this temperature range.
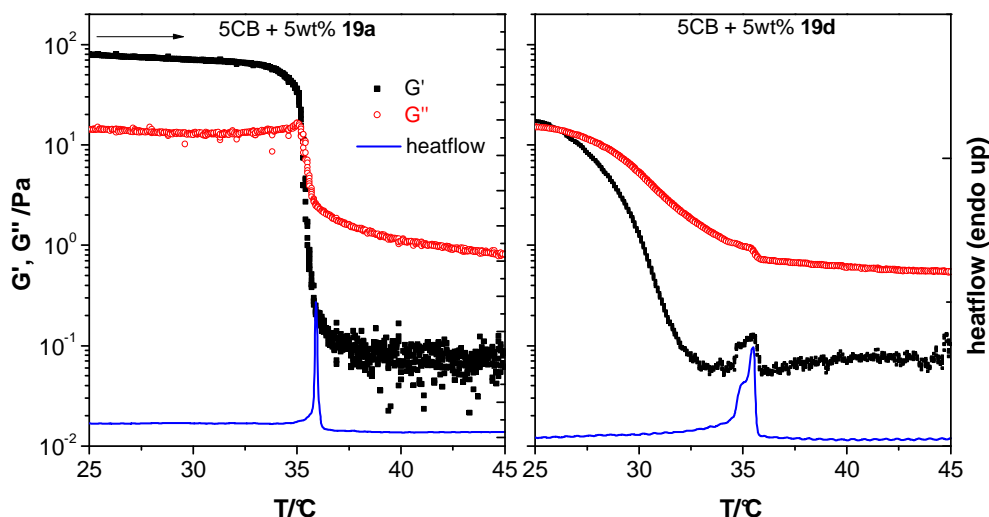
Figure 5.28   Temperature dependence of linear dynamic viscoelastic behavior of 5CB gel samples with 5 wt% of **19a** (*left*) and **19d** (*right*) on heating with a heating rate of 1 K/min. Overlaid are respective the second heating DSC traces at a heating rate of 1 K/min (arrows indicates direction of sweep).

From this comparison of the gelators with a rather short B-block (ru$_{CB}$ ≈ 680, 930) it is evident that at a gelator concentration of 5 wt% the lengths of the PS A-blocks of **19d** (ru$_{PS}$ = 190, 120) is insufficient to ensure a reasonable physical crosslinking. In contrast the PS A-block in gelator **19a** (ru$_{PS}$ ≈ 490) are about two times the length of **19d** and achieves a stable physical crosslinking.

The gelator **19a** with a relatively short functionalized B-block and short A-blocks reflects the situation as schematically shown in Figure 5.3 (right). As expected, in this case the resulting gel shows a high elasticity due to the high network density.

Length of functionalized B-block

The influence of the cyanobiphenyl-functionalized B-block was investigated using to different sets of gelators for the comparison. In the first set **19a** and **19e** are used. The lengths of the PS A-block are quite similar for **19a** (ru_{PS} = 490) and **19e** (ru_{PS} ≈ 550) but the B-block of **19e** (ru_{CB} = 3740) is four times the length as in **19a** (ru_{CB} = 930).

	19a	19e
a	490	530
b	930	3740
a	490	550
w_{CB}/wt%	76	91
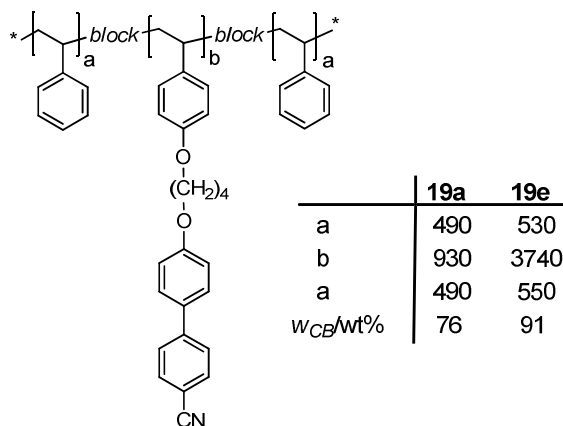
The double logarithmic plots of G' and G'' against ω for 5CB with 5 wt% of **19a** and **19d** at different temperatures, are given Figure 5.29. The sample containing **19a** was already described above. For **19e** G'(ω) is higher than G''(ω) and exhibits a plateau over nearly the whole frequency range. Up to 32 °C no temperature dependency is observed. Thus, the sample with **19e** shows a gel-like behavior. The characteristics of a gel are more pronounced for this gelator compared to **19a**.

Figure 5.29:   Linear dynamic viscoelastic curves for 5CB gel samples with 5 wt% of **19a** (*left*) and **19e** (*right*). Measurements were performed at different temperatures.

The temperature dependence of the linear dynamic viscoelastic behavior for both samples is given in Figure 5.30. The sample with gelator **19e** exhibits a high storage modulus

(G' = 43 Pa) in the gels state and a crossing point of G' and G'' at 35.1 °C. In the liquid state G' as well as G'' show relatively high values (>1 Pa) indicating a significant higher viscosity compared to **19a**. This might be caused by the very high molecular weight of the gelator **19e** compared to **19a**. Around the crossing point of G' and G'' both moduli show an abrupt increase in modulus and a local maximum at 34.5 °C which is directly below the onset of the clearing transition determined in the DSC. In the second heating DSC curve a double peak can be observed for the clearing transition. One peak maximum (35.6 °C) corresponds to the clearing temperature found for 5CB whereas the second, stronger peak maxium is observed at higher temperature at 36.7 °C.

Figure 5.30   Temperature dependence of linear dynamic viscoelastic behavior of 5CB gel samples with 5 wt% of **19a** (*left*) and **19e** (*right*) on heating with a heating rate of 1 K/min. Overlaid are respective the second heating DSC traces at a heating rate of 1 K/min (arrows indicates direction of sweep).

In the second set of samples containing the gelators **19b** and **19c** were compared. The PS A-blocks are of similar lengths (**19b** ($ru_{PS} = 430$), **19c** ($ru_{PS} \approx 360$)) while the functionalized B-block of **19c** ($ru_{CB} = 2670$) is 1.5 times the length as in **19b** ($ru_{CB} = 1860$).

	19b	19c
a	430	360
b	1860	2670
a	430	360
w_{CB}/wt%	87	92
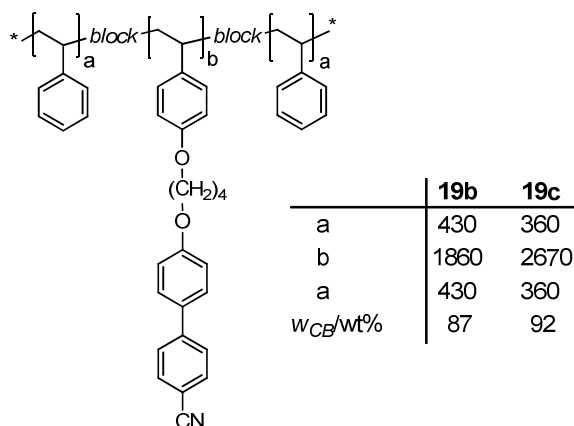
In the frequency dependent experiment both samples show a similar evolution. Gel-like behavior is observed for a wide frequency range, although a crossing of G'(ω) and G''(ω) takes place a higher frequency for both samples, indication a viscous liquid above the crossing frequency. For both samples the moduli show a dependency on the frequency as well as on the temperature. For the sample with **19b** at 34 °C G''(ω) is higher than G'(ω) over the whole frequency range indicating a liquid state.
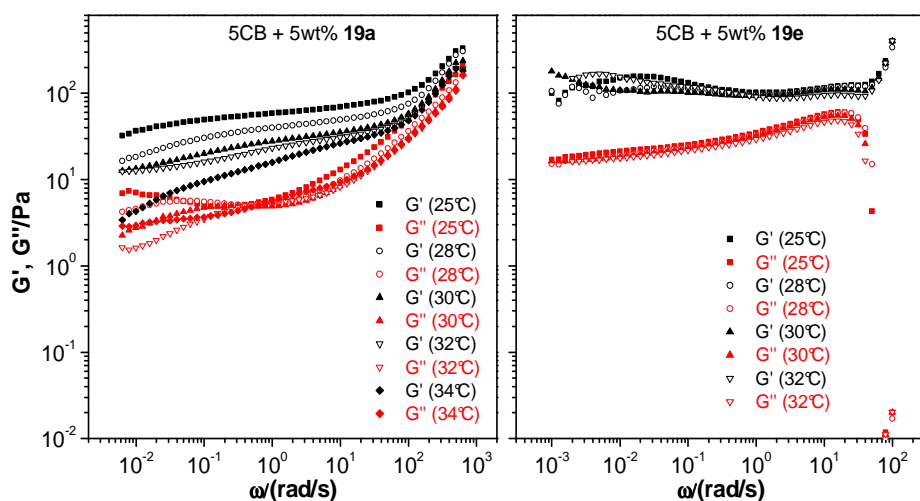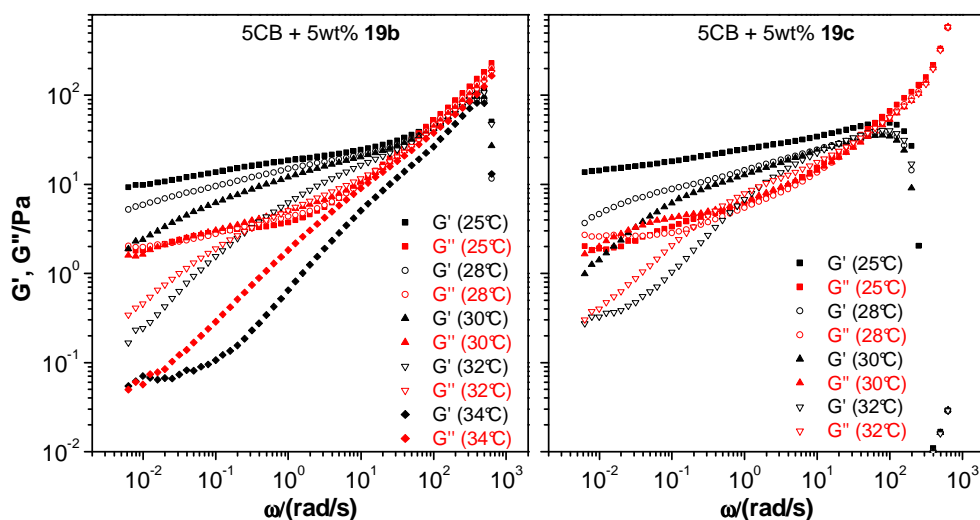

Figure 5.31:   Linear dynamic viscoelastic curves for 5CB gel samples with 5 wt% of **19b** (*left*) and **19c** (*right*). Measurements were performed at different temperatures.

The temperature-dependent measurements are shown in Figure 5.32.Both samples exhibit a gel-like behavior and similar temperature dependence at the fixed frequency of 1Hz (6.28 rad/s). The storage modulus in the gel state for the sample containing **19c** (G' = 29 Pa) is slightly higher than for **19b** (G' = 23 Pa). The crossover of G' and G'' is at 33.4 °C for **19b** while it is shifted to lower temperatures for **19c** at 32.8 °C. This shift might also be caused by the lower A-block length of **19c** (ru_{PS} = 360) compared to **19b**

(ru_{PS} = 430), as observed above for **19a** and **19d**. In the second heating DSC curves a single clearing transition is detected for both samples, for **19b** the peak maximum is 35.3 °C while it is slightly lower for **19c** at 34.7 °C. Both samples exhibit the intermediate maximum in storage modulus, discussed above, albeit to a very low degree. In the liquid state sample **19b** shows a lower viscosity than **19c** that might be attributed to the shorter B-block.
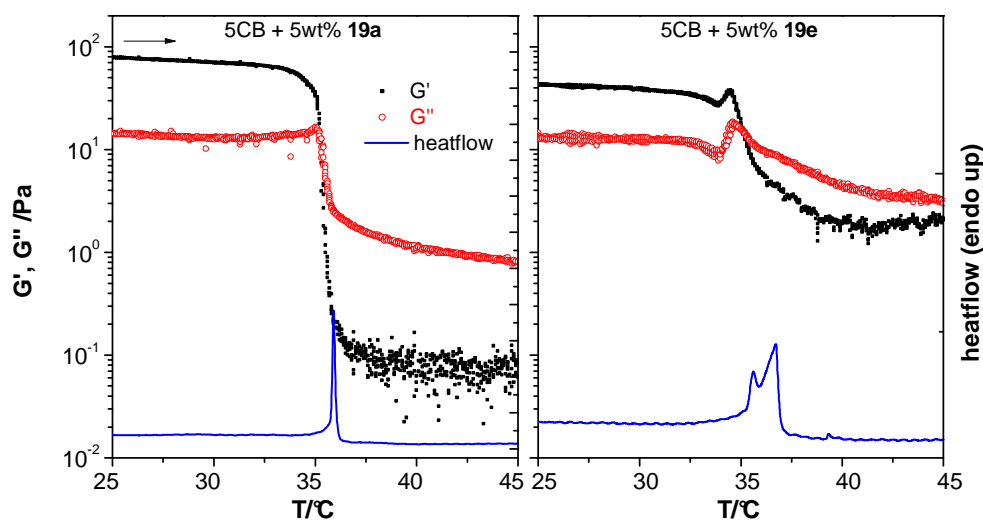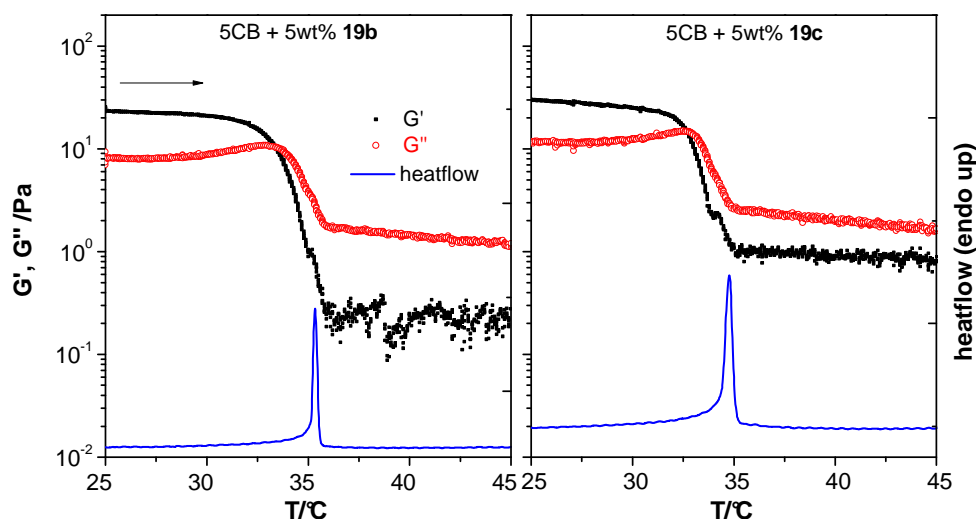

Figure 5.32:   Temperature dependence of linear dynamic viscoelastic behavior of 5CB gel samples with 5 wt% of **19b** (*left*) and **19c** (*right*) on heating with a heating rate of 1 K/min. Overlaid are respective the second heating DSC traces at a heating rate of 1 K/min (arrows indicates direction of sweep).

The gelators investigated in this series resulted in the formation of very weak gels at a concentration of 5 wt% in 5CB. The difference in G' and G'' was typically below the orders of magnitude often referred to as a strong gel.

A shorter B-block with relatively long A-blocks (**19a**) seems to result in gel with a higher elasticity and stability due to the high network density and large nodes. If the length of the middle block is significantly increased (**19e**) the resulting gel exhibits more gel-like behavior (frequency independence, larger difference between G' and G''), although this might also be attributed to the higher viscosity of the system due to the high molecular weight of the gelator. For gelators with B-block length in between the aforementioned but shorter A-block lengths (**19b** and **19c**) a stronger dependency on the frequency is observed as well as shear thinning a high frequencies. This is attributed to the shorter A-block that might result in less stable nodes. Thus, under strain A-blocks might dissociate from the physical crosslinking points. If the A-block lengths are drastically reduced as in

the case for **19d** the resulting nodes are not formed or at least are not stable enough to yield a physical thermoreversible network at a gelator concentration of 5 wt% With decreasing length of the A-blocks also the gelation temperature seems to decrease and the temperature dependency in the frequency dependent experiment increases slightly. The formation of a biphasic region around the clearing temperature cannot be correlated with the length of either block in this work.

5.7.4 Influence of the gelator backbone architecture

If the block copolymer architecture is changed from a linear ABA structure to a three arm star architecture, this change is expected to result in higher number of physical crosslinking points per gelator molecule due to the introduction of a chemical crosslinking connecting the arms (see chapter 5.6). This increase in the number of network point should increase the network density, thus creating a more elastic gel structure. Additionally, by the introduction of the chemical crosslink the probability for the formation of back loops might be reduced.

In Figure 5.33 the molecules are schematically shown. The linear ABA' triblock copolymer gelator **19d** is compared to the star-shaped block copolymer gelator **25a**. Each arm in the star consists of a ABA' triblock copolymer **19d**. **25a** is comprised of a mixture of three arm stars, dimers and unimers.
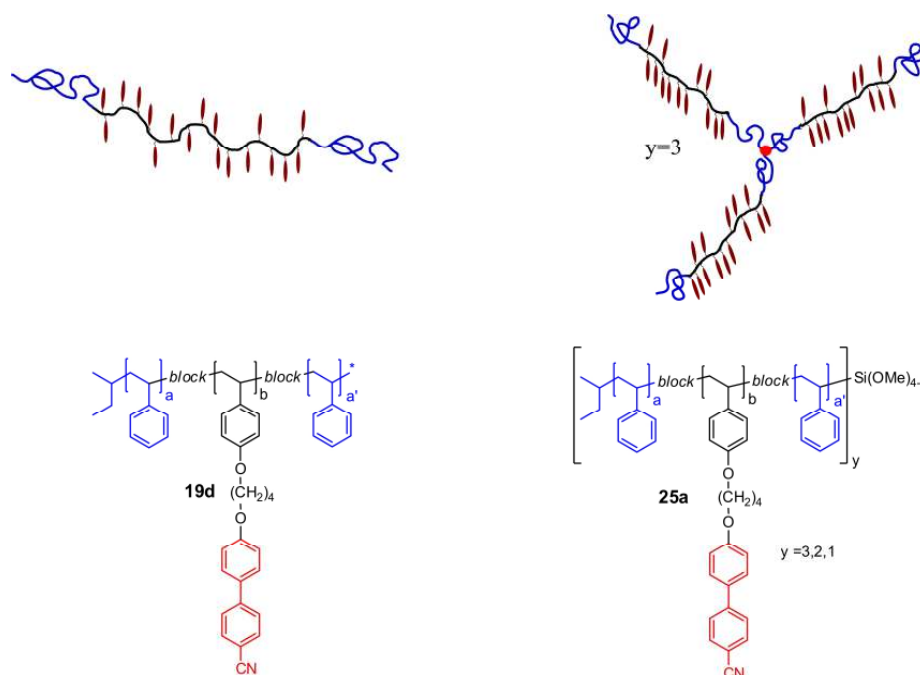
Figure 5.33: Schematic representation and chemical structure of the linear ABA triblock copolymer gelator **19d** (*left*) and the mixture containing the three arm star-shaped block copolymer **25a** (*right*). Schematical representation is shown for y = 3.

Samples containing 5CB with 5 wt% of **19d** or **25a** were analyzed in the same way as discussed above. In the frequency-dependent measurement, shown in Figure 5.34, both samples show a temperature dependency. The frequency dependency is much more pronounced for the sample with **19d**, although the sample with **25a** exhibits a crossing in $G'(\omega)$ and $G'(\omega)$ at $\omega \geq 31$ rad/s and, thus, shows liquid-like behavior above that frequency.
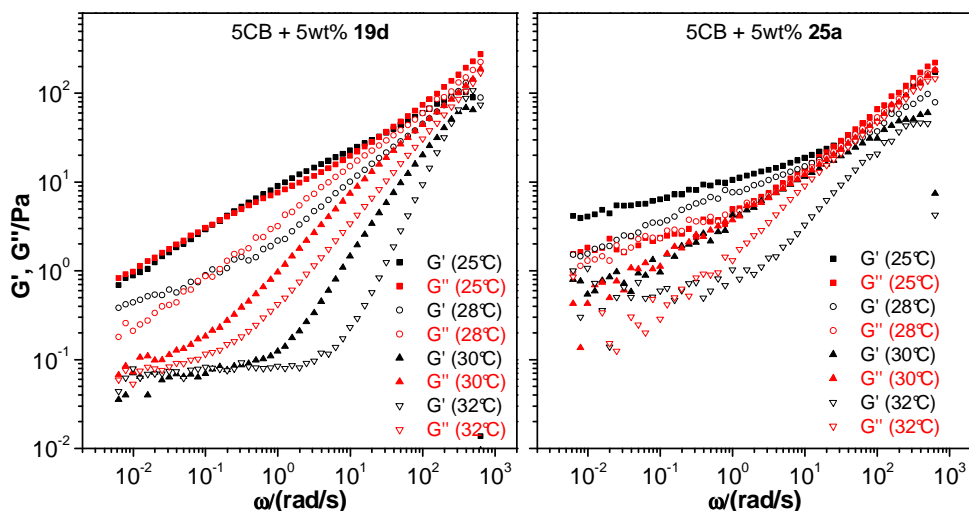
Figure 5.34: Linear dynamic viscoelastic curves for 5CB gel samples with 5 wt% of linear triblock copolymer **19d** (*left*) and the gelator mixture containing the star-shaped block copolymer **25a** (*right*). Measurements were performed at different temperatures.

The temperature dependence of the linear dynamic viscoelastic behavior for both sample is given in Figure 5.35. The behavior of the sample containing **19d** was already described above in detail. Apparently, no gel is formed that corresponds to the gel definition in chapter 5.1. For the sample containing the star-shaped block copolymer gelator **25a** a gel like behavior is observed. In the gel state a high storage modulus ($G' = 111$ Pa) is determined that sharply decreases around the crossover point of G' and G''. This temperature at which the gel network disassembles is at 31.4 °C and thus significantly shifted to lower temperature compared to the clearing transition. The second heating DSC trace exhibits a broadened clearing transition with two peak maxima of equal heights at 35.2 ° and 35.6 °C.
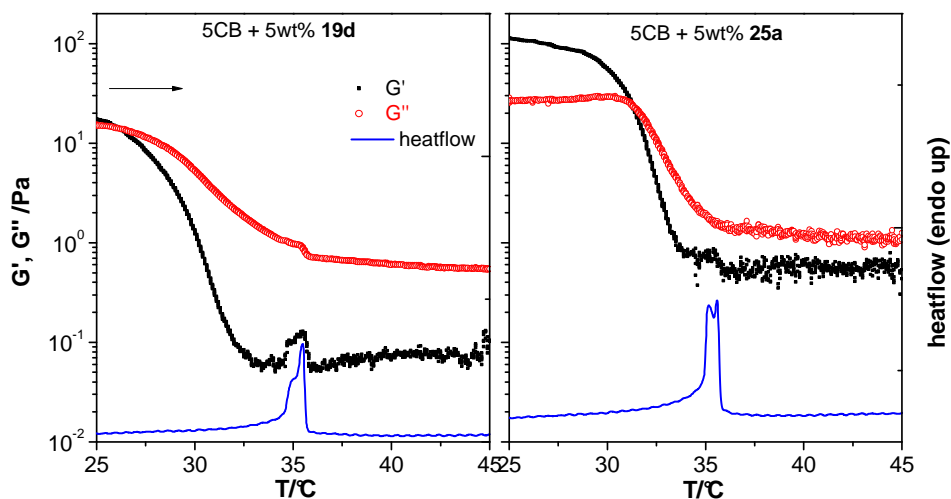
Figure 5.35:   Temperature dependence of linear dynamic viscoelastic behavior of 5CB gel samples with 5 wt% of linear ABA triblock copolymer gelator **19d** (*left*) and the star-shaped block copolymer gelator **25a** (*right*) on heating with a heating rate of 1 K/min. Overlaid are respective the second heating DSC traces at a heating rate of 1 K/min (arrows indicates direction of sweep).

The change of the block copolymer architecture from linear to a mixture of three arm star-shaped block copolymers, dimers of ABA triblock copolymers and unimers results in a significant increase in the quality of network formation. At the same gelator mass concentration where the linear triblock copolymer gelator **19d** failed to produce a gellating network the corresponding star-shaped block copolymer gelator **25a** yielded a sample filling network. The storage modulus for the resulting gel was the highest value at 25 °C determined in the series of gelators that were investigated. The high temperature dependency as well as the shift in gelation temperature is attributed to the short A-blocks, although the increase in crosslinking points, resulting from the partial star architecture, leads to a network formation. For gelator based on star-shaped block copolymers with longer A-blocks a significantly improved performance might be expected.

5.8 Electrooptical investigation of LC gels [1]

In cooperation with Dr. Maxim Khazimullin and Prof. Ingo Rehberg of Experimental Physics V electro-optical methods have been employed to characterize the viscoelastic properties of binary mixtures of the block copolymer gelators as well as the cyanobiphenyl-containing homopolymers in 5CB. All measurements and data analysis in this chapter have been performed by Dr. Maxim Khazimullin. For the different experiments a wide range of samples containing different concentration of homopolymer or gelators have been prepared by myself as well as Dr. Klaus Kreger using the sample preparation method described in chapter 5.7.

In this chapter exemplary investigations are presented to illustrate the usage of the discussed materials for fundamental studies. Results obtained for the gelator **19c** and the respective cyanobiphenyl-containing homopolymer **IX** were selected that were also submitted as a publication.[230]

The transition from the diluted regime to the gel state of solutions of triblock copolymer **19c** in 5CB by varying the polymer concentration was investigated. To this end, the viscoelastic properties of a binary mixture of the gelator **19c** in 5CB and the homopolymer **IX** in 5CB were characterized over a mass concentration (c) range from 0.2 % up to 2.5 %. . Infiltration of the mixtures with **IX** in 5Cb and **19c** in 5CB into liquid crystal cells coated with rubbed polyamide produced well aligned samples that behaved like usual nematics up to mass concentrations of c = 2.5 % as shown in Figure 5.36
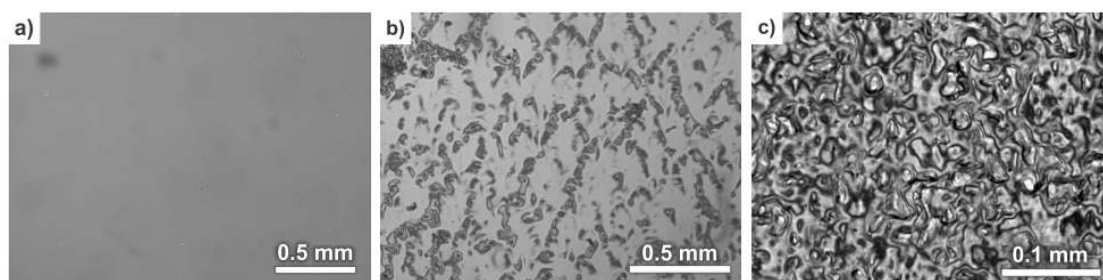
Figure 5.36: Microscopic images taken between crossed polarizers of cells filled with samples of different concentrations c of the block copolymer **20c**. a) c = 1.1 %; b) c = 3.0 %; c) c = 5.0 %. Note the different scales.

For the characterization of the viscoelstic properties the dynamic Fréedericksz transition technique was used.[231] This electro-optical technique is based on the optical detection of the reorientation of the liquid crystal in an electric field thus, the dependence of the splay elastic constant and the rotational viscosity on the polymer concentration could be obtained. The anisotropy of the dielectric permittivity, as well as the splay elastic constant, of the mixtures did not exhibit any pronounced dependence on concentration within the accuracy of the measurements. In contrast, the dynamic properties, namely the rotational viscosity ($\delta\gamma_1$), display a more pronounced influence of the polymer concentration.

The self-assembly of the A-blocks of the gelator was investigated by comparing the behavior of samples containing homopolymer **IX** to samples of the same concentration of gelator **19c**. The increase of rotational viscosity of the samples depending of the mass concentration of homopolymer **IX** and triblock copolymer **19c** is shown in Figure 5.37. For small concentrations $c < 1$ %, the rotational viscosities of both mixtures increase with c and show similar values. With increasing concentrations $c > 1$ %, the rotational viscosity of the mixture with **20c** sharply increases and tends to diverge while the rotational viscosity for the mixtures with **IX** exhibits an almost linear dependence on c.
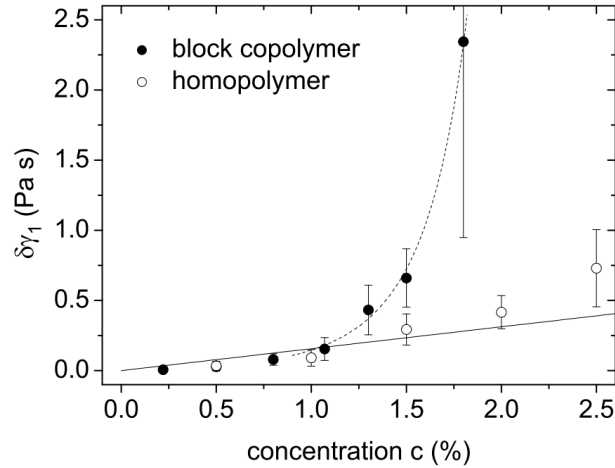
Figure 5.37:   Increase of the rotational viscosity for the homopolymer ($\delta\gamma^h_1$) and for the block copolymer ($\delta\gamma^c_1$) solutions. The solid line is a linear fit with $\delta\gamma^h_1 = 0.156$ c, while the dashed line is a guide to the eye.

By the comparison of the homopolymer to the ABA triblock copolymer the influence of the A-blocks can be isolated as shown in Figure 5.38. The increase of the ratio $\delta\gamma^c_1/\delta\gamma^h_1$ with concentration yields a measure for the effective size of the attached block copolymer chains in units of a single chain size. These measurements of the dynamic behavior reveal that above a mass concentration of 1 % self-assembling of the block copolymer chain segments in clusters occurred resulting in a gel state at higher concentrations. The effective cluster size was estimated as a function of the gelator concentration.

Until the critical gelator concentration $\delta\gamma^c_1/\delta\gamma^h_1$ should obey a scaling law. The experimental values were fitted as shown in Figure 5.38. Using this fitting procedure the critical gelator concentration could be calculated to a mass concentration of 2.7 %. As discussed in chapter 5.7.2, the critical concentration determined by rheological measurements resulted in a mass concentration of c ≈ 3 %.The value obtained from the rotational viscosity data is very close to the value extrapolated from rheological measurements. Thus, the dynamic Freedericksz transition technique can serve as an alternative approach for the determination of the critical concentration and has apparent advantages in comparison with rheological and dynamic light scattering measurements.
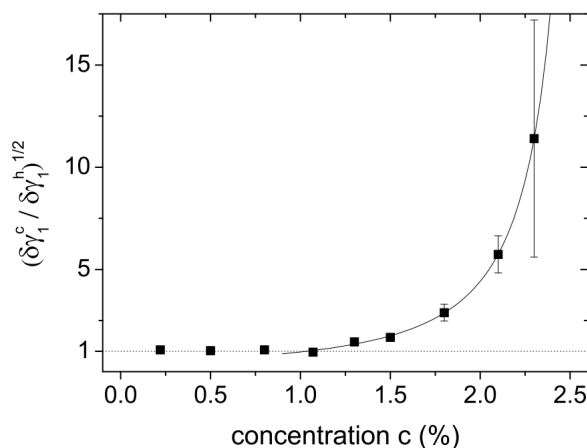
Figure 5.38:   Dependence of $(\delta\gamma^c_1 / \delta\gamma^h_1)^{1/2}$ on the block copolymer concentration c. The solid line is obtained by a fitting procedure for the data above c = 1 %.

Achievements

In this chapter functional ABA triblock copolymers were synthesized and characterized that were designed as block copolymer gelators for the low molecular weight liquid crystal 5CB. Two different synthetic routes were employed for the anionic polymerization of the ABA and ABA' block copolymer backbone with varying block lengths and compositions. Cyanobiphenyl-containing homopolymers and block copolymers were prepared in a polymer analogous reaction and structure-property relations regarding the required solubility of the functionalized B-block in the liquid crystal 5CB were established using the respective functionalized homopolymers. Combination of oscillating rheology measurements and DSC measurements were performed to study gels containing 5 wt% of the gelators. The influence of the gelator backbone on the gel properties was investigated. In cooperation with the Department of Experimental Physics V the gel formation was investigated by electro-optical techniques on selected examples.

6   Summary

This thesis covers the design, synthesis, characterization, and application of functional block copolymers. In polymer science the term functional has several meanings. The term *functional* is used if at least one polymer segment bears chemical functions or if the block copolymers fulfill a specific function due to their distinct physical properties or inducible changes in properties. Here, block copolymers carrying functional groups in one block copolymer segment that allow chemical reactions are denoted as *functionalizable* polymers.

The general synthetic approach towards functional block copolymers utilized in this thesis is shown below and is based on three steps: (i) anionic polymerization of the block copolymers bearing protected functional side-groups, (ii) subsequent conversion into a functionalizable block copolymer by deprotection and (iii) attachment of side-group with specific function in a polymer analogous reaction.
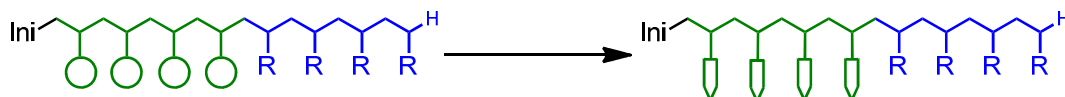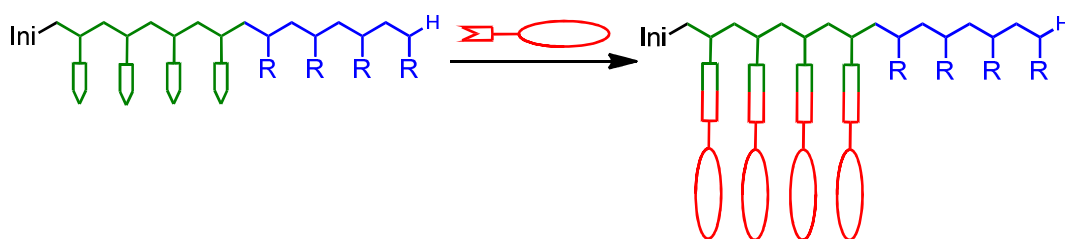
The resulting functional block copolymers were designed for two different purposes, namely, materials for holographic data storage and gelators for low molecular weight crystals.

This thesis covers three main subjects: (I) the combinatorial synthesis of block copolymers by anionic polymerization, (II) azobenzene-containing block copolymers for holographic experiments and (III) cyanobiphenyl-functionalized ABA block copolymers as gelators for liquid crystals.

The *first subject* is the implementation of a specially constructed reactor setup for sequential anionic polymerization that is capable of performing *parallel block copolymer*

synthesis based on one identical A-block on a lab scale. For this reason, this setup facilitates the *preparation of block copolymer series in a combinatorial fashion*. It consists of one main reactor and three secondary reactors with individual temperature control, and the addition of monomers or additives to each reactor can be handled separately. To conduct anionic polymerizations of block copolymers in this reactor setup without termination of the living polymers during pumping and distribution processes, operating procedures were established and optimized. For the combinatorial synthesis of AB diblock copolymers, shown below, the A-block is polymerized in the main reactor and the living polymer solution is subsequently distributed to the secondary reactors. The final B-segment can be polymerized in each of the four reactors resulting in a block copolymer series based on an identical A-block.
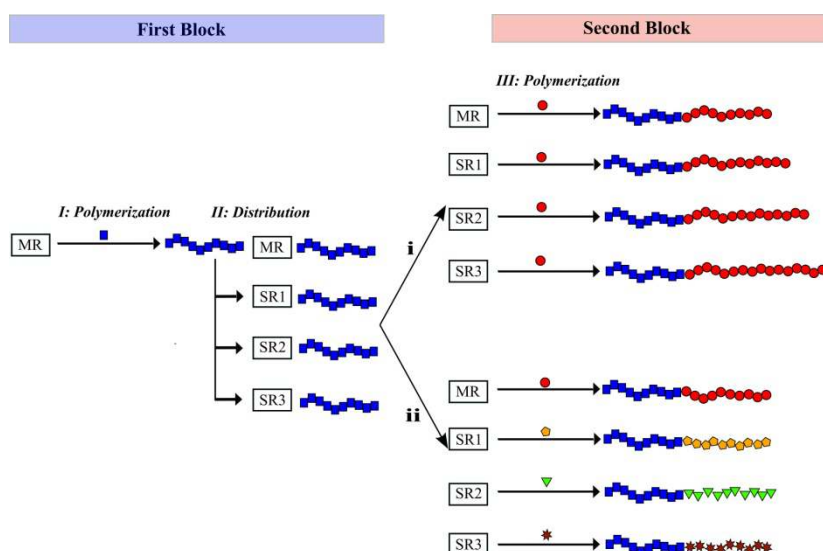
This procedure can also be expanded for the synthesis of ABC triblock copolymer series or even more complex block copolymer architectures. From the wide range of combinatorial variations two basic variants were selected to demonstrate the capabilities of the reactor. An AB diblock copolymer series and an ABC triblock copolymer series were prepared with *different lengths of the final block* as well as a diblock copolymer *series with different chemical structures of the last block.*

Using this reactor setup, complex series of block copolymers are conveniently obtainable to facilitate composition-dependent investigations as well as process optimization in block copolymer applications such as lithography, nano-templating, and holographic data storage.

The *second subject* covers the synthesis, characterization, processing and application of new liquid crystalline azobenzene-containing block copolymers. Most of the *azobenzene-containing diblock copolymers* were designed in view of their application as materials for holographic data storage and, thus, contained an amorphous, optical inert *poly(methyl methacrylate) (PMMA) or polystyrene (PS) matrix*. As a functionalizable segment

polyhydroxystyrene was introduced enabling polymer analogous reactions to functional photoadressable homopolymers, copolymers and block copolymers with a high glass transition temperature. *Different lengths of flexible spacers* and/or mixtures of two spacer lengths were employed to connect the mesogenic chromophores to the polymer backbone. *The structure-property relation* of functionalized block copolymers and the resulting mesophase was investigated. The respective homopolymer and copolymers were used as reference materials.
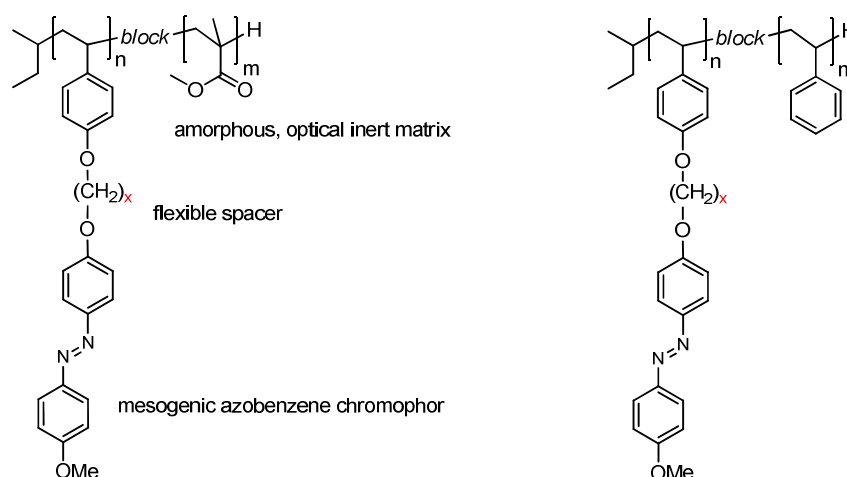
Holographic experiments were conducted on selected examples of the prepared azobenzene-containing polymers and several relations on the holographic behavior were revealed. *Smectic annealed samples* or *amorphous quenched samples* were obtained by different sample preparation methods to investigate the influence of the liquid crystalline order. While the sensitivity to light induced orientation of the polymer systems remained unaffected in the beginning, the writing times and level of postdevelopment were improved for quenched samples but with slight loss of the achievable maximum refractive index modulation. *Variation in spacer lengths* resulted in decreasing smectic order with decreasing spacer length as well as for mixtures of two different spacer lengths. The reduced order promoted lower writing times in the holographic experiments while the maximum refractive index modulation was not significantly affected. Additionally, *the temperature dependence* of the temporal evolution of the refractive index modulation in the *smectic polymers* was studied. A significant decrease of writing times and an enhancement of the postdevelopment were revealed at elevated temperatures. Stable holographic gratings could be obtained even at 100 °C due to the liquid crystalline phase of the storage materials. Thus, the high writing temperatures in combination with amorphous quenched samples facilitated short writing times and an exceptionally high stability of the holographically inscribed gratings.

1.1 mm *thick samples*, that are a prerequisite for volume holographic data storage with a high data storage density, were prepared by injection molding of blends of photoaddressable block copolymer and PMMA or PS. Preliminary results confirmed the

long-term stability of holographic inscribed gratings. Additionally, *angular multiplexing of holographic volume gratings was demonstrated* on thick samples. Based on these results smectic azobenzene-containing block copolymer systems can be seen as promising candidates to further develop faster rewritable holographic data storage materials with improved long-term stability of the inscribed information.

The *third subject* covers the synthesis and characterization of new *cyanobiphenyl-containing ABA triblock copolymers* and their application as *block copolymer gelators* for the low molecular weight liquid crystal 4-cyano-4'-(pentyl)biphenyl (5CB). Liquid crystalline solvents cause an abrupt change in solvent quality due to their first-order transition from the isotropic into the liquid crystalline phase. Based on the selective solubility of the A and B blocks in the nematic solvent, ABA triblock copolymers can be used for the thermoreversible gelation of 5CB. To this end, ABA and ABA' triblock copolymers comprised of polystyrene A-blocks and a cyanobiphenyl-functionalized polyhydroxystyrene B-block with a high degree of polymerization were prepared by the combination of anionic polymerization, using two different synthetic routes, and polymer analogous attachment of the mesogens. Using this approach, *series of gelators were prepared with variations in the B-block length, the A-block lengths.* Different *polymer architectures*, e.g. star shaped block copolymers, were obtained by the use of a coupling agent.
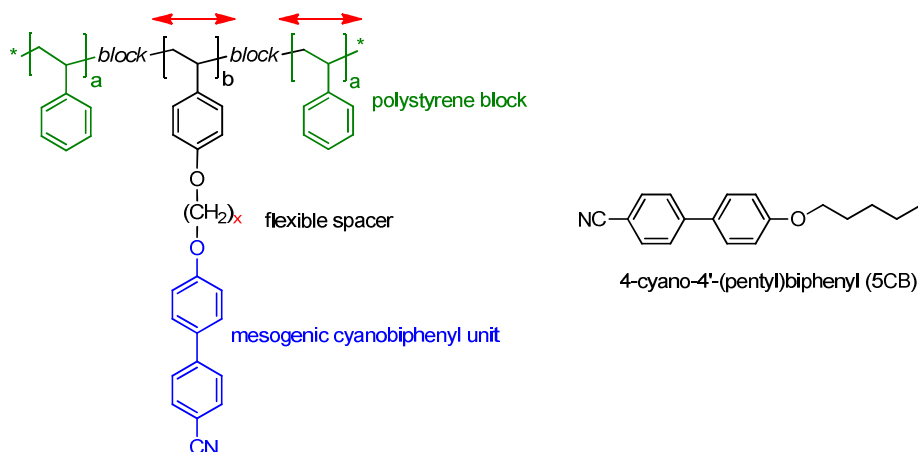
Structure-property relations regarding the mesophase characterization revealed that cyanobiphenyl-functionalized polymers with long spacers feature highly ordered smectic phases. On reducing the spacer length this order was significantly lowered enhancing the solubility in the nematic 5CB. A comprehensive study was conducted to investigate the structure-property relation of the triblock copolymer gelators regarding the gelation of 5CB. A combination of *oscillating rheology measurements* and *thermal characterization by DSC* was employed to investigate the behavior of the thermoreversible liquid crystalline gels. Most of the block copolymer gelators achieved gelation of the low molecular weight liquid crystal 5CB at a concentration of 5 wt%. The properties of the

different gels where compared at this fixed concentration. The *influence of the gelator backbone on the gel properties* was investigated by comparing different sets of triblock copolymers that differed only in the length either the A-blocks or the functionalized B-block. While a short functionalized B-block resulted in high network density and, thus, a high elasticity of the gel the length of the A-blocks proved critical to the gelation process. The gelator with the shortest A-blocks failed to form a gel network at the fixed gelator concentration, whereas the stability of the physical network nodes formed by the self assembled polystyrene segments seemed to increase for longer A-blocks.

Additionally, the influence of the block copolymer architecture, namely linear and star-shaped block copolymers, was investigated. Comparing a linear ABA' triblock copolymer gelator to a three arm star gelator revealed that the star-shaped gelator resulted in a significantly higher elasticity of the liquid crystalline gel.

In cooperation with the Department of Experimental Physics V at the University of Bayreuth, the gel formation was investigated using the electro-optical Fréedericksz transition technique on selected samples. These measurements investigated the dynamic properties of dilute solutions of 5CB and a cyanobiphenyl-containing gelator as well as the respective homopolymer with increasing concentrations. The concentration dependency of the rotational viscosity could be fitted by a scaling law. By extrapolation of the fitting curve the critical gelator could be assumed that coincided with the value that was experimentally determined by rheology measurements on liquid crystalline gel samples.

7 Zusammenfassung

Diese Arbeit umfasst Design, Synthese, Charakterisierung und Anwendung von funktionellen Blockcopolymeren. Die Bezeichnung *funktionell* besitzt in den Polymerwissenschaften mehrere Bedeutungen. Sie wird benutzt, wenn mindestens ein Polymersegment chemische Funktionen beinhaltet oder die Blockcopolymere aufgrund ihrer originären physikalischen Eigenschaften oder induzierbaren Änderungen in diesen Eigenschaften spezielle Funktionen erfüllen. Blockcopolymere, die in einem Segment funktionelle Gruppen tragen, welche eine chemische Reaktion ermöglichen, werden als *funktionalisierbare* Polymere bezeichnet.

Der generelle synthetische Ansatz zu funktionellen Blockcopolymeren, der in dieser Arbeit benutzt wurde, und basiert auf drei Schritten: (i) die anionische Polymerisation von Blockcopolymeren mit geschützten funktionellen Seitengruppen, (ii) die anschließende Umwandlung in funktionalisierbare Blockcopolymere durch Entschützung und (iii) die Einführung von komplexen Seitengruppen mit spezifischen Funktionen durch polymeranaloge Reaktion.
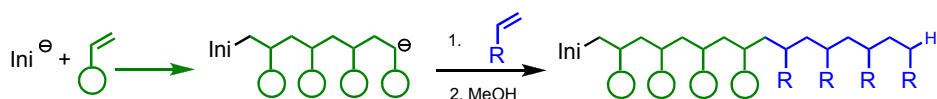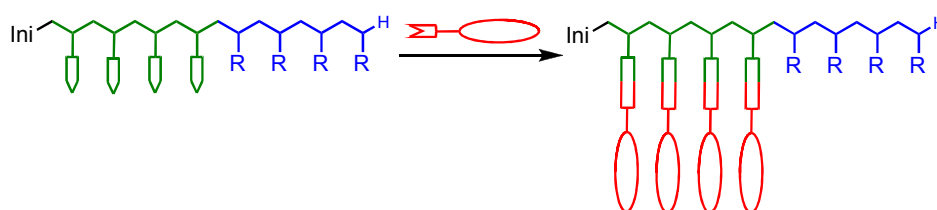
Die so hergestellten funktionellen Blockcopolymere wurden speziell für zwei unterschiedliche Zielsetzungen maßgeschneidert und zwar als Materialien für wiederbeschreibbare holographische Datenspeicher und als Gelatoren für niedermolekulare Flüssigkristalle.

Diese Arbeit behandelt drei übergreifende Themengebiete: (I) die kombinatorische Synthese von Blockcopolymere durch anionische Polymerisation, (II) azobenzolhaltige Blockcopolymere für holographische Experimente und (III) Cyanobiphenyl-funktionalisierte ABA Blockcopolymere als Gelatoren für niedermolekulare Flüssigkristalle.

Für das *erste Themengebiet* wurde eine speziell angefertigte Reaktoranlage realisiert, welche die *parallele anionische Synthese von Blockcopolymeren* im Labormaßstab erlaubt. Dadurch wird die *Synthese von Blockcopolymerserien auf kombinatorische Art* ermöglicht. Die Anlage besteht aus einem Hauptreaktor und drei Nebenreaktoren. In diesen kann sowohl die jeweilige Temperatur individuell kontrolliert als auch die Zugabe von Additiven oder Monomeren separat gehandhabt werden. Um die anionische Polymerisation von Blockcopolymeren in dieser Reaktoranlage ohne Abbruchsreaktionen während der Pump- und Verteilungsvorgänge zu gewährleisten, wurden spezifische Arbeitsrichtlinien ausgearbeitet und optimiert. Für die kombinatorische Synthese von AB Diblockcopolymeren wird der A-Block im Hauptreaktor polymerisiert und die lebende Polymerlösung, wie unten gezeigt, anteilig in die Nebenreaktoren gepumpt. Der abschließende B-Block kann so, basierend auf dem identischen A-Block, in jedem der vier Reaktoren separat polymerisiert werden.
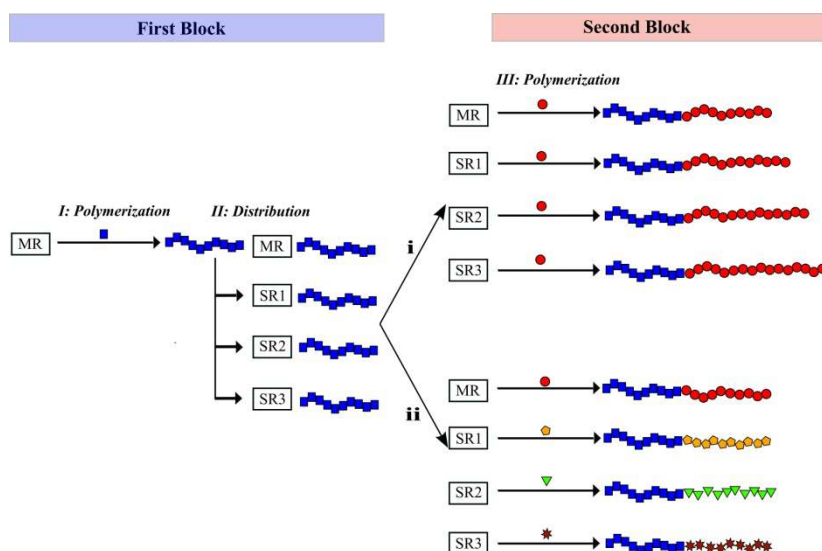
Diese Technik kann auch für die Synthese von ABC Triblockcopolymeren oder noch komplexeren Blockcopolymerarchitekturen entsprechend erweitert werden. Aus dieser großen Bandbreite an möglichen kombinatorischen Herangehensweisen wurden zwei einfache Varianten ausgewählt, um die die Möglichkeiten dieser Reaktoranlage zu demonstrieren. Es wurde je eine Serie aus AB Diblockcopolymeren und ABC Triblockcopolymeren mit *variierender Länge des abschließenden Blockes* erfolgreich hergestellt sowie eine Serie von *Diblockcopolymeren mit unterschiedlicher chemischer Struktur der letzen Blockes*.

Komplexe Blockcopolymerserien, welche sich für zusammensetzungsabhängige Untersuchungen und Prozessoptimierungen in komplexen Blockcopolymeranwendungen eignen, sind nun leicht zugänglich. Beispiele dafür sind die Nanostrukturierung mittels Blockcopolymertemplaten oder auch die holographische Datenspeicherung.

199

Das *zweite Themengebiet* behandelte Synthese, Charakterisierung, Verarbeitung und Anwendung von neuen *azobenzolhaltigen Blockcopolymeren*. Die meisten dieser fotoadressierbaren Diblockcopolymere wurden im Hinblick auf ihre Anwendung als Materialien für die holgraphische Datenspeicherung designt und enthielten deshalb *Poly(methyl methacrylat) (PMMA) oder Polystyrol (PS) als amorphen, optisch inerten Matrixblock. Polyhydroxystyrol* wurde als funktionalisierbares Segment für die polymer analoge Synthese von funktionellen Homopolymeren, Copolymeren und Blockcopolymeren mit hohen Glasübergangstemperaturen eingeführt. *Flexible Spacer verschiedener Länge* und/oder Mischungen zweier unterschiedlicher Spacerlängen wurden eingesetzt, um die Farbstoffmesogene mit dem Polymerrückgrat zu verbinden. Die *Struktur-Eigenschaftsbeziehung* der resultierenden Flüssigkristallphase wurde mit Hilfe der funktionalisierten Blockcopolymere sowie der entsprechenden Homopolymere als Referenzmaterialien untersucht.
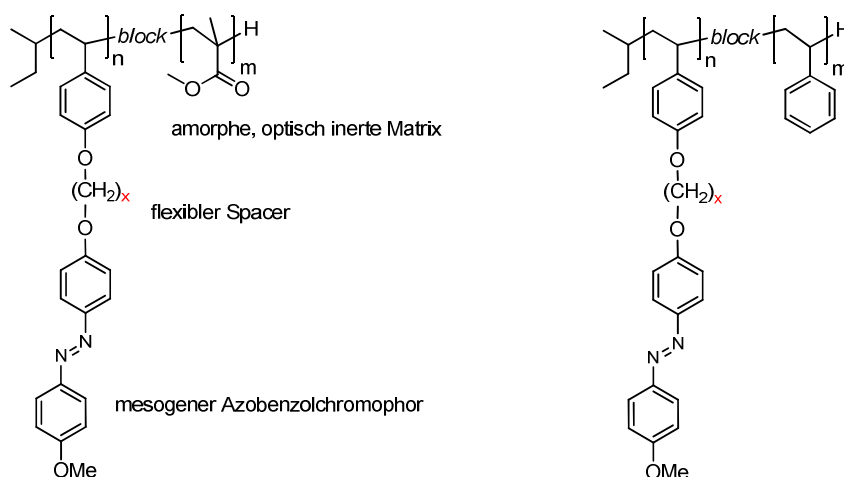
In Zusammenarbeit mit dem Bayreuther Institut für Makromolekülforschung (BIMF) wurden an ausgewählten Beispielen *holographische Experimente* mit azobenzolhaltigen Polymeren durchgeführt und verschiedene Einflussfaktoren auf das holographische Verhalten gefunden. *Smektische getemperte Proben* und *amorphe gequenschte Proben* wurden durch unterschiedliche Probenpräparationsverfahren hergestellt, um den Einfluss der flüssigkristallinen Ordnung zu untersuchen. Es zeigte sich, dass dadurch die Sensitivität im Anfangsbereich gegenüber lichtinduzierter Orientierung nicht beeinflusst wurde. Im Gegensatz dazu verbesserten sich die Schreibzeit und der Grad der Nachentwicklung durch den Einsatz von amorph gequenschten Proben, wobei die maximale Brechungsindexmodulation leicht reduziert war. *Variationen der Spacerlängen* zeigten eine Reduzierung der smektischen Ordnung bei abnehmender Länge oder Mischung zweier Längen. Diese reduzierte Ordnung führte zu kürzeren Schreibzeiten in den holographischen Experimenten, wobei die Brechungsindexmodulation nicht stark beeinflusst wurde.

Zusätzlich wurde die *Temperaturabhängigkeit* des zeitlichen Verlaufs der Brechungsindexmodulation in den *smektischen Polymeren* untersucht. Bei höheren Temperaturen reduzierte sich die Schreibzeit deutlich, während die Nachentwicklung verstärkt auftrat. Durch die flüssigkristalline Phase konnten stabile holographische Gitter sogar bei einer Temperatur von 100 °C erhalten werden, wo die verstärke thermische Relaxation in den meisten Systemen zum Einbrechen der Stabilität führt. Der Einsatz hoher Schreibtemperaturen in Kombination mit amorph gequenschten Proben führte zu kurzen Schreibzeiten bei gleichzeitig außergewöhnlich hoher Stabilität der holographischen Gitter.

1,1 mm *dicke Proben* sind eine Voraussetzung für die Anwendung in der holographischen Datenspeicherung mit hohen Speicherdichten und wurden durch Spritzgussverfahren aus Blends aus fotoadressierbaren Blockcopolymeren mit PMMA oder PS hergestellt. Vorläufige Ergebnisse bestätigten die Langzeitstabilität der eingeschriebenen holographischen Gitter. Zusätzlich wurde die Möglichkeit *des Winkelmultiplexing von Volumengittern* demonstriert.

Basierend auf diesen Ergebnissen dürfen smektische azobenzolhaltige Blockcopolymere als vielversprechende Kandidaten betrachtet werden, um schnellere, wiederbeschreibbare holographische Datenspeichermaterialien mit verbesserter Langzeitstabilität weiterzuentwickeln.

Im *dritten Themengebiet* wurde Synthese und Charakterisierung von neuen *cyanobiphenylhaltigen ABA Triblockcopolymeren* sowie ihre Anwendung als *Blockcopolymergelatoren* für den niedermolekularen Flüssigkristall 4-cyano-4'-(pentyl)biphenyl (5CB) behandelt. Beruhend auf der selektiven Löslichkeit der A-Blöcke und des B-Blocks in einem nematischen Lösungsmittel, können ABA Triblockcopolymere für die thermoreversible Gelierung von 5CB eingesetzt werden. Zu diesem Zweck wurden zuerst ABA und ABA' triblockcopolymere, bestehend aus Polystyrol A-Blöcken und einem funktionalisierbaren Polyhydroxystyrol B-Block, mit einem hohen Polymerisationsgrad, über anionische Polymerisation hergestellt, wobei zwei unterschiedliche synthetische Routen genutzt wurden. Anschließend wurden die Cyanobiphenyleinheiten durch polymer analoge Reaktion eingeführt. Mittels dieses Ansatzes wurde eine *Serie aus linearen Triblockcopolymergelatoren mit variierenden Längen der A und B-Blöcke sowie ein Blockcopolymer mit Sternarchitektur* hergestellt.
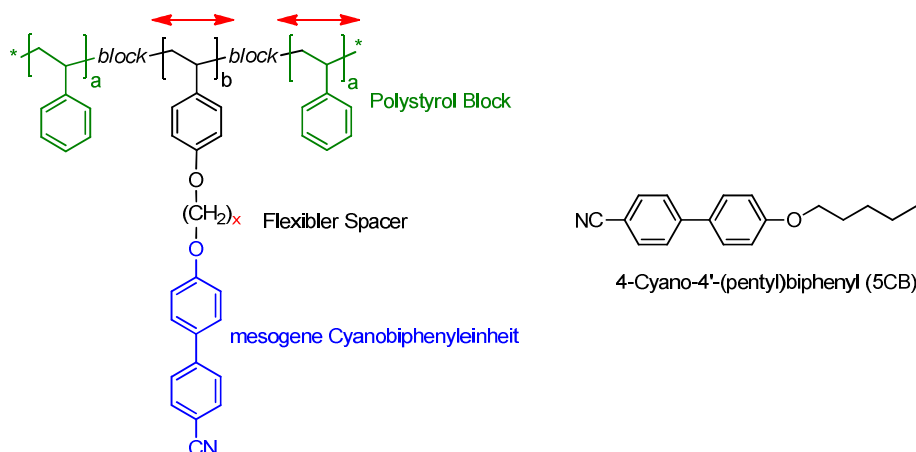
Untersuchungen der Struktur-Eigenschaftsbeziehungen im Hinblick auf die Mesophasencharakterisierung ergaben, dass cyanobiphenyl-funktionalisierte Polymere mit langen Spacern eine hoch geordnete smektische Phase aufweisen. Mit abnehmender Spacerlänge wird diese Ordnung deutlich herabgesetzt, wodurch sich die Löslichkeit im nematischen 5CB erhöht. Eine umfassende Studie zum Einfluss des Polymerrückgrats und der Polymerarchitektur der entsprechenden Gelatoren auf die Gelierung von 5CB wurde durchgeführt. Eine Kombination von *oszillierenden rheologischen Messungen* und *thermischer DSC Charakterisierung* wurde eingesetzt, um das Verhalten der thermoreversiblen flüssigkristallinen Gele zu untersuchen. Die meisten eingesetzten Blockcopolymergelatoren waren in der Lage, den niedermolekularen Flüssigkristall 5CB bei einer Massenkonzentration von 5 Gew.% zu gelieren. Die Eigenschaften der verschiedenen Gele wurden bei dieser festgelegten Konzentration untersucht. Der *Einfluss des Gelatorrückgrats auf die Geleigenschaften* wurde untersucht, indem verschiedene Paare von Triblockcopolymer verglichen wurden, die sich jeweils nur in der Länge der A-Blöcke oder des funktionalisierten B-Blocks unterschieden. Während ein kurzer funktionalisierter B-Block eine hohe Netzwerkdichte bedingte und dadurch zu einer hohen Elastizität des entsprechenden Gels führte, erwies sich die Länge der A-Blöcke als kritisch für den Gelierungsprozess. Der Gelator mit den kürzesten A-Blöcken war nicht in der Lage, bei der festgelegten Konzentration ein gelierendes Netzwerk auszubilden. Mit steigender Länge der A-Blöcke schien sich auch die Stabilität der physikalischen Verknüpfungspunkte des Netzwerks zu erhöhen, welche sich durch Selbstorganisation der Polystyrolsegmente bilden.

Zusätzlich wurde der Einfluss der Blockcopolymerarchitektur untersucht, im Speziellen an linearen und sternförmigen Blockcopolymeren. Beim Vergleich eines linearen ABA' Triblockcopolymergelators mit einem Dreiarmsterngelator ergab sich eine signifikant höhere Elastizität des resultierenden flüssigkristallinen Gels für den sternförmigen Gelator.

In Kooperation mit dem Fachbereich Experimentalphysik V an der Universität Bayreuth wurde die Gelbildung an ausgewählten Beispielen mittels elektro-optischer Fréedericksz Übergangsmessungen untersucht. Diese Messungen verglichen die dynamischen Eigenschaften von verdünnten Lösungen von 5CB und sowohl cyanobiphenyl-funktionalisierten Gelatoren als auch den entsprechenden Homopolymeren mit steigender Konzentration. Die Konzentrationsabhängigkeit der Rotationsviskosität konnte mittels eines Skalierungsgesetzes angenähert werden. Durch Extrapolation dieser Kurve konnte eine kritische Gelatorkonzentration ermittelt werden, die mit dem durch rheologische Untersuchungen an flüssigkristallinen Gelproben bestimmten Wert übereinstimmte.

8   Experimental part

8.1   Methods

Size exclusion chromatography (SEC) measurements were performed on three different setups. The first one, utilizes a Waters 515-HPLC pump with stabilized THF as eluent at a flow rate of 0.5 mL/min. 20 µl of a solution with a concentration of approx. 1 mg/mL were injected into a column setup, which consists of a guard column (PSS; 5 x 0.8 cm; SDV- gel; pore size 100Å; particle size 5 µm) and two separation columns (PL; 30 x 0.8 cm; mixed C gel; particle size 5 µm). The molecular-weight distribution was monitored with a Waters 486 tunable UV detector at 254 nm and a Waters 410 differential RI detector. Molecular weights were given with respect to an added internal standard (*o*-dichlorobenzene) and to narrowly distributed polystyrene standards.

The second setup, uses a Waters 510-HPLC pump with a column setup which consists of a guard column (PSS; 5 x 0.8 cm; SDV- gel; pore size 100 Å; particle size 5 µm) and three separation columns (PL; 30 x 0.8 cm; pore size 100, 10^3, 10^4Å; particle size 5 µm). THF with 0,25 wt% tetrabutylammonium bromide (TBAB) was used as eluent at a flow rate of 0.5 mL/min. 100 µl of a solution with a concentration of approx. 1 mg/mL were injected for each measurement. All other parameters equal the Poly-SEC setup.

Oligo-SEC measurements were performed utilizing a Waters 515-HPLC pump with stabilized THF as eluent at a flow rate of 0.5 mL/min. 20 µl of a solution with a concentration of approx. 1 mg/mL were injected into a column setup, which consists of a guard column (Varian; 5 x 0.8 cm; mesopore gel; particle size 3 µm) and two separation columns (Varian; 30 x 0.8 cm; mesopore gel; particle size 3 µm). The compounds were monitored with a Waters 486 tuneable UV detector at 254 nm and a Waters 410 differential RI detector. Molecular weights were given with respect to an oligo-styrene calibration.

^{1}H-NMR spectra were recorded on a Bruker AC 250 spectrometer (250 MHz) and Bruker AC 300 spectrometer (300 MHz) using CDCl$_3$ as solvent and tetramethylsilane (TMS) as internal standard.

Thermogravimetric analysis (TGA) was conducted under N$_2$ atmosphere at a scan rate of 10 °C/min with a Mettler Toledo TGA/SDTA851^e.

Differential scanning calorimetry (DSC) was carried out on a PerkinElmer DSC Diamond instrument utilizing 10–20 mg of the polymers in 50 mL pans at a scanning rate of 10 K/min or 1 K/min. Indium standard was used to calibrate the instrument.

Polarized optical microscopy (POM) experiments were performed using a Leitz Laborlux 12PolS microscope equipped with a Mettler FP 802 hot-stage.

Fourier transform infrared spectroscopy (FT-IR) was performed in attenuated total reflectance (ATR) mode on a PerkinElmer Spectrum 100 with universal ATR accessory.

8.1.1   X-ray diffraction

A crystalline material can be described as the translational shift of a unit cell thus, forming a crystal lattice. The unit cell contains the complete array of symmetry properties of the crystal lattice and hence is sufficient for a complete description of the crystal structure. The unit cell is characterized by the lattice constants a, b, c (the absolute values of the vectors of the unit cell) and the angle between them. For the description of the coordinates in a unit cells fractions of the lattice constants are used (fractional (atomic) coordinates). A plane within a lattice can be completely described by the coordinates of three lattice points within the plane. The fractional coordinates (a/h, b/k, c/l) of these points are expressed using the integers h, k, l, as shown in Figure 8.1. For the denotation of the lattice planes normally only the integers are used in the form (hkl) and are called Miller indices. In Figure 8.1 (100), (200) and (110) are given as illustration.
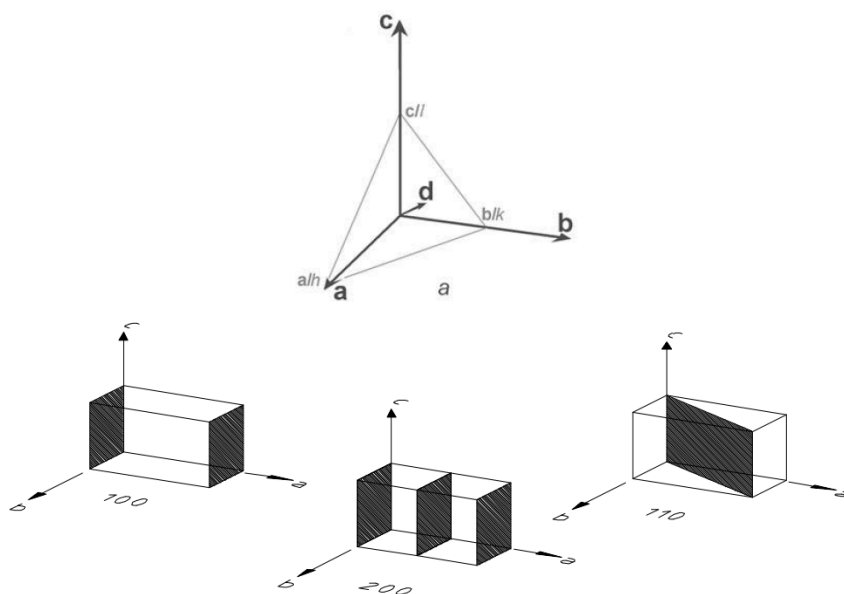
Figure 8.1:   An exemplary plane (122) characterized by fractional coordinates using the integers h, k, l (left)[232] and three different sets of lattice planes with the respective (hkl) notation (right).[233]

The distance (d_{hkl}) between two lattice planes (lattice distance) is given by the absolute value of the vector $\vec{d}_{hkl}$.and can be calculated in an orthorhombic lattice (all angles = 90°, a ≠ b ≠ c) from the lattice constants and the Miller indices by using equation (8.1).

$$\frac{1}{d_{hkl}^2} = \left(\frac{h}{a}\right)^2 + \left(\frac{k}{b}\right)^2 + \left(\frac{l}{c}\right)^2 \qquad (8.1)$$

h, k, l: Miller indices of the lattice plane

d_{hkl}: distance between two planes (lattice distance)

X-ray diffraction is based on the elastic scattering of X-rays from the electron clouds of the individual atoms in the system and is used to investigate the atomic structures in a material. In most directions, the combining resulting waves are out of phase, called a destructive interference, and thus, no resultant energy leaves the solid sample. If atoms are arranged in a regular pattern, well-defined X-ray beams leave the sample in various directions. In these cases the combining resulting waves are in phase thus, having a constructive interference. A diffracted beam may be described as a being comprised of a large number of scattered rays. Commonly the X-ray reflections from a series of parallel planes inside the crystal are detected as shown in Figure 8.2. Positive interference is observed if the difference in path length between the wave reflected by the first plane and the wave reflected by the second plane is an integral number of the wavelengths. Thus, the observation of diffraction is depending on the lattice distance d_{hkl} and the angle between the plane normal and the beam (θ).
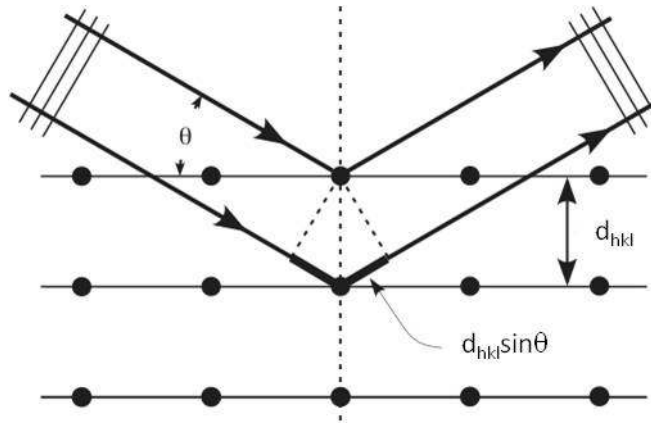
Figure 8.2:   Schematical illustration of the Bragg diffraction.[234]

This relationship is expressed by equation (8.2) that is called the Bragg equation.

$$\lambda = 2d_{hkl}\sin\theta \qquad (8.2)$$

Setup

X-ray diffraction (XRD) was performed on powder samples using a transmission diffractometer with focusing beam path after Guinier (*Guinier diffractometer*). The schematical setup is shown in Figure 8.3. The setup operates with monochromatic Cu-$K_{\alpha 1}$-radiation. A monochromator (Huber Type 616-2) is used for focusing the beam on the samples. The powder samples were filled in glass tubes with diameters of 1.5 mm or 2.0 mm. Temperature dependent measurements were possible due to the electrically heated copper chamber in which the tubes were fixated. A position-sensitive detector (position sensitive proportional counter, PSPC) was used to collect all diffracted beams into a 2θ range of 1-30°.
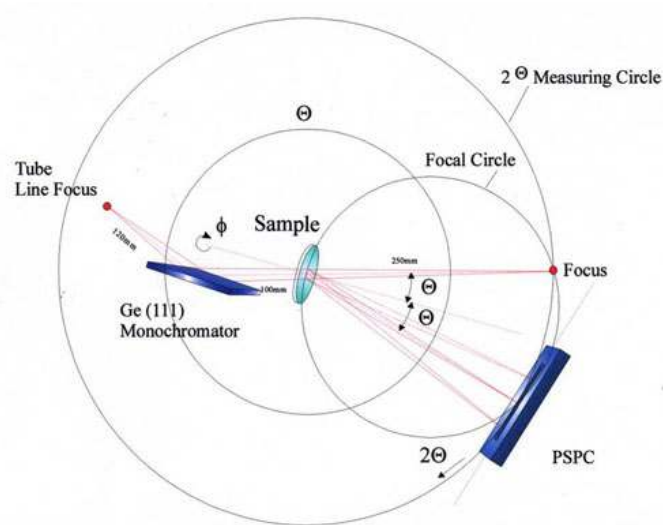
Figure 8.3:   Schematically illustration of a Guinier diffractometer.[235]

8.1.2   Holographic measurements

Introduction to holography

In holographic data experiments an optical interference pattern is created by intersecting two coherent laser beams within the storage material. A coherent beam is split into two beams. The first beam, called the signal or object beam, contains the information. The second beam, called the reference beam, generates a coherent background. Both beams are superimposed in the storage medium. In the simplest case of transmission holographic writing, an interference pattern is created by intersecting two coherent plane waves (no object) in the storage material. The resulting intensity grating is a sinusoidal light intensity gradient that is stored in the photosensitive material as a local change of the refractive index. The grating constant (Λ), that is the distance between the intensity

maxima or minima of the intensity grating, is dependent on the wavelength (λ) and the angle of incidence of the beams (θ).

$$\Lambda = \frac{\lambda}{2n_0 \sin\theta} \tag{8.3}$$

Λ: grating constant

λ: writing wavelength

θ: angle of incidence of the laser beams

n: refractive index

In this writing process the intensity grating is stored in the photosensitive material as a change in the refractive index (n) of the material:

$$n = n_0 + n_1 cos\left(\frac{2\pi x}{\Lambda}\right) + \ldots = \sum_{m=0}^{\infty} \alpha_m \left(\frac{2\pi x}{\Lambda}\right) \tag{8.4}$$

n_m: amplitude of the m-th spatial Fourier component of the refractive index

Holographic reading process

The reading process has to be conducted without influencing the storage material and the inscribed grating. Thus a laser with a wave length outside the absorption band of the azobenzene containing material is used. The reading beam is used to illuminate the storage material where it diffracted at the inscribed interference grating.

The diffraction efficiency (η) is the most basic indicator used to evaluate the quality of holographic storage materials.

$$\eta = \frac{I_1}{I_0} \tag{8.5}$$

I_1: intensity of the light diffracted into the first order

I_0: intensity of the incident laser light

η uses only the first order diffraction of the incident light beam and is therefore dependent on the diffraction type of the grating. Only the amplitude of the first Fourier component of the refractive index, n_1, determines the diffraction into the first order (see (8.10)). In an approximation the following the higher orders are neglected and n_1 is called refractive index modulation.

At this point it has to be distinguished between two different conditions: thin and thick gratings. The parameters Q' and γ are used for the determination:[137,236]

$$Q' = \frac{2\pi\lambda d_0}{n_0 \Lambda^2 \cos\theta} \tag{8.6}$$

$$\gamma = \frac{\pi n_1 d_0}{\lambda \cos\theta} \tag{8.7}$$

d_0: thickness of the hologram

n_0: refractive index of the material

n_1: first spatial component of the refractive index modulation

A grating is called thick if Q' and $\gamma \cdot Q'$ are greater than unity. Thin gratings show *Raman-Nath* diffraction with multiple diffraction orders and the theoretical maximum diffraction efficiency is 33.9 %. Thick gratings exhibit *Bragg* diffraction and only a single diffraction order. Thus they provide a theoretical maximum diffraction efficiency of 100 % with a high angular selectivity. Therefore angular multiplexing, the inscription of many holographic gratings in the same volume under different angles, is only possible using thick gratings.[137,178]

η can now be calculated for thin gratings using Magnusens theory[237] and for thick gratings using Kogelnik's *Coupled Wave Theory*.[238] Under the conditions of light incident at the Bragg angle and only small refractive-index modulations, the calculations of the diffraction efficiencies for thin and thick gratings are the same:

$$\eta \approx \left(\frac{\pi n_1 d_0}{\lambda \cos\theta} \right)^2 \tag{8.8}$$

To compare different holographic storage materials η is not fully suited. The above derived equations are only valid for samples without absorption. For a given writing angle and laser intensity, η depends not only on the properties of the material, but also on the thickness of the sample thus it is not a material constant. In contrast the first Fourier component of the spatial modulation of the refractive index, called the refractive index modulation n_1, is independent of the thickness.[239] Equation (8.8) can be used to calculate the changes n_1 from the diffraction efficiency that is directly measured in the holographic experiment:

$$n_1 \approx \frac{\lambda \cos\theta \sqrt{\eta}}{\pi d_0} \tag{8.9}$$

For all descriptions of holographic measurements presented in this thesis n_1 was used.

A further important material characteristic is the material sensitivity S that describes the slope of the holographic growth curve.[140] The sensitivity is a parameter for the photo-physical response of the whole photochromic system. Since the growth of the writing curve does not increasing linear, the sensitivity is usually determined at the beginning of the writing process ($t \sim 0$) where it exhibits the maximum value (S_{max}).

$$S = \frac{\frac{\partial \sqrt{\eta}}{\partial t}}{I_0 d_0} \qquad (8.10)$$

Holographic setup

If not noted otherwise the samples were spin-coated from THF solution on cleaned glass slides and annealed on a hot stage at 60 °C for 1 h to remove the solvent. The holographic measurements were performed with the standard holographic setup depicted in Figure 8.4. Two s-polarized plane waves at 488 nm with an intensity of each 1 W/cm^2 are brought to interference in the plane of the sample. Due to the s:s-polarization a light-intensity grating is generated in the material. The read out was performed at 685 nm. From the grating experiment, the diffraction efficiency is obtained. The refractive index modulation, n_1, was calculated according to Kogelniks theory. The temporal evolution of the refractive index modulation in thin films of all polymers was recorded until the maximum of n_1 (n_{1max}) was reached at the writing time t_{max}. Technical details about the setup and the measurements can be found in lit.[147]

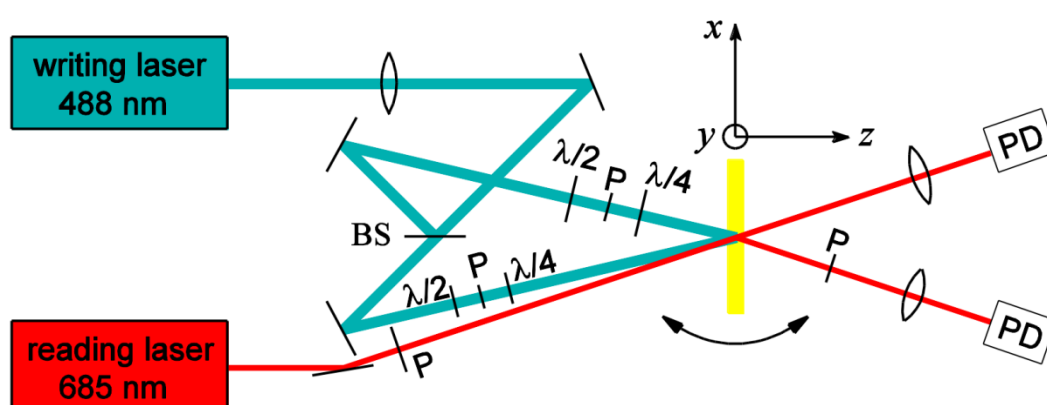

Figure 8.4: Optical set-up for the holographic experiments with plane waves. (P: polarizer, BS: beam splitter, PD: photodiode, λ/2: half-wave plate, λ/4: quarter-wave plate).[147]

This specific writing wavelength of 488 nm is used to avoid an overpopulation of the *cis*-azobenzene species that would result if the maximum absorption wave length of the $\pi\pi^*$-

transition would be used. The writing wavelength is in the range of the maximum absorption of the nπ^*-transition, thus this absorption is much larger than the also exited $\pi\pi^*$-transition. Therefore, during inscription, most azobenzene chromophores are already in the *trans*-state and only few isomers are the *cis*-state.

8.1.3 Rheological measurements

Introduction to rheology

Gels are viscoelastic materials, they behave partly as elastic solids as well as viscous liquids.[227] The rheological properties of these components are described in the following.

Ideal elastic (*Hookean*) solids exhibit an elastic response to an applied external stress. If stress, i.e. the force (F) per unit area (A), acts on a material a deformation or strain, defined as the ratio of the change in dimension relative to the original dimensions, is induced. This deformation is fully reversible and recovers upon removal of the applied stress. For tensile deformation the strain is *dl/l* (*l*: original (dimension) length, *dl*: change in dimension) resulting in a tensile modulus (*E*):

$$E = \frac{\sigma}{\varepsilon} = \frac{F/A}{dl/l} \tag{8.11}$$

σ: tensile stress

ε: tensile strain

In the case of an applied shear stress the resulting shear strain is given by *tanα*. For small strains tan$\alpha \approx \alpha$. Thus the shear modulus is given by:

$$G = \frac{\tau}{\gamma} = \frac{F/A}{\tan \alpha} \tag{8.12}$$

τ: shear stress

γ: shear strain

For ideal fluids (*Newtonian*) the applied energy is fully dissipated and cannot be recovered. The stress depends upon the rate of change of strain with time rather than the amount of deformation. The shear viscosity (η) is defined by:

$$\eta = \frac{\tau}{d\gamma/d\tau} = \frac{\tau}{\dot{\gamma}} \tag{8.13}$$

$\dot{\gamma}$: shear rate

These equations are valid for non oscillating experiments. However dynamic rheological measurements often use oscillatory strain experiments that allow the investigation of materials over a broad range of frequencies.[240] A sinusoidal oscillation of maximum strain γ_M and oscillatory frequency ω is applied to a sample using parallel plate geometry and the response is determined. For ideal elastic materials the response stress wave is in phase with the applied strain wave. For purely viscose materials the phase difference (δ) of the response stress will be exactly 90 °C. For a viscoelastic material δ will be in between these limits (0<δ<90°) thus δ, or more commonly tanδ, is a measure of the viscous/elastic ratio of a material at a given ω (see Figure 8.5).
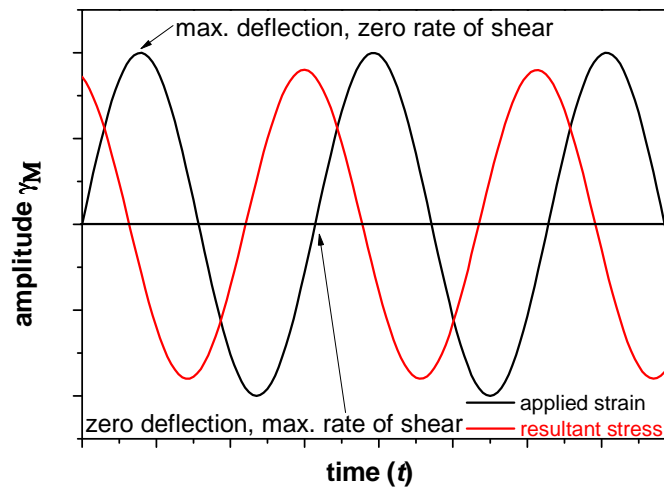
Figure 8.5   Principle of sinusoidal oscillation of max. strain γM with the frequency ω in a parallel plate geometry rheometer. (after lit.[227])

Under these conditions:

$$\gamma = \gamma^0 \sin(\omega t) \tag{8.14}$$

γ^0: maximum amplitude of strain

t: time

$$\tau = \tau^0 \sin(\omega t + \delta) \tag{8.15}$$

τ^0: maximum amplitude of stress

The elastic (in-phase) and viscous (out-of-phase) components of the stress wave can be seperated. The in-phase, *shear storage modulus* (*G'*) defines the dissipation of energy and the out-of-phase, *shear loss modulus* (*G"*) defines the energy stored in the material by the

applied strain and that is completely regained as expected for an elastic solid according to Hooke's law. They are given by:

$$\tau = \tau^0 G' \sin(\omega t) + \tau^0 G'' \cos(\omega t) \tag{8.16}$$

The ratio of loss to storage modulus is called *loss tangent* (tanδ) and is proportional to the energy loss per cycle:

$$\tan \delta = \frac{G''}{G'} \tag{8.17}$$

Rheological measurements

Oscillatory rheological measurements were performed, using an Anton-Paar MCR301 rheometer. The measurement system was a cone-plate geometry with a diameter of 50 mm and an angle of 1°. The temperature was adjusted by Peltier devices in the plate. For loading a sample, the plate as well as the sample were heated to T=50 °C. The liquid was transferred onto the plate with a syringe and the cone was lowered to the measurement position. Prior to every measurement, the sample was kept at the respective temperature for one hour. For temperature depended measurements a heating/cooling rate of 1 K/min was used and a frequency of f =1 Hz. All measurements were performed within the linear viscoelastic regime, which was determined by strain dependence measurements of the dynamic shear storage modulus G' and loss modulus G''. Typically strain in the range of 0.1 % or 1 % was used depending on the concentration and temperature of the solution.

8.2 Materials

Until noted otherwise all other chemicals were purchased from Aldrich or Acros and were used as received.

In the following the syntheses used in this work are described. Not all of the presented compounds were used in the results and discussion chapters. Nevertheless, the additional compounds are intended for further work and, thus, are included here for reference.

Compounds discussed in this thesis will be additionally denoted as in the previous chapters.

8.2.1 Purification of solvents and monomers for anionic polymerization

Purification of the required solvent, monomers and additives was performed as described in ref.. [241], [242]

Tetrahydrofuran (THF; Riedel-deHaën) was first refluxed for 3 days over CaH_2 and distilled off. Prior to use THF was additionally refluxed for 3 days over potassium and distilled off. 1.3 M *sec*-butyllithium solution in cyclohexane/hexane (*s*-BuLi; Acros) was used as received. 0.013 M. Sodium naphthalene (Na-naptha) solution in THF was prepared by reacting sodium metal (Aldrich) with a slight excess of naphthalene (Aldrich) in dry THF under inert atmosphere for 1 d. Afterwards the dark green solution was filtered under inert atmosphere and stored in the freezer under argon atmosphere.[243] Methanol (abs.; Acros) was degassed with argon for 15 min before use.

Styrene

Styrene was purified in a one step procedure. Usually, prior to purification, all glassware was flame-dried under high vacuum to remove traces of moisture. Then, 100 mL of styrene (S, Aldrich) were placed in a flask and 1 M solution dibutyl magnesium in heptane (Aldrich) was added to the styrene until a yellow color appeared; as a typical amount, 6 mL were sufficient for 100 mL of styrene. After the solution was stirred in the dark for 15 min, it was degassed by three freeze-pump-thaw cycles (i.e. freezing the monomer in liquid nitrogen followed by thawing under high vacuum). The heptane was carefully removed under low vacuum while the solution was cooled with an ice bath. Afterwards, the styrene was condensed into an ampoule under high vacuum (~5×10^{-4} mbar) and stored in liquid nitrogen until usage.

tert-Butoxystyrene

As a styrene derivative *tert*-butoxystyrene (*t*BS, Aldrich) purified similar to the procedure described above. Due to its high boiling point (72-73 °C/0.1 mmHg) it could not be condensed into an ampoule at rt. Therefore it had to be distilled under high vacuum (~5x10^{-6} mbar) at 90 °C oil bath temperature using a micro distillation unit connected to a graded ampoule cooled with liquid nitrogen. The whole setup had to be wrapped in tin foil to prohibit polymerization of the purified monomer. It was stored in liquid nitrogen until usage.

Methyl methacrylate

The glassware for the purification of methyl methacrylate (MMA, Aldrich) was pretreated in the same way as described above for the purification of styrene. Typically 100 mL MMA were placed in a flask and 1 M solution of triethyl aluminum in hexane (Aldrich) was added until a light yellowish color appeared. An amount of 8 mL was sufficient to purify 100 mL MMA. After stirring the solution for 15 min in the dark, the monomer was degassed with two freeze-pump-thaw cycles and condensed into a frozen ampoule. However, the hexane could not be separated from the MMA and had to be taken into account when the desired amount of MMA for the anionic polymerization was calculated.

Ethyl methacrylate, n-butyl methacrylate, tert-butyl methacrylate

Ethyl methacrylate (EMA, Aldrich), n-butyl methacrylate (nBMA, Acros) and tert-butyl methacrylate (tBMA, Aldrich) were purified as described above for MMA.

2-Ethylhexyl methacrylate

2-Ethylhexyl methacrylate (EHMA, Aldrich) was purified similar to the procedure described for MMA. Due to its high boiling point (218 °C) it had to be distilled under high vacuum at 60 °C oil bath temperature using the same setup as described for tBuOS. It was stored in liquid nitrogen until usage

8.2.2   Purification of additives for anionic polymerization

1,1-Diphenylethylene

The glassware for the purification of methyl 1,1-diphenylethylene (DPE; Aldrich) was pretreated in the same way as described above for the purification of styrene. DPE was dried over s-BuLi and distilled from deep red (diphenylmethyl)lithium under high vacuum using the same setup as for tBOS. It was stored in liquid nitrogen until usage. For long term storage it could be stored under inert gas atmosphere in the freezer at -20 °C.

Lithium chloride

Lithium chloride (LiCl) was dried under high vacuum at 250 °C for several days before being dissolved in dry THF yielding a 0.236 mol/L solution.

8.3   Side-groups

8.3.1   General reaction procedures

General method for azocoupling reactions **GM1**[207]

The aminobenzene derivative (51 mmol, 1 eq) was dissolved in EtOH (120 mL). The solution was cooled and semi concentrated HCl (2.4 eq) was added drop wise forming a suspension. After further cooling with a MeOH/dry ice mixture, $NaNO_2$ solution (2.5 M, 20.4 mL) was added drop wise without the temperature exceeding 5 °C. Full conversion of the aminobenezene derivative was monitored by thin-layer chromatography (TLC). In a second flask, phenol (53.5 mmol, 1.1 eq) was dissolved in NaOH solution (2 M, 50 mL) and cooled in an ice bath. The diazonium salt solution was transferred to a coolable dropping funnel and added slowly to the alkaline solution. During the reaction, the pH value was monitored and adjusted to a pH of 10 by adding additional NaOH solution (2 M) to the reaction mixture. The mixture was allowed to warm to rt and was stirred for further 12 h. The solution was precipitated in an acidified water (HCl) solution and filtered off. The crude product was dissolved in CH_2Cl_2 and filtered through a column containing 100 g of silica gel.

General method for attachment of spacer **GM2**

The phenol derivative (30.7 mmol, 1 eq) was dissolved in dry acetone. α,ω-Dibromoalkane (8 eq) (if monobromides were used: 1.2 eq), K_2CO_3 (1.1 eq) and KI (tip of a spatula) were added. The solution was heated to reflux for 48 h. The spacer unit was distilled off (HV, 40 °C oil bath), the residue dissolved in THF and the salts were filtered off.

General ester derivative saponification method **GM3**

Cyanobiphenyl (CB) derivatives:

The CB ethyl ester derivative (6.46 mmol, 1 eq) was dissolved in dry THF (50 mL), KOH (0.47 g, 8.40 mmol, 1.3 eq) was added and the solution was stirred at rt over night. The precipitate was filtered off and dissolved in THF/H_2O (1:1). The solution was poured into

$NaHCO_3$ (0.1 M) and the pH was adjusted to pH=6 with glacial acetic acid. The precipitate was filtered off and purified by soxhlet extraction with $CHCl_3$.

Azobenzene derivatives:

The azobenzene ethyl ester (32.0 mmol, 1 eq) was suspended in EtOH/THF (1:1; 200 mL). Aqueous KOH solution (53.9 mL; 10 wt%) were added. The reaction mixture was refluxed for 6 h. A clear solution was obtained. Full conversion was monitored by TLC. Approx. two-thirds of the solution were removed under reduced pressure and the remaining solution was precipitated in 1 l of acidified water (HCl). The solid was filtered off and washed several times with water.

General method for the preparation of the acid chlorides **GM4**

The synthesis was carried out under inert atmosphere (i.e. dry argon). The N_2-flask was flame dried under HV prior to use. The acid derivative (1.78 mmol, 1 eq) was suspended in dry THF (20 mL) and DMF (3 drops) and cooled to 0 °C. $SOCl_2$ (8.44 mmol, 4.75 eq, for CB derivatives) or $C_2O_2Cl_2$ (8.44 mmol, 4.75 eq, for azobenzene derivatives) was added slowly. After warming to rt and stirring for 3 h excess $SOCl_2$ /$C_2O_2Cl_2$ and solvents were removed under HV.

8.3.2   Synthesis of azobenzene chromophores

Azo1a *4-(4-Methoxyphenylazo)phenol*

The synthesis was carried out as described **GM1**. After evaporation the product was obtained as a red powder (8.84 g, 76%).

Chemical Formula: $C_{13}H_{12}N_2O_2$
Molecular Weight: 228,25

^{1}H-NMR (CDCl$_3$-d$_1$): δ(ppm)= 7.80 (d, 4H, CH^{3,5,9,13}), 6.92 (d, 4H, CH^{2,6,10,12}), 5.29 (s, 1H, OH^{11}), 3.80 (s, 3H, CH$_3^7$).
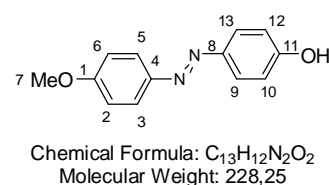
α-Bromo-ω-(4-methoxyazobenzene-4'-oxy)alkanes

Azo1 *4-[4-[(4-Methoxyphenyl)azo]phenoxy] butyl bromide*

The synthesis was carried out according to the **GM2** using Azo5a (6.00 g, 26.3 mmol, 1.0 eq), 1,4-dibromobutane (34.05 g, 0.158 mol, 6.0 eq) and K_2CO_3 (4.00 g, 28.9 mmol, 1.1 eq) in aceton (110 mL) yielding an orange solid (7.89 g, 72%).

Chemical Formula: $C_{17}H_{19}BrN_2O_2$
Molecular Weight: 363,25
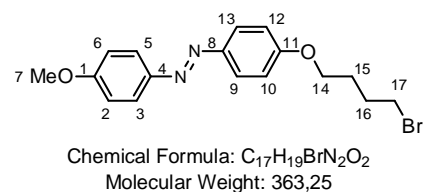
^{1}H-NMR (CDCl$_3$-d$_1$): δ(ppm)= 7.88 (d, 4H, CH^{3,5,9,13}), 6.99 (d, 4H, CH^{2,6,10,12}), 4.07 (t, 2H, CH$_2$^{14}), 3.88 (s, 3H, CH$_3$^{7}), 3.50 (t, 2H, CH$_2$^{17}), 2.14-1.93 (m, 4H, CH$_2$^{15,16}).

El.Vol. (Oligo-SEC): 18.20 mL.

Azo2 *6-[4-[(4-Methoxyphenyl)azo]phenoxy] hexyl bromide*

The synthesis was carried out according to the **GM2** using Azo5a (6.00 g, 26.3 mmol, 1.0 eq), 1,6-dibromohexane (38.48 g, 0.158 mol, 6.0 eq) and K$_2$CO$_3$ (4.00 g, 28.9 mmol, 1.1 eq) in aceton (110 mL) yielding an orange solid (9.05 g, 88 %).

Chemical Formula: C$_{19}$H$_{23}$BrN$_2$O$_2$
Molecular Weight: 391,30

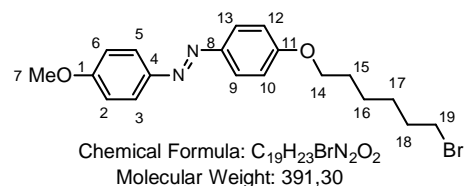^{1}H-NMR (CDCl$_3$-d$_1$): δ(ppm)= 7.87 (d, 4H, CH^{3,5,9,13}), 6.99 (d, 4H, CH^{2,6,10,12}), 4.04 (t, 2H, CH$_2$14), 3.88 (s, 3H, CH$_3$^{7}), 3.45 (t, 2H, C^{19}H$_2$), 1.95-1.79 (m, 4H, CH$_2$^{15,18}), 1.53-1.35 (m, 4H, CH$_2$^{16,17}).

El.Vol. (Oligo-SEC): 17.82 mL

DSC: T$_m$ (ΔH) = 110 °C (126.7 J/g); T$_{cryst}$ (ΔH) = 92 °C (115.7 J/g)

Azo3 *8-[4-[(4-Methoxyphenyl)azo]phenoxy] octyl bromide*

The synthesis was carried out according to the **GM2** using Azo5a (4.00 g, 17.5 mmol, 1.0 eq), 1,8-dibromooctane (28.60 g, 0.105 mol, 6.0 eq) and K$_2$CO$_3$ (2.664 g, 19.3 mmol, 1.1 eq) in aceton (110 mL) yielding an orange solid (6.6 g, 84%).

Chemical Formula: C$_{21}$H$_{27}$BrN$_2$O$_2$
Molecular Weight: 419,36
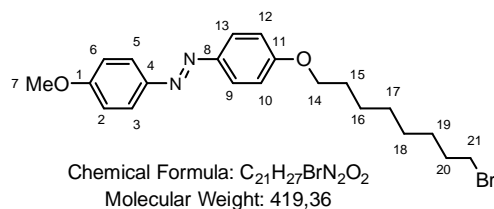
^{1}H-NMR (CDCl$_3$-d$_1$): δ(ppm)= 7.87 (d, 4H, CH^{3,5,9,13}), 6.99 (d, 4H, CH^{2,6,10,12}), 4.02 (t, 2H, CH$_2$^{14}), 3.88 (s, 3H, CH$_3$^{7}), 3.42 (t, 2H, CH$_2$^{21}), 1.91-1.76 (m, 4H, CH$_2$^{15,20}), 1.51-1.31 (m, 8H, CH$_2$$^{16-19}$).

El.Vol. (Oligo-SEC): 17.69 mL

DSC: T$_m$ (ΔH) = 114 °C (138.3 J/g); T$_{cryst}$ (ΔH) = 97 °C (134.1 J/g)

Azo4 *10-[4-[(4-Methoxyphenyl)azo]phenoxy] decyl bromid*

The synthesis was carried out according to the **GM2** using Azo5a (3.00 g, 13.1 mmol, 1.0 eq), 1,8-dibromodecane (24.77 g, 78.9 mol, 6.0 eq) and K_2CO_3 (2.00 g, 14.5 mmol, 1.1 eq) in aceton (110 mL) yielding an orange solid (4.2 g, 72%).
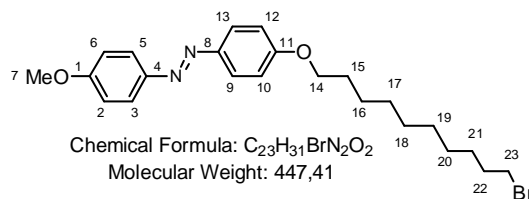
Chemical Formula: $C_{23}H_{31}BrN_2O_2$
Molecular Weight: 447,41

^{1}H-NMR (CDCl$_3$-d$_1$): δ(ppm)= 7.87 (d, 4H, CH^{3,5,9,13}), 6.99 (d, 4H, CH^{2,6,10,12}), 4.03 (t, 2H, CH$_2$^{14}), 3.88 (s, 3H, CH$_3$^{7}), 3.41 (t, 2H, CH$_2$^{23}), 1.90-1.76 (m, 4H, CH$_2$^{15,22}), 1.50-1.31 (m, 12H, CH$_2$$^{16-21}$).

El.Vol. (Oligo-SEC): 17.43 mL

DSC: T_m (ΔH) = 113 °C (130.5 J/g); T_{cryst} (ΔH) = 104 °C (126.6 J/g)

4-[4-[(4-Methoxyphenyl)azo]phenoxy] butyric acid ethyl ester (MeO-Azo-3-COOEt)

The synthesis was carried out according to **GM2**, although only 1.3 eq ethyl 4-bromobutanoate were used, yielding an orange solid (11.04 g, 92 %).

Chemical Formula: $C_{19}H_{22}N_2O_4$
Molecular Weight: 342,39
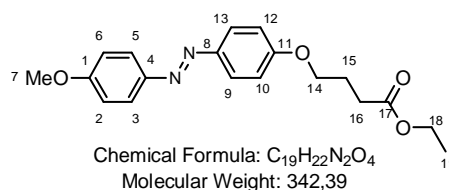
^{1}H-NMR (CDCl$_3$-d$_1$): δ(ppm)= 7.87 (d, 4H, CH^{3,5,9,13}), 6.99 (d, 4H, CH^{2,6,10,12}), 4.15 (q, 2H, CH$_2$^{18}), 4.07 (t, 2H, CH$_2$^{14}), 3.88 (s, 3H, CH$_3$^{7}), 2.54 (t, 2H, CH$_2$^{16}), 2.14 (t, 2H, CH$_2$^{15}), 1.26 (t, 2H, CH$_3$^{19}).

4-[4-[(4-Methoxyphenyl)azo]phenoxy] butyric acid (MeO-Azo-3-COOH)

The synthesis was carried out according to **GM3:** Recrystallization from acetone/H_2O yielded orange-yellow crystals (95 %).

Chemical Formula: $C_{17}H_{18}N_2O_4$
Molecular Weight: 314,34
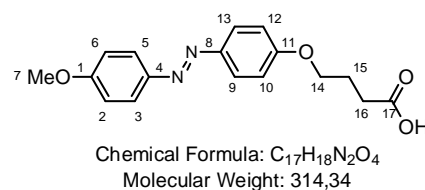
^{1}H NMR (DMSO-d$_6$): δ (ppm) = 12 (br, 1H), 7.81 (d, 4H, CH^{3,5,9,13}), 7.05 (d, 4H, CH^{2,6,10,12}), 4.07 (t, 2H, CH$_2$^{14}), 3.84 (s, 3H, CH$_3$^{7}), 2.39 (t, 2 H, CH$_2$^{16}), 1.96 (quintet, 2 H, CH^{15}).

4-[4-[(4-Methoxyphenyl)azo]phenoxy] butyryl chloride (MeO-Azo-3-COCl)

The synthesis was carried out as described in **GM4** using *MeO-Azo-3-COOH* (2.27 g, 7.34 mmol, 1.0 eq), oxalyl

Chemical Formula: $C_{17}H_{17}ClN_2O_3$
Molecular Weight: 332,78
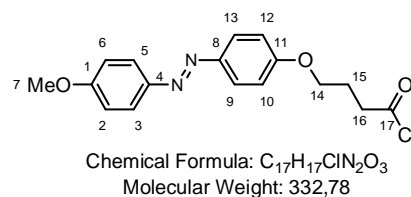
chloride (3.73 g, 29.40 mmol, 4.0 eq) and DMF (0.1 mL) in dry THF (50 mL). The product was obtained as an orange solid (quantitative).

^{1}H-NMR (CDCl$_{3}$-d$_{1}$): δ(ppm)=. 7.96 (m, 4 H, CH^{3,5,9,13}), 7.02 (m, 4 H, CH^{2,6,10,12}), 4.12 (t, 2 H, CH$_{2}$^{14}), 3.91 (s, 3 H, CH$_{3}$^{7}), 3.18 (t, 2 H, CH$_{2}$^{16}), 2.25 (quintet, 2 H, CH^{15}).

Azo5a *4-[4-(Cyanophenyl)azo] phenol*

The synthesis was carried out according to **GM1**. After recrystallization from AcOH/H$_{2}$O red-brown crystals were obtained (yield: 49 %).

Chemical Formula: C$_{13}$H$_{9}$N$_{3}$O
Molecular Weight: 223,23

^{1}H-NMR (DMSO-d$_{6}$): δ(ppm)= 10.6 (br, 1H), 7.99 (d, 2 H, CH^{3,5}), 7.89 (d, 2 H, CH^{2,6}), 7.82 (d, 2 H, CH^{9,13}), 6.92 (d, 2 H, CH^{10,12}).
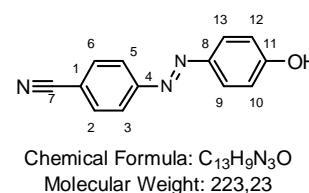
Azo5b *4-[4-[(4-Cyanophenyl)azo]phenoxy] butyric acid ethyl ester*

The synthesis was carried out according to the **GM2**, although only 1.3 eq ethyl 4-bromobutanoate were used. After recrystallization from EtOH orange crystals were obtained (yield: 71 %).

Chemical Formula: C$_{19}$H$_{19}$N$_{3}$O$_{3}$
Molecular Weight: 337,37

^{1}H-NMR (CDCl$_{3}$-d$_{1}$): δ(ppm)= 7.92 (d, 2 H, CH^{3,5}), 7.77 (m, 4H, CH^{2,6,9,13}), 7.01 (d, 2 H, CH^{10,12}), 4.14 (m, 4 H, CH$_{2}$^{14,18}), 2.54 (t, 2 H, CH$_{2}$^{16}), 2.16 (quintet, 2 H, CH$_{2}$^{15}), 1.27 (t, 3 H, CH$_{3}$^{19}).
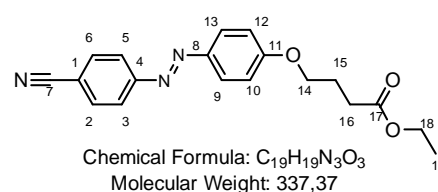
Azo5c *4-[4-[(4-Cyanophenyl)azo]phenoxy] butyric acid*

The synthesis was carried out analog to **GM3**. After recrystallization from CHCl$_{3}$/hexane orange crystals were obtained (yield 74 %).

Chemical Formula: C$_{17}$H$_{15}$N$_{3}$O$_{3}$
Molecular Weight: 309,32

^{1}H NMR (DMSO-d$_{6}$): δ (ppm) = 12.2 (br, 1H). 8.02 (m, 2H, CH^{3,5}), 7.92 (m, 4 H, CH^{2,6,9,13}), 7.13 (d, 2 H, CH^{10,12}), 4.10 (t, 2 H, CH$_{2}$^{14}), 2.40 (t, 2 H, CH$_{2}$^{16}), 1.97 (quintet, 2 H, CH$_{2}$^{15}).
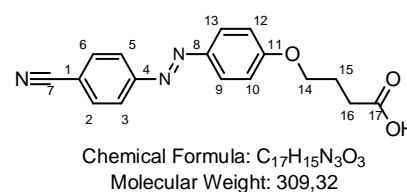
Azo5 *4-[4-[(4-Cyanophenyl)azo]phenoxy] butyryl chloride*

The synthesis was carried out as described in **GM4** using **Azo5c** (2.27 g, 7.34 mmol, 1.0 eq), oxalyl chloride (3.73 g, 29.40 mmol, 4.0 eq) and DMF (0.1 mL) in dry THF

Chemical Formula: C$_{17}$H$_{14}$ClN$_{3}$O$_{2}$
Molecular Weight: 327,76
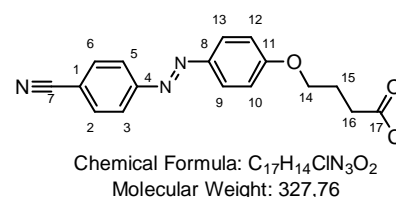
(50 mL). The product was obtained as an orange solid (quantitative).

^{1}H NMR (THF-d$_8$): δ(ppm)= 7.7-7.9 (m, 6 H, CH^{2,3,5,6,9,13}), 6.99 (m, 2 H, CH^{10,12}), 4.05 (t, 2 H, CH$_2$^{14}), 3.12 (t, 2 H, CH$_2$^{16}), 2.09 (quintet, 2 H, CH$_2$^{15}).

8.3.3 Synthesis of cyanobiphenyl containing mesogens

α-Bromo-ω-(4-cyanobiphenyl-4'-oxy)alkanes

The α-bromo-ω-(4cyanobiphenyl-4'-oxy)alkanes were prepared by the reaction of 4-cyano-4'-hydroxybiphenyl with a large excess of the appropriate dibromoalkane in dry acetone with potassium carbonate as base according to a procedure described by Crivello *et al.*[122]

CB1 *4'-(4-bromobutoxy)biphenyl-4-carbonitrile*

CB1 was synthesized according to **GM2** using 4'-hydroxy-(1,1'-biphenyl)-4-carbonitrile (3.00 g, 15.4 mmol, 1.0 eq), 1,4-dibromobutane (19.09 g, 92.2 mmol, 6.0 eq) and K$_2$CO$_3$ (2.34 g, 16.9 mmol, 1.1 eq) in aceton (100 mL). Recrystallisation from ethanol yielded a white solid (3.70 g, 73%).

Chemical Formula: C$_{17}$H$_{16}$BrNO
Molecular Weight: 330,22
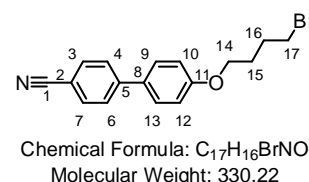
^{1}H-NMR (CDCl$_3$-d$_1$): δ(ppm)= 7.6 (q, 4H, CH^{3,4,6,7}), 7.5 (d, 2H, CH^{10,12}), 7.0 (d, 2H, CH^{9,13}), 4.0 (t, 2H, CH$_2$^{14}), 3,5 (t, 2H, CH$_2$^{17}), 2.1-1.9 (m, 4H, CH$_2$^{15,16}).

El.Vol. (Oligo-SEC): 17.77 mL

CB2 *4'-(6-bromohexyloxy)biphenyl-4-carbonitrile (CB-6-Br)*

The synthesis of CB-6-Br was carried out according **GM2** using 4'-hydroxy-(1,1'-biphenyl)-4-carbonitrile (5.00 g, 25.6 mmol, 1.0 eq), 1,6-dibromohexane (37.49 g, 154.0 mmol, 6.0 eq) and K$_2$CO$_3$ (3.89 g, 28.2 mmol, 1.1 eq) in aceton (150 mL). The oil bath temperature was set to 60 °C for the distillation of 1,6-dibromohexane. Recrystallisation from ethanol yielded a white solid (7.5 g, 82%).

Chemical Formula: C$_{19}$H$_{20}$BrNO
Molecular Weight: 358,27
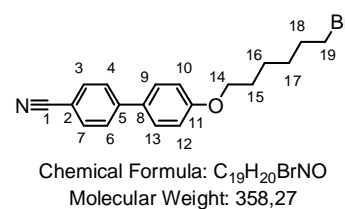
^{1}H-NMR (CDCl$_3$-d$_1$): δ(ppm)= 7.6 (q, 4H, CH^{3,4,6,7}), 7.5 (d, 2H, CH^{10,12}), 7.0 (d, 2H, CH9,13), 4.0 (t, 2H, CH$_2$^{14}), 3.4 (t, 2H, CH$_2$^{19}), 1.9-1.8 (m, 4H, CH$_2$^{15,18}), 1.5 (m, 4H, CH$_2$^{16,17}).

El.Vol. (Oligo-SEC): 16.92 mL

CB3 *4'-(8-bromooctyloxy)biphenyl-4-carbonitrile (CB-8-Br)*

The synthesis of CB-8-Br was carried out according **GM2** using 4'-hydroxy-(1,1'-biphenyl)-4-carbonitrile (5.00 g, 25.6 mmol, 1.0 eq), 1,8-dibromooctane (41.80 g, 154.0 mmol, 6.0 eq) and K_2CO_3 (5.31 g, 38.4 mmol, 1.5 eq) in aceton (110 mL). **T**he oil bath temperature was set to 100 °C for the distillation of 1,8-dibromooctane. Recrystallisation from ethanol yielded a white solid (7.96 g, 80%).

Chemical Formula: $C_{21}H_{24}BrNO$
Molecular Weight: 386,33

^{1}H-NMR (CDCl$_3$-d$_1$): δ(ppm)= 7.6 (q, 4H, CH^{3,4,6,7}), 7.5 (d, 2H, CH^{10,12}), 7.0 (d, 2H, CH^{9,13}), 4.0 (t, 2H, CH$_2$^{14}), 3.4 (t, 2H, CH$_2$^{19}), 1.9-1.7 (m, 4H, CH$_2$^{15,20}), 1.5-1.4 (m, 8H, CH$_2$$^{16-19}$).

El.Vol. (Oligo-SEC): 16.70 mL

CB4 *4'-(10-bromodecyloxy)biphenyl-4-carbonitrile (CB-10-Br)*

The synthesis of CB-10-Br was carried out according **GM2** using 4'-hydroxy-(1,1'-biphenyl)-4-carbonitrile (2.00 g, 10,2 mmol, 1.0 eq), 1,10-dibromodecane (19.31 g, 61.5 mmol, 6.0 eq) and K_2CO_3 (1.56 g, 11.3 mmol, 1.1 eq) in aceton (90 mL). The 1,10-dibromohexane was not distilled off. Recrystallisation from ethanol yielded a white solid (2.97 g, 70%).

Chemical Formula: $C_{23}H_{28}BrNO$
Molecular Weight: 414,38

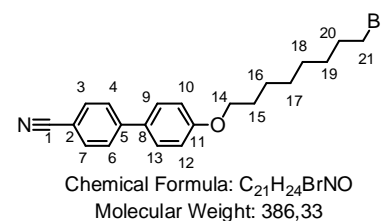^{1}H-NMR (CDCl$_3$-d$_1$): δ(ppm)= 7.6 (q, 4H, CH^{3,4,6,7}), 7.5 (d, 2H, CH^{10,12}), 7.0 (d, 2H, CH^{9,13}), 4.0 (t, 2H, CH$_2$^{14}), 3.4 (t, 2H, CH$_2$^{19}), 1.9-1.7 (m, 4H, CH$_2$^{15,22}), 1.5-1.3 (m, 12H, CH$_2$$^{16-21}$).
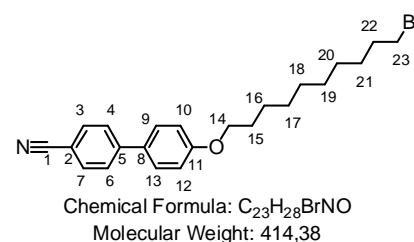
El.Vol. (Oligo-SEC): 17.41 mL

Ethyl 4-(4'-cyanobiphenyl-4-yloxy)butanoate (CB-3-COOEt)

The synthesis was carried out according to **GM2** using 4'-hydroxy-(1,1'-biphenyl)-4-carbonitrile (4.00 g, 20.5 mmol, 1.0 eq), bromobutanoate (5.447 g, 27.9 mmol, 1.4 eq) and K_2CO_3 (4.00 g, 29.0 mmol, 1.4 eq) in aceton (150 mL) yielding a white solid (6.15 g, 96 %).

Chemical Formula: $C_{19}H_{19}NO_3$
Molecular Weight: 309,36

223
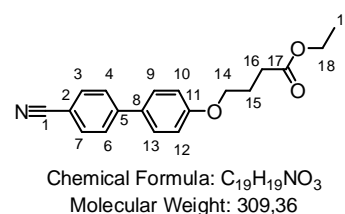
^{1}H-NMR (CDCl$_3$-d$_1$): δ(ppm)= 7.66 (q, 4H, CH^{3,4,6,7}), 7.52 (d, 2H, CH^{10,12}), 6.98 (d, 2H, CH^{9,13}), 4.15 (q, 2H, CH$_2$^{18}), 4.06 (t, 2H, CH$_2$^{14}), 2,53 (t, 2H, CH$_2$^{16}), 2.14 (q, 2H, CH$_2$^{15}), 1.26 (t, 3H, CH$_3$^{19}).

4-(4'-Cyanobiphenyl-4-yloxy)butanoic acid (CB-3-COOH)

The synthesis was carried out according to **GM3** using *CB-3-COOEt* (1.16 g, 3.75 mmol, 1.0 eq), KOH (0.32 g, 5.62 mmol, 1.5 eq) in THF/ethanol (1:5, 30 mL). The product was obtained as a white solid (1.31 g, 72%).

Chemical Formula: C$_{17}$H$_{15}$NO$_3$
Molecular Weight: 281,31
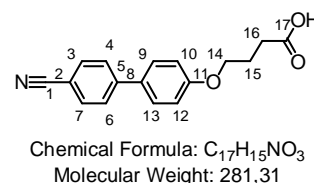
^{1}H-NMR (DMSO-d$_6$): δ(ppm)= 12.14 (s, 1H, OH^{17}), 7.84 (q, 4H, CH^{3,4,6,7}), 7.68 (d, 2H, CH^{10,12}), 7.04 (d, 2H, CH^{9,13}), 4.02 (t, 2H, CH$_2$^{14}), 2.39 (t, 2H, CH$_2$^{16}), 1.95 (m, 2H, CH$_2$^{15}).

4-(4'-Cyanobiphenyl-4-yloxy)butanoyl chloride (CB-3-COCl)

The synthesis was carried out according to **GM4** using CB-3-COOH (0.50 g, 1.78 mmol, 1.0 eq) and SOCl$_2$ (1.00 g, 8.44 mmol, 4.8 eq) in dry THF (20 mL). The product was obtained as a white solid (quantitative).

Chemical Formula: C$_{17}$H$_{14}$ClNO$_2$
Molecular Weight: 299,75
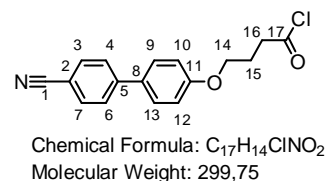
^{1}H-NMR (THF-d$_8$): δ(ppm)= 7.74 (m, 4H, CH^{3,4,6,7}), 7.63 (d, 2H, CH^{10,12}), 7.02 (d, 2H, CH^{9,13}), 4.08 (t, 2H, CH$_2$^{14}), 3.58 (t, 2H, CH$_2$^{16}), 2.17 (m, 2H, CH$_2$^{15}).

Ethyl 6-(4'-cyanobiphenyl-4-yloxy)hexanoate (CB-5-COOEt)

The synthesis was carried out according to **GM2** using 4'-hydroxy-(1,1'-biphenyl)-4-carbonitrile (4.00 g, 20.5 mmol, 1.0 eq), ethyl 6-bromohexanoate (6.86 g, 3.07 mmol, 1.5 eq) and K$_2$CO$_3$ (4.00 g, 29.0 mmol, 1.4 eq) in aceton (150 mL) yielding a white solid (5.42 g, 79%).

Chemical Formula: C$_{21}$H$_{23}$NO$_3$
Molecular Weight: 337,41
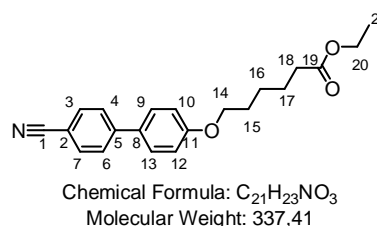
^{1}H-NMR (CDCl$_3$-d$_1$): δ(ppm)= 7.66 (q, 4H, CH^{3,4,6,7}), 7.52 (d, 2H, CH^{10,12}), 6.98 (d, 2H, CH^{9,13}), 4.15 (q, 2H, CH$_2$^{20}), 4.06 (t, 2H, CH$_2$^{14}), 2,53 (t, 2H, CH$_2$^{18}), 1.88-1.46 (m, 6H, CH$_2$$^{15-17}$), 1.26 (t, 3H, CH$_3$^{21}).

6-(4'-Cyanobiphenyl-4-yloxy)hexanoic acid (CB-5-COOH)

The synthesis was carried out as described in **GM3** using *CB-5-COOEt* (2.00 g, 5.93 mmol, 1.0 eq), KOH (0.43 g, 7.71 mmol, 1.5 eq) in THF (50 mL). The product was obtained as a white solid (1.30 g, 72%).

Chemical Formula: $C_{19}H_{19}NO_3$
Molecular Weight: 309,36
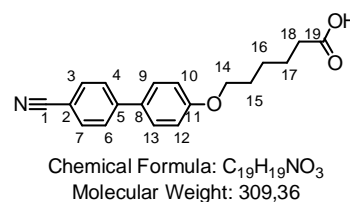
^{1}H-NMR (DMSO-d$_6$): δ(ppm)= 12.00 (s, 1H, COH^{17}), 7.84 (q, 4H, CH^{3,4,6,7}), 7.68 (d, 2H, CH^{10,12}), 7.04 (d, 2H, CH^{9,13}), 4.01 (t, 2H, CH$_2$^{14}), 1.77-1.66 (m, 2H, CH$_2$^{18}), 1.64-1.50 (m, 4H, CH$_2$^{15,17}), 1.47-1.35 (m, 2H, CH$_2$^{16}).

6-(4'-Cyanobiphenyl-4-yloxy)hexanoyl chloride (CB-6-COCl)

The synthesis was carried out as described **GM4** using *CB-5-COH* (0.90 g, 2.91 mmol, 1.0 eq) and SOCl$_2$ (1.64 g, 13.80 mmol, 4.8 eq) in dry THF (40 mL). The product was obtained as a white solid (quantitative).

Chemical Formula: $C_{19}H_{18}ClNO_2$
Molecular Weight: 327,80
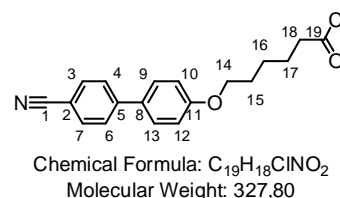
^{1}H-NMR (THF-d$_8$): δ(ppm)= 7.74 (m, 4H, CH^{3,4,6,7}), 7.63 (d, 2H, CH^{10,12}), 7.02 (d, 2H, CH^{9,13}), 4.04 (t, 2H, CH$_2$^{14}), 3.03 (t, 2H, CH$_2$^{18}), 1.85-1.77 (m, 4H, CH$_2$^{15,17}), 1.61-1.51 (m, 2H, CH$_2$^{16}).

8.4 Anionic polymerization

Denomination of polymers

For easier references in text and tables all polymers are named using the following schema:

if not stated otherwise all copolymer are block copolymers and the *block* or *b* is omitted

P(M1)$_{ru1}$P(M2)$_{ru2}$P(M3)$_{ru3}$

(M1,2,3,…= Monomer 1,2,3,... ; ru1,2,3,.. = repeating units in respective block)

In case of functionalized polymers the monomer (M) is replaced by the abbreviation used for the functional moiety and the connection to the polymer backbone.

Ie. PS$_{190}$P(**CB4OS**)$_{680}$PS$_{120}$

In this case the middle block contains **CB** = 4'-(4-bromobutoxy)biphenyl-4-carbonitrile (CB4Br) connected via an ether linkage (**O**) to a styrene (**S**) backbone.

8.4.1 General polymerization methods

General polymerization method for AB diblock copolymers in a single reactor **GP1**

All block polymers were synthesized by sequential anionic polymerization in tetrahydrofuran (THF) with *sec*-butyllithium as initiator.

If methacrylates were polymerized, lithium chloride (LiCl) was used as a µ-ligand to ensure the controlled polymerization of the methacrylates.[169] Before the polymerization of methacrylate block, DPE was added to reduce the reactivity of the living anions. In this way crossover steps and transfer reactions due to too high nucleophilicity could be suppressed.

All operations were performed under an inert atmosphere, i.e. dry nitrogen. Prior to every polymerization the reactor unit was flushed with a THF/*s*-BuLi solution. After five minutes the solution was exhausted and the setup was evacuated. After initiation of the first block, the polymer solution was kept under temperature controlled conditions until completion of synthesis. THF was transferred into the main reactor (MR) from the adjacent distillation unit with reduced pressure. The THF/LiCl solution (0.263 mol/l), prepared in a separate flask under inert conditions at room temperature, was injected into the MR via septum. The absence of protic impurities was ensured via titration. *s*-BuLi was injected into the reactor at -30°C until the solution turned slightly yellow, then heated to -5 °C whereas the yellow color vanished upon reaction of s-BuLi with THF. After the reactor was cooled to -66 °C and the predetermined amount of initiator was added, the first styrenic monomer was injected into the vigorously stirred solution via septum and syringe. The polymerization was continued at the given temperature under nitrogen overpressure for 40 min. Then DPE (3 fold excess on initiator) was injected and allowed to react for 20 min. A sample of this precursor block was drawn. To this end a sample of the precursor solution was transferred into the graduated transfer vessel with reduced pressure. Using nitrogen overpressure the living polymer sample was pumped into a flask containing 1 mL dry methanol, in order to obtain the precursor polymer for analytical purposes. Subsequently, the second monomer was injected with a syringe through the septum. The polymerization of the second block continued for 35 min and was terminated by injecting dry methanol into the reactor. After warming to rt the reactor was exhausted using nitrogen overpressure. The block copolymer was isolated and purified by precipitation in methanol.

General combinatorial polymerization method for AB diblock copolymers **GP2**

Procedure was the same as **GP1** up to the addition of the second monomer.

After a sample of the first block was isolated and the secondary reactors (SRs) were cooled to -78 °C, parts of the precursor solution were distributed from the MR to the SRs. To control the transfer volume for each reactor, the solution was first pumped into the graduated transfer vessel and from there into the SRs. Each SR was filled with 100 mL, and rest remained in the MR. Subsequently, the second monomer was added in predetermined amounts to all four reactors. The polymerization of the second block was continued for 35 min and terminated by injecting dry methanol into each reactor. The reactors were exhausted via line 2 using nitrogen overpressure. All block copolymers were isolated and purified by precipitation in methanol.

General polymerization method for ABA triblock copolymers with bifunctional initiator **GP3**

The polymerizations were carried out in the main reactor (MR) of the reactor setup under inert atmosphere (i.e. dry nitrogen). Dry THF was transferred directly from the distillation unit into the MR. After cooling to -65 °C the solvent was titrated with Na-Naptha until a persistent slightly green color appeared. The calculated amount of initiator was injected. The incomplete initiator reaction had to be taken into account; therefore the amount of initiator was increased by 50%. *t*BS was added and allowed to polymerize for 100 min. A sample precursor was terminated with degassed methanol yielding P*t*BS (**I**). Subsequently styrene was introduced into the reactor and polymerized for 60 min. Finally, the living chain ends were terminated by adding degassed methanol yielding polystyrene-*block*-poly(4-*tert*-butoxystyrene)-*block*-polystyrene (PS-P*t*BS-PS).

8.4.2   Combinatorial series for chapter 3

AB diblock copolymers with variable B-block length **1a-1d**
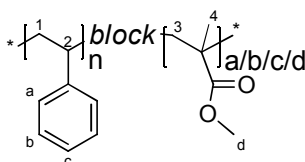
PS-PMMA (**1a-1d**) was prepared according to **GP1** using s-BuLi (0,1 mL, 0.12 mmol), LiCL solution (5.23 mL), styrene (7.50 mL, 65.24 mmol), DPE (0.07 mL, 0.37 mmol)

and MMA (MR: 20.0 mL, 187.8 mmol; SR1: 6.5 mL, 61.0 mmol; SR2: 4.5 mL, 42.2 mmol; SR3: 3.0 mL, 28.2 mmol).

sample	$M_n^{b)}$	$M_w^{b)}$	PDI[c)]	A:B[c)]
	kg/mol			
1n PS	55.1	57.1	1.04	-
1a PS$_{530}$-PMMA$_{1450}$	167	176	1.05	1 : 2.7
1b PS$_{530}$-PMMA$_{2170}$	244	253	1.04	1 : 4.1
1c PS$_{530}$-PMMA$_{290}$	282	294	1.04	1 : 5.5
1d PS$_{530}$-PMMA$_{4550}$	509	539	1.06	1 : 8.6

a) determined by SEC (eluent: THF) with polystyrene standards, RI-detection; b) polydispersity index; c) molar block composition determined by ^{1}H-NMR

Typical ^{1}H-NMR data:

^{1}H-NMR (CDCl$_3$-d$_1$): δ(ppm) = 7.20-6.85 (CH^{b,c}), 6.82-6.27 (CH^a), 3.59 (CH$_3^d$), 2.21-0.72 (CH$_3^4$, CH$_2^{1,3}$, CH^2).

ABC triblock copolymers with variable C-block length **2a-2d**

Polystyrene-block-poly(2-ethylhexyl methacrylate)-block-poly(methyl methacrylate) (PS-PEHMA-PMMA)
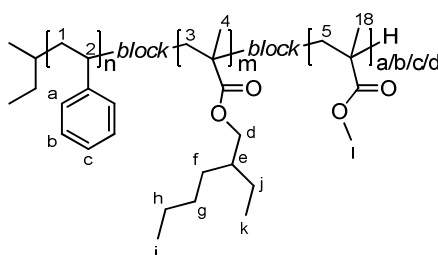
PS-PEHMA-PMMA (**2a; 2b; 2c; 2d**). The polymerization was performed similar to **GP2** in THF (430 mL) and a THF/LiCl-solution (70 mL) with styrene (5.52 mL, 480.1 mmol) and s-BuLi (1.28 mL, 1.7 mmol). After the addition of DPE (0.59 mL, 3.3 mmol) to the PS precursor, the solution was stirred for 20 min. Then the second monomer EHMA (16 mL, 71.2 mmol) was injected into the MR. The polymerization of the EHMA block was allowed to proceed for 4h at -66 °C. A sample of the precursor (120 mL) was withdrawn prior to the distribution to all reactors (i.e. SR1: 50 mL; SR2: 50 mL; SR3: 100 mL). Subsequently, the third monomer MMA (i.e. MR: 15 mL, 140.8 mmol; SR1: 8 mL, 75.1 mmol; SR2: 10 mL, 93.9 mmol; SR3: 10 mL, 93.9 mol) was added to all four reactors and the procedure described above was resumed.

| sample	$M_n^{b)}$	$M_w^{b)}$	$PDI^{c)}$	$A:B:C^{c)}$
	kg/mol			
2n PS_{30}	3.2	3.3	1.06	-
2nm PS_{30}-$PEHM_{45}$	9.1	10.2	1.05	1 : 1.5
2a PS_{30}-$PEHM_{45}$-$PMMA_{260}$	30.7	32.4	1.06	1 : 1.5 : 8.7
2b PS_{30}-$PEHM_{45}$-$PMMA_{310}$	34.5	36.3	1.05	1 : 1.5 : 10.4
2c PS_{30}-$PEHM_{45}$-$PMMA_{516}$	49.9	53.1	1.06	1 : 1.5 : 17.2
2d PS_{30}-$PEHM_{45}$-$PMMA_{540}$	53.9	56.3	1.04	1 : 1.5 : 18.0

a) determined by SEC (eluent: THF) with polystyrene standards, RI-detection; b) polydispersity index; c) molar block composition determined by ^{1}H-NMR

Typical ^{1}H-NMR data:

^{1}H-NMR (CDCl$_3$-d$_1$): δ(ppm) = 7.20-6.85 (CH^{b,c}), 6.82-6.27 (CH^a), 3.81 (CH^d), 3.59 (CH$_3^1$), 2.12-0.72 (CH$_3^{4,6,i,k}$, CH$_2^{1,3,5,f,g,h,j}$, CH^{2,e}).

AB diblock copolymers with variable chemical composition of the B-block **3a-3d**
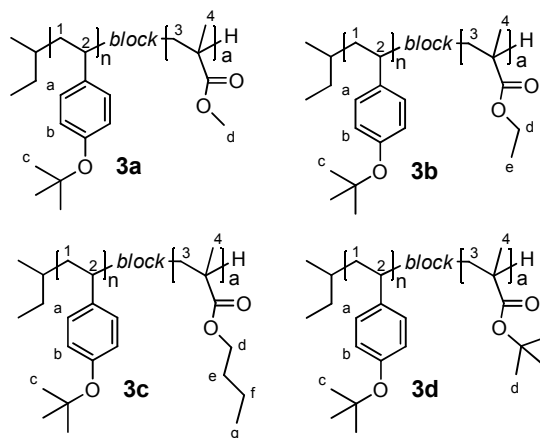
P*t*BS-PMMA/PEMA/P*n*BMA/P*t*BMA (**3a; 3b; 3c; 3d**). The polymerization was conducted according to the **GP2** using THF (510 mL), THF/LiCl-solution (40 mL), *tert*-butoxystyrene (6.00 mL, 318.6 mmol) and *s*-BuLi (0.72 mL, 0.94 mmol). 20 min after the addition of DPE a sample of the precursor (50 mL) was withdrawn prior to the distribution to all reactors (i.e. SR1: 100 mL, SR2: 100 mL, SR3: 100 mL). The four different monomers were injected into the four reactors: MMA (16 mL, 150.2 mmol) in MR, EMA (7 mL. 56.2 mmol) in SR1, *n*BMA (8 mL, 50.1 mmol) in SR2 and tBMA (7 mL, 43.1 mmol) in SR3. The temperature of SR3 was set to -45 °C for the polymerization of *t*BMA. The conditions in the other reactors equaled the above described. The polymerization in all reactors was continued for the 1h and terminated by injecting methanol in all reactors.

sample	$M_n^{b)}$	$M_w^{b)}$	$PDI^{c)}$	$A:B^{c)}$
	kg/mol			
3n PtBS$_{30}$	5.5	5.8	1.06	-
3a PtBS$_{30}$-PMMA$_{410}$	44.0	45.8	1.04	1 : 13.3
3b PtBS$_{30}$-PEMA$_{280}$	36.9	38.3	1.04	1 : 9.1
3c PtBS$_{30}$-PnBMA$_{280}$	41.7	43.3	1.04	1 : 8.9
3d PtBS$_{30}$-PtBMA$_{210}$	34.3	35.4	1.03	1 : 6.7$^{d)}$

a) determined by SEC (eluent: THF) with polystyrene standards, RI-detection; b) polydispersity index; c) molar block composition determined by ^{1}H-NMR d) not clearly detectable by ^{1}H-NMR

3a: ^{1}H-NMR (CDCl$_3$-d$_1$): δ(ppm) = 6.87-6.08 (CH^{b,c}), 3.59 (CH$_3^d$), 2.31-0.59 (CH$_3^{4,c}$, CH$_2^{1,3}$, CH^2).

3b: ^{1}H-NMR (CDCl$_3$-d$_1$): δ(ppm) = 6.92-6.10 (CH^{b,c}), 4.01 (CH$_2^d$), 2.20-0.63 (CH$_3^{4,c,e}$, CH$_2^{1,3}$, CH^2).

3c: ^{1}H-NMR (CDCl$_3$-d$_1$): δ(ppm) = 6.86-6.11 (CH^{b,c}), 3.93 (CH$_2^d$), 2.07-0.53 (CH$_3^{4,c,g}$, CH$_2^{1,3,e,f}$, CH^2).

3d: ^{1}H-NMR (CDCl$_3$-d$_1$): δ(ppm) = 6.86-6.13 (CH^{b,c}), 3.74 (CH$_3^d$), 2.37-0.65 (CH$_3^{4,c}$, CH$_2^{1,3}$, CH^2).

8.4.3   Synthesis of AB diblock copolymers

Poly(4-tert-butoxystyrene)-block-polystyrene
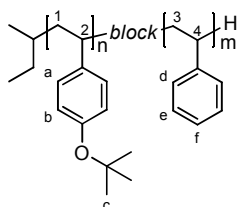
Several poly(4-*tert*-butoxystyrene)-*block*-polystyrene (P*t*BS-PS) batches were polymerized. One combinatorial polymerization was conducted yielding a series with increasing PS-block length. Additionally a single batch of P*t*BS-PS was polymerized in the MR alone. Characteristic data of all P*t*BS-PS block copolymers are shown below.

Single reactor batch

The polymerization was carried out similar to the **GP1**. *t*BS (20 mL, 0.106 mol) in THF (900 mL) for 95 min at -65 °C with s-BuLi (0.41 mL, 0.535 mmol) as initiator. After an aliquot (50 mL) was terminated in dry methanol the second monomer styrene (40 mL, 0.348 mol) was injected. After 100 min the polymerization was terminated with dry methanol. The block copolymer was purified by precipitation in methanol.

Combinatorial batch

The polymerization was carried out according to the **GP2**. *t*BS (8 mL, 42,5 mmol) was polymerized in THF (900 mL) for 100 min at -65 °C with s-BuLi (0.58 mL, 0.749 mmol) as initiator. After 40 mL of the polymer solution were terminated in dry methanol aliquots were distributed to the secondary reactors (SR1-3: 100 mL each). The second monomer styrene (MR: 25 mL, 0.217 mol; SR1: 10 mL, 87.0 mol; SR2: 7.7 mL, 67.0 mol; SR3: 5 mL, 43.5 mol) was injected in each reactor. After 35 min the polymerization was terminated with dry methanol. The block copolymers were purified by precipitation in methanol.

sample	$M_n^{b)}$	$M_w^{b)}$	$PDI^{c)}$	$A:B^{c)}$
	kg/mol			
Ie P*t*BS$_{188}$	33.11	34.06	1.03	-
10a P*t*BS$_{188}$PS$_{651}$	99.21	102.7	1.04	22.41
If P*t*BS$_{48}$	8.47	8.81	1.04	-
10b P*t*BS$_{48}$PS$_{1340}$	143.39	147.08	1.02	3.46
10c P*t*BS$_{48}$PS$_{1407}$	158.58	162.74	1.03	3.30
10d P*t*BS$_{48}$PS$_{630}$	92.20	94.89	1.03	7.08
10e P*t*BS$_{48}$PS$_{445}$	66.78	69.18	1.04	9.735

a) determined by SEC (eluent: THF) with polystyrene standards, UV-detection; b) polydispersity index; c) molar block composition determined by ^{1}H-NMR

Typical characteristic data for P*t*BS-PS:

^{1}H-NMR (CDCl$_3$-d$_1$): δ(ppm) = 7.21-6.89 (CH^{e,f}), 6.88-6.19 (CH^{a,b,d}), 2.21-0.72 (CH$_3^c$, CH$_2^{1,3}$, CH^{2,4}).

FT-IR (ATR): $\tilde{v}$ (cm^{-1}) 3028, 2972, 2924, 1603, 1505, 1452, 1365, 1236, 1162, 1027, 899, 851, 756, 697.

DSC (10 K/min, N$_2$, heating): T$_g$ = 105-111 °C

Poly(4-tert-butoxystyrene)-block-poly(methyl methacrylate)
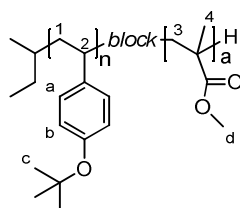
Several single reactor batches were polymerized according to the **GP1**.

*t*BS in THF for 95 min at -65 °C with *s*-BuLi as initiator and a tenfold excess of LiCl solution with respect to the initiator. A twofold excess of DPE was added and allowed to react for 20 min. After an aliquot (typically 100 mL) was terminated in dry methanol the calculated amount of methyl methacrylate for the second block was injected. After 45 min the polymerization was terminated with dry methanol. The block copolymer was purified by precipitation in methanol.

sample	$M_n^{b)}$	$M_w^{b)}$	$PDI^{c)}$	$A:B^{c)}$
	kg/mol			
Ia P*t*BOS$_{19}$	3.36	3.60	1.07	-
4a P*t*BOS$_{19}$PMMA$_{241}$	28.3	29.3	1.04	7.3
Ib P*t*BOS$_{60}$	10.7	11.1	1.04	-
4b P*t*BOS$_{60}$PMMA$_{785}$	72.9	76.0	1.04	7.1
Ic P*t*BOS$_{245}$	43.13	44.37	1.03	-
4c P*t*BOS$_{245}$PMMA$_{878}$	128.32	137.01	1.07	21.81

a) determined by SEC (eluent: THF) with polystyrene standards, RI-detection; b) polydispersity index; c) molar block composition determined by ^{1}H-NMR

Typical characteristic data for P*t*BS-PMMA:

^{1}H-NMR (CDCl$_3$-d$_1$): δ(ppm) =   6.85-6.12 (CH^{b,c}), 3.59 (CH$_3^d$), 2.21-0.72 (CH$_3^{4,c}$, CH$_2^{1,3}$, CH^2).

FT-IR (ATR): $\tilde{\nu}$ (cm^{-1})   2977, 2950, 1727, 1606, 1505, 1448, 1389, 1365, 1237, 1147, 1065, 988, 898, 851, 749.

DSC (10 K/min, N$_2$, heating):   T$_{g(1)}$ = 104-110 °C, T$_{g(2)}$ = 126-130 °C

Poly(4-tert-butoxystyrene)-block-poly(2-ethylhexyl methacrylate)-block-poly(methyl methacrylate)
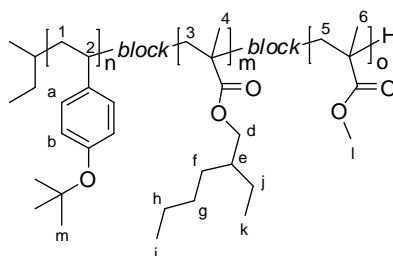
The polymerizations of PtBS-PEHMA-PMMA were carried out according to the **GP1** in dry THF (430 mL) and THF/LiCl-solution (83 mL) with tBS (8.01 mL, 42.6 mmol) and s-BuLi (1.92 mL, 2.5 mmol) for 45 min at -65 °C. After the addition of DPE (0.69 mL, 3.89 mmol) to the PtBOS precursor, the solution was stirred for 20 min. A sample of the PtBS precursor was quenched in degassed dry methanol Then the second monomer EHMA (23 mL, 0.102 mol) was injected into the MR. The polymerization of the EHMA block was allowed to proceed for 2 h at -65 °C. A sample of the AB-precursor was withdrawn prior to the distribution to all reactors (i.e. SR1: 50 mL; SR2: 50 mL; SR3: 100 mL). Subsequently, the third monomer MMA (i.e. MR: 12 mL, 113 mmol; SR1: 12 mL, 113 mmol; SR2: 8 mL, 75.1 mmol; SR3: 10 mL, 93.9 mol) was added to all four reactors and the polymerization proceeded for 70 min before termination with methanol. The polymers were purified by reprecipitation in cyclohexane.

sample	M_n[b]	M_w[b]	PDI[c]	A:B:C[c]
	kg/mol			
Id PtBS$_{16}$	2.80	3.05	1.08	-
8 PtBS$_{16}$PEHMA$_{66}$	10.4	11.2	1.11	1:4.1
PtBS$_{16}$PEHMA$_{66}$PMMA$_{155}$	25.4	27.2	1.07	1:4.1:9.71
PtBS$_{16}$PEHMA$_{66}$PMMA$_{571}$	62.4	70.8	1.12	1:4.1:35.7
9 PtBS$_{16}$PEHMA$_{66}$PMMA$_{472}$	54.3	57.3	1.06	1:4.1:29.5
PtBS$_{16}$PEHMA$_{66}$PMMA$_{240}$	33.6	32.5	1.06	1:4.1:15.02

a) determined by SEC (eluent: THF) with polystyrene standards, RI-detection; b) polydispersity index; c) molar block composition determined by ^{1}H-NMR

Typical characteristic data for PtBS-PEHMA-PMMA:

^{1}H-NMR (CDCl$_3$-d$_1$): δ(ppm) =   6.85-6.12 (CH[b,c]), 6.83-6.25 (CH[a]), 3.80 (CH[d]), 3.59 (CH$_3$[l]), 2.18-0.69 (CH$_3$[4,6,i,k,m], CH$_2$[1,3,5,f,g,h,j], CH[2,e]).

8.4.4 Synthesis of ABA triblock copolymers

Polystyrene-block-poly(4-tert-butoxystyrene)-block-polystyrene)
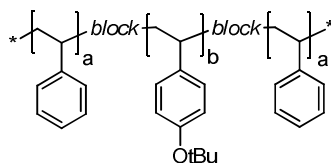
Route A: ABA' triblock copolymers via linear sequential polymerization with monofunctional initiator

The polymerizations were carried out similar to the **GP1** regarding preparations and cleaning procedures. The block copolymers were obtained by anionic polymerization (60 min) of styrene in THF at -70 °C with s-BuLi as initiator. An aliquot of the first block was isolated for analysis after termination with degassed methanol. Subsequently *t*BS was added to the solution and allowed to polymerize for 100 min. Again a sample of the AB diblock precursor was isolated after termination in degassed methanol. Styrene was introduced into the reactor to polymerize the last block for 70 min. Finally, the living chain ends were terminated by adding degassed methanol yielding PS-P*t*BuS-PS The block copolymers were isolated and purified by precipitation in methanol.

|	$M_n^{b)}$	$M_w^{b)}$	$PDI^{c)}$	$A:B^{c)}$
	kg/mol			
VIIIa PS$_{190}$	20.1	20.8	1.04	-
16a PS$_{190}$P*t*BS$_{680}$	112	115	1.03	1:3.5
17d PS$_{190}$P*t*BS$_{680}$PS$_{120}$	124	125	1.03	1:2.2
VIIIb PS$_{530}$	55.4	57.0	1.03	-
16b PS$_{530}$P*t*BS$_{3740}$	912	953	1.05	1:7.0
17e PS$_{530}$P*t*BS$_{3740}$PS$_{550}$	1000	1120	1.06	1:3.5

a) determined by SEC (eluent: THF) with polystyrene standards, UV-detection; b) polydispersity index; c) molar block composition determined by ¹H-NMR
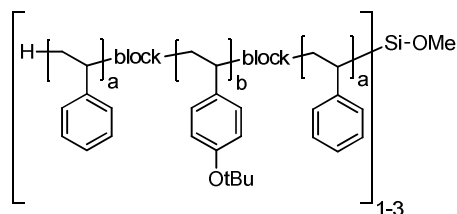
Route B: ABA triblock copolymers via linear polymerization with bifunctional initiator

The polymerizations were carried out according to **GP3** yielding PS-P*t*BS-PS. The block copolymer was isolated and purified by precipitation in methanol. Typical characteristic data can be found on page 231.

sample	$M_n^{b)}$	$M_w^{b)}$	$PDI^{c)}$	$A_2:B^{c)}$
	kg/mol			
Ij $PtBS_{930}$	163	171	1.05	-
17a $PS_{490}PtBS_{930}PS_{490}$	278	306	1.10	1 : 1.0
Ik $PtBS_{1860}$	327	345	1.07	-
17b $PS_{430}PtBS_{1860}PS_{430}$	403	436	1.08	1 : 2.2
Il $PtBS_{2670}$	470	499	1.06	-
17c $PS_{360}PtBS_{2670}PS_{360}$	528	558	1.06	1 : 3.7

a) determined by SEC (eluent: THF) with polystyrene standards, UV-detection; b) polydispersity index; c) molar block composition determined by ^{1}H-NMR

Synthesis of (A-B-A)$_{1-3}$ star block copolymer **23**

Triarm star polymers which each arm consisting of a ABA triblock copolymer **(A-B-A)$_{1-3}$** were synthesized via linear sequential anionic polymerization and subsequent coupling of the living carbanions with silicon tetrachloride. The coupling of living styrene anions with silicon tetrachloride is typically not quantitative therefore a triarm star is to be expected.[224]

The synthesis of the ABA block copolymer is the same as described for **17d**. In this polymerization the termination step with dry methanol was replaced with the coupling reaction with the silicon tetrachloride.

The polymerizations were carried out similar to the **GP1** using only the main reactor (MR) of the reactor setup. The block copolymers were obtained by anionic polymerization (40 min) of styrene (5,44 mL, 52.2 mmol) in THF (900 mL) at -70 °C with *s*-BuLi (0.2 mL, 0.261 mmol) as initiator. An aliquot of the first block was isolated for analysis after termination with degassed methanol. Subsequently *t*BS (24 mL, 0.127 mol) was added to the solution and allowed to polymerize for 100 min. Again a sample of the AB diblock precursor was isolated after termination in degassed methanol. Styrene (3 mL, 26.1 mmol) was introduced into the reactor to polymerize the last block for 40 min. A sample of the ABA triblock precursor poly(styrene-*block*-4-*tert*-butoxystyrene-*block*-styrene) (PS-P*t*BS-PS) was isolated after termination in degassed methanol.

Silicon tetrachloride was diluted in dry THF to yield a solution of 0.05 mol/L. The SiCl$_4$ (0.55 mL, 0.029 mmol, ¼ eq of remaining living anions) solution was introduced slowly into the reactor. After stirring for 15 h at -65 °C the temperature was raised to -44 °C for 5 h. More SiCl$_4$ solution was added until the yellow color vanished. The reaction was terminated by the addition of dry methanol. The block copolymer was isolated and purified by precipitation in methanol.

SEC (eluent: THF, UV-detection): M_n = 239 kg/mol, M_w = 298 kg/mol, PDI = 1.24

Typical characteristic data can be found on page 231.

8.5 Polymer analogous reaction

Prior to the functionalization of the polymers with mesogens or chromophores the PtBS block bearing the protected hydroxyl group has to be deprotected. The quantitative removal of the tBu group can be confirmed with ^{1}H-NMR. The hydroxylated polymers were acetylated to verify the quantitative deprotection.

8.5.1 General deprotection procedure

The general procedure is described for PtBS$_{1860}$ (**Ik**). The synthesis was carried out under inert atmosphere (i.e. dry argon). The N$_2$-flask was flame dried under HV prior to use. The polymer PtBS$_{1860}$ (0.5 g, 2.84 mmol, 1 eq) was dissolved in THF. HCl solution (31-33%, 1.42 mL, 5 eq) was added and the mixture was heated to reflux over night (~15 h). The polymer was precipitated in alkaline water. After precipitation the pH was adjusted to pH= 6 and the polymer was filtered off. After thorough drying under high vacuum at rt the polymer was purified by reprecipitation from THF in methanol to ensure the removal of potential terminated PHS homopolymer.
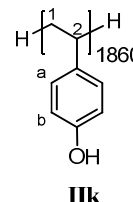
Typical FT-IR of polyhydroxystyrene homopolymers:

FT-IR (ATR): $\tilde{v}$ (cm^{-1})   3293, 3017, 2919, 1882, 1749, 1611, 1595, 1509, 1444, 1366, 1226, 1171, 1103, 1014, 827, 728, 693.

Acetylation of polyhydroxystyrene containing polymer

The synthesis was carried out under inert atmosphere (i.e. dry argon). The N$_2$-flask was flame dried under HV prior to use. The PHS$_{1860}$ (**IIk**) (0.1 g, 0.832 mmol) was dissolved in dry THF (20 mL) and pyridine (0.27 mL).
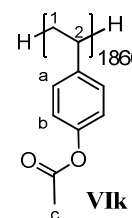
After cooling to -5 °C acetyl chloride (0.18 mL, 2.50 mmol, 3 eq) were added slowly. After warming to rt the mixture was stirred over night (~15 h) and heated to reflux for 1 h afterwards. Dry methanol (2 mL) was added to terminate the reaction and to dissolve the pyridinium salt. The polymer was purified by precipitation in methanol.

^{1}H-NMR analysis verified the quantitative conversion. SEC results confirmed slight reduction of molecular weight (M_n: 271 kg/mol, M_w: 292 kg/mol, PDI: 1.07).

Typical ^{1}H-NMR data of polyacetoxystyrene:

^{1}H-NMR (CDCl$_3$-d$_1$): δ(ppm) =   7.06-6.20 (CH^{a,b}), 2.25 (CH$_3$^{c}), 6.78-6.09 (CH^{a,b}), 2.05-1.04 (CH$_2$^{1}, CH^2).

The deprotection proceeds always quantitative under the described reaction conditions, therefore the characterization sequence for every single polymer was omitted.

8.5.2 Polymer analogous functionalization of polymers

General polymer analogous reaction procedure 1 **GPRP1**

The synthesis was carried out under inert atmosphere (i.e. dry argon). The N$_2$-flask was flame dried under HV prior to use. After thorough drying under HV, poly(4-vinylphenyloxy) PHS$_{2670}$ (**17c**) (0.2 g, 1.66 mmol, 1 eq) was dissolved in dry DMF 35 mL). 4'-(4-bromobutoxy)biphenyl-4-carbonitrile **CB4** (0.77 g, 2.33 mmol, 1.3 eq), K$_2$CO$_3$ (0.345 g, 2.5 mmol, 1.5 eq), 18-crown-6 (tip of a spatula) and KI (tip of a spatula) were added. The mixture was heated to 100 °C for 20 h. The mixture was concentrated by evaporation under HV at 60 °C. The polymer solution was first precipitated in water and afterwards purified by repeated reprecipitation in MeOH from THF.

General polymer analogous reaction procedure 2 **GPRP2**

The synthesis was carried out under inert atmosphere (i.e. dry argon). The N$_2$-flask was flame dried under HV prior to use. After thorough drying under HV, poly(4-vinylphenyloxy) PHS$_{1860}$ (**17b**) (0.12 g, 1.00 mmol, 1 eq) was dissolved in dry THF (40 mL) and pyridine (0.323 mL). The solution was cooled to 0 °C in an ice bath and **CB-3-COCl** (4.19 g, 1.4 mmol, 1.4 eq) was added. The mixture was allowed to warm to rt and was stirred for 20 h. Dry MeOH was added to quench excess acid chloride. The polymer was precipitated in MeOH and purified by reprecipitation in MeOH from THF.
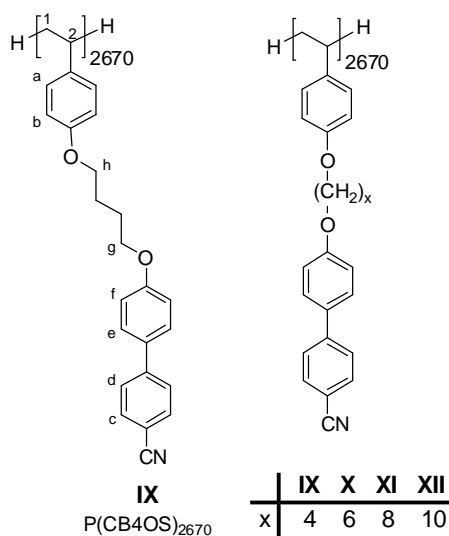
General polymer analogous reaction procedure 3 **GPRP3**

The synthesis was carried out under inert atmosphere (i.e. dry argon). The N_2-flask was flame dried under HV prior to use. After thorough drying under HV, poly(4-vinylphenyloxy) PHS_{1860} (**17b**) (0.15 g, 1.28 mmol, 1 eq) was dissolved in dry DMF (35 mL). **Azo1** (0.256 g, 0.7 mmol, 0.55 eq), **Azo2** (0.276 g, 0.7 mmol, 0.55 eq), K_2CO_3 (0.3 g, 2.18 mmol, 1.7 eq), 18-crown-6 (tip of a spatula) and KI (tip of a spatula) were added. The mixture was heated to 110 °C for 25 h. The second portion of mesogens was added, **Azo1** (0.07 g, 0.192 mmol, 0.15 eq) and **Azo2** (0.075 g, 0.192 mmol, 0.15 eq) and the reaction was continued for 17 h at 110 °C. The mixture was concentrated by evaporation under HV at 60 °C. The polymer was first precipitated in water and afterwards purified by repeated reprecipitation in EtOH from THF.

8.5.3 Synthesis of cyanobiphenyl-containing homopolymers

Cyanobiphenyl-functionalized poly(hydroxystyrene) with ester linkage

The synthesis of P(CB4OS) (**IX-XII**) was carried out according to **GPRP1.** This synthesis was carried out for several mesogens with spacer length x= 4, 6, 8, 10.

IX
P(CB4OS)$_{2670}$

	IX	X	XI	XII
x	4	6	8	10

sample	$DC^{a)}$	$M_n^{b)}$	$M_w^{b)}$	$PDI^{c)}$	$T_g^{d)}$	$T_{cl}\ (\Delta H)^{d)}$
	x	%	kg/mol			°C	°C (J/g)
IX P(CB4OS)$_{2670}$	4	97	1637	1898	1.16	80	98
X P(CB6OS)$_{2670}$	6	89	1600	2128	1.34	63	90
XI P(CB8OS)$_{2670}$	8	99	1732	2176	1.26	62	112 (4.8)
XII P(CB10OS)$_{2670}$	10	87	1865	2099	1.12	68	105 (6.0)

a) degree of conversion of polymer analogous reaction, determined by ^{1}H-NMR, b) determined by SEC, molecular weight with respect to polystyrene standards, UV-detection; c) polydispersity index; d) determined from second heating in DSC experiment at a heating rate of 10 K/min under N_2
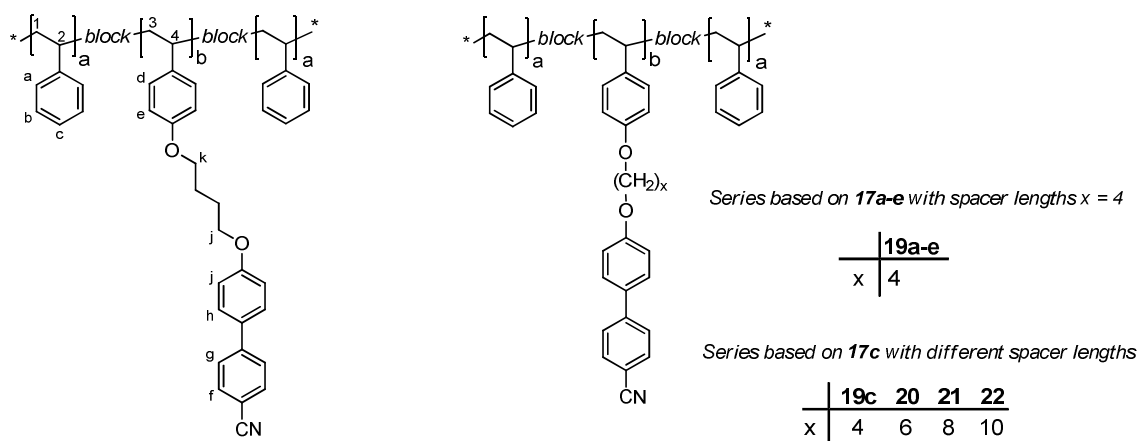
Typical FT-IR and ^{1}H-NMR data for cyanobiphenyl functionalized homopolymers. ^{1}H-NMR example given for **IX**, differences only in intensity of spacer signal (CH$_2$^{spacer}) with slight shift.

^{1}H-NMR (CDCl$_3$-d$_1$): δ(ppm) =   7.78-7.36 (CH^{c,d,e}), 7.09-6.85 (CH^f), 6.78-6.09 (CH^{a,b}), 4.31-3.61 (CH$_2$^{g,h}), 2.21-0.72 (CH$_2$$^{1,\ spacer}$, CH^2).

FT-IR (ATR): $\tilde{\nu}$ (cm^{-1})   3032, 2924, 2870, 2225, 1603, 1580, 1509, 1494, 1469, 1393, 1291, 1241, 1177, 1110, 1013, 819.

8.5.4 Synthesis of cyanobiphenyl-containing ABA and ABA' triblock copolymers

Cyanobiphenyl-functionalized polystyrene-block-poly(hydroxystyrene)-block-polystyrene with ether linkage

Series based on **17a-e** with spacer lengths x = 4

	19a-e
x	4

Series based on **17c** with different spacer lengths

	19c	20	21	22
x	4	6	8	10

The syntheses were conducted according to **GPRP1**. In this case the reaction was allowed to proceed for at least 48 h. This synthesis was carried out for several mesogens with spacer length x= 4, 6, 8, 10.

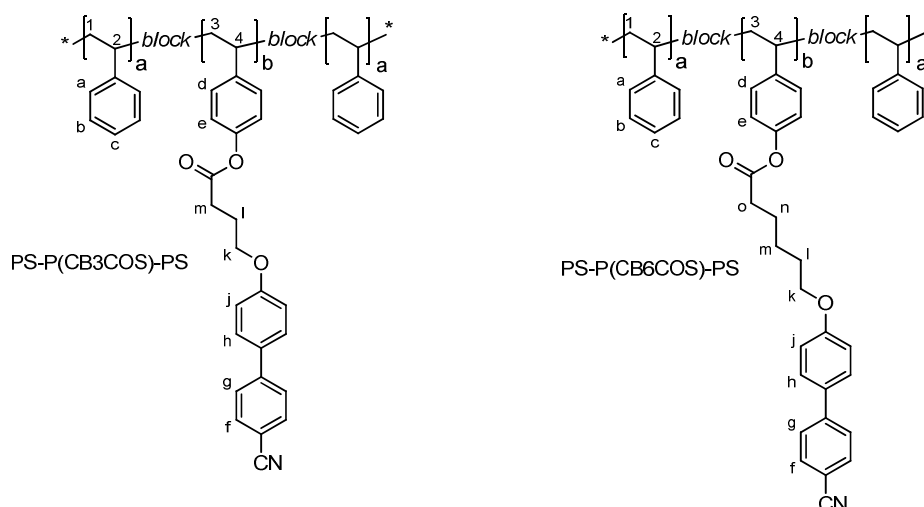| sample	spacer	DC[a]	M_n[b]	M_w[b]	PDI[c]	$T_{g(1)}$[d]	$T_{g(2)}$[d]	T_{cl}[d]
	x	%	kg/mol			°C	°C	°C
19a PS$_{490}$P(CB4OS)$_{930}$PS$_{490}$	4	88	894	947	1.06	87	109	n.f.
19b PS$_{430}$P(CB4OS)$_{1860}$PS$_{430}$	4	78	1409	1713	1.22	81	n.f.	n.f.
19c PS$_{360}$P(CB4OS)$_{2670}$PS$_{360}$	4	83	1560	2107	1.30	80	n.f.	n.f.
19d PS$_{190}$P(CB4OS)$_{680}$PS$_{120}$	4	87	601	630	1.05	90	n.f.	n.f.
19e PS$_{550}$P(CB4OS)$_{3740}$PS$_{530}$	4	59	2460	3052	1.24	91	n.f.	n.f.
20 PS$_{360}$P(CB6OS)$_{2670}$PS$_{360}$	6	70	2068	2560	1.24	74	n.f.	n.f.
21 PS$_{360}$P(CB8OS)$_{2670}$PS$_{360}$	8	80	1954	2348	1.21	n.f.	n.f.	94
22 PS$_{360}$P(CB10OS)$_{2670}$PS$_{360}$	10	84	1812	2184	1.21	70	n.f.	97
PS$_{550}$P(CB8OS)$_{3740}$PS$_{530}$	8	73	2672	3550	1.33	83	n.f.	n.f.
PS$_{190}$P(CB8OS)$_{680}$PS$_{120}$	8	78	564	586	1.04	58	n.f.	80

a) degree of conversion of polymer analogous reaction, determined by ^{1}H-NMR, b) determined by SEC eluent: THF + 0.25 wt% electrolyte), molecular weight with respect to polystyrene standards, UV-detection; c) polydispersity index, d) determined from second heating in DSC experiment at a heating rate of 10 K/min under N_2

Typical FT-IR and ^{1}H-NMR data for cyanobiphenyl functionalized homopolymers. ^{1}H-NMR example given for **19c**, differences only in intensity of spacer signal (CH$_2$[spacer]) with slight shift.

^{1}H-NMR (CDCl$_3$-d$_1$): δ(ppm) =   7.76-7.29 (CH[f,g,h]), 7.17-6.05 (CH[a-f,i]), 4.12-3.63 (CH$_2$[j,k]), 2.50-0.72 (CH$_2$[1,3, spacer], CH[2,4]).

FT-IR (ATR): $\tilde{\nu}$ (cm^{-1})   3033, 2930, 2870, 2225, 1666, 1603, 1580, 1509, 1494, 1471, 1388, 1289, 1241, 1171, 1047, 819, 699.

Cyanobiphenyl-functionalized polystyrene-block-poly(hydroxystyrene)-block-polystyrene with ester linkage

The syntheses of PS-P(CB3COS)-PS and PS-P(CB5COS)-PS were conducted according to **GPRP2**.

sample	x	DC[a)]	M$_n$[b)]	M$_w$[b)]	PDI[c)]	T$_{g(1)}^{d)}$	T$_{g(2)}^{d)}$	T$_{cl}$[d)]
		%	kg/mol			°C	°C	°C
PS$_{490}$P(CB3COS)$_{930}$PS$_{490}$	3	95	957	1150	1.20	105	n.f.	n.f.
PS$_{430}$P(CB3COS)$_{1860}$PS$_{430}$	3	86	1630	2100	1.29	94	n.f.	n.f.
PS$_{360}$P(CB3COS)$_{2670}$PS$_{360}$	3	92	1820	2320	1.28	n.d.	n.d.	n.d.
PS$_{360}$P(CB5COS)$_{2670}$PS$_{360}$	5	88	2220	3160	1.42	76	n.f.	95

a) degree of conversion of polymer analogous reaction, determined by ^{1}H-NMR, b) determined by SEC eluent: THF + 0.25 wt% electrolyte), molecular weight with respect to polystyrene standards, UV-detection; c) polydispersity index; d) determined from second heating in DSC experiment at a heating rate of 10 K/min under N$_2$
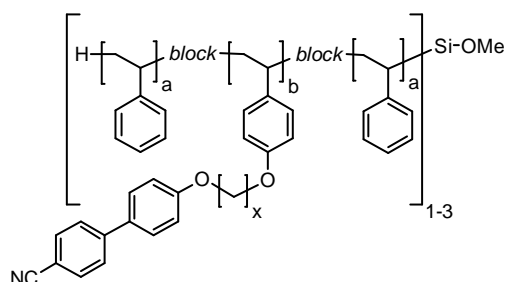
PS-P(CB3COS)-PS

^{1}H-NMR (CDCl$_3$-d$_1$): δ(ppm) =   7.69-7.34 (CH[f,g,h]), 7.22-6.19 (CH[a-e,i]), 4.02 (CH$_2$[k]), 2.70 (CH$_2$[j]), 2.16 (CH$_2$[l]), 2.02-0.72 (CH$_2$[1,3], CH[2,4]).

PS-P(CB5COS)-PS

^{1}H-NMR (CDCl$_3$-d$_1$): δ(ppm) =   7.75-7.35 (CH[f,g,h]), 7.18-6.13 (CH[a-e,i]), 3.94 (CH$_2$[k]), 2.51 (CH$_2$[o]), 2.00-0.88 (CH$_2$[1,3,l,m,n], CH[2,4]).

Cyanobiphenyl-functionalized star block copolymer

The syntheses were conducted according to **GPRP1**. In this case the reaction was allowed to proceed for 117 h.
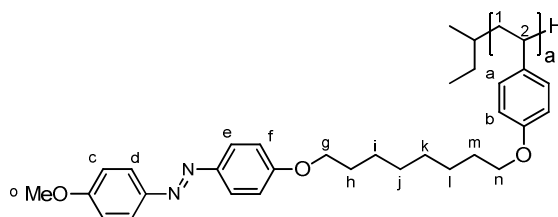

sample	x	DC[a)]	M$_n$[b)]	M$_w$[b)]	PDI[c)]	T$_{g(1)}^{d)}$	T$_{g(2)}^{d)}$	T$_{cl}$[d)]
		%	kg/mol			°C	°C	°C
25a (PS$_{190}$P(CB4OS)$_{680}$PS$_{120}$)$_{1-3}$	4	75	849	1035	1.22	105	n.f.	n.f.
25b (PS$_{190}$P(CB8OS)$_{680}$PS$_{120}$)$_{1-3}$	8	81	737	862	1.17	58	n.f.	80

a) degree of conversion of polymer analogous reaction, determined by ^{1}H-NMR, b) determined by SEC eluent: THF + 0.25 wt% electrolyte), molecular weight with respect to polystyrene standards, UV-detection; c) polydispersity index; d) determined from second heating in DSC experiment at a heating rate of 10 K/min under N$_2$

Typical data are given on page 240.

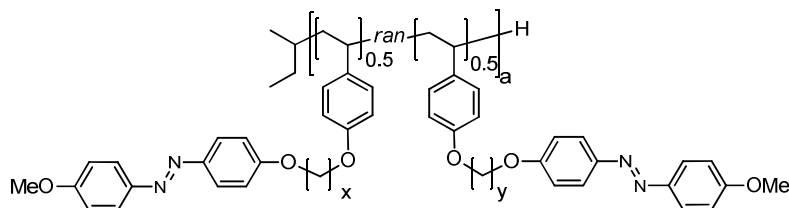### 8.5.5 Synthesis of azobenzene-containing homopolymers and copolymers

Methoxy azobenzene-functionalized poly(hydroxystyrene) with ether linkage

The syntheses were conducted according to **GPRP1**.

sample	x	DC[a]	M_n[b]	M_w[b]	PDI[c]	T_g[d]	T_{cl} (ΔH)[d]
		%	kg/mol			°C	°C (J/g)
III P(MeAzo8OS)$_{245}$	8	93	122	128	1.05	92	156 (15.6)
P(MeAzo8OS)$_{245}$	8	90	120	126	1.05	91	155 (14.8)

a) degree of conversion of polymer analogous reaction, determined by ^{1}H-NMR, b) determined by SEC eluent: THF + 0.25 wt% electrolyte), molecular weight with respect to polystyrene standards, UV-detection; c) polydispersity index; d) determined from second heating in DSC experiment at a heating rate of 10 K/min under N_2

This synthesis was carried out according to **GPRP3** for several mesogens.

sample	x/y	DC[a]	M_n[b]	M_w[b]	PDI[c]	T_g	T_{cl} (ΔH)[d]
		%	kg/mol			°C	°C (J/g)
IV P(MeOAzo4/6OS)$_{188}$	4/6	85	123	131	1.06	105	156 (10.0)
V P(MeOAzo4/8OS)$_{188}$	4/8	86	87	92	1.06	99	152 (14.5)
VI P(MeOAzo4/8OS)$_{188}$	6/8	75	161	169	1.05	92	142 (5.8)

a) degree of conversion of polymer analogous reaction, determined by ^{1}H-NMR, b) determined by SEC eluent: THF + 0.25 wt% electrolyte), molecular weight with respect to polystyrene standards, UV-detection; c) polydispersity index; d) determined from second heating in DSC experiment at a heating rate of 10 K/min under N_2
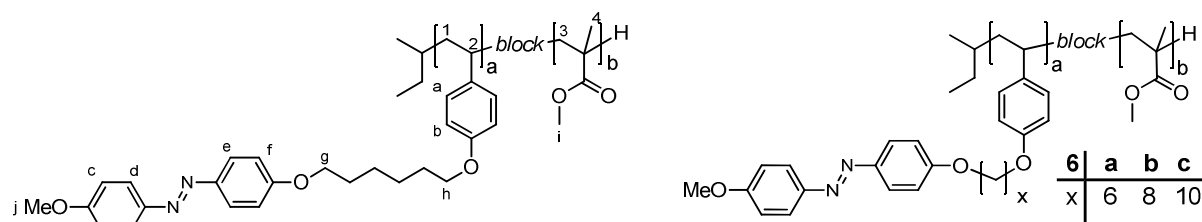
Typical FT-IR and ^{1}H-NMR data for methoxy azobenzene-functionalized homopolymers and copolymers. ^{1}H-NMR example given for **III**, differences only in intensity of spacer signal (CH_2^{spacer}) with slight shift.

^{1}H-NMR (CDCl$_3$-d$_1$): δ(ppm) = 8.10-7.67 (CH^{d,e}), 7.15-6.79 (CH^{c,f}), 6.56-6.17 (CH^{a,b}), 4.10-3.62 (CH$_3^{o}$, CH$_2^{g,n}$), 2.06-0.92 (CH$_2^{1,h-m}$, CH^2).

FT-IR (ATR): $\tilde{v}$ (cm^{-1}) 2929, 2865, 1598, 1581, 1500, 1470, 1296, 1241, 1177, 1146, 1104, 1027, 837, 756.

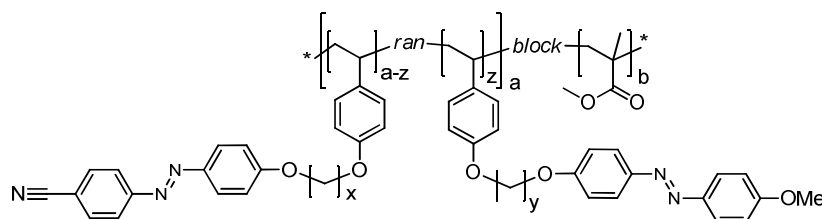## 8.5.6 Synthesis of azobenzene-containing homopolymers and copolymers

Methoxy azobenzene-functionalized poly(hydroxystyrene)-block- poly(methyl methacrylate) with ether linkage

The syntheses were conducted according to **GPRP1**. In this case the reaction was allowed to proceed for at least 48 h.

sample	x	$DC^{a)}$	$M_n^{b)}$	$M_w^{b)}$	$PDI^{c)}$	$T_{g(1)}^{d)}$	$T_{g(2)}^{d)}$	T_{cl} $(\Delta H)^{d)}$
		%	kg/mol			°C	°C	°C (J/g)
6a P(MeOAzo6OS)$_{245}$PMMA$_{878}$	6	90	249	261	1.05	101	128	152 (5.9)
6b P(MeOAzo8OS)$_{245}$PMMA$_{878}$	8	86	266	282	1.06	100	n.f.	145 (6.3)
6c P(MeOAzo10OS)$_{245}$PMMA$_{878}$	10	86	293	306	1.04	93	127	142 (6.6)

a) degree of conversion of polymer analogous reaction, determined by ^{1}H-NMR, b) determined by SEC eluent: THF + 0.25 wt% electrolyte), molecular weight with respect to polystyrene standards, UV-detection; c) polydispersity index; d) determined from second heating in DSC experiment at a heating rate of 10 K/min under N$_2$

This synthesis was carried out according to **GPRP3** for several mesogens.

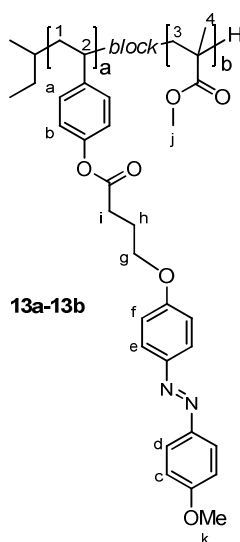| sample	x/y	$DC^{a)}$	$M_n^{b)}$	$M_w^{b)}$	$PDI^{c)}$	$T_{g(1)}^{d)}$	$T_{g(2)}^{d)}$	T_{cl} $(\Delta H)^{d)}$
		%	kg/mol			°C	°C	°C (J/g)
7a P(MeOAzo4/6OS)$_{245}$PMMA$_{878}$	4/6	82	291	304	1.04	107	130	150 (5.2)
7b P(MeOAzo4/8OS)$_{245}$PMMA$_{878}$	4/8	84	300	322	1.07	100	n.f.	135 (4.3)
P(MeOAzo6/8OS)$_{245}$PMMA$_{878}$	6/8	77	305	317	1.04	-	-	-
7c P(MeOAzo6/8OS)$_{245}$PMMA$_{878}$	6/8	84	297	309	1.04	105	n.f.	141 (5.5)

a) degree of conversion of polymer analogous reaction, determined by ^{1}H-NMR, b) determined by SEC eluent: THF + 0.25 wt% electrolyte), molecular weight with respect to polystyrene standards, UV-detection; c) polydispersity index; d) determined from second heating in DSC experiment at a heating rate of 10 K/min under N$_2$

Typical FT-IR and ^{1}H-NMR data for methoxy azobenzene-functionalized block copolymers with PMMA matrix. ^{1}H-NMR example given for **6a**, differences only in intensity of spacer signal (CH$_2$^{spacer}) with slight shift.

^{1}H-NMR (CDCl$_3$-d$_1$): δ(ppm) = 7.92-7.67 (CH^{d,e}), 7.04-6.79 (CH^{c,f}), 6.73-6.15 (CH^{a,b}), 4.02-3.38 (CH$_3$^{i,j}, CH$_2$^{g,h}), 2.13-0.63 (CH$_3$^{4}, CH$_2$^{1,spacer}, CH^2).

FT-IR (ATR): $\tilde{v}$ (cm^{-1}) 2982, 2947, 2860, 1725, 1598, 1581, 1501, 1436, 1388, 1240, 1144, 1028, 836, 749.

Cyano azobenzene-functionalized poly(hydroxystyrene)-block- poly(methyl methacrylate) with ether linkage

13a-13b

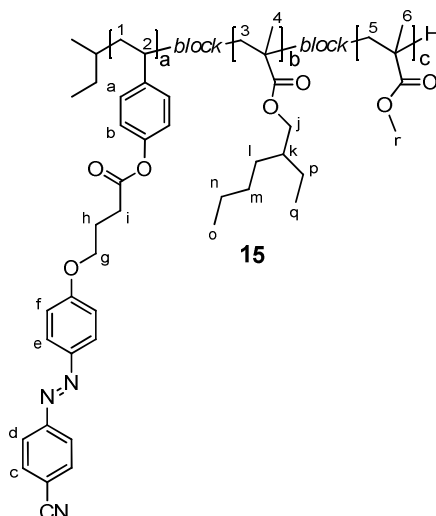The syntheses were conducted according to **GPRP2**.

sample	DC$^{a)}$	M$_n$$^{b)}$	M$_w$$^{b)}$	PDI$^{c)}$	T$_g$$^{d)}$	T$_{cl}$$^{d)}$
	%	kg/mol			°C	°C
13a P(CNAzo3COS)$_{19}$PMMA$_{241}$	87	3.06	3.36	1.10	n.d.	n.d.
13b P(CNAzo3COS)$_{61}$PMMA$_{455}$	84	78.7	84.1	1.07	128	135

a) degree of conversion of polymer analogous reaction, determined by ^{1}H-NMR, b) determined by SEC eluent: THF + 0.25 wt% electrolyte), molecular weight with respect to polystyrene standards, UV-detection; c) polydispersity index; d) determined from second heating in DSC experiment at a heating rate of 10 K/min under N$_2$

^{1}H-NMR (CDCl$_3$-d$_1$): δ(ppm) = 7.93-7.64 (CH^{d,e}), 7.02-6.28 (CH^{a,b,c,f}), 4.16-3.93 (CH$_2$^{g}), 3.80-337 (CH$_3$^{j,k}), 3.80-3.37 (CH$_2$^{i}), 2.82-2.58 (CH$_3$^{4}, CH$_2$^{1,h}, CH^2).

FT-IR (ATR): $\tilde{v}$ (cm^{-1}) 2997, 2950, 1727, 1599, 1435, 1387, 1241, 1192, 1142, 987, 843, 749.

Cyano azobenzene-functionalized poly(hydroxystyrene)-block-poly(2-ethylhexyl methacrylate)-block poly(methyl methacrylate) with ether linkage
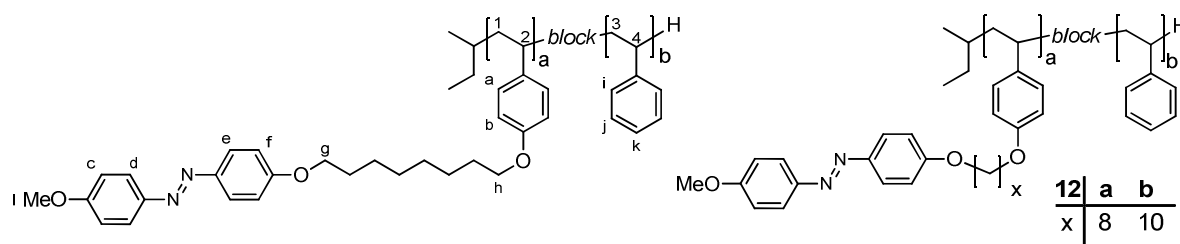

15

The syntheses were conducted according to **GPRP2**.

SEC (eluent: THF + 0.25 wt% electrolyte, RI-detection): $M_n = 51.2$ kg/mol, $M_n = 55.0$ kg/mol, PDI = 1.08; DC = 46% (by ^{1}H-NMR)

^{1}H-NMR (CDCl$_3$-d$_1$): δ(ppm) = 8.05-7.63 (CH^{d,e}), 7.13-6.16 (CH^{a,b,c,f}), 4.27-3.11 (CH$_3^r$, CH$_2^{g,j}$), 2.61-2.34 (CH$_2^i$), 2.82-2.58 (CH$_3^{4,6,o,q}$, CH$_2^{1,3,5,h,l,m,n,p}$, CH^{2,k}).

Methoxy azobenzene-functionalized poly(hydroxystyrene)-block-polystyrene with ether linkage

12	a	b
x	8	10

The syntheses were conducted according to **GPRP1**.

sample	x	DC[a]	M_n [b]	M_w [b]	PDI [c]	T_g [d]	T_{cl} (ΔH) [d]
		%	kg/mol	kg/mol		°C	°C (J/g)
12a P(MeAzo8OS)$_{188}$PS$_{651}$	8	87	234	244	1.04	106	143 (7,4)
12b P(MeAzo10OS)$_{188}$PS$_{651}$	10	63	243	253	1.04	104	135 (4.9)

a) degree of conversion of polymer analogous reaction, determined by 1H-NMR, b) determined by SEC eluent: THF + 0.25 wt% electrolyte), molecular weight with respect to polystyrene standards, UV-detection; c) polydispersity index; d) determined from second heating in DSC experiment at a heating rate of 10 K/min under N_2

Typical FT-IR and ^{1}H-NMR data for methoxy azobenzene-functionalized block copolymers with PS matrix. ^{1}H-NMR example given for **12a**, differences only in intensity of spacer signal (CH$_2$^{spacer}) with slight shift.

^{1}H-NMR (CDCl$_3$-d$_1$): δ(ppm) = 7.99-7.77 (CH^{d,e}), 7.24-6.87 (CH^{c,f,p,q}), 6.83-6.17 (CH^{a,b,o}), 4.06-3.67 (CH$_2$^{1}, CH$_2$^{g,h}), 2.18-0.96 (CH$_2$^{1,3,spacer}, CH^{2,4}).

FT-IR (ATR): $\tilde{v}$ (cm^{-1}) 3026, 2933, 2850, 1599, 1582, 1494, 1452, 1246, 177, 1147, 1104, 1028, 839, 755. 697.

8.6 Optical characterization of injection molded samples of blends of azobenzene-containing block copolymer and PMMA

The quality of the samples prepared by injection molding was analyzed using a micro-haze *plus* (BYK Gardner) to determine the transmission, haze and clarity. While haze is defined as the percentage of light that is deflected more than 2.5° from the incoming light direction (wide angle scattering) clarity is defined as the percentage of light that is deflected less than 2.5° (small angle scattering). The results of this characterization for all samples are given in Table 8.1. Samples of pure PMMA 7H that were used to optimize the processing conditions. These samples were compared to photoaddressable samples containing 1.5 wt% or 0.75 wt% of the azobenzene-containing block copolymer **6b**. The samples 1-9 containing **6b** all show lower transmission and higher haze compared to the neat PMMA samples 10-17. In contrast the clarity was not significantly influenced by the addition of the block copolymer. If the polymer mixture was prepared by precipitation prior to the injection molding process the resulting specimen showed Schlieren and turbidity when viewed with the naked eye that were not apparent in the results obtained by the micro-haze *plus*. These observations might be due to residual solvent in the mixture. Also, processing additives that are commonly used in commercial PMMA grades might have removed the precipitation procedure, causing a higher thermal degradation during the injection molding process.

Table 8.1:   Optical data of all samples prepared by injection molding (d = 1.1 mm) by different
preparation methods

Sample	polymer	Nr	transmission	haze	clarity	comment
1	PMMA 7H + 1.5 wt% **6b**	1	69.6	12.9	96.8	a), b), e)
2	PMMA 7H + 1.5 wt% **6b**	1	68..8	16.5	95.7	a), b), f), g)
3		2	68.6	16.0	95.4	
4	PMMA 7H + 0.75 wt% **6b**	1	79.5	9.8	97.0	a), c), e)
5	PMMA 7H + 0.75 wt% **6b**	1	79.6	10.4	96.1	a), c), f), g)
6		2	79.8	10.7	96.4	
7	PMMA 7H + 0.75 wt% **6b**	1	77.1	14.6	94.5	d), e), i)
8	PMMA 7H + 0.75 wt% **6b**	1	80.5	15.0	97.5	d), f)
9	PMMA 7H + 0.75 wt% **6b**	1	81.0	10.8	96.9	d), h), e)
10		1	94.7	0.8	99.3	
11	PMMA 7H	2	94.3	3.2	98.4	a), e)
12		3	95.0	1.4	99.4	
13	PMMA 7H	1	94.9	1.5	97.5	a), f), g)
14		2	94.8	1.3	98.3	
15	PMMA 7H	1	93.8	1.4	98.9	d), e)
16		2	94.7	1.6	986	
17	PMMA 7H	1	91.2	13.6	96.3	d), f), i)

a)   PMMA, (ground,) pre-dried

b)   powder-powder-mixture, powder mixer

c)   powder-powder-mixture, mortar and pestle

d)   polymer (mixture) precipitated in MeOH

e)   non-annealed

f)   annealed 135-140°C, 20h

g)   bubble formation during annealing (140°C), possible deformation on mold opening

h)   MicroInjector flushed with PMMA

i)   black Schlieren

9 References

[1]   L. Leibler, *Macromolecules* **1980**, *13*, 1602–1617.

[2]   G. H. Fredrickson, F. S. Bates, *Annu. Rev. Mater. Sci.* **1996**, *26*, 501–550.

[3]   A.-V. Ruzette, L. Leibler, *Nat. Mater.* **2005**, *4*, 19–31.

[4]   C. Tang, E. M. Lennon, G. H. Fredrickson, E. J. Kramer, C. J. Hawker, *Science* **2008**, *322*, 429–432.

[5]   F. Reinitzer, *Monatsh. Chem.* **1888**, *9*, 421.

[6]   O. Lehmann, *Flüssige Kristalle, sowie Plastizität von Kristallen im Allgemeinen, molekulare Umlagerungen u. Aggregatzustände*, Engelmann, Leipzig, **1904**.

[7]   D. Demus, *Mol. Cryst. Liquid Cryst.* **2001**, *364*, 25–91.

[8]   B. Bahadur, *Liquid crystals. Applications and uses*, World Scientific, Singapore, **1994**.

[9]   D. Pauluth, K. Tarumi, *J. Mater. Chem.* **2004**, *14*, 1219–1227.

[10]   R. Hołyst, P. Oswald, *Macromol. Theory Simul.* **2001**, *10*, 1–16.

[11]   F. S. Bates, G. H. Fredrickson, *Annu. Rev. Phys. Chem.,* **1990**, *41*, 525–557.

[12]   V. Abetz, P. F. W. Simon, *Adv. Polym. Sci.* **2005**, *189*, 125–212.

[13]   D. J. Meier, *J. Polym. Sci., Part C: Polym. Symp.* **1969**, *26*, 81-98.

[14]   M. W. Matsen, F. S. Bates, *Macromolecules* **1996**, *29*, 1091–1098.

[15]   A. K. Khandpur, S. Foerster, F. S. Bates, I. W. Hamley, A. J. Ryan, W. Bras, K. Almdal, K. Mortensen, *Macromolecules* **1995**, *28*, 8796–8806.

[16]   a) Y. Mogi, M. Nomura, H. Kotsuji, Matsuhita Y, I. Noda, *Macromolecules* **1994**, *27*, 6755–6760. b) R. Stadler, C. Auschra, J. Beckmann, U. Krappe, I. Voight-Martin, L. Leibler, *Macromolecules,* **1995**, *28*, 3080–3097. c) C. Auschra, R. Stadler, *Macromolecules* **1993**, *26*, 2171–2174.

[17]   IUPAC, *Pure Appl. Phys.,* **2004**, *76*, 889–904.

[18]   J. Adams, W. Gronski, *Makromol. Chem. Rapid Commun.* **1989**, *10*, 553–557.

[19]   C. Frenz, A. Fuchs, H.-W. Schmidt, U. Theissen, D. Haarer, *Macromol. Chem. Phys.* **2004**, *205*, 1246–1258.

[20]   E. Verploegen, T. Zhang, N. Murlo, P. T. Hammond, *Soft Matt.* **2008**, *4*, 1279–1287.

[21]   R. Fernández, I. Zalakain, J. A. Ramos, L. Martin, I. Mondragon, *Eur. Polym. J.* **2011**, *47*, 1176–1185.

[22]   F. H. Schacher, T. Rudolph, M. Drechsler, A. H. E. Müller, *Nanoscale* **2011**, *3*, 288–297.

[23]   T. Breiner, K. Kreger, R. Hagen, M. Haeckel, L. Kador, A. H. E. Müller, E. J. Kramer, H.-W. Schmidt, *Macromolecules* **2007**, *40*, 2100–2108.

[24]   E. Yoshida, S. Kuwayama, *Colloid. Polym. Sci.* **2008**, *286*, 1621–1627.

[25]   P.-H. Tung, S.-W. Kuo, S.-C. Chen, C.-L. Lin, F.-C. Chang, *Polym.* **2007**, *48*, 3192–3200.

[26]   A. Shishido, *Polym J* **2010**, *42*, 525–533.

[27]   T. Seki, *Bull. Chem. Soc. Jpn* **2007**, *80*, 2084–2109.

[28]   A. S. Matharu, S. Jeeva, P. S. Ramanujam, *Chem. Soc. Rev.* **2007**, *36*, 1868–1880.

[29]   H. Audorff, K. Kreger, R. Walker, D. Haarer, L. Kador, H.-W. Schmidt, *Adv. Polym. Sci.* **2010**, *228*, 59–121.

[30]   H. Yu, T. Kobayashi, *Molecules* **2010**, *15*, 570-603.

[31]   T. Ikeda, J.-i. Mamiya, Y. Yu, *Angew. Chem. Int. Ed.* **2007**, *46*, 506–528.

[32]   BASF, "Brands: Pluronic®", can be found under http://worldaccount.basf.com/wa/NAFTA~en_US/Catalog/ChemicalsNAFTA/pi/ BASF/Brand/pluronic, **04.04.11**.

[33]   a) E. V. Batrakova, A. V. Kabanov, *Journal of Controlled Release* **2008**, *130*, 98–106. b) A. K. Bhowmick, H. L. Stephens, *Handbook of elastomers*, M. Dekker, New York, **2001**. c) P. Desbois, V. Warzelhan, N. Niessner, A. Deffieux, S. Carlotti, *Macromol. Symp.* **2006**, *240*, 194–205.

[34]   Kraton, "Kraton SBS", can be found under http://kraton.com/Products/Kraton_D_SBS/, **04.04.11**.

[35]   BASF Styrolutions, "Styroflex® (SBC)", can be found under http://www.styrolution.com.sg/wa/stap~en_GB/portal/show/content/products/styre nics/styroflex, **04.04.11**.

[36]   BASF Styrolutions, "Styrolux® (SBC)", can be found under http://www.styrolution.com.sg/wa/stap~en_GB/portal/show/content/products/styre nics/styrolux, **04.04.11**.

[37]   a) I. Hamley, *Prog. Polym. Sci.* **2009**, *34*, 1161–1210. b) W. H. Jeu, Y. Séréro, M. Al-Hussein, *Adv. Polym. Sci.* **2006**, *200*, 71–90.

[38]   D. A. Bernards, T. A. Desai, *Soft Matt.* **2010**, *6*, 1621.

[39]   J. K. Kim, S. Y. Yang, Y. Lee, Y. Kim, *Prog. Polym. Sci.* **2010**, *35*, 1325–1349.

[40]   M. C. Orilall, U. Wiesner, *Chem. Soc. Rev.* **2011**, *40*, 520.

[41]   J. K. Bosworth, M. Y. Paik, R. Ruiz, E. L. Schwartz, J. Q. Huang, A. W. Ko, D.-M. Smilgies, C. T. Black, C. K. Ober, *ACS Nano,* **2008**, *2*, 1396–1402.

[42]   a) I. Bita, J. K. W. Yang, Y. S. Jung, C. A. Ross, E. L. Thomas, K. K. Berggren, *Science* **2008**, *321*, 939–943. b) S. Park, O. Yavuzcetin, B. Kim, M. T. Tuominen, T. P. Russell, *Small* **2009**, *5*, 1064–1069. c) S. Park, D. H. Lee, J. Xu, B. Kim, S. W. Hong, U. Jeong, T. Xu, T. P. Russell, *Science* **2009**, *323*, 1030–1033. d) M. Li, C. A. Coenjarts, C. K. Ober, *Adv. Polym. Sci.* **2005**, *190*, 183–226. e) D. Bratton, D. Yang, J. Dai, C. K. Ober, *Polym. Adv. Technol.* **2006**, *17*, 94–103.

[43]   R. Ruiz, H. Kang, F. A. Detcheverry, E. Dobisz, D. S. Kercher, T. R. Albrecht, J. J. de Pablo, P. F. Nealey, *Science* **2008**, *321*, 936–939.

[44]   a) M. A. Hillmyer, *Adv. Polym. Sci.* **2005**, 137–181. b) G. R. Whittell, M. D. Hager, U. S. Schubert, I. Manners, *Nat. Mater.* **2011**, *10*, 176–188. c) M. Lazzari,

G. Liu, S. Lecommandoux, *Block copolymers in nanoscience*, Wiley-VCH, Weinheim, **2006**.

[45]   Y. Zhou, W. Huang, J. Liu, X. Zhu, D. Yan, *Adv. Mater.* **2010**, *22*, 4567–4590.

[46]   a) M. Sommer, S. Huettner, M. Thelakkat, *J. Mater. Chem.* **2010**, *20*, 10788–10797. b) M. Sommer, S. Huettner, M. Thelakkat, *Adv. Polym. Sci.* **2010**, *228*, 123–153. c) M. Sommer, S. Huttner, U. Steiner, M. Thelakkat, *Appl. Phys. Lett.* **2009**, *95*, 183308. d) A. S. Lang, F. R. Kogler, M. Sommer, U. Wiesner, M. Thelakkat, *Macromol. Rapid Commun.* **2009**, *30*, 1243-1248.

[47]   O. W. Webster, *Science* **1991**, *251*, 887–893.

[48]   M. Szwarc, M. Levy, R. Milkovich, *J. Am. Chem. Soc.* **1956**, *78*, 2656–2657.

[49]   M. Szwarc, *Nature* **1956**, *178*, 1168–1169.

[50]   H. L. Hsieh, R. P. Quirk, *Anionic Polymerization. Principles and practical applications*, Marcel Dekker Inc, New York, **1996**.

[51]   D. Baskaran, A. H. E. Müller, *Prog. Polym. Sci.* **2007**, *32*, 173–219.

[52]   A. H. E. Müller, K. Matyjaszewski, *Controlled and living polymerizations. Methods and materials*, Wiley-VCH, Weinheim, **2009**.

[53]   N. Hadjichristidis, M. Pitsikalis, H. Iatrou, *Adv. Polym. Sci.* **2005**, *189*, 1–124.

[54]   N. Hadjichristidis, M. Pitsikalis, S. Pispas, H. Iatrou, *Chem. Rev.* **2001**, *101*, 3747–3792.

[55]   R. P. Quirk, T. Yoo, Y. Lee, J. Kim, B. Lee, *Adv. Polym. Sci.,* **2002**, *153*, 67–162.

[56]   S. Nosov, H. Schmalz, A. H. E. Müller, *Polym.* **2006**, *47*, 4245–4250.

[57]   A. Hirao, Y. Tokuda, K. Morifuji, M. Hayashi, *Macromol. Chem. Phys.* **2001**, *202*, 1606–1613.

[58]   T. Suzuki, J.-i. Kusakabe, T. Ishizone, *Macromolecules* **2008**, *41*, 1929–1936.

[59]   A. Hirao, S. Loykulnant, T. Ishizone, *Prog. Polym. Sci.* **2002**, *27*, 1399–1471.

[60]   S. Aoshima, S. Kanaoka, *Chem. Rev.* **2009**, *109*, 5245–5287.

[61]   O. W. Webster, W. R. Hertler, D. Y. Sogah, W. B. Farnham, T. V. RajanBabu, *J. Am. Chem. Soc.* **1983**, *105*, 5706–5708.

[62]   J. Raynaud, Y. Gnanou, D. Taton, *Macromolecules* **2009**, *42*, 5996–6005.

[63]   M. R. Buchmeiser, *Chem. Rev.* **2000**, *100*, 1565–1604.

[64]   M. Mayr, B. Mayr, M. R. Buchmeiser in *Studies in Surface Science and Catalysis : Scientific Bases for the Preparation of Heterogeneous Catalysts, Proceedings of the 8th International Symposium* (Eds.: E. n. Gaigneaux, D. Vos, P. Grange, P. Jacobs, J. Martens, P. Ruiz, G. Poncelet), Elsevier, **2000**.

[65]   K. Matyjaszewski, J. Xia, *Chem. Rev* **2001**, *101, 2921–2990.*

[66]   C. J. Hawker, A. W. Bosman, E. Harth, *Chem. Rev.,* **2001**, *101*, 3661–3688.

[67]   J. Chiefari, Y. K. Chong, F. Ercole, J. Krstina, J. Jeffery, T. P. T. Le, R. T. A. Mayadunne, G. F. Meijs, C. L. Moad, G. Moad et al., *Macromolecules,* **1998**, *31*, 5559–5562.

[68] O. Lehmann, *Zs. Phys. Ch.* **1889**, *4*, 862.

[69] D. Vorländer, *Kristallinisch-flüssige Substanzen*, Enke, Stuttgart, **1908**.

[70] S. Kumar, J. D. Brock, *Liquid crystals. Experimental study of physical properties and phase transitions*, Cambridge Univ. Press, Cambridge, **2001**.

[71] Dr. Robert P. Lemieux, can be found under http://www.chem.queensu.ca/people/faculty/lemieux/images/web-Fig.%201.jpg.

[72] D. Demus, *Handbook of Liquid Crystals. Low molecular weight liquid crystals I*, Wiley-VCH, Weinheim, **1998**.

[73] M. Schadt, W. Helfrich, *Appl. Phys. Lett.* **1971**, *18*, 127–128.

[74] H. Kelker, B. Scheurle, *Angew. Chem. Int. Ed.* **1969**, *8*, 884-885.

[75] a) G. W. Gray, *Liq. Cryst.* **1998**, *24*, 5–14. b) G.W. Gray, K.J. Harrison, J.A. Nash, *Electronics Letters* **1973**, *9*, 130–131.

[76] H. Finkelmann, H. Ringsdorf, J. H. Wendorff, *Makromol. Chem.* **1978**, *179*, 273.

[77] S. Poser, H. Fischer, M. Arnold, *Prog. Polym. Sci.* **1998**, *23*, 1337–1379.

[78] L. Noirez, P. Keller, J. P. Cotton, *Liq. Cryst.* **1995**, *18*, 129–148.

[79] C. Pugh, A. L. Kiste, *Prog. Polym. Sci.* **1997**, *22*, 601–691.

[80] G. Trimmel, S. Riegler, G. Fuchs, C. Slugovc, F. Stelzer, *Adv. Polym. Sci.* **2005**, *176*, 43–87.

[81] a) E. Novotná, S. G. Kostromin, H. Kresse, *Liq. Cryst.* **1995**, *18*, 73–79. b) C. T. Imrie, F. E. Karasz, G. S. Attard, *J. Macromol. Sci. Part A Pure Appl. Chem.* **1994**, *31*, 1221–1232.

[82] M. Yamada, T. Itoh, R. Nakagawa, A. Hirao, S.-i. Nakahama, J. Watanabe, *Macromolecules* **1999**, *32*, 282–289.

[83] Y. Tian, K. Watanabe, X. Kong, J. Abe, T. Iyoda, *Macromolecules* **2002**, *35*, 3739–3747.

[84] V. Percec, A. Keller, *Macromolecules* **1990**, *23*, 4347–4350.

[85] A. A. Craig, C. T. Imrie, *Macromolecules* **1999**, *32*, 6215–6220.

[86] A. A. Craig, C. T. Imrie, *Macromolecules* **1995**, *28*, 3617–3624.

[87] C. T. Imrie, F. E. Karasz, G. S. Attard, *Macromolecules* **1992**, *25*, 1278–1283.

[88] P. Martinoty, L. Hilliou, M. Mauzac, L. Benguigui, D. Collin, *Macromolecules* **1999**, *32*, 1746–1752.

[89] Q. Wang, C.-a. Yang, H. Xie, X. Wang, H. Zhang, *Liq. Cryst.* **2010**, *37*, 435–443.

[90] O. Lehmann, S. Förster, J. Springer, *Macromol. Rapid Commun.* **2000**, *21*, 133–135.

[91] R. Bohnert, H. Finkelmann, *Macromol. Chem. Phys.* **1994**, *195*, 689–700.

[92] M. Yamada, T. Iguchi, A. Hirao, S. Nakahama, J. Watanabe, *Polym. J* **1998**, *30*, 23–30.

[93] W. Y. Zheng, P. T. Hammond, *Macromol. Rapid Commun.* **1996**, *17*, 813–824.

[94]   V. Percec, M. Lee, *J. Macromol. Sci. Part A Pure Appl. Chem.* **1992**, *29*, 723–740.

[95]   A. Omenat, R. A. M. Hikmet, J. Lub, P. van der Sluis, *Macromolecules* **1996**, *29*, 6730–6736.

[96]   W. Kreuder, O. W. Webster, H. Ringsdorf, *Makromol. Chem. Rapid Commun.* **1986**, *7*, 5–13.

[97]   M. Hefft, J. Springer, *Makromol. Chem. Rapid Commun.* **1990**, *11*, 397–401.

[98]   G. Mao, Christopher K. Ober in *High Molecular Weight Liquid Crystals*, *Vol. 3* (Ed.: D. Demus), Wiley-VCH, Weinheim, **1998**.

[99]   J.-S. Wang, K. Matyjaszewski, *Macromolecules* **1995**, *28*, 7901–7910.

[100]   L.-Y. Wang, K.-C. Li, H.-C. Lin, *Polym.* **2010**, *51*, 75–83.

[101]   X. He, H. Zhang, X. Wang, *Polym. Bull.* **2002**, *48*, 337–344.

[102]   H. Yu, Y. Naka, A. Shishido, T. Ikeda, *Macromolecules* **2008**, *41*, 7959–7966.

[103]   X. He, W. Sun, D. Yan, M. Xie, Y. Zhang, *J. Polym. Sci., Part A: Polym. Chem.* **2008**, *46*, 4442–4450.

[104]   a) L. Ding, H. Mao, J. Xu, J. He, X. Ding, T. P. Russell, D. R. Robello, M. Mis, *Macromolecules* **2008**, *41*, 1897–1900. b) P. Forcen, L. Oriol, C. Sanchez, R. Alcala, S. Hvilsted, K. Jankova, J. Loos, *J. Polym. Sci., Part A: Polym. Chem.* **2007**, *45*, 1899–1910. c) Y.-K. Han, B. Dufour, W. Wu, T. Kowalewski, K. Matyjaszewski, *Macromolecules* **2004**, *37*, 9355–9365. d) P. Forcen, L. Oriol, C. Sanchez, F. J. Rodriguez, R. Alcala, S. Hvilsted, K. Jankova, *Eur. Polym. J.* **2007**, *43*, 3292–3300.

[105]   Y. Zhang, W. Zhang, X. Chen, Z. Cheng, J. Wu, J. Zhu, X. Zhu, *J. Polym. Sci., Part A: Polym. Chem.* **2008**, *46*, 777–789.

[106]   L. Cui, Y. Zhao, A. Yavrian, T. Galstian, *Macromolecules* **2003**, *36*, 8246–8252.

[107]   a) R. Maeda, T. Hayakawa, M. Tokita, R. Kikuchi, J. Kouki, M.-a. Kakimoto, H. Urushibata, *React. Funct. Polym.* **2009**, *69*, 519–529. b) E. Yoshida, M. Ohta, *Colloid. Polym. Sci.* **2005**, *283*, 521–531.

[108]   a) X. Hao, M. H. Stenzel, C. Barner-Kowollik, T. P. Davis, E. Evans, *Polym.* **2004**, *45*, 7401–7415. b) S. Boissé, J. Rieger, A. Di-Cicco, P.-A. Albouy, C. Bui, M.-H. Li, B. Charleux, *Macromolecules* **2009**, *42*, 8688–8696. c) Y. Zhang, Z. Cheng, X. Chen, W. Zhang, J. Wu, J. Zhu, X. Zhu, *Macromolecules* **2007**, *40*, 4809–4817.

[109]   Y. Zhao, B. Qi, X. Tong, Y. Zhao, *Macromolecules* **2008**, *41*, 3823–3831.

[110]   C. W. Bielawski, R. H. Grubbs, *Prog. Polym. Sci.* **2007**, *32*, 1–29.

[111]   Z. Komiya, R. R. Schrock, *Macromolecules* **1993**, *26*, 1387–1392.

[112]   K. Wewerka, A. Wewerka, F. Stelzer, B. Gallot, L. Andruzzi, G. Galli, *Macromol. Rapid Commun.* **2003**, *24*, 906-910.

[113]   S. Koltzenburg, M. Ungerank, F. Stelzer, O. Nuyken, *Macromol. Chem. Phys.* **1999**, *200*, 814-820.

[114] A. J. Gabert, E. Verploegen, P. T. Hammond, R. R. Schrock, *Macromolecules* **2006**, *39*, 3993–4000.

[115] G. Mao, J. Wang, S. R. Clingman, C. K. Ober, J. T. Chen, E. L. Thomas, *Macromolecules* **1997**, *30*, 2556–2567.

[116] J. Wang, G. Mao, Christopher K. Ober, E. J. Kramer, *Macromolecules* **1997**, *30*, 1906–1914.

[117] T. Hayakawa, S. Horiuchi, H. Shimizu, T. Kawazoe, M. Ohtsu, *J. Polym. Sci., Part A: Polym. Chem.* **2002**, *40*, 2406–2414.

[118] M. D. Kempe, N. R. Scruggs, R. Verduzco, J. Lal, J. A. Kornfield, *Nat. Mater.* **2004**, *3*, 177–182.

[119] M. D. Kempe, R. Verduzco, N. R. Scruggs, J. A. Kornfield, *Soft Matt.* **2006**, *2*, 422–431.

[120] B. Zaschke, W. Frank, H. Fischer, K. Schmutzler, M. Arnold, *Polym. Bull.* **1991**, *27*, 1–8.

[121] C. T. Imire, F. E. Karasz, G. S. Attard, *Liq. Cryst.* **1991**, *9*, 47–57.

[122] J. V. Crivello, M. Deptolla, H. Ringsdorf, *Liq. Cryst.* **1988**, *3*, 235–247.

[123] a) Z. Li, Y. Zhang, L. Zhu, T. Shen, H. Zhang, *Polym. Chem,* **2010**, *1*, 1501–1511. b) W. H. Binder, C. Kluger, *Macromolecules* **2004**, *37*, 9321–9330.

[124] a) A. Schneider, J. J. Zanna, M. Yamada, H. Finkelmann, R. Thomann, *Macromolecules* **2000**, *33*, 649–651. b) H. Finkelmann, M. Walther, *Prog. Polym. Sci.* **1996**, *21*, 951–979.

[125] H. Fischer, S. Poser, M. Arnold, W. Frank, *Macromolecules* **1994**, *27*, 7133–7138.

[126] H. Fischer, S. Poser, M. Arnold, *Macromolecules* **1995**, *28*, 6957–6962.

[127] M. Anthamatten, W. Y. Zheng, P. T. Hammond, *Macromolecules* **1999**, *32*, 4838–4848.

[128] a) E. Verploegen, L. C. McAfee, L. Tian, D. Verploegen, P. T. Hammond, *Macromolecules* **2007**, *40*, 777–780. b) I. W. Hamley, V. Castelletto, Z. B. Lu, C. T. Imrie, T. Itoh, M. Al-Hussein, *Macromolecules* **2004**, *37*, 4798–4807. c) I. A. Ansari, V. Castelletto, T. Mykhaylyk, I. W. Hamley, Z. B. Lu, T. Itoh, C. T. Imrie, *Macromolecules* **2003**, *36*, 8898–8901.

[129] a) M. Shah, V. Pryamitsyn, V. Ganesan, *Macromolecules* **2008**, *41*, 218–229. b) M. Anthamatten, P. T. Hammond, *J. Polym. Sci. B Polym. Phys* **2001**, *39*, 2671–2691.

[130] I. I. Potemkin, A. S. Bodrova, *Macromolecules* **2009**, *42*, 2817–2825.

[131] Y. Zhao, J. He, *Soft Matt.* **2009**, *5*, 2686–2693.

[132] R. E. Bohn, J. E. Short, *How Much Information? 2009. Report on American Consumers*, San Diego, **2009**.

[133] D. A. Thompson, J. S. Best, *IBM J. Res. Dev.* **2000**, *44*, 311B.M.

[134] Pioneer, *The world's first multi-layer (16) optical disk technology. Blu-ray Disc has a compatible with progress towards the realization of large capacity archival system - Capacity 400 GB*, **2008**.

[135] a) D. Gabor, *Science* **1972**, *177*, 299–313. b) D. Gabor, *Nature* **1948**, *161*, 777–778.

[136] G. Ekspong, T. Frängsmyr, S. Lundquist, *Nobel Lecures: Physics 1981-1990*, River Edge, NJ; World Scientific, Singapore ;, **1992**.

[137] K. R. D. L. Curtis, A. Hill, W. Wilson, M. Ayres, *Holographic data storage. From theory to practical systems*, Wiley, Hoboken, NJ, **2010**.

[138] R. Hagen, T. Bieringer, *Adv. Mater.* **2001**, *13*, 1805–1810.

[139] a) G. Barbastathis, D. Psaltis in *Holographic data storage* (Ed.: H. P. D. S. G. T. Coufal), Springer-Verlag, Berlin, **2000**. b) D. A. Waldmann, C. J. Butler, D. H. Raguin, *Proc. SPIE Int. Soc. Opt. Eng.* **2003**, *5216*, 10–25. c) M. Schnoes, B. Ihas, L. Dhar, D. Michaels, S. Settachayanon, G. L. Schomberger, W. L. Wilson, *Proc. SPIE Int. Soc. Opt. Eng.* **2003**, *4988*, 68–76. d) J. Ashley, M. P. Bernal, G. W. Burr, H. Coufal, H. Guenther, J. A. Hoffnagle, C. M. Jefferson, B. Marcus, R. M. Macfarlane, R. M. Shelby and G. T. Sincerbox, *IBM J. Res. Dev.* **2000**, *44*, 341-368. e) M. L. Schilling, V. L. Colvin, L. Dhar, A. L. Harris, F. C. Schilling, H. E. Katz, T. Wysocki, A. Hale, L. L. Blyler, C. Boyd, *Chem. Mater.* **1999**, *11*, 247–254.

[140] L. Hesselink, S. S. Orlov, M. C. Bashaw, *Proc. IEEE,* **2004**, *92*, 1231–1280.

[141] InPhase Technologies, *Tapestry Product Brochure*, **2011**.

[142] M. Eich, J. H. Wendorff, H. Ringsdorf, H.-W. Schmidt, *Makromol. Chem.* **1985**, *186*, 2639–2647.

[143] H. Ringsdorf, H.-W. Schmidt, *Makromol. Chem.* **1984**, *185*, 1327–1334.

[144] M. Eich, J. H. Wendorff, B. Reck, H. Ringsdorf, *Makromol. Chem. Rapid Commun.* **1987**, *8*, 59–63.

[145] a) K. Anderle, J. H. Wendorff, *Mol. Cryst. Liq. Cryst. Sci. Technol., Sect. A* **1994**, *243*, 51–75. b) G. S. Kumar, D. C. Neckers, *Chem. Rev.,* **1989**, *89*, 1915–1925.

[146] F. Weigert, J. Matulis, *Fortschrittsberichte über Kolloide und Polymere* **1933**, *38*, 384–411.

[147] H. Audorff, *Dissertation*, Universität Bayreuth, Bayreuth, **2011**.

[148] S.-k. Ahn, R. M. Kasi, S.-C. Kim, N. Sharma, Y. Zhou, *Soft Matt.* **2008**, *4*, 1151–1157.

[149] T. Kato, Y. Hirai, S. Nakaso, M. Moriyama, *Chem. Soc. Rev.,* **2007**, *36*, 1857–1867.

[150] N. Mizoshita, Y. Suzuki, K. Kishimoto, K. Hanabusa, T. Kato, *J. Mater. Chem.* **2002**, *12*, 2197–2201.

[151] a) C. A. Guymon, E. N. Hoggan, N. A. Clark, T. P. Rieker, D. M. Walba, C. N. Bowman, *Science* **1997**, *275*, 57–59. b) D. Coates, *J. Mater. Chem.,* **1995**, *5*, 2063–2072. c) S. M. Kelly, *J. Mater. Chem.,* **1995**, *5*, 2047–2061.

[152] Y. Xia, R. Verduzco, R. H. Grubbs, J. A. Kornfield, *J. Am. Chem. Soc.* **2008**, *130*, 1735–1740.

[153] R. Vendamme, U. Maschke, *E-POLYMERS* **2006,** 069.

[154] T. Kato, N. Mizoshita, K. Kishimoto, *Angew. Chem. Int. Ed.* **2006**, *45*, 38-68.

[155] R. Pettau, C. Erdelen, H.-W. Schmidt, *Macromol. React. Eng.* **2010**, *4*, 65–72.

[156] a) A. Furka, F. Sebestyen, J. Gulyas, *Proc. Int. Conf. Biochem. Sep. 2nd* **1988**, *35*. b) A. Furka, *Notariell Beglaubigtes Dokument Nr. 36237/1982*, Budapest, **1982**.

[157] H. M. Geysen, R. H. Meloen, S. J. Barteling, *Proc. Nat. Acad. Sci. U.S.A.* **1984**, *81*, 3998.

[158] R. A. Houghten, *Proc. Nat. Acad. Sci. U.S.A.* **1982**, *85*, 5131.

[159] E. J. Amis, X.-D. Xiang, J.-C. Zhao, *MRS Bull.* **2002**, *27*, 295–300.

[160] Meier, Michael A. R., R. Hoogenboom, U. S. Schubert, *Macromol. Rapid Commun.* **2004**, *25*, 21–33.

[161] M. Thelakkat, C. Schmitz, C. Neuber, H.-W. Schmidt, *Macromol. Rapid Commun.* **2004**, *25*, 204–223.

[162] C. Guerrero-Sanchez, R. M. Paulus, Fijten, Martin W. M., de la Mar, Mariska J., R. Hoogenboom, U. S. Schubert, *Appl. Surf. Sci.* **2006**, *252*, 2555–2561.

[163] a) A. Ekin, D. C. Webster, *Macromolecules* **2006**, *39*, 8659–8668. b) Meier, Michael A. R., J.-F. Gohy, C.-A. Fustin, U. S. Schubert, *J. Am. Chem. Soc.* **2004**, *126*, 11517–11521.

[164] a) S. Ludwigs, A. Boker, V. Abetz, A. H. E. Müller, G. Krausch, *Polym.* **2003**, *44*, 6815–6823. b) H. Huckstadt, A. Gopfert, V. Abetz, *Polym.* **2000**, *41*, 9089–9094.

[165] H. Schmalz, A. Boeker, R. Lange, G. Krausch, V. Abetz, *Macromolecules* **2001**, *34*, 8720–8729.

[166] C. Guerrero-Sanchez, C. Abeln, U. S. Schubert, *J. Polym. Sci., Part A: Polym. Chem.* **2005**, *43*, 4151–4160.

[167] J. Jagur-Grodzinski, *J. Polym. Sci., Part A: Polym. Chem.* **2002**, *40*, 2116–2133.

[168] M. H. Acar, K. Matyjaszewski, *Macromol. Chem. Phys.* **1999**, *200*, 1094–1100.

[169] J. P. Hautekeer, S. K. Varshney, R. Fayt, C. Jacobs, R. Jerome, P. Teyssie, *Macromolecules* **1990**, *23*, 3893–3898.

[170] T. Higashimura, K. Kojima, M. Sawamoto, *Makromol. Chem.* **1989**, *15*, 127–136.

[171] M. Haller, J. Luo, H. Li, T.-D. Kim, Y. Liao, B. H. Robinson, L. R. Dalton, A. K. Y. Jen, *Macromolecules* **2004**, *37*, 688–690.

[172] R. H. Berg, S. Hvilsted, P. S. Ramanujam, *Nature* **1996**, *383*, 505–508.

[173] A. Natansohn, P. Rochon, *Chem. Rev.,* **2002**, *102*, 4139–4175.

[174] Y. Zhao, T. Ikeda (Eds.) *Smart light-responsive materials. Azobenzene-containing polymers and liquid crystals*, Wiley, Hoboken, N.J, **2009**.

[175] a) V. Cimrova, D. Neher, S. Kostromine, T. Bieringer, *Macromolecules* **1999**, *32*, 8496–8503. b) X. Meng, A. Natansohn, P. Rochon, *Polym.* **1997**, *38*, 2677–2682.

[176] X. Meng, A. Natansohn, C. Barrett, P. Rochon, *Macromolecules* **1996**, *29*, 946–952.

[177] M. Häckel, L. Kador, D. Kropp, C. Frenz, H.-W. Schmidt, *Adv. Funct. Mater.* **2005**, *15*, 1722–1727.

[178] M. Ishiguro, D. Sato, A. Shishido, T. Ikeda, *Langmuir* **2007**, *23*, 332–338.

[179] L. L. Nedelchev, A. S. Matharu, S. Hvilsted, P. S. Ramanujam, *Appl. Opt.* **2003**, *42*, 5918-5927.

[180] M. Kidowaki, T. Jujiwara, S. Morino, K. Ichimura, J. Stumpe, *Appl. Phys. Lett.* **2000**, *76*, 1377–1379.

[181] a) P. Rochon, E. Batalla, A. Natansohn, *Appl. Phys. Lett.* **1995**, *66*, 136–138. b) D. Y. Kim, S. K. Tripathy, L. Li, J. Kumar, *Appl. Phys. Lett.* **1995**, *66*, 1166–1168.

[182] R. Walker, H. Audorff, L. Kador, H. W. Schmidt, *Adv. Funct. Mater.* **2009**, *19*, 2630–2638.

[183] J. Minabe, T. Maruyama, S. Yasuda, K. Kawano, K. Hayashi, Y. Ogasawara, *Jpn. J. Appl. Phys.* **2004**, *43*, 4964–4967.

[184] H. Audorff, K. Kreger, R. Walker, D. Haarer, L. Kador, H.-W. Schmidt in *Advances in Polymer Science* (Eds.: A. H. E. Müller, H.-W. Schmidt), Springer Berlin / Heidelberg, **2010**.

[185] M. Haeckel, L. Kador, D. Kropp, H.-W. Schmidt, *Adv. Mater.* **2007**, *19*, 227–231.

[186] M. Walther, H. Faulhammer, H. Finkelmann, *Macromol. Chem. Phys.* **1998**, *199*, 223-237.

[187] A. Martin, C. Tefehne, W. Gronski, *Macromol. Rapid Commun.* **1996**, *17*, 305-311.

[188] S. Gimeno, P. Forcen, L. Oriol, M. Pinol, C. Sanchez, F. J. Rodriguez, R. Alcala, K. Jankova, S. Hvilsted, *Eur. Polym. J.,* **2009**, *45*, 262–271.

[189] J.-H. Liu, Y.-H. Chiu, *J. Polym. Sci., Part A: Polym. Chem.* **2010**, *48*, 1142-1148.

[190] X. Tong, L. Cui, Y. Zhao, *Macromolecules* **2004**, *37*, 3101–3112.

[191] A. Gomes, K. S. Carvalho, M. R. Pinto, *Macromol. Rapid Commun.* **1995**, *16*, 543–548.

[192] X. He, W. Sun, D. Yan, L. Liang, *Eur. Polym. J.* **2008**, *44*, 42–49.

[193] L. Cui, X. Tong, X. Yan, G. Liu, Y. Zhao, *Macromolecules* **2004**, *37*, 7097–7104.

[194] X. Tang, L. Gao, X. Fan, X. Liang, Q. Zhou, *Macromol. Chem. Phys.* **2009**, *210*, 1556-1562.

[195] C. Stillings, R. Pettau, J. H. Wendorff, H.-W. Schmidt, K. Kreger, *Macromol. Chem. Phys.* **2010**, *211*, 250–258.

[196] a) A. Hirao, H. Kato, K. Yamaguchi, S. Nakahama, *Macromolecules* **1986**, *19*, 1294–1299. b) T. Breiner, *Dissertation*, Universität Bayreuth, Bayreuth, **2001**.

[197] a) K. Se, K. Miyawaki, K. Hirahara, A. Takano, T. Fujimoto, *J. Polym. Sci., Part A: Polym. Chem.* **1998**, *36*, 3021–3034. b) D. A. Conlon, J. V. Crivello, J. L. Lee, M. J. O'Brien, *Macromolecules* **1989**, *22*, 509–516.

[198] A. Hirao, S. Nakahama, *Acta Polym.* **1998**, *49*, 133–144.

[199] K. Kreger, P. Wolfer, H. Audorff, L. Kador, N. Stingelin-Stutzmann, P. Smith, H. W. Schmidt, *J. Am. Chem. Soc.* **2010**, *132*, 509–516.

[200] D. Demus, *Handbook of Liquid Chrystals*, Wiley-VCH, Weinheim, **1998**.

[201] C. T. Imrie, T. Schleeh, F. E. Karasz, G. S. Attard, *Macromolecules* **1993**, *26*, 539–544.

[202] W.-W. Wang, W.-Y. Ren, L. Jiang, Y. Dan, *J. Appl. Polym. Sci* **2010**, *118*, 2379–2388.

[203] U. Breiner, U. Krappe, E. L. Thomas, R. Stadler, *Macromolecules* **1998**, *31*, 135–141.

[204] S. Ivanov, I. Yakovlev, S. Kostromin, V. Shibaev, L. Läsker, J. Stumpe, D. Kreysig, *Makromol. Chem. Rapid Commun.* **1991**, *12*, 709–715.

[205] A. Bobrovsky, V. Shibaev, J. Wendorff, *Liq. Cryst.* **2007**, *34*, 1–7.

[206] S. Yoneyama, T. Yamamoto, O. Tsutsumi, A. Kanazawa, T. Shiono, T. Ikeda, *Macromolecules* **2002**, *35*, 8751–8758.

[207] K. Kreger, C. Loeffler, R. Walker, N. Wirth, D. Bingemann, H. Audorff, E. A. Rössler, L. Kador, H.-W. Schmidt, *Macromol. Chem. Phys.* **2007**, *208*, 1530–1541.

[208] C. Frenz, *PhD Thesis*, Bayreuth.

[209] a) Q. T. Pham, W. B. Russel, J. C. Thibeault, W. Lau, *Macromolecules* **1999**, *32*, 2996–3005. b) J. M. Yu, P. Dubois, P. Teyssié, R. Jérôme, S. Blacher, F. Brouers, G. L'Homme, *Macromolecules* **1996**, *29*, 5384–5391. c) T. Annable, R. Buscall, R. Ettelaie, D. Whittlestone, *Journal of Rheology* **1993**, *37*, 695–726. d) T. Annable, R. Buscall, R. Ettelaie, *Colloids and Surfaces A: Physicochemical and Engineering Aspects* **1996**, *112*, 97–116.

[210] T. Sato, H. Watanabe, K. Osaki, *Macromolecules* **1996**, *29*, 6231–6239.

[211] H. Watanabe, T. Sato, K. Osaki, M.-L. Yao, A. Yamagishi, *Macromolecules* **1997**, *30*, 5877–5892.

[212] H. Watanabe, T. Sato, K. Osaki, *Macromolecules* **2000**, *33*, 2545–2550.

[213] E. Raspaud, D. Lairez, M. Adam, J.-P. Carton, *Macromolecules* **1996**, *29*, 1269–1277.

[214] D. A. Vega, J. M. Sebastian, Y.-L. Loo, R. A. Register, *J. Polym. Sci., Part B: Polym. Phys.* **2001**, *39*, 2183-2197.

[215] H. Soenen, H. Berghmans, H. H. Winter, N. Overbergh, *Polymer* **1997**, *38*, 5653–5660.

[216] D. Dutta, H. Fruitwala, A. Kohli, R. A. Weiss, *Polym. Eng. Sci* **1990**, *30*, 1005–1018.

[217] a) N. Crawford, M. D. Dadmun, *Liquid Crystals* **2006**, *33*, 195–203. b) N. Gogibus, U. Maschke, F. Benmouna, B. Ewen, X. Coqueret, M. Benmouna, *J. Polym. Sci., Part B: Polym. Phys.* **2001**, *39*, 581–588. c) F. Benmouna, A. Daoudi, F. Roussel, J.-M. Buisine, X. Coqueret, U. Maschke, *J. Polym. Sci., Part B: Polym. Phys.* **1999**, *37*, 1841–1848.

[218] N. R. Scruggs, J. A. Kornfield, J. Lal, *Macromolecules* **2006**, *39*, 3921–3926.

[219] H. Ringsdorf, H. W. Schmidt, A. Schneller, *Makromol. Chem. Rapid Commun.* **1982**, *3*, 745–751.

[220] a) G. Sigaud, M. F. Achard, F. Hardouin, C. Coulon, H. Richard, M. Mauzac, *Macromolecules* **1990**, *23*, 5020–5024. b) M. L. Auad, M. D. Kempe, J. A. Kornfield, S. Rendon, W. R. Burghardt, K. Yoon, *Macromolecules* **2005**, *38*, 6946–6953. c) A. M. Jamieson, D. Gu, F. L. Chen, S. Smith, *Prog. Polym. Sci.* **1996**, *21*, 981–1033.

[221] C. T. Imrie, F. E. Karasz, G. S. Attard, *Macromolecules* **1993**, *26*, 3803–3810.

[222] a) H. Ren, S.-T. Wu, *Appl. Phys. Lett.* **2002**, *81*, 1432–1434. b) K. Urayama, S. Honda, T. Takigawa, *Macromolecules* **2006**, *39*, 1943–1949.

[223] a) E. Raspaud, D. Lairez, M. Adam, J.-P. Carton, *Macromolecules* **1994**, *27*, 2956–2964. b) K. Inomata, D. Nakanishi, A. Banno, E. Nakanishi, Y. Abe, R. Kurihara, K. Fujimoto, T. Nose, *Polym.* **2003**, *44*, 5303–5310.

[224] R. P. Quirk, T. Yoo, B. Lee, *J. Macromol. Sci., Pure Appl. Chem.* **1994**, *A31*, 911–926.

[225] a) Z. Li, M. A. Hillmyer, T. P. Lodge, *Macromolecules* **2004**, *37*, 8933–8940. b) K. A. Switek, F. S. Bates, M. A. Hillmyer, *Macromolecules* **2004**, *37*, 6355–6361. c) A. Hirao, M. Hayashi, A. Matsuo, *Polym.* **2002**, *43*, 7125–7131.

[226] a) *Gels: Structures, Properties, and Functions*, Springer Berlin Heidelberg, Berlin, Heidelberg, **2009**. b) in *Encyclopedia of Materials: Science and Technology* (Ed.: H. H. Winter), Elsevier, **2008**. c) K. Almdal, J. Dyre, S. Hvidt, O. Kramer, *Polymer Gels and Networks* **1993**, *1*, 5–17. d) S. B. Ross-Murphy, *Polymer Gels and Networks* **1994**, *2*, 229–237.

[227] G. M. Kavanagh, S. B. Ross-Murphy, *Prog. Polym. Sci.* **1998**, *23*, 533–562.

[228] Anton Paar, "MCR301 rheometer", can be found under http://www.anton-paar.com/MCR-Rheometer/Rheometer/60_Germany_de?product_id=45, **08.04.11**.

[229] N. R. Scruggs, R. Verduzco, D. Uhrig, W. Khan, S.-Y. Park, J. Lal, J. A. Kornfield, *Macromolecules* **2009**, *42*, 299–307.

[230] M. Khazimullin, T. Müller, S. Messlinger, W. Schöpf, I. Rehberg, A. Krekhov, R. Pettau, K. Kreger, H.-W. Schmidt, *Phys. Rev. E,* **2011**, *submitted*.

[231] a) P. Pieranski, F. Brochard, E. Guyon, *J. Phys. France* **1973**, *34,*, 35–48. b) P. Pieranski, F. Brochard, E. Guyon, *J. Phys. France* **1972**, *33,*, 681–689.

[232] W. Massa, *Kristallstrukturbestimmung*, Vieweg + Teubner, Wiesbaden, **2009**.

[233] Scintag, "Basics of X-ray Diffraction", can be found under http://epswww.unm.edu/xrd/xrdbasics.pdf, **06.05.11**.

[234] Wikipedia, "Bragg_diffraction", can be found under http://en.wikipedia.org/wiki/File:Bragg_diffraction.png, **06.05.11**.

[235] LabXA, "GUINIER DIFFRACTOMETER", can be found under http://www.labxa.de/content/guinier.htm, **06.05.11**.

[236] R. Magnusson, T. K. Gaylord, *J. Opt. Soc. Am.* **1978**, *68*, 809.

[237] R. Magnusson, T. K. Gaylord, *J. Opt. Soc. Am.* **1978**, *68*, 806–809.

[238] H. Kogelnik, *Bell Syst. Tech. J.* **1969**, *48*, 2909–2947.

[239] a) T. Bieringer, *PhD Thesis*, Universität Bayreuth, Bayreuth, **1996**. b) M. Huber, *PhD Thesis*, Universität Bayreuth, Bayreuth, **2001**.

[240] G. Schramm, *Einführung in Rheologie und Rheometrie -2. Auflage*, Thermo Fisher Scientific, Karlsruhe, **2004**.

[241] R. D. Allen, T. E. Long, J. E. McGrath, *Polym. Bull.* **1986**, *15*, 127–134.

[242] N. Hadjichristidis, H. Iatrou, S. Pispas, M. Pitsikalis, *J. Polym. Sci., Part A: Polym. Chem.* **2000**, *38*, 3211–3234.

[243] M. Morton, R. Milkovich, D. B. McIntyre, L. J. Bradley, *J. Polym. Sci., Part A* **1963**, *1*, 443–459.

List of Publications

M. Khazimullin, T. Müller, S. Messlinger, I. Rehberg, W. Schöpf, A. Krekhov, R. Pettau, K. Kreger, H.-W. Schmidt, „Gel formation in a mixture of a block copolymer and a nematic liquid crystal",*Phys. Rev. E* **2011**, *84*, 2171.

R. Pettau, C. Erdelen, H.-W. Schmidt, „Design and Implementation of a Reactor Setup for Combinatorial Anionic Synthesis of Block Copolymer Series with Well-Defined Compositions", *Macromol. React. Eng.* **2010***, 4*, (1), 65–72.

C. Stillings, R. Pettau, J. H. Wendorff, H.-W. Schmidt, K. Kreger, „Lamellar Nanoconfinements Effects in Discotic Liquid Crystalline Block Copolymers", *Macromol. Chem. Phys.* **2010***, 211*, (2), 250–258.

C. Stillings, E. Martin, M. Steinhart, R. Pettau, J. Paraknowitsch, M. Geuss, J. Schmidt, G. Germano, H. W. Schmidt, U. Gösele, J. H. Wendorff, „Nanoscaled Discotic Liquid Crystal/Polymer Systems: Confinement Effects on Morphology and Thermodynamics", Mol. Cryst. Liquid Cryst. **2008**, *495*, 285–293.

Erklärung

Hiermit erkläre ich, dass ich die Arbeit selbstständig verfasst und keine anderen als die angegebenen Hilfsmittel verwendet habe.

Ferner erkläre ich, dass ich nicht versucht habe, anderweitig mit oder ohne Erfolg, eine Dissertation einzureichen oder mich der Doktorprüfung zu unterziehen.

Bayreuth, Mai 2011

Robin Pettau